EXPERIMENTAL AND FINITE ELEMENT ANALYSIS OF PRESSURE VESSEL STEEL SA 387 WITH SUBMERGED ARC WELDING

A THESIS SUBMITTED TO
GRADUATE SCHOOL OF NATURAL AND APPLIED SCIENCES
OF
KOCAELI UNIVERSITY

BY
MERT TURGUT ŞENOL

IN PARTIAL FULLFILLMENT OF THE REQUIREMENTS
FOR
THE DEGREE OF MASTER OF SCIENCE
IN
MECHANICAL ENGINEERING

KOCAELI 2023

EXPERIMENTAL AND FINITE ELEMENT ANALYSIS OF PRESSURE VESSEL STEEL SA 387 WITH SUBMERGED ARC WELDING

A THESIS SUBMITTED TO
GRADUATE SCHOOL OF NATURAL AND APPLIED SCIENCES
OF
KOCAELI UNIVERSITY

BY
MERT TURGUT ŞENOL

IN PARTIAL FULLFILLMENT OF THE REQUIREMENTS
FOR
THE DEGREE OF MASTER OF SCIENCE
IN
MECHANICAL ENGINEERING

Assoc.Prof.Dr. Murat MAKARACI
Supervisor, Kocaeli University ……………………….

Assist.Prof.Dr. Ali ÖZTÜRK
Jury Member, Necmettin Erbakan University ……………………….

Assist.Prof.Dr. Okan GÜL
Jury Member, Kocaeli University ……………………….

Thesis Defense Date : 03.07.2023

ETHICAL STATEMENT AND RESEARCH FUND SUPPORT

In this thesis/project study, which I prepared in accordance with the thesis writing rules of Kocaeli University Graduate School of Natural and Applied Sciences,

I declare that,

- This thesis/project is my own and original work,
- I act in accordance with scientific ethical principles and rules at all stages of my study, including preparation, data collection, analysis, and presentation of information,
- I have cited all data and information obtained within the scope of this study and that I have included these sources in the bibliography,
- This study complies with the similarity criteria determined by the Graduate School of Natural and Applied Sciences in terms of the plagiarism software to which Kocaeli University is subscribed,
- I have not done any falsification of the data used,
- I have not submitted any part of this thesis/project as another thesis/project work at this university or another university,

☒ Any stage of this thesis/project work has not been provided any financial/infrastructural support by any institution/organization.

☐ The data and information produced within the scope of this thesis/project work were carried out by …………………………….. with the financial/infrastructure support within the scope of the project no …………………………….. .

I declare that I accept all the moral and legal consequences at any time that may arise regarding my work in the event of situation contrary of this statement.

…..…..………………
(Signature)
……......………………
(Mert Turgut ŞENOL)

PUBLISHING AND INTELLECTUAL PROPERTY RIGHTS

…..…..………………
(Signature)
……......………………
(Mert Turgut ŞENOL)

PREFACE AND ACKNOWLEDGEMENTS

Welding is a fairly prevalent process in the industrial industry . A construction or artistic procedure called welding coalesces the materials it is joining. The product's life cycle may be shortened by residual stress. The final result gets distorted by welding due to a variety of reasons, not just one. Numerical solutions are the best method for analysing the temperature and stress distributions since welding makes it challenging to utilise an analytical solution to calculate the product's temperature distribution and stress distribution.

My deepest gratitude and foremost to my supervisor Asc.Prof.Dr. Murat Makaracı, for his supervision, constant encouragement and guidance.

A part of this research would not have been possible without the sincere help and advice of my managers and colleagues: Malik Arun, Mehmet Emin Bilgin, Ediz Sezginel, Özgür Köksal, Ramazan Polat, Engin Deniz and Tufan Alkan.

I would like to express my high appreciation to Mr. Yusuf Öztürk and Mr. Bilal Alcan from TÜBİTAK Marmara Research Center, for their kindness, great help and technical support.

Last, my thanks would go to my familiy for their loving consideration and great confidence in me all through these years.

July – 2023 Mert Turgut ŞENOL

CONTENTS

LIST OF FIGURES

LIST OF TABLES

INDEX OF SYMBOLS AND ABBREVIATIONS

a	: Thermal diffusivity $mm^{2/}sec$
d	: Interplanar spacing between crystallaographic planes (m)
E	: Poisson's ratio or Elastisite Modulus (Pa)
Q	: Welding power (watt)
I	: Welding current (amper)
U	: Arc voltage (volt)
k	: Thermal conductivity (Wm^{-1}/K^{-1})
ɳ	: Efficiency
v	: Welding speed (m/sec)
α	: Coefficient of thermal expansion (K^{-1})
ε	: Emissivity
σ	: Stefan Boltzman constant (W/m^2K)
m	: Slope
n	: Constant
λ	: Wavelength (m)
θ	: Diffraction angle (°)
Ψ	: Bragg reflection
σ_θ	: surface stress (Pa)
υ	: Poisson's ratio

Abbreviations

AC	: Alternatig Current
APDL	: Ansys parametric Design Language
ASME	: The American Society of Mechanical Engineers
AWS	: American Welding Society
BS	: British Standards
C	: Carbon
Cr	: Crom
Cu	: Copper
CAW	: Carbon arc welding
CMM	: Coordinate Measuring Machine
CSEF	: Creep Strenth Enhanced Ferrite
DC	: Direct current
EBD	: Element Birth and Death
Eq	: Equation
HAZ	: Heat Effected Zone
EDM	: Electrical Discharge Machine
FE	: Finite Element
FEA	: Finite Element Analysis
FEM	: Finite Element Method
GMAW	: Gas Metal Arc Welding
GTAW	: Gas Tungsten Arc Welding
Mn	: Manganese
Mo	: Molybdenum

Ni	: Nickel
P	: Phosphorus
S	: Sulfur
Si	: Silicon
V	: Vanadium
PDE	: Partial Differential Equation
SAW	: Submerged Arc Welding
SEY	: Sonlu Elemanlar Yöntemi
S	: Sulfur
Si	: Silicon
V	: Vanadium
SMAW	: Shielded Metal Arc Welding
TC	: Thermocouple
TIG	: Tungsten Inert Gas

BASINÇLI KAP ÇELİĞİ SA 387'NİN TOZALTI ARK KAYNAĞI İLE KAYNAĞININ DENEYSEL VE SONLU ELEMAN ANALİZİ

ÖZET

Kaynak, malzemenin erimesini ve katılaşmasını içeren bir metal birleştirme işlemidir. Çok çeşitli malzemeleri birleştirmek için uygulanabilir. Malzemenin erime ve katılaşma aşamaları çok yüksek sıcaklık gradyanı ile fakat küçük bir bölgede meydana gelir. Kaynak tekniklerinin çoğu, birleştirilecek yüzeylerin dolgu metali olsun veya olmasın (yüzey kaplama kaynakları dahil) eritilmesini ve ardından soğutulmasını içerir. Eritme, yerel ısı girişi uygulayarak, bileşene ısı difüzyonunu ve çevreye ısı dağılımını en aza indirerek gerçekleştirilir.

Kaynak işlemi artık gerilmelere, çatlamaya, bozulmaya ve ITAB'ın (Isı tesiri altındaki bölge) oluşumuna vb. neden olur. Çünkü kaynak sırasında ısıtme ve soğutma aşamaları düzensizdir. Kaynaklı bölgenin soğuma aşamalarında malzemenin büzülmesi gerçekleşir. Kaynaklı bölge çevre alan tarafından sınırlandırılmıştır. Bu nedenle kaynak bölgesi artık çekme gerilimi gösterir ve çevreleyen alan, soğuduktan sonra artık basma gerilimi gösterir.

Araştırmacılar ve tasarım mühendisleri için artık gerilim ve distorsiyon miktarını tahmin etmek önemlidir. Bu tez çalışmasında, numuneyi analiz etmek ve numune içerisinde kaynaklamanın neden olduğu kalıntı gerilme miktarını hesaplamak için ANSYS Programı kullanılmıştır. Numunenin 3 boyutlu görüntüsü SpaceClaim uygulaması ile hazırlanmıştır. Bu tezin ana amacı, Tozalyı kaynak işlemi sırasındaki termal çevrimi ve tozaltı kaynağı tarafından indüklenen artık gerilimi deneysel test plakasına kıyasla daha yüksek doğrulukla tahmin edebilen bir FEA modeli geliştirmektir. Bunu gerçekleştirmek için Goldak'ın çift elipsoidal ısı kaynağı modeli kullanılmıştır.

Anahtar Kelimeler: Artık Gerilme, Basınçlı Kap Çeliği, Kaynak Defermasyonu, Sonlu Elemanlar Analizi, Tozaltı Kaynağı

EXPERIMENTAL AND FINITE ELEMENT ANALYSIS OF PRESSURE VESSEL STEEL SA 387 WITH SUBMERGED ARC WELDING

ABSTRACT

Welding is a metal joining process involving melting and solidification of material. It may be applied in order to join wide range of materials. Melting and solidification stages of material occur with very high temperature gradient but within a small region. The majority of welding techniques include melting the surfaces to be connected, with or without filler metal (including surfacing welds), and then cooling them. Melting is accomplished by applying local heat input, minimising heat diffusion into the component and heat dissipation into the environment.

Welding process results into residual stresses, cracking, distortion, formation of Heat Affected Zone and etc. Because heating and cooling stages during welding are uneven. During cooling stages of welded region, contraction of material takes place. Welded region is contracted by surrounding area. Therefore the weld region shows tensile residual stress and the surrounding area shows compressive residual stress after cooling down.

It is important for reseachers and design engineers to predict the amount of residual stress and distortion. In this thesis, ANSYS Program was used in order to analyse the specimen and calculate the amount of residual stresses caused by welding inside the specimen. 3D view of specimen was prepared by SpacaClaim Aplication. The main aim of this thesis is to develop a FEA model which can be predict thermal cycle during SAW process and residual stress induced by SAW with higher accuracy compare to experimental test plate. To realize this, Goldak's double ellipsoidal heat source model was used.

Keywords: Residual Stress, Pressure Vessel Steel, Welding Deformation, Finite Elemanlar Analizi, Submerged Arc Welding

BASINÇLI KAP ÇELİĞİ SA 387'NİN TOZALTI ARK KAYNAĞI İLE KAYNAĞININ DENEYSEL VE SONLU ELEMAN ANALİZİ

GENİŞLETİLMİŞ ÖZET

Kaynak, malzemenin erimesini ve katılaşmasını içeren bir metal birleştirme işlemidir. Çok çeşitli malzemeleri birleştirmek için uygulanabilir. Malzemenin erime ve katılaşma aşamaları çok yüksek sıcaklık gradyanı ile fakat küçük bir bölgede meydana gelir. Kaynak tekniklerinin çoğu, birleştirilecek yüzeylerin dolgu metali olsun veya olmasın (yüzey kaplama kaynakları dahil) eritilmesini ve ardından soğutulmasını içerir. Eritme, yerel ısı girişi uygulayarak, bileşene ısı difüzyonunu ve çevreye ısı dağılımını en aza indirerek gerçekleştirilir. Kaynak işleminin ana avantajı, birleştirilecek parçalar arasında, bileşenin temel malzemesi ile karşılaştırılabilir veya hatta ondan daha yüksek bir mukavemet düzeyine sahip metalurjik bir bağ oluşturmasıdır. Kaynak işleminin ortaya çıkmasından önce perçinleme, yapılar, gemiler ve hatta bazı basınçlı kaplar gibi bileşenlerin imalatı için ana metal birleştirme işlemi idi. Perçinleme, kaynağa göre daha düşük ekipman maliyeti, basit kullanım, daha düşük operatör beceri seviyesi, ön ısıtma ve kaynak sonrası ısıl işlem gibi herhangi bir ek işlem olmaksızın farklı malzemeler için standartlaştırılmış prosedür, daha az sarf malzemesi gereksinimi, basit kalite kontrol prosedürleri vb. gibi çeşitli avantajları vardır.

Kaynak işlemi artık gerilmelere, çatlamaya, bozulmaya ve ITAB'ın (Isı tesiri altındaki bölge) oluşumuna vb. neden olur. Çünkü kaynak sırasında ısıtma ve soğutma aşamaları düzensizdir. Kaynaklı bölgenin soğuma aşamalarında malzemenin büzülmesi gerçekleşir. Kaynaklı bölge çevre alan tarafından sınırlandırılmıştır. Bu nedenle kaynak bölgesi artık çekme gerilimi gösterir ve çevreleyen alan, soğuduktan sonra artık basma gerilimi gösterir. Kaynak işleminin son derece yerel veya yarı sürekli olması dışında, metallerin dökümü ile bir benzetme yapılabilir. Karakteristik olarak, soğuyan kaynak metali bölgesi, termal olarak indüklenen gerilmelerin ortaya çıkmasına yol açan şiddetli kısıtlama koşulları altında büzülür. Büzülme gerçekleşmeye çalışırken ve stress sitemi kararlılığını sağlamak için en düşük seviyesine ulaşmaya çalışırken, akma gerçekleşiren bozulma meydana gelir. Kısıtlamalar ve düşük süneklik ile birleşen yüksek gerilmeler çatlama şeklinde başarısızlığa neden olur.

Sonlu Elemanlar Yöntemi kaynakla ilgili çeşitli art etkileri analiz etmek için kullanılabilen güçlü bir araçtır. Sonlu Elemanlar Yönetmini kullanılarak elde edilen bilgi, uygulayıcı bir mühendisin kritik bileşenlerde yeniden işleme kapsamını en aza indirecek optimum prosedüre ulaşmasına yardımcı olabilir. Ancak SEY'ni kullanarak anlamlı bir sonuç elde etmek kolay bir iş değildir ve kaynakla ilgili önemli olguları gerçekten temsil eden girdi verileri oluşturmak için büyük çaba ve bilgi gerektirir. Geniş veri çıktısını gözden geçirmek ve sonuçları yorumlamak için eşit miktarda çaba gerekebilir. Bu nedenle mühendis kaynak ile ilgili fenomenler hakkında iyi bir bilgiye ve bunları girdi verileri olarak ifade edecek matematiksel beceriye sahip olmalıdır. Kaynak işleminin karmaşık doğası sayısal yöntemlerle analiz ve modellemede zorluklara neden olur. Karmaşıklık, sıcaklığa bağlı malzeme özelliklerine, doğrusal olmayan sınır koşullarına, hareketli ısı kaynaklarına, faz değişimlerine ve dönüşümlerine, karmaşık artık gerilme durumlarına ve yüksek sıcaklıklarda deneysel ölçüm yapmanın zorluklarını içerir. Bu karmaşıklıkların bir sonucu olarak, kaynak işleminin sonlu eleman modellemesi, bir kaynak işlemini simüle ederken karmaşık termomekanik etkileşimleri, dolgu malzeme birikimini ve hareketli ısı kaynaklarını içerir.

Araştırmacılar ve tasarım mühendisleri için artık gerilim ve distorsiyon miktarını tahmin etmek önemlidir. Bu tez çalışmasında, numuneyi analiz etmek ve numune içerisinde kaynaklamanın neden olduğu kalıntı gerilme miktarını hesaplamak için ANSYS Programı kullanılmıştır.

Numunenin 3 boyutlu görüntüsü SpaceClaim uygulaması ile hazırlanmıştır. Bu tezin ana amacı, Tozaltı kaynak işlemi sırasındaki termal çevrimi ve tozaltı kaynağı tarafından indüklenen artık gerilimi deneysel test plakasına kıyasla daha yüksek doğrulukla tahmin edebilen bir FEA modeli geliştirmektir.

Numune malzemesi olarak Basınçlı kap çeliği olarak kullanılan SA 387 GR 11 Class 2 basınçlı kap çeliği seçilmiştir. Bu çelik yüksek sıcaklık çalışma ortamnda çalışabilecek basınçlı kap sınıfı çelik olarak çeşitli endüstrilerde kullanılmaktadır. Özellikle sıvıların ve gazların genellikle daha yüksek sıcaklıklarda depolandığı petrol, gaz ve petrokimya endüstrisinde oldukça etkilidir. Daha yüksek krom seviyeleri ayrıca atık gaz uygulamalarında bir zorunluluk olan mükemmel korozyon ve oksidasyon direnci sağlar.

Numune parçanın kaynak işlemi için Tozaltı kaynak yöntemi kullanılmıştır. 100x100x8 mm ölçülerinde hazırlanan numune parça için 1 mm kare şeklinde kaynak ağzı açılmıştır. Kaynak hızı olarak 0,01 m/s ve kaynak gerilimi olarak 31 volt daha önce bu parça için yapılan kaynak prosedürlerinden tespit edilmiştir. Kaynak işlemi için gerekli akım değerini belirlemek için 430, 530, 560 ve 600 amper değerlerinde testler gerçekleştirilmiştir. Kaynak nufuziyeti en uygun 600 amperde elde edilmiştir. Kaynak işleminde sıcaklık değerlerini analiz sonuçları ile karşılaştırmak için parça üzerinden 5 noktadan sıcaklık ölçümü alınmıştır. Sıcaklık ölçümü için K tipi termokupl ve sıcaklıkların kaydedilmesi için de Honeywell marka dijital sıcaklık kayıt cihazı kullanılmıştır. Numune parça üzerinden ölçülen sıcaklık değerleri sonlu elemanlar yöntemi ile elde edilen sıcaklık değerleri ile karşılaştırılmıştır.

Artık gerilme değerlerini karşılaştırmak için, Tübitak MAM araştırma merkezinde bulunan Panalyytical X'Pert Pro MPD cihazı kullanımış ve X-Ray difraction yöntemi ile parça üzerinde belirlenen 9 noktadan (5 nokta parçanın tam ortasından enine yönde, 5 nokta kaynak hattı boyunca, orta nokta her iki yönün ortak noktası olacak şekilde) artık gerilme ölçümleri yapılmıştır ve sonlu elemanlar yöntemi ile elde edilen sonuçlar ile karşılaştırılmıştır. X-Ray difraction yöntemi ile artık gerilme ölçümü tahribatsız ölçüm metodlarındandır. Stres, belirli bir Bragg yansımasının açısal kaymasının eğiminin (Ψ) bir fonksiyonu olarak kaydedilmesi ile belirlenir. Bu aslında numunede bir gerinim ölçüsü sağlar ve bundan sonra $\sin^2 \Psi$'ye karşılık d-aralığındaki değişikliğin grafiği çizilerek gerilim buradan hesaplanır.

Kaynak işleminin sonlu elemanlar yöntemi ile analizi için hareketli ısı kaynağı modeli kullanmak gerekmektedir. Bu hareketli ısı kaynağı modeli Ansys programında APDL kodu olarak yazılmıştır. Hareketli ısı kaynağı modeli olarak Goldak'ın çift elipsoidal ısı kaynağı modeli kullanılmıştır. Bu ısı kaynağı ile ilgili deneyim, arkın önündeki tahmin edilen sıcaklık gradyanlarının deneysel olara gözlemlenenlerden daha az dik olduğunu ve arkın arkasındaki gradyanların ölçülenlerden az dik olduğunu göstermiştir. Bunun üstesinden gelmek için çift elipsoidal ısı kaynağı adı verilen bir ısı kaynağı önerilmiştir. Yeni ısı kaynağını vermek için iki farklı yarı elipsoid birleştirildiğinden, her bir yarı elipsoid içindeki ısı akışı farklı denklemlerle tanımlanmıştır. Goldak çift elipsodial ısı kaynağı hacimsel bir ısı kaynağıdır ve ark kaynak uygulamalarının sonlu elemanlar yöntemi ile analizinde en çok kullanlan modeldir. Goldak çift elipsoid model için gerekli geometrik ölçüler numune parça üzerinden alınmıştır.

Ağ yapısı olarak 1x1x1 mm lik ağlar kullanılmıştır. Toplamda 358743 nod ve 80800 eleman kullanılmıştır. Ağ yapısını küçültmek sonuçların doğruluğunu arttırmaktadır fakat hesaplama zamanını da oldukça arttırmaktadır. Bu yüzden en uygun ağ yapısı olarak 1x1x1 mm lik ağlar tercih edilmiştir.

3 ısı transferi çeşidi olan iletim, konveksiyon ve radiasyon çeşitlerinden konveksiyon gözönünde bulundurulmamıştır. İletim ve radiasyon gözönünde bulundurulmuştur. Parçanın üst tarafı tozaltı tozu ile kaplandığı için tamamen izolasyonlu olarak kabul edilmiştir. Parçaya ön ısıtma yapıldığı için parçanın başlangıç sıcaklığı 150ºC çevre ortam sıcaklığı ise 25ºC olarak kabul edilmiştir. Parçanın öz ısısı ve iletim katsayısı sıcaklığa bağlı değerler olarak girilmiştir. Yapısal analizde de elastisite modülü, termal genşleşme katsayısı sıcaklığa bağlı değerler olarak girilmiştir. Yoğunluğu 7750 kg/m^3 ve poisson oranı 0,3 olarak sabit değer girilmiştir. Isı transfer katsayısı olarak 5 W/m^{2}ºC, radiasyon yayınım değeri de 0,9 olarak alınmıştır.

Zaman bağlı termal analizden elde edilen sonuçlar yapısal analizde sınır şartı olarak kullanılmıştır. Yapısal analizde iki yöntem ile analiz gerçekleştirilmiştir. Birinci yöntemde termal analizden elde edilen sonunçlar yapısal analizde kullanılmış, ikinci yöntemde kaynak dolgu metalinin etkisini görmek için kaynak dikişi ve dolgu metalinin olduğu kısım eleman doğum ve ölüm yöntemi ile modellenmiştir. Yapısal bir analizde bir eleman öldüğünde sertliği sıfıra yakın bir değer olarak ayarlanmaktadır. Bu varsayılan değer 10^{-6}'dır. Eleman ölümünün bir diğer etkisi eleman yüklerinin sıfıra ayarlanmasıdır ve tekrar doğduklarında bu sıfır değerinde tekrar devreye girmeleridir.

Sıcaklık analizinde elde edilen deneysel ve analiz sonuçları karşılaştırılmış ve deneysel sonuçlar ile analiz sonuçlarında iyi bir uyum bulunmuştur. 5 noktadaki sonuçlarda birbirine benzer ısınma ve soğuma eğrilerini göstermektedir. 5 sonuçtada deneysel sonuçlardaki soğuma hızı analiz sonuçlarına göre daha yavaştır. Fakat deneysel sonuçlarda da aynı noktalarda elde edilen değerler birbirinden farklılık gösterdiği tespit edilmiştir. Bunun nedeni torchun yükseklik ayarı, amper değerinin kaynak esnasında değişimi, tozlatı tozunun parça üzerinde kapsadığı alan ve soğumaya etkisi gibi hem çevresel hem de kaynak işleminin doğasından kaynaklanan nedenlerdir.

Yapısal analiz sonuçları her iki durumda deneysel souçlar ile karşılaştırılmıştır. Analiz sonuçlarından beklediğimiz parça simetrik olduğundan sonuçların da simetrik olmasıdır. Deneysel sonuçlarda simetrik noktalara karşılık gelen yerlerdeki ölçüm sonuçları birbirinden farklılık göstermiştir. Bu farklılık X-Ray diffraction metodunun ölçüm hassasiyetinden kaynaklanmaktadır. Çünkü bu yöntem ile doğru sonuç almak için parça yüzeyinin pürüzsüz ve çok düzgün olması gerekmektedir. Kaynak yapılan parça kaynak dikişi oval olduğu için kaynak boyunca artık gerilme sonuçlarını ölçebilmek amacı ile kaynak dikişi taşlama yöntemi ile parça üzerinde kaldırılmış ve parçanın düz olması sağlanmıştır. Fakat taşlama işlemi esnasında parça yüzeyinde hafif oyuk yüzeylerde oluşmuştur bu girinti ve çıkıntı olan noktalarda X-Ray diffraction yöntemi ile hatalı sonuçlar alınmış ve ölçüm bu noktaya yakın ve daha düzgün olan yüzeyden alınmaya çalışılmıştır. Ayrıca X-ray diffraction yöntemi ile parça makinenin tablası üzerine çift taraflı bant ile yapıştırılmıştır. Fakat ölçüm esnasında bu bant parçayı tabla üzerinde sabitlemeyi bazen başaramamıştır. Bu da sonuçların yanlış ölçülmesine neden olmuştur.

Yapılan iki analiz modelinde de simetrik sonuçlar elde edilmiştir. Eleman doğum/ölüm yöntemini kullanmak parçayı bir bütün olarak kabul ettiğimiz yönteme göre daha zordur ve daha fazla çaba gerektirmektedir. Her iki yöntemde de elde edilen sonuçlar karşılaştırıldığında kayak boyunca elde edilen sonuçlarda eleman doğum ve ölüm yönteminde farklılık tespit edilmiştir. Elaman doğum / ölüm yönteminde elde edilen bu farklılık yöntemin eleman yüklerini her ölümde sıfıra yakın bir değer olan 10^{-6} ‘a ayarlaması ve ve tekrar doğduklarında bu sıfır değerinde tekrar devreye girmeleridir. Gerilişm sonuçlarını karşılaştırırken hat üzerinde gerilim değerlerine karşılaştırılmış ve ayrıca deneysel ölçümlerde ölçüm noktalarına karşılık gelen analiz sonuçlarında nodlardaki değerlerde karşılaştırılmıştır. Nodal olarak değerleri karşılaştırma daha uygun sonuçlar vermektedir.

1. INTRODUCTION

FEM is a useful tool for analysing different welding-related effects. The knowledge can help a practicing engineer to arrive at the optimum procedure, which will minimize the extent of rework in critical components. However, getting a meaningful result using FEM is no easy task and it requires a great amount of effort to create input data that truly represent the important phenomena associated with welding. An equal amount of effort may be required to sift through the vast data output and interpret the results. Thus, an engineer must have a good knowledge of the phenomena associated with welding as well as the mathematical skill to express them as input data.

Welding is widely employed in the fabrication industry for the manufacture of many types of components involving different shapes, sizes and materials. The primary benefit a of the welding procedure is that it produces a metallurgical bond between the members to be joined which has a strength level comparable to or even higher than that of the base material of the component. Before the advent of the welding process, riveting was the main metal joining process for the fabrication of components such as structures, ships, and even some pressure vessels. Riveting has several advantages over welding like lower equipment cost, simple operation, lower operator skill level, standardized procedure for different materials without any additional operations like preheating and post-weld heat treatment, less consumable requirement, simple quality control procedures, etc.

However, the advantage of higher joint strength in the case of welding gives it an edge over riveting in many types of components. The welding process enables the designer to optimally design the component for maximum performance with minimum size, shape, and weight of the component.

Today, industrial components are designed with advanced materials and thicker sections for operating at increasingly higher load levels. The challenges in the joining of these critical components are effectively met by welding. Much research work has been undertaken to address the various issues which are faced during welding and the welding process owes its premier position to these developments. Many welding processes, procedures, consumables and equipment have been developed which are suitable for various types of components for different end applications. The productivity of the welding process is continually being improved, and automation has been successfully implemented for large-scale manufacture of many welded components. Suitable welding procedures which minimize the metallurgical damage in different materials are under constant development. The deleterious effect of weld discontinuities on the load carrying capability has been studied in detail, and steps to overcome the problems are widely known to the industry. Advanced testing methods have been developed for better reliability of the welded components. Fabrication codes have been formulated so that the welding procedure is standardized and safe performance of welded components during service is ensured. There are many trained welders and welding operators who meet the skill requirement of various fabrication codes. Thus the process of welding has come to occupy an important position in the fabrication industry.

The metallurgical bond in the case of welding is achieved by the conversion of different forms of energy into the energy for coalescence. This energy is focused in 2 Finite Element Analysis of Weld Thermal Cycles Using ANSYS the localized region at the interface between the two members. In the case of arc welding processes which account for a major share of welding, the electric arc provides the required energy for fusion of the members.

In many cases, extra metal is deposited to fill the groove between the members, and this additional metal also receives the heat from the electric arc. After solidification, the required metallurgical bond between the abutting members is created. The localised release of heat along the joint line is essential for the welding process to be successful., but this localized heat has its own aftereffects and unless these detrimental aftereffects are suitably tackled, the resulting quality of the weld will not be satisfactory. The zone in the parent metal which is closest to the weld is heated to very high temperature, which causes metallurgical phase changes in the material. The parts that are joined are known as a parent material. This zone which is metallurgically affected by the high temperature is called the heat affected zone. Heat affected zone is the weakest link in the entire weldment, unless steps are taken to contain the weakness within limits, the resulting weld will not meet the quality requirements. The heat due to welding produces different effects in different materials under different conditions. In materials like carbon steel and low alloy steel, it produces hardening due to rapid cooling whereas in materials like aluminium alloys, it has a softening effect due to recrystallization which takes away the beneficial effects of cold work. In steels, faster cooling rates during welding affect ductility whereas slow cooling rates affect toughness. The welding heat causes grain refinement in the previously deposited weld metal in multipass welding whereas it has a grain coarsening effect in the heat affected zone which affects the strength and toughness. The welding heat leads to depletion of elements like chromium, which give the required properties, whereas it may cause segregation of impure elements, which weakens the weld joint. In stainless steel, the welding heat may lead to the precipitation of unfavourable carbides, and in some other cases, the heat leads to dissolution of the favourable carbide in the matrix. The inadequate liberation of the welding heat results in improper fusion of the weld metal with the base metal but in some steels, the excess liberation of heat causes melting of more parent metal which alters the chemical composition of the weld metal and makes the weld metal inferior. The non-uniform heating and cooling cycle associated with welding also causes problems including distortion and residual stresses which affects the integrity of the welded structure. The differential thermal expansion during the heating cycle causes localized plastic deformation in the weld and adjacent regions, and as a result, shrinkage forces are developed in this region during the cooling phase. These shrinkage forces produce residual stresses or distortion depending on the restraint offered by the component. In steels containing non-metallic inclusions in the form of thin lamella at the mid-section, the shrinkage forces in the thickness direction may lead to tearing of the member, and this phenomenon is known as lamellar tearing.

The root cause of all these detrimental aftereffects can be traced to the application of localized heat during welding, and hence the total elimination of these after effects is not possible. But the damage may be contained within limits by controlling the heat input to the exact minimum requirement. Any indiscreet application of heat during welding will aggravate the problem, and post correction becomes more difficult. Thus the successful application of welding requires a careful balancing of the heat input for achieving proper fusion without severe degradation of the properties of the weld.

There are analytical methods for the study of temperature history in the weldment. These methods are easy to use and have been successfully employed in some cases. But these methods employ many simplifying assumptions which affect the accuracy of the results.

With the improvement in computing power, numerical techniques like the finite element method have become popular as various phenomena may be incorporated easily in these models and reasonably accurate thermal results can be obtained. There are many phenomena associated with welding and accounting all these phenomena will make the analysis very complex and time consuming. The phenomena which have major effects must be considered in the model, leaving out the other less important ones so that the accuracy of the results will be reasonable while the cost of computation is kept within limits. Incorporating the phenomena in the model must be done carefully, and improper representation of these phenomena will have adverse effects on the accuracy of the results.

There are commercially available finite element method based softwares which can help a researcher to perform the analysis without the need to go through the basic steps in formulation and solution of the problem. These softwares enable the user to visualize the results for better understanding. Even though there are many advantages in using these softwares, the user has to exercise caution during the data input since there may be some underlying limitations for a particular case, and if the researcher tries to run the analysis without really understanding the effect of these limitations, it will only lead to inaccurate and unreliable results (Ravichandran, 2021).

2. WELDING PROCESSES

2.1. Basic Concepts of Welding and Welding Mechanics

The welding procedure is a fabrication step that is used to fuse the metal parts together. An energy source of heat is used to locally raise the temperatures of the surfaces that will be bonded by welding to their melting points. The energy source may alter depending on whether you're welding using electrical resistance, an electric arc or a flame. The junction is formed when small or thin structural components fuse together on their own. It is necessary to inject a filler material during the welding process. The process energy obtained by welding machines creates a localised molten pool. This pool is hosting the welding process consumable, and/or previously deposited weld metal and the component surface

The heating and cooling stages of the welding process are consequently uneven because the molten pool into which the consumable is introduced is shifted along the joint axis. During welding, adjacent pieces of the material attempt to expand and contract to varying degrees in line with the timing of the localized heat cycle. Figure 2.1 shows distortion caused by welding.

Casting of metals is a similar process to welding, but there is a difference. When compared to the casting process, the welding process has a very localized and semi-continuous application. The weld metal zone's cooling stafe contracts in conditions of severe restriction. Stresses caused by heat will be introduced as a result of this restriction.

The metal that has been welded attempts to contract. As a result, the stress system tries to stabilize at its lowest level. Metal yielding results in distortion.

Figure 2.1. Distortion caused by welding (Croft D.N., 1996)

High stresses will be coupled with joint restraint and these high stresses causes cracking problems with low ductility. Let’s consider a 2-dimensional rectangular body as shown in Figure 2.2 in order to comprehend the causes of the residual strains brought on by the welding process' heat cycles.

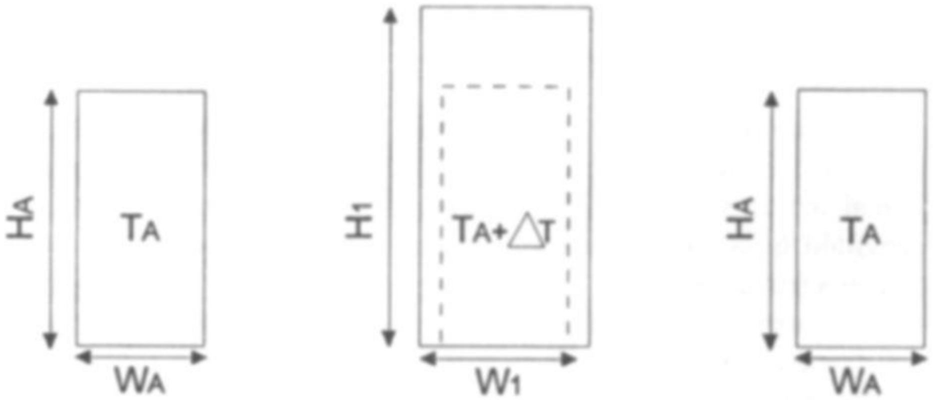

Figure 2.2. Unrestrained expansion and contraction (Croft D.N., 1996)

Characteristically metals will expand when they will be heated. In the case of unrestrained situation, they independently alter their size in accordance with their coefficient of thermal expansion. Dimensions H_A and W_A grow to H_1 and W_1 correspondingly when the body is heated to from ambient temperature T_A by an amount ΔT.

$$H_1 = H_A (1 + \alpha\Delta T) \tag{2.1}$$

$$W_1 = W_A (1 + \alpha\Delta T) \tag{2.2}$$

Where α is the coefficient of thermal expansion, generally this value can take as 12.7-14.6 x 10^{-6} K^{-1} for ferritic steels. When the temperature drops to the ambient level during cooling stages, the body will resume its former shape. In a case of a restriction on free expansion in the vertical axis, the H dimension in Figure 2.3.

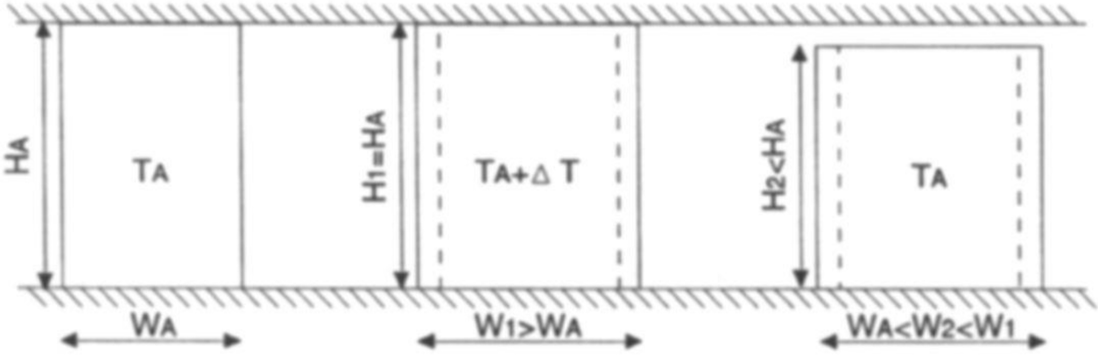

Figure 2.3. Restrained expansion unrestrained contraction (Croft D.N., 1996)

The structure cannot simultaneously expand its dimension in the H direction and temperature if the temperature is raised as previously. Only W dimension can increase its dimension. It will undergo a larger expansion than in Fgure 2.2. When the metal's temperature is changed sufficiently, plastic deformation occurs at the higher temperature, stabilising the structure. There are no restrictions on contraction when welded metal cools to room temperature from a high temperature. As a result, when compared to the original proportions, the height will be decreased but the width will be enlarged.

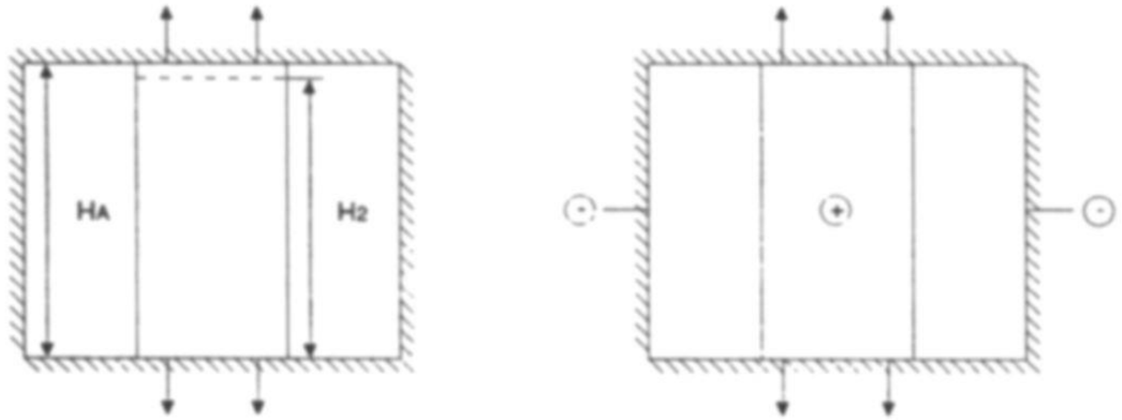

Figure 2.4. Restrained expansion and contraction (Croft D.N., 1996)

Now it can be explained it by giving an example. Let's try to weld the metal with the body representing but this metal should be firmly attached to the two boundaries an in Figure 2.4. The body is restrained and therefore it will not long freely from H_A to H_2 as the temperature returns to ambient. It is in stretched position and tensile stress is actiong to the body. Unless another sort of treatment is used to reduce it, this stress will last forever. Compressive stresses will be generated elsewhere to permit a self-balancing state since every stress system must be in balance to be stable. The mechanism of residual welding tensions that develop during the welding process is explained using this example in a very simplistic manner.

In actuality, the area around the joint will have a distribution of these stresses that is greater than the size of the yield point. Figure 2.5 illustrates the two main longitudinal and parallel directions in which residual stresses will act. Gaps would arise at the plate ends if the weld metal were allowed to expand and contract without limitation while creating the connection. (See Figure 2.6).

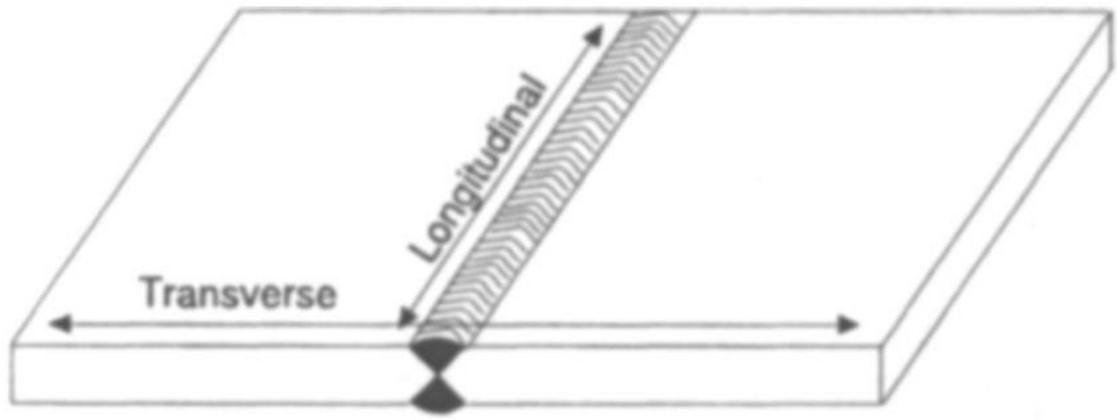

Figure 2.5. Direction of principal stresses (Croft D.N., 1996)

Figure 2.6. Effects of restraint on weld metal (a) Unfused (b) Fused (Croft D.N., 1996)

The distribution of longitudinal residual stresses is depicted in section in Figure 2.7(a), with the tensile component limited to the area around the joint. The resultant transverse stress distribution is shown in Figure 2.7 (b). Midlength is where the largest tensile stress will build, and some compressive residual stresses will work near the junction to provide balance.

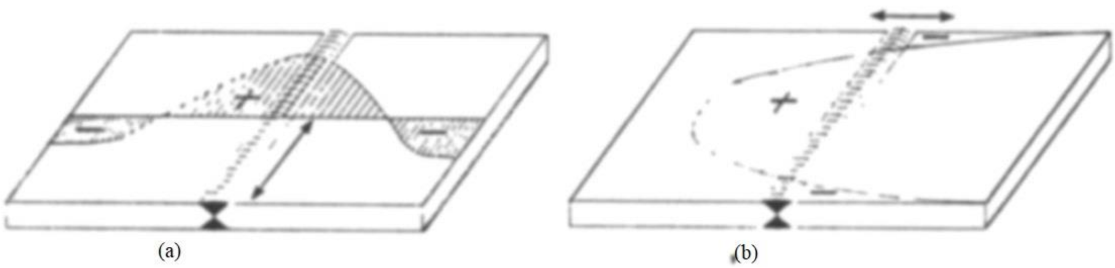

Figure 2.7. Residual stress distribution (a) longitudinal (b) transverse (Croft D.N., 1996)

The localized melting of the component joint faces and the deposition of weld metal in a molten pool, followed by cooling, are metallurgical effects that are changing the microstructure of these areas.

After the welding process, the cooling steps can go rather quickly. An as-cast-type structure emerges from the molten pool of weld metal. Metallurgical restructuring takes place when the parent metal is heated to its melting point at the fusion face. The rapid cooling creates a metallurgical structure. Mechanical properties of this structure will be different from the bulk parent material. The heat affected zone refers to this portion of the parent material in the welded junction.

Because steels lose their resistance to impact and ductility during welding, the heat impacted zones in steels are often tougher than the parent material.

There are some reason of failure of a weld, these are;

- The harshness of heat cycles, which results in significant residual stresses
- Because the characteristics of the heat-affected zone and the weld metal differ significantly from those of the parent material.

Thermal behavior is the cause of the weld failure. Heating application can be applied to prevent these failure. Heat treatment engineering is the study of a sequence of heat treatment activities that are performed prior to, during, and after welding in order to regulate metallurgical changes. (Croft D.N., 1996).

Products that are to be welded always experience heat strains, deformations, and residual stresses as a result of fusion welding. Design engineers are very interested in how stress and deformation are produced, as well as how they affect welded constructions' performance. The theoretical basis for comprehending these effects is provided by welding mechanics theory. Theories in traditional welding mechanics are derived from simplified models and an empirical formula. Products that are to be welded always experience heat strains, deformations, and residual stresses as a result of fusion welding. Design engineers are very interested in how stress and deformation are produced, as well as how they affect welded constructions' performance. The theoretical basis for comprehending these effects is provided by welding mechanics theory. Theories in traditional welding mechanics are derived from simplified models and an empirical formula. Engineers can modify their designs in response to the findings of FEM. In reality, generic structures are created using a variety of manufacturing techniques, including cutting, bending, connecting, straightening, releasing residual tension, etc. These procedures may be divided into the following three categories: use of a mechanical process, chemical reaction, and thermal process. The first category includes welding, also known as "fusion joining," which is the process of attaching components by melting a tiny amount of metal. Metal melting energy sources include gas, arc, plasma, electron beams, lasers, and others. The type of construction and the production efficiency should be taken into consideration while choosing these approaches. For instance, because a heavy pressure vessel is made up of several thick plates, it is frequently preferred to use an extremely effective heat source, such as electron beam welding, which concentrates a significant amount of heat input. Arc welding is frequently utilized for huge buildings like ships and bridges since the equipment is affordable and simple to use. In order to perform fusion welding, a heat source is typically moved along the weld line.

Various welded joint types, such as butt joints, fillet joints, etc., are employed according on the form parameters of the structural components, as shown in Figure 2.8. To achieve appropriate penetration, the groove type also varies depending on plate thickness, as illustrated in Figure. 2.9.

Arc heating is used in arc welding to melt the base metal on the surface of the groove. The electrode melts and fills the groove at the same time.

In arc welding, the surface of the groove of the base metal is heated and molten by arc heating. Simultaneously, the electrode is also molten and fills into the groove. After cooling down, the joint is formed.

The type of welding power source, such as direct current, alternating current, and pulse current, must be selected to fit the type of welded joint. In arc welding, the heat input per unit. The energy sources for melting metal are gas, arc, plasma, electron beam, laser, etc. These are selected according to the type of structure and the efficiency of the manufacturing. For example, since a heavy pressure vessel is composed of many thick plates, a highly efficient heat source such as electron beam welding, which provides a concentrated large amount of heat input, is often adopted. For large structures such as ships, bridges, etc., arc welding is widely used because its machine is cheap and can be handled easily.

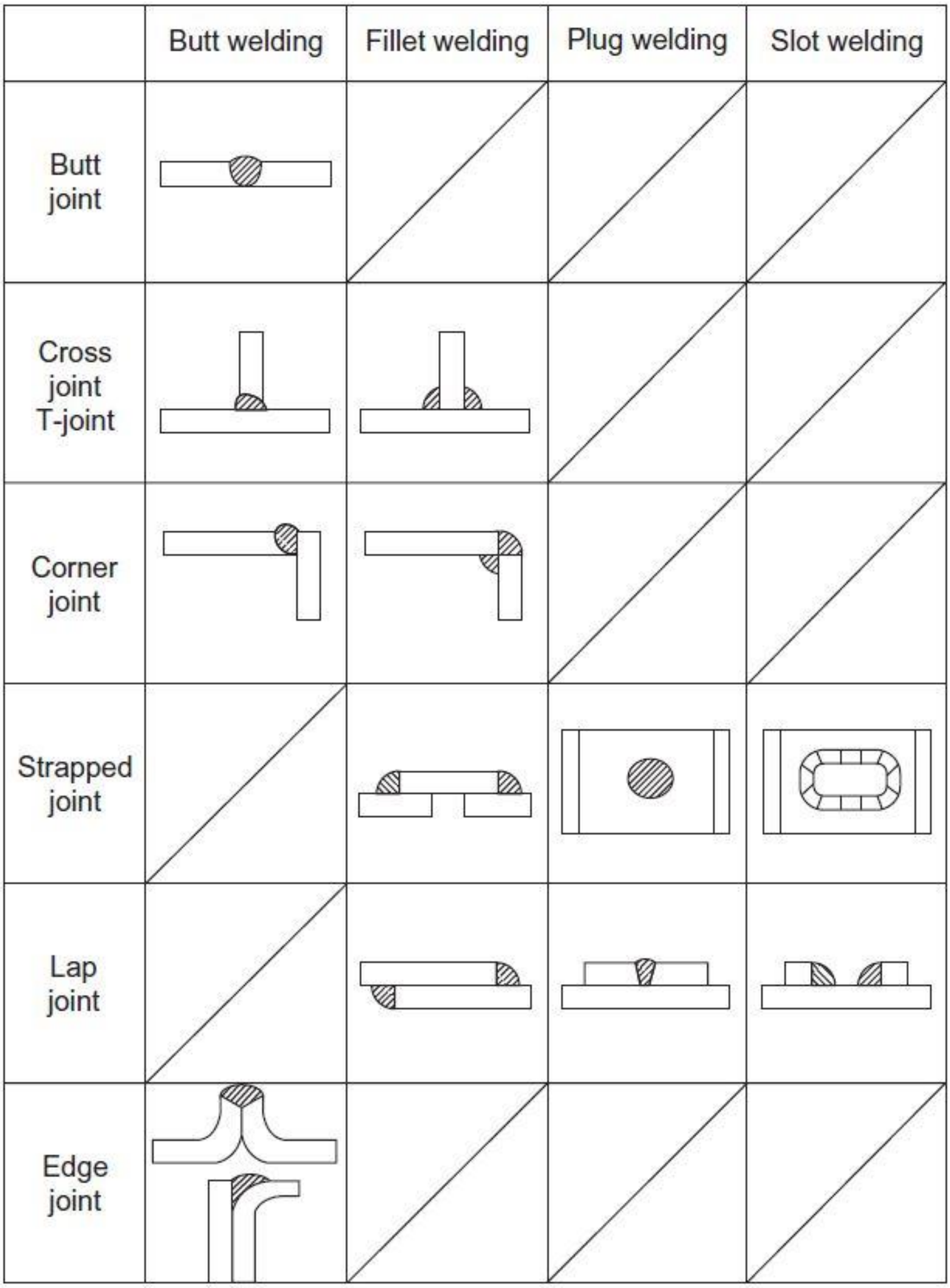

Figure 2.8. Types of welded joints (Ueda and et al., 2012)

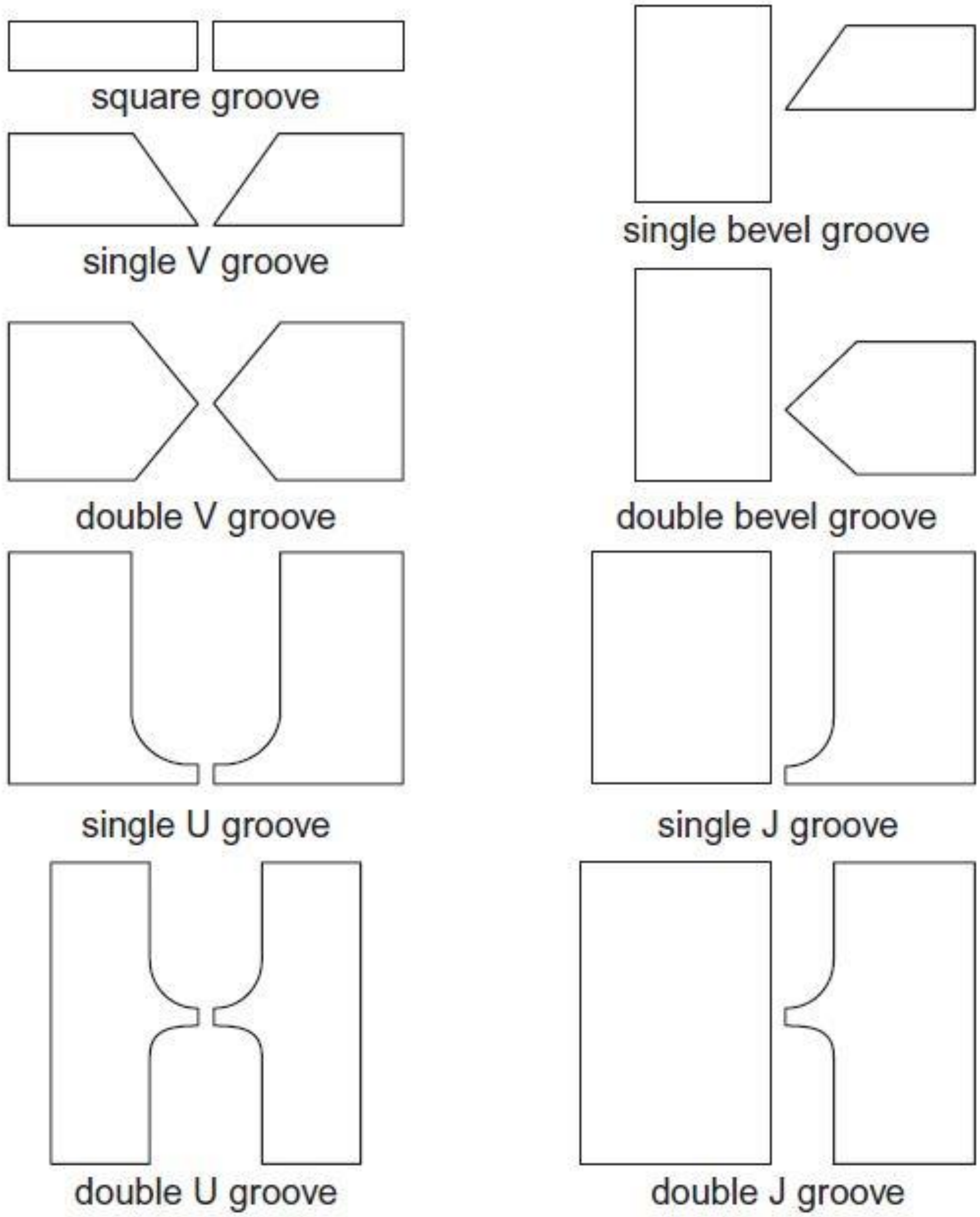

Figure 2.9. Types of grove shapes (Ueda and et al., 2012)

The joint is produced following the cooling stage. The schematic representation of the electrical power supply and the welding arc is shown in Figure 2.10.

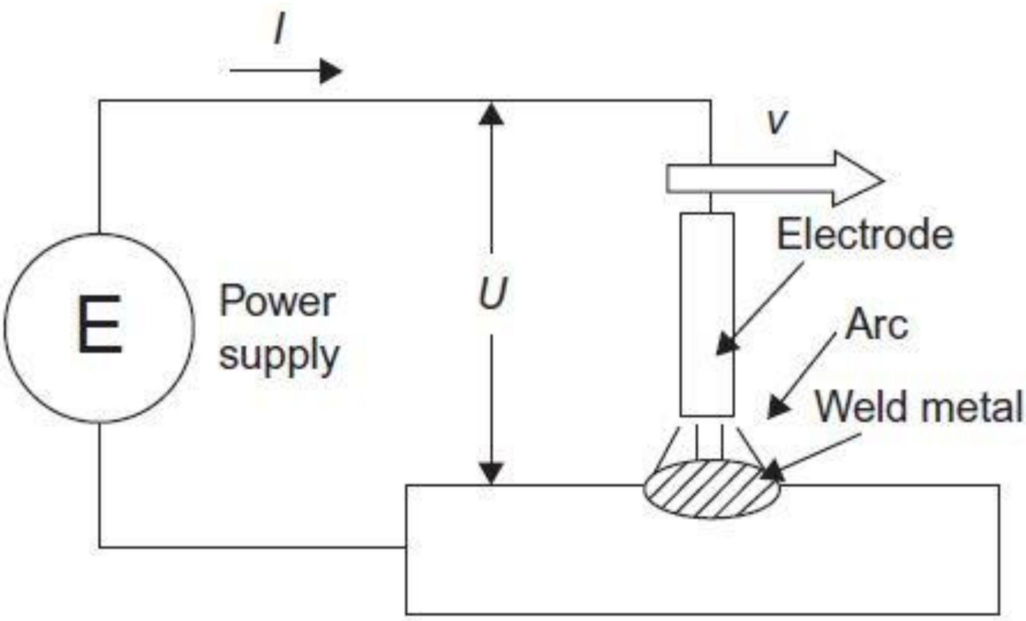

Figure 2.10. Electric power and welding arc (Ueda and et al., 2012)

The heat input per unit weld length in arc welding is represented by;

$$Q = \frac{\eta * I * U}{v} \tag{2.3}$$

Where, I stands for direct-current source's current, U for the voltage between the base plate and electrode, and v for the electrode's speed of movement. η is the heat input's efficiency, which accounts for the loss of electrical energy by, convection, conduction, radiation etc.

The temperature distributions are determined, for instance, when a point heat source passes across the surface of a thick plate as shown in Figure 2.1.

The temperature is maximum just beneath the heat source and progressively drops as one moves toward the welding start.

A concentric circle is shown by the temperature distribution in the vertical plane opposite the weld line. The area that is heated above the Ac1 transition temperature (723°C) in the case of steel is considered to be the weld metal as a consequence, and the area around it is known as the heat-affected zone, as shown in Figure 2.12. The hardness and ductility of the HAZ vary, and these differences have an impact on the dependability and strength of the welded junction.

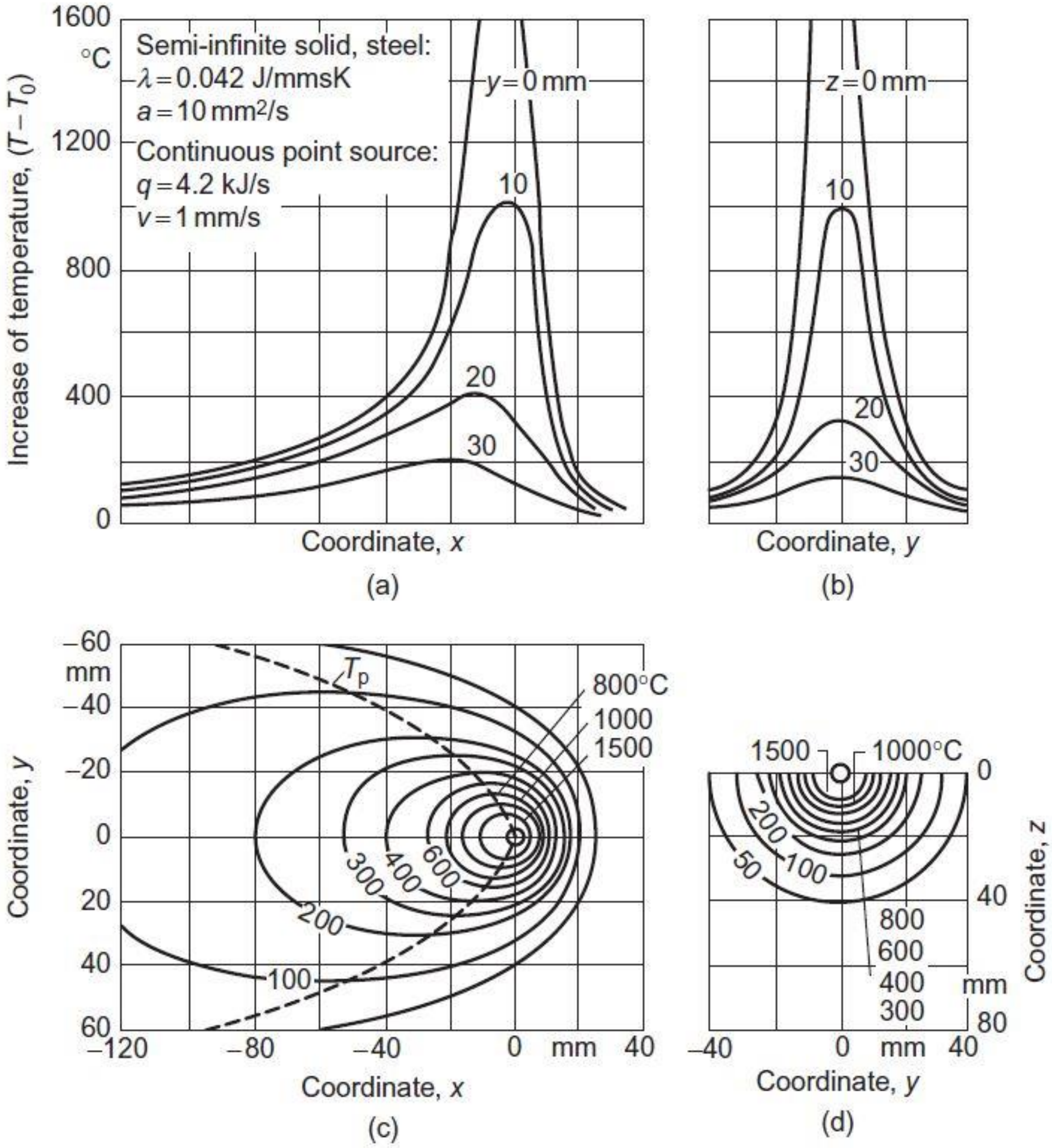

Figure 2.11. Temperature distributions on a thick plate's surface that were calculated using a point heat source (Ueda and et al., 2012)

There are three categories into which welding-related issues can be divided:

1. Metallurgical modifications brought on by thermal history.
2. Heat is utilized during welding to help the metal melt and solidify.
3. Mechanical effects of the welding process, including as deformation and residual stress

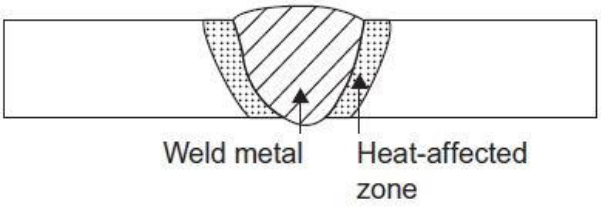

Figure 2.12. Section of welded joints (Ueda and et al., 2012)

Plastic shrinkage, which is brought on by thermal shrinkage and expansion in the welded section during heating processes, causes welding deformation and residual stress like shown in Figure 2.13. Basic welding deformation patterns in a butt joint are shown in Figure 2.14. They consist of rotational and angular distortions as well as transverse and longitudinal shrinkages.

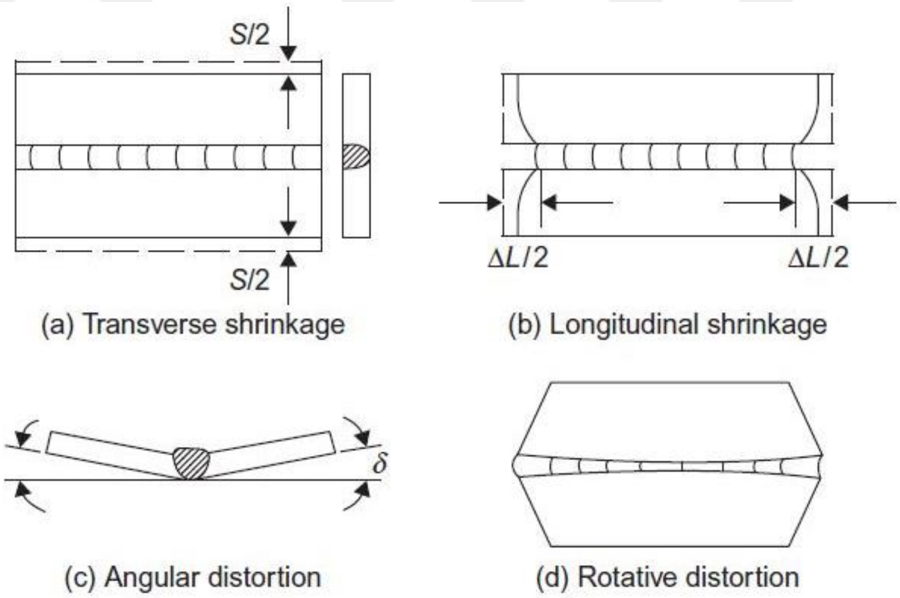

Figure 2.13. Basic types of welding deformation (Ueda and et al., 2012)

The maximum longitudinal stress is almost equivalent to the yield stress in magnitude. Weld cracks may develop in the welded part if the base and filler metal ratio and the welding circumstances are not chosen correctly. As shown in Table 2.1, residual stress, deformation, and weld fractures might weaken the welded structure's strength and reduce the product's dependability. High thermal gradients result from the surrounding area's fast heating during the welding process. The heated material expands, but the expansion is constrained by the mass that is around it, which is colder and stronger. Thermal stress will result from this. Plastic stresses will form in the weld zone because the yield limit is decreased in the area of higher temperature. The material in the weld region will be "too small" after it cools down since the volume has decreased. Due to plastic hardening, which also causes latent stresses, the material will recover its strength upon cooling, usually at a higher level. The residual stress, distortion, and weld cracks may deteriorate the strength of the welded structure and lower the reliability of the product as described in Table 2.1.

Table 2.1. Welding-induced Problems and Countermeasures (Ueda and et al. 2012)

	Influential Factors	Countermeasures
Residual stress	Brittle fracture, fatigue, stress corrosion crack (SCC), buckling	Heat input, welding sequence, post-weld heat trteatment (PWHT)
Distortion	Geometry inaccuracy, anti-automation	Clamping, Constraint, Prediction, offset, straightening
Crack	Cold/Hot cracking	Material selection, pre-/postheating Weld condition,

Then, it is advised to implement the necessary actions based on simulation and/or forecast. For instance, residual stress can be reduced and metallurgical characteristics can be enhanced by using stress relief annealing. Prestrain may be applied to correct welding distortion in order to reduce the resultant distortion. It is vital to forecast or estimate residual stress and deformation in order to be ready for the effects of welding. One of the most effective techniques is to replicate welding activity using a computer (Ueda and et al. 2012).

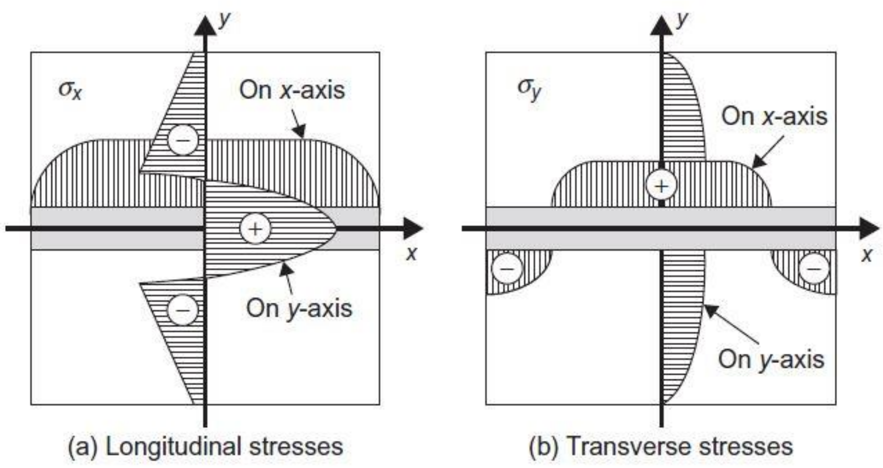

Figure 2.14. Typical residual stress distribution patterns (Ueda and et al., 2012)

2.2. Welding and Joining Processes

Fusion and solid phase welding applications are the two basic categories for welding processes. Two edges or surfaces are welded together via fusion welding. The melting point is reached on these edges or surfaces that will be welded. The joint gap is filled by mixing in molten filler material. With solid phase welding, two spotless solid metal surfaces are pushed close enough to one another to produce a metallic connection. At temperatures as low as room temperature, solid phase welding is possible. The Figure 2.15 below shows various welding and joining process (Singh 2021).

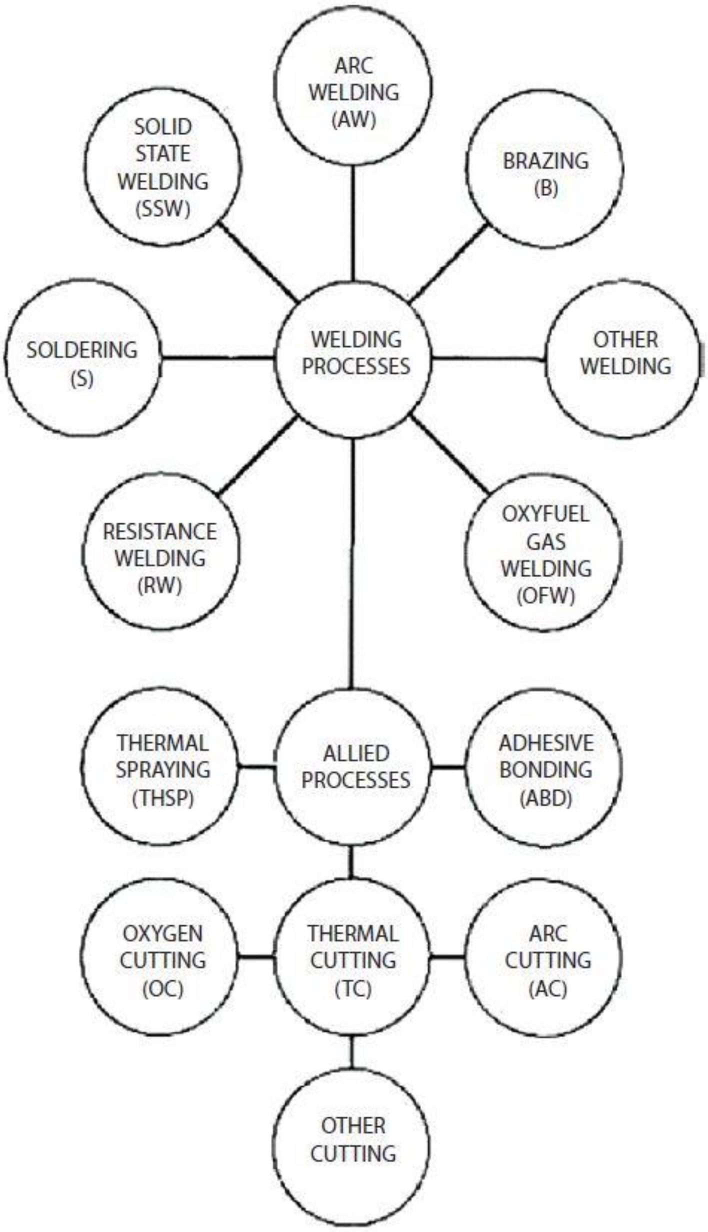

Figure 2.15. General layout welding and joining processes (Singh, 2021)

2.3. Efficiency of Energy Use

An electric arc is produced by an electrode and the base material using a welding power source, melting the metals at the welding site. This process is known as arc welding. To thoroughly melt the metals for welding, however, not all of the arc energy is used. The product current and voltage that flow through the arc are what give welding its strength. The process results in a large energy loss. Heat is produced when power is transferred to it, however there are heat losses due to convection, conduction, radiation, and splatter. Based on a variety of variables, the process efficiency of different arc welding processes varies greatly. These considerations include the type of gas to utilize (if any) and the material to be welded. These variables' effects depend on a single factor or a mix of factors. How a process uses the energy it produces has a significant impact on how muchelectrical current should be required to provide the necessary heating for weld applications. The efficiency of a procedure for joining various materials depends on the heat generated.

2.4. Preheating Process

Preheating process is to raise locally parent material's temperature on both sides of welding joint which is welded over ambient temperature prior to welding. Preheating is required for the four reason below.

1. "To lower the metal's cooling rate in the HAZ below 805 ºC in the HAZ, to decrease hardness value of the welded part."

Low alloy steels and high carbon steels are capable of being hardened by quenching from high temperatures (above 850 ºC) The fusion face with the parent material is where the same process can take place in a welded junction. By increasing the base metal's temperature, the hardening process may be slowed down when the weld cools and the temperature difference between the base material and the weld pool is minimized. The likelihood that the metal to be welded may crack is decreased by reducing hardness.

2. "To regulate the rate of hydrogen diffision in a welded joint."

Moisture exists in the metals, and it contains both hydrogen and oxygen. Moisture is broken down into its constituent parts, hydrogen and oxygen, by the welding arc. At high temperatures, both of these fundamental substances may be readily absorbed into the metal of the weld and may even be stuck during the cooling process. Hydrogen, also known as cold cracking or hydrogen cracking, plays a significant role in weld and heat affected zone cracking at lower temperatures. The preheating method aids in the steel's hydrogen dissolution. By making sure that the weld region is dry and stays dry during the welding process, the preheating procedure delivers. Additionally, materials used in welding consumables like fluxes and electrodes contain moisture.

3. “To reduce thermal stresses.”

As the molten weld pool cools, thermal stresses are created. Because the parent metal resists or restrains the weld metal's contraction and the joint's cross sectional area is insufficient to handle the resulting tensile stress, partially formed welds are susceptible to cracking. Prehat may reduce temperature differences and slow cooling rates to control the amount of strain.

4. “Compensation for heat losses.”

Preheating during welding may be necessary for thicker section steels with high thermal conductivity to achieve fusion.

Figure 2.16, 2.17, 2.18 show some preheating application. In Figure 2.16 and 2.18 preheating were performed with electrical resistance heater and In Figure 2.17 preheating was performed with gas fired system.

Figure 2.16. Welding with Preheat (Ueda and et al., 2012)

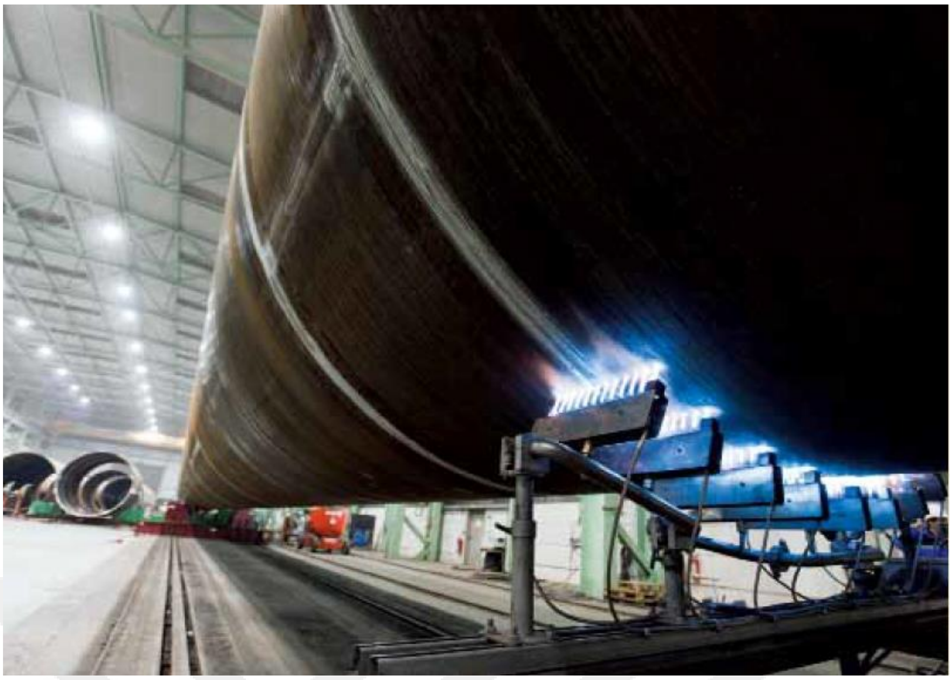

Figure 2.17. Preheating of special pipes prior to SAW Welding (Ueda and et al., 2012)

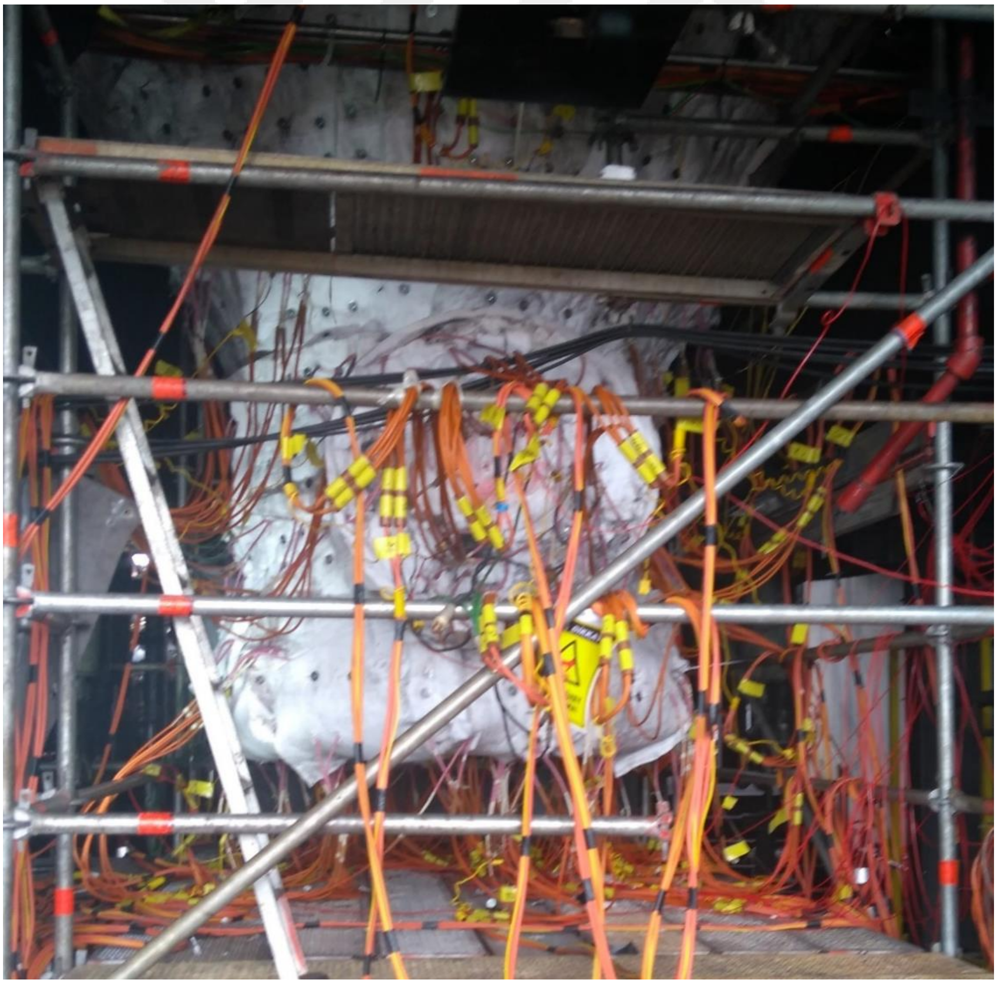

Figure 2.18. A local heat treatment application view 3

Figure 2.19 shows application temperatures for preheating process in Code BS 2663: 1987. Figure 2.20 shows application temperatures for preheating process in Code ASME 31.3-2016). Preheating temperatures may vary according to relevant code for the same type of material.

Table 5. Pre-heating for welding (see also 18.3)

Type of steel	Minimum pre-heating temperature for TIG welding of root runs			Hydrogen controlled weld metal (note 1)		Non-hydrogen controlled weld metal	
	Carbon steel root run		Matching root run, all diameters and thicknesses	Material thickness	Minimum pre-heating temperature	Material thickness	Minimum pre-heating temperature
	≤ 127 mm dia. and ≤ 12.5 mm thick	> 127 mm dia. or > 12.5 mm thick					
	°C	°C	°C	mm	°C	mm	°C
C and C-Mn, (≤ 0.25 C)	5	≤ 30 mm*: 5 > 30 mm*: 100	≤ 30 mm*: 5 > 30 mm*: 100	≤ 30 > 30	5 100	≤ 20 > 20	5 100
C and C-Mn, (> 0.25 C ≤ 0.4 C)	50	100	100	All	150	All	200
C-Mo	5	100	≤12.5mm*: 20 >12.5mm*: 100	≤ 12.5 > 12.5	20 100	≤ 38 (note 5)	150
1 Cr ½ Mo 1¼ Cr ½ Mo	5	100	100	≤ 12.5 > 12.5	100 150 } (note 3)	≤ 12.5 > 12.5 ≤ 20 (note 5)	150 200
1.25 Ni Cu Mo Nb	50 (note 7)	100 (note 7)	100	≤ 12.5 >12.5	100 150	Note 6	Note 6
½ Cr ½ Mo ¼ V	50	100	100	≤ 12.5 > 12.5	150 200 } (note 3)	Note 6	Note 6
2¼ Cr 1 Mo	50	100	100	≤ 12.5 > 12.5	150 200 } (note 3)	≤ 12.5 (note 5)	200
5 Cr ½ Mo 7 Cr ½ Mo 9 Cr 1 Mo	Note 2	Note 2	150	All	200 (note 3)	Note 6	Note 6
9 Cr 1 Mo V Nb N	Note 2	Note 2	100 (note 3)	All	200 (note 3)	Note 6	Note 6
12 Cr Mo V (W)	Note 2	Note 2	150	All	150 (note 4)	Note 6	Note 6
3½ Ni 9 Ni	Note 2	Note 2	100	All	150	Note 6	Note 6

NOTE 1. Hydrogen controlled weld metal as defined in BS EN 499 contains no more than 5, 10, or 15 mL of diffusible weld metal for type H5, H10 and H15 respectively.

NOTE 2. A carbon steel root run is not to be used.

NOTE 3. When TIG welding is used a lower pre-heating temperature may be applied provided it is proved to be satisfactory by procedure tests.

NOTE 4. A welding process with extra low hydrogen potential (less than 5 mL per 100 g of deposited weld metal) should be employed. If a high pre-heating temperature is used, e.g. 300 °C, then the joint should be cooled to between 100 °C and 150 °C to ensure full transformation before post-weld heat treatment is applied. Welding at a pre-heating temperature in the region of 150 °C to 200 °C will ensure that a high degree of transformation and some tempering will occur during welding and will assist in the removal of hydrogen from the joint.

NOTE 5. Above the maximum thickness stated hydrogen controlled weld metal only to be used.

NOTE 6. Hydrogen controlled weld metal only to be used.

NOTE 7. A C-Mo root run is to be treated as a carbon steel root run.

NOTE 8. Both 9 Cr 1 Mo and 9 Cr 1 Mo V Nb N are considered to be matching root run compositions.

*Thickness.

Figure 2.19. Guidance on preheating process in national codes (BS2633: 1987)

Table 330.1.1 Preheat Temperatures

Base Metal P-No. [Note (1)]	Base Metal Group	Greater Material Thickness		Additional Limits [Note (2)]	Required Minimum Temperature	
		mm	in.		°C	°F
1	Carbon steel	≤25	≤1	None	10	50
		>25	>1	%C ≤ 0.30 [Note (3)]	10	50
		>25	>1	%C > 0.30 [Note (3)]	95	200
3	Alloy steel, Cr ≤ ½%	≤13	≤½	SMTS ≤ 450 MPa (65 ksi)	10	50
		>13	>½	SMTS ≤ 450 MPa (65 ksi)	95	200
		All	All	SMTS > 450 MPa (65 ksi)	95	200
4	Alloy steel, ½% < Cr ≤ 2%	All	All	None	120	250
5A	Alloy steel	All	All	SMTS ≤ 414 MPa (60 ksi)	150	300
		All	All	SMTS > 414 MPa (60 ksi)	200	400
5B	Alloy steel	All	All	SMTS ≤ 414 MPa (60 ksi)	150	300
		All	All	SMTS > 414 MPa (60 ksi)	200	400
		≤13	≤½	%Cr > 6.0 [Note (3)]	200	400
6	Martensitic stainless steel	All	All	None	200 [Note (4)]	400 [Note (4)]
9A	Nickel alloy steel	All	All	None	120	250
9B	Nickel alloy steel	All	All	None	150	300
10I	27Cr steel	All	All	None	150 [Note (5)]	300 [Note (5)]
15E	9Cr–1Mo–V CSEF steel	All	All	None	200	400
. . .	All other materials	. . .	. . .	None	10	50

NOTES:
(1) P-Nos. and Group Nos. from BPV Code, Section IX, QW/QB-422.
(2) SMTS = Specified Minimum Tensile Strength.
(3) Composition may be based on ladle or product analysis or in accordance with specification limits.
(4) Maximum interpass temperature 315°C (600°F).
(5) Maintain interpass temperature between 150°C and 230°C (300°F and 450°F).

Figure 2.20. Guidance on preheating process in national codes (ASME 31.3-2016)

As the alloying content of a ferritic steel increaes, prehating has more important role. Due to the hardenability's relationship to an elevated danger of cracking during the cooling process.

The relevant guideline document for organizing welding technique trials for general welding carbon-manganese steels is BS5135 (pr EN1011). This considers the steel's chemical composition as represented by the carbon equivalent, or C_{eq}, written as follows:

$$C_{eq} = C + \frac{\text{Mn}}{6} + \frac{\text{Cr+Mo+V}}{5} + \frac{Cu+Ni}{15} \tag{2.4}$$

The joint's total thickness (heat sink effect), the welding process's energy input (kJ/mm = [arc voltages x amps] /travel speed), and the electrode coatings' hydrogen potential (scale A> 15 ml/100 g to scale D 5 ml/100 g). Figure 2.21 is an example of a chart that would be used to calculate the values of the prehating process based on the interaction of various factors.

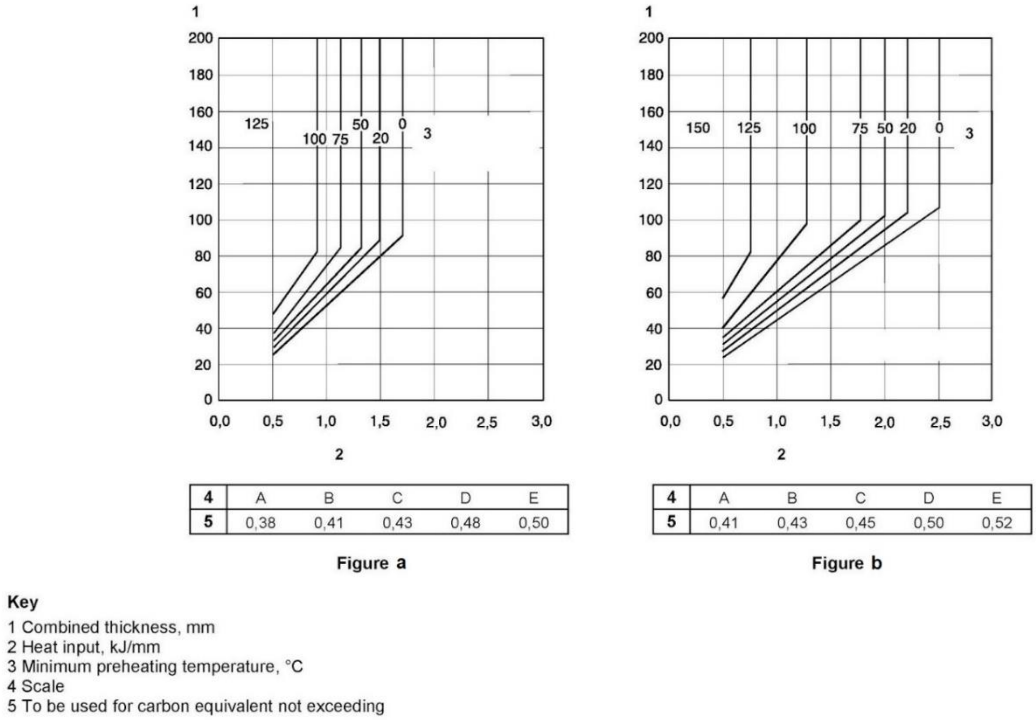

Figure 2.21. Conditions for welding steels with defined carbon equivalents (URL-1)

The preheating temperature is kept to a minimum during the welding operation. Heat input has the potential to raise the temperature to a dangerously high point, impairing the welded structure's mechanical qualities or changing the welding process's parameters enough to create flaws. Additionally, it is possible to alter the maximum interpass temperature, frequently by 100–150 ºC (Croft D.N. 1996).

2.5. Measuring and Determent of Residual Stresses in Weldments

Metal residual stresses may be measured using a variety of techniques. These techniques, which may be categorized into three categories, are also typically used in weldments;

1. “Stress-relaxation”,
2. X-ray diffraction methods” (and, more recently, neutron)
3. “Cracking of metal” methods.

These methods are not perfect, all of them has its merits, advocates, and appropriateness.

By cutting a sample holding the residual stresses and measuring the amount, sign, and direction of the strain that is released using an electrical or mechanical gauge, stress-relaxation techniques can determine the residual stresses. These techniques deliver quantitative data that is essentially correct and trustworthy. The sample geometry, notably the 3-D intricacy, has a constraint. There are specific methods for handling samples of various shapes and sizes, particularly thin 2D sheets or plates and thick 3D solids. These methods involve a variety of cutting techniques (such as drilling, boring, sectioning, and machine milling) as well as a variety of methods for observing the release of strain, such as the physical distortion of overlaying grids, mechanical measurement devices or gauges, and electrical resistance.

By assessing the impact of residual stresses on the metal's lattice parameter, X-ray diffraction techniques may identify these stresses. The lattice expands as a result of tensile residual stresses, increasing the typical lattice parameter. However, compressive residual stresses result in a contraction of the lattice and a reduction in the normal lattice parameter, both of which are proportional to the intensity of the stresses. These procedures typically have long processing times, a need for specialized tools and knowledgeable operators, and poor accuracy.

There are just a few techniques. These methods can track the impact of residual stresses on stress corrosion or hydrogen-induced cracking (embrittlement) (Çelik, 2009).

3. PREVIOUS STUDIES

In the late 1930s, Rosenthal and Rykalin used Fourier to create the fundamental theory of heat flow, which they then extended to moving heat sources. The most common analytical technique for determining the thermal history of welds is still this idea. Rosenthal's point or line heat source models have a considerable error for temperatures in or near the fusion zone (FZ) and heat impacted zone (HAZ). The heat source's temperature is considered to be unlimited in this scenario. As the heat source is closer, the inaccuracy increases due to this temperature and the material's temperature sensitivity. The finite element technique (FEM) has been utilized by numerous authors (Goldak, Andersson, Krutz, Taylor, Segerlind, and Friedman) to examine heat flow in welds in order to overcome the majority of these restrictions. (Çelik, 2009).

Goldak et al. (1986) created an analytical model to obtain heat source for welding. The Gaussian power density distribution served as the model's foundation. In order to represent the form and magnitude of the heat source of shallow and deeper penetrations, they developed a double ellipsoidal distribution.

Biswas and Mandal (2009), created a numerical model based on the finite element package ANSYS. For single-pass and single-sided submerged arc welding of square butt joints, they created this model. In order to take top and bottom reinforcements, a time step, and a meshing method into consideration, they attempted to model the scenario of a moving dispersed heat source. They created the required macros. In this model, the effect of bead geometry was considered. To take into consideration the effect of filler metal deposition, they employed the element birth and death theory. They discovered that employing reusable backing strip which is flux-filled and the appropriate parameters for welding process, through-thickness fusion, proper top and bottom reinforcements, and square butt edge preparation could be performed in a single run of submerged arc welding. There is an overall decrease in angular distortion. The element death and birth approach is used to successfully include the influence of top and bottom reinforcements into the theoretical model. Theoretical findings indicated less angular deformations. This is because the calculations took into account the restraint impact of the reinforcements. Theoretical findings closely matched those obtained through experimental measurement.

Only 4 to 10% of the anticipated distortions and the experimentally measured distortions differ from one another.

A brand-new Goldak heat source distribution model for SAW was created by Nezamdost et al. (2016). It is being attempted to construct both 2D and 3D finite element models utilizing the solution of heat transfer equations in ABAQUS Standard implicit. Their findings demonstrated the effectiveness of using the 2D axi-symmetric model to predict the heat cycles and welding residual stresses for the test steel. Both 3D and 2D analyses were compared. When compared to 3D analysis, they found that the 2D model greatly reduced the FE computation's time and cost. The bead-on-plate welds' experimentally observed values and the projected fusion zone geometry's numerical accuracy are compared. The current model's predictions and experimental observations were found to accord rather well.

To investigate the impact of welding in passes on residual stress and ultimate angular deformation of fillet welded mild steel joints, Mondal and et al. (2017) constructed a 3-D FEM. An elasto-plastic thermomechanical model is developed to predict residual stresses occuered during SAW process. The simulation results show that the single sided fillet weld has more residual stress than the double sided fillet weld and that this residual stress is not balanced on both sides of welded part. The predicted results was confirmed by experimental results and published literature.

Ghosh and et al (2013), tried to present a mathematical model for temperature distribution in the case of submerged arc welding to join two steel. The thermal behavior of the submerged arc welding process was demonstrated using the conservation of energy equation. They are thinking of using a volumetric heat source with a double-paraboloid form in three dimensions and a Gaussian distribution for welding. The weld pool's cross section might have a parabolic form. To determine the geometric parameters, they performed a series of tests. They contrasted the predictions' outcomes with temperatures anticipated empirically. They observed the outcomes and discovered good agreement.

Sirivella (2014) concentrated on investigating how temperatures vary during SAW welding. In this study with 2D heat flow mesh model was used. According to the analysis, the heat source operates for 0.001 to 1.000 seconds before ceasing, and by that point, the shape of the weld has not been produced. Additionally, it makes note of the fact that the node at the upper surface of the plate located near to the weld's border achieves its maximum temperature value after 10 seconds. The comparable node on the plate's bottom reaches its maximum temperature at 15 and may detect incremental temperature equalization.

Taskaya and et al (2019), welded Ramor 500 steel with 65×55 mm and with 3 mm thick. Ramor Steel is a special steel developed for army industry. It is used as the main combat vehicle. They are using submerged arc welding (SAW) method to weld Ramor Steel. They carried out some experiment at different conditions. The ANSYS package software was used to evaluate the thermomechanical analyses. They discovered that all welded connections had full penetration, hence there were no macro or microcracks visible after the radiography diagnostic test. A grain structure is seen in the microstructure analysis. in the shape of a uniform distribution starting at the weld stitch and moving down to the base material. The results of SEM-EDS investigation demonstrate the homogenous distribution of elemental phase structures. Welding width rose as welding speed increased, and welding width decreased as welding speed increased as a result of the impact of welding stitch shapes on the current strength and velocity. The thermomechanical research performed using ANSYS software revealed that welding stresses increased as heat was added, and that mechanical and elastic stresses peaked quite high before being replaced by permanent stresses as a result of deformation.

Suman and Biswas (2020) used a Creep Strength Enhanced Ferritic (CSEF) steel plate that was 10 mm thick to evaluate residual stresses and deformations with and without the preheating effect. For greater accuracy, the bead geometry in FE models was compared to that of a weld junction. Modeling also took into account the solid-state phase change or austenitic-martensitic transformation typical of CSEF steel. For as welded and preheated weld models, thermal history, distortion, and residual stresses were predicted; these predictions were then confirmed by empirically observed data. For measuring residual stress, deep hole drilling methods were used. A coordinate measuring machine was used to measure the residual deformation. The edge deflection and angular deformation values were found to be successfully decreased by preheating by 41.7% and 54.1%, respectively. By lowering the results by a maximum difference of 90%, preheating had a favorable influence on longitudinal residual stress distribution. They discovered that the residual stresses and deformation findings were accurately predicted by FE modeling with solid state phase transition effect, with errors of up to 16.67% and 26.57% (highest) and down to 3.15% and 4.35% (lowest), respectively.

Suman and Biswas (2022) are employing submerged arc welding to join single- and double-side single-pass square butts to 9Cr-1Mo-V steel plates using the same welding materials. To estimate welding-induced residual stresses, they use deep hole drilling and contour measuring. Investigations are also conducted on the following changes in microstructure and mechanical characteristics. The birth and death of elements, the double ellipsoidal Gaussian distributed heat source model, temperature-dependent material characteristics, phase transformation, etc. are all taken into account while simulating and analyzing these weld joints. In comparison to double-side single-pass welding, it has been found that single-side single-pass welding creates stronger transverse characteristics. In the fusion zone, the single-pass weld showed a compressive longitudinal residual stress throughout its thickness. The top and bottom areas of the double-sided weld's fusion zone, on the other hand, have compressive residual stress, whereas the mid-thickness region of the FZ shows tensile residual stress.

Biswas and Mandal (2009) welded by using shielded metal arc welding (SMAW) some metals. Three different finite element (FE) based models were used for distortion prediction of orthogonally stiffened plate panels. The three different approaches of FE analysis were developed as elastoplastic transient thermomechanical analysis, transient cooling phase analysis, Inherent strain method. Of these three methods, the inherent strain method was found to be highly computationally efficient leading to almost 70 times less CPU time compared with that of transient elastoplastic analysis. At the same time, the deviation in the magnitude of distortion was found to vary within 7 to 10% only. Hence the inherent strain method enables us to predict weld-induced distortions of full-size complex structures as used in ship construction. It is observed that inherent strain method in general overestimates the extent of distortion, thereby making it a conservative analysis. In a real life case the implication is the actual distortion will be less than what is predicted.

Suman and Ant et al. (2019) used single pass double sided submerged arc to weld P91 steel with a square butt weld joint in order to calculate welding-induced residual stress. A component's distribution can be tracked via the strain connected to trapped stresses. For the welded plate, the relevant deformation was identified. Using a wire EDM (Electrical Discharge Machine), the weld sample was divided into two equal halves throughout the weld length. The coordinate measuring machine (CMM) was used to record the surface deformations. Data conditioning was done since there may be factors affecting the deformation data, such as how the sample is positioned on the CMM bed or the cutting process' lack of homogeneity. The residual stress distribution in longitudinal direction, or to put it another way, perpendicular to the targeted surface, is produced by the structural findings of the FE study. In contrast to how other steels weld, they notice a compressive residual stress distribution in the weld zone.

A machine learning approach is suggested by Sarkar and colleagues (2020) to forecast and assess temperature in the SAW process. By placing an infrared camera on the workpiece's bottom surface, they are able to capture thermal video. The temperature history is extracted using MATLAB programs, and transient isotherms are produced using image processing methods. A quantitative analysis is done of the transient isotherm's evolution during the heating and cooling cycle. For application in machine learning, the experimental datasets are adequately prepared. The suggested machine learning algorithm predicts the local temperature, temperature-time curve, and temperature field map. The temperature field map's other features are examined and forecasted. They use experiments to support the suggested methodology. The results match the experimental data quite well.

Residual stress was analyzed experimentally and numerically by Uzun (2014). The numerical analysis uses the finite element method. ANSYS finite element software simulates submerged arc welding of carbon steels. The movement of the heat source during submerged arc welding is precisely modeled in APDL code. Experimental residual stress measurements utilizing a nondestructive ultrasonic method are used to validate the finite element model. His study included a number of experimental phases, including metallography, ultrasonic examination, and finite element modeling. He came to the conclusion that carbon concentration affects the production of thermal stress and residual stress in steel materials. While it varies in different areas of the weld beam, this effect demonstrates a tendency for the acoustoelastic constant related to thermal stress. He noted that the use of ultrasonic technology is appropriate in this situation. It offers adequate information for examining residual tension in base metal plates.

By employing a butt joint for St37 steel, Yıldız (2011) compares the results from an experimental research with an analysis using the finite element approach and MAG welding. By adjusting the settings for the distance between the pieces, gas flow, and current input, the distribution of temperature and displacement may be shown. Tensile tests, hardness measurements, studies of the microstructure, and welding penetration have all been carried out to determine the mechanical and microstructural features of welded samples. Due to the physical laws, modeling using the finite element method is a crucial tool for simulating welding operations. HyperMesh 10.0 is carried out to performe the finite element technique analysis. The comparison of simulation and experimental research reveals that the distribution of temperature and displacement data are consistent with one another.

4. MATERIAL AND METHODS

Figure 4.1. below shows project flow chart performed during this study.

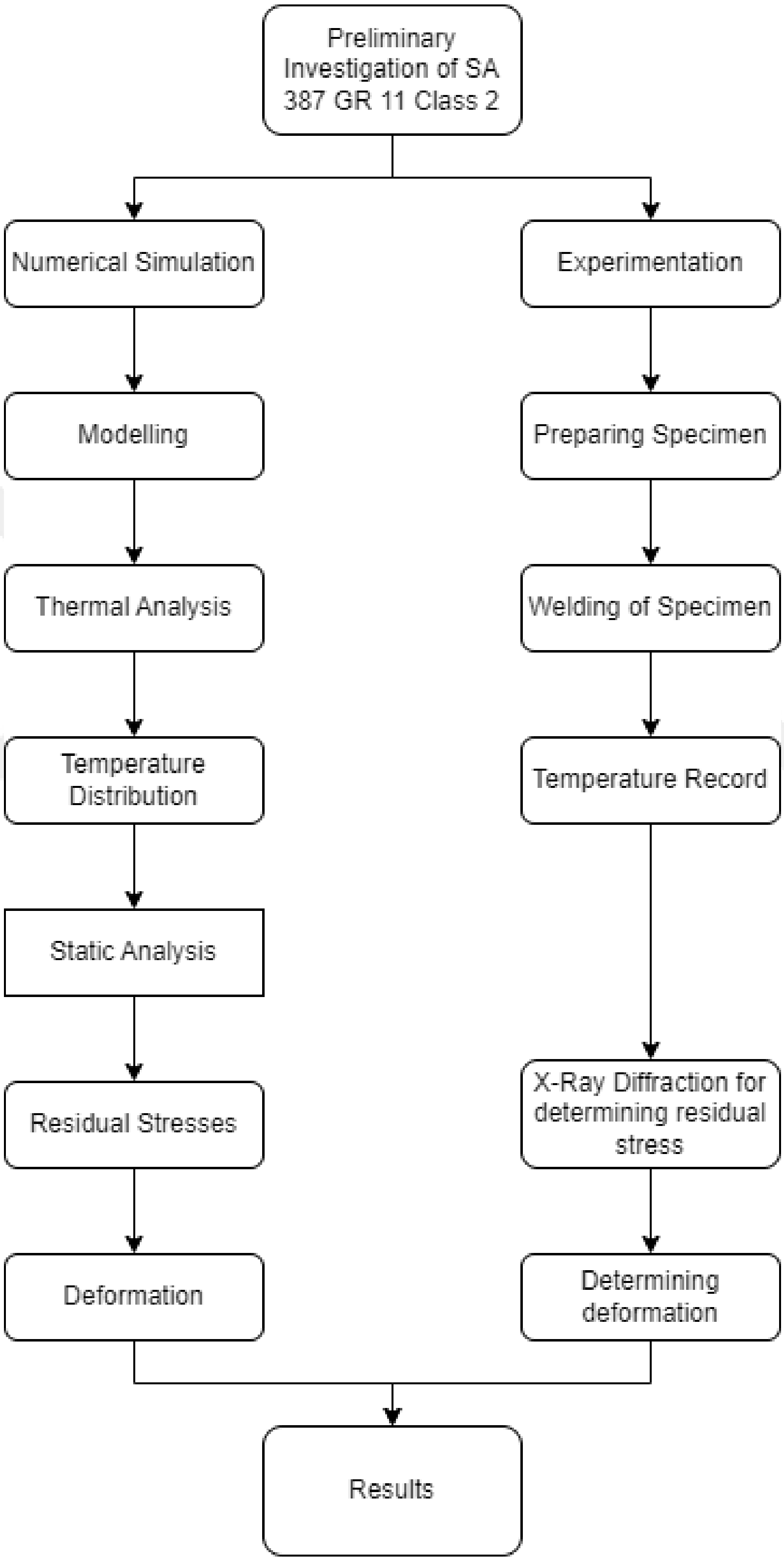

Figure 4.1. Project Flow Chart

4.1. Material SA 387 GR 11

The material used for specimen is SA 387 Gr 11 C2 which is 8 mm thick and 100 mm x 100 mm x long. Since gases and liquids are routinely stored at higher temperatures in the oil, gas, and petrochemical industries, it is very helpful in these fields. Pressure vessel grade steel SA 387 Grade 11 Class 2 is used for activities at high temperatures. Higher chromium concentrations also offer superior oxidation and corrosion resistance. This properties are essential in applications using sour gas (URL-3). Because of its better capacity to withstand the high temperature, SA 387 Gade 11 Class 2 plate is employed in elevated and high temperature service in various industries. This plate's high chromium content provides oxidation and corrosion resistance, which is crucial for applications with sour gas. Because of their exceptional qualities and the manner they are produced in the manufacturing sector, these plates are used in a variety of applications around the globe. High tensile strength, durability, outstanding dimensional precision, great surface finishes, weldability, longevity, flexibility, and the ability to support huge loads are some of these characteristics. Additionally, it can totally resist pitting, crevice corrosion, and stress corrosion cracking. Table 4.1, Table 4.2, Table 4.3 show equivalent grades, chemical composition mechanical properties of SA 387 Gr 11 Cl2 respectively (URL-2).

Table 4.1. SA 387 GR 11 Equivalent grades (URL-2)

BS	ASTM/ASME	UNS	EN
621 B	A387 / SA 387	K11789	-

Table 4.2. Chemical Composition of SA387 GR.11 CL.2 Plate (URL-2)

C	MN	P	S	Si	CR	Mo
0,05 – 0,17	0,40-0,65	0,025	0,025	0,50 – 0,80	1,00 – 1,50	0,45 – 0,65

Table 4.3. Mechanical Properties of SA 387 GR.11 CL.2 Plate (URL-2)

Tensile Strength	Yield Strength	Elongation in 200 mm (%)	Elongation in 50 mm (%)
70-90 ksi, 485-620 MPa	45 ksi, 310 MPa	18	22

4.2. Welding Method

4.2.1. Submerged Welding (SAW)

Submerged arc welding process is commonly used for heavy welding. With SAW, the thick section materials can be weld with faster production rate. By heating the metal with an arc or several arcs between the bare metal electrode or electrodes and the work, this arc welding procedure causes coalescence of the metal. Submerged arc welding with high amperage (over 1,000 amps) may weld carbon steel plates with strong penetration and high deposition rates. A thick layer of granular, fusible flux, which melts and shields the weld pool from ambient gases, completely covers the arc and the weld zone. These fluxes can be used to add alloying components to welds that are created using electrode- and filler-wire combinations. One of the most popular welding techniques is submerged arc welding in the heavy manufacturing sector. There are various restrictions associated with its unpotable status. The work piece should be easier to reach from where the machine is set up. The process's constrained mobility is a natural byproduct of its design, which comprises the following.

1. It is necessary to move nozzle, head gun of welding system etc. Along the weld line, which might be either longitudinal or radial. Nevertheless, lie horizontally or flat.
2. Flux should be used and deliverid from a fixed location.

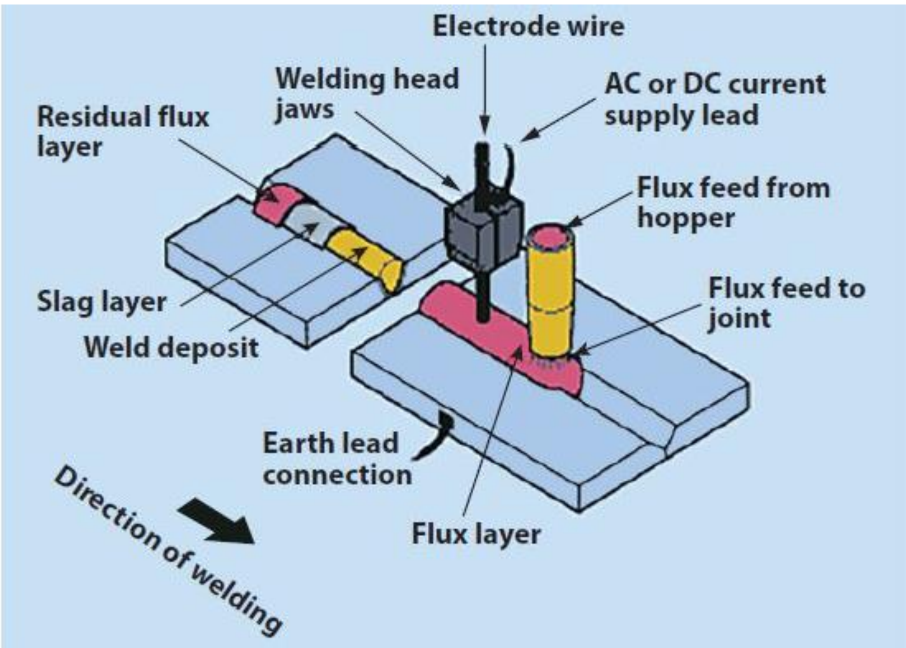

Figure 4.2. SAW process's schematic display (Singh, 2021)

The residual flux, which is used just to provide blanket coverage to the weld underneath but is not consumed during the welding process, is at the top of the weld. The fused layer of the flux, in the form of hardened slag, is located underneath that blanket. The actual weld is located underneath the slag. Flux is provided through the hopper, while the power source, electrode wire, and wire feed through the welding head.

The SAW welding technique includes creating an arc between the workpiece and a constantly supplied bare wire electrode through nozzle, much like the GMAW welding process. This blanket technique, which uses the flux running through the hopper and the force of gravity to completely cover the weld region, is a flexible way to create welds with little contamination.

The adaptability of submerged arc welding is, however, constrained by this benefit of safeguarding weld pool which is molten metal. Except in extremely rare circumstances, the flux is delivered vertically down over the weld region. These extremely rare circumstances include vertical and horizontal welds made with specially made tools, including belts or shoes that would keep the flux in place. The SAW method does not require a shielding gas to protect the weld pool and surrounding region from air contaminations, similar to GMAW-S but different from GMAW-G. The flux itself acts as a shield in the SAW process. Before welding, a small layer of flux powder is applied to the workpiece's surface; as previously mentioned, this activity serves numerous crucial purposes.

1. The molten flux flows continually down and melts around the arc, ensuring appropriate flux flow to the weld.
2. It creates a tiny flux dust trail that aids in arc initiation in the shielding environment.,
3. It begins the flux's two primary tasks of (i) shielding the weld pool from air contamination and (ii) adding alloying components to the weld.

Along the joint line, excess flux is dumped onto the arc through a hopper. As the weld is being completed, the flux that is closest to the arc heat and the weld pool gets consumed and turns into a dense layer of slag. As seen in the aforementioned pictures, the residual flux is collected; pay attention to the suction head that follows the weld. Some of the leftover flux is occasionally recycled for new welds, although not all fluxes can be recycled. Any leftover layers of fused slag after welding are easily removed. Heat loss is incredibly minimal since the flux layer fully encloses the arc. Compare the thermal efficiency of this process, which may reach 60%, to the 25% heat efficiency of the SMAW method. Figure 4.3 above illustrates the findings of one such research concerning the deposition rate increasing when the diameter of the wire is increased and the associated current is raised, demonstrating how high the deposition rate of the SAW process is in comparison to other arc welding techniques. Another benefit of using SAW is that there is no visible arc light, there is no welding spatter, and no requirement for fume extraction. (Singh 2021).

Figure 4.3. Flat plate welded with SAW (Singh, 2021)

Figure 4.4. A pipe welded with SAW (Singh, 2021)

Figure 4.5. Pipe welded with SAW completely (Singh, 2021)

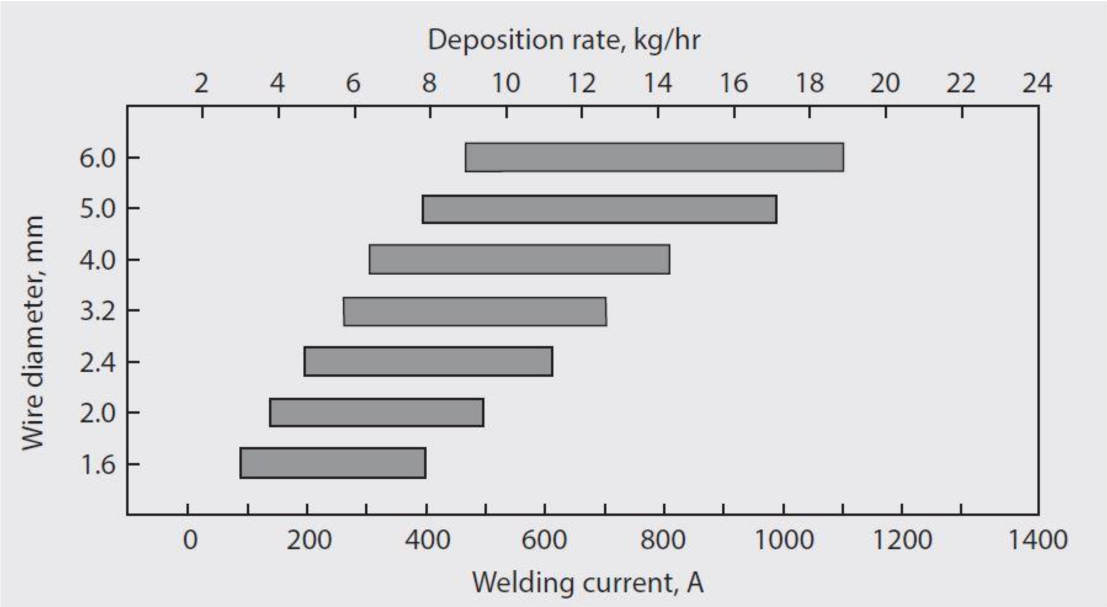

Figure 4.6. Deposition rate of SAW (Singh, 2021)

Limitations and Advantages of Submerged Arc Welding can be explained like below. A prominent welding technique in the structural and vessel manufacturing sectors is submerged arc welding (SAW). The method is often used to make pressure tanks, bridge constructions, columns, beams, booms, tractor,girders members, and sub-assemblies in shipyards, offshore.

The method is known as "Sub Arc" or "SAW" locally.

The benefits of this flux blanket are as follows:

1. Protects against pollution from atmosphere.
2. Keeps the arc stable during welding
3. Prevents the spread of sparks and splatter.
4. Has a better rate and efficiency of deposition,
5. Reduces the fumes and radiation according to the other arc welding process, such as GMAW and SMAW are known for.

The method included a number of crucial benefits that were beneficial for large manufacturing operations. The following are some benefits of submerged arc welding:

1. It is simple to create strong and reliable welds.
2. Very little welding fume is released.
3. Very little arc light is produced.
4. It may be used for both indoor and outdoor projects.
5. It reduces distortion rate.
6. It creates deeper weld penetration.
7. Mininmal edge preparation.
8. It has high rates of deposition.
9. Thick materials may be welded, low alloy steels, carbon-manganese steels, and stainless steels are the most common materials to be welded.
10. Half or more of the flux can be recovered at least.

Submerged arc welding has several restrictions.

1. “Welding position.” Welding is often only possible in a flat posture.

2. “The requirement of using a granular flux and the fluidity of the molten weld pool.” These issues are limiting to 1G, 1F, and 2F positions.

3. “Welding is often only used for rotating containers or pipelines or long, straight seams.” Flux handling systems may be fairly complex, and they need to be regularly inspected.

4. " Without some sort of support material to place the root weld, it cannot be utilised to deposit the root pass," is still another restriction.” (Singh 2021).

4.3. Finite Element Analysis

A numerical approach for the analysis of engineering components is the finite element method. With this approach, the operational domain is split up into a number of pieces. The elements are connected to each other by the corner points which are called nodes. The field variable is assigned to the nodes and within each element, the field variable is assumed to vary as per linear or quadratic relationship while maintaining continuity at the nodes. Thus, it is argued that the field variable is piecewise continuous and that it may be defined in terms of the shape function or interpolation function for the elements as well as the nodal values of the field variable.

Numerical analysis and modelling of the welding process are challenging due to its complexity. A few of the factors contributing to complexity are temperature-dependent material characteristics, non-linear boundary conditions, moving heat sources, phase shifts and transformations, complicated residual stress states, and the challenges associated with doing experimental measurements at high temperatures. Due to these complications, finite element modelling of the welding process must take into account intricate thermo-mechanical interactions, the deposition of filler material, and moving heat sources.

Using a minimization process for the functional formulation of the governing equation, the partial differential equation which represents the three-dimensional transient heat flow is converted into a set of linear equations which are best represented in matrix form. A global matrix is created by combining all of these elemental matrices once the equation has been evaluated for each element. The matrix equation is then solved to yield the nodal field variable once the specific circumstances, known as boundary conditions, are applied.

In a transient analysis, the procedure is repeated for a series of time steps in order to get the nodal values of field variable for various time intervals.

4.3.1. Shape Function

Thermal analysis uses temperature as the field variable, and every point's temperature is described in terms of shape functions and nodal temperatures.

$$T = [N].\{T\} \tag{4.1}$$

The evaluation of shape function begins with the assumption of a polynomial relationship for representing the temperature as a function of spatial coordinates. The evaluation of shape functions in the case of a simple one-dimensional analysis and a two-dimensional analysis using a quadrilateral element are presented in the following sections.

4.3.1.1. Shape Function For A One-Dimensional Simplex Element

In the case of a one-dimensional analysis, the simplex element is a line element with two nodes at the two ends as shown in Figure 4.7. Let the x coordinate of the two nodes be x_1 and x_2. Let the temperature at the two nodes be T1 and T2. The following linear connection represents the temperature at any location within the element.

$$T = a0 + a1.x \tag{4.2}$$

Figure 4.7. One-dimensional simple element (Ravichandran, 2021)

The equation contains two unknown parameters a0 and a1 which may be evaluated using the defined values of temperatures at two nodes. Substituting x coordinate values and the nodal temperatures, we get

$$T = a0 + a1.x1$$

T2 = a0 + a1.x2

By solving for two unknown parameters from the equations, we get

A0 = T1 – (T2-T1) / (x2 – x1).x1

a1 = (T2-T1) / (x2 – x1)

Substituting the values of a0 and a1 in these equations, we get

T = T1 – (T2-T1) / (x2 – x1).x1 + (T2-T1) / (x2 – x1).x

Simplifying,

T = ((x2 – x) / (x2 – x1)).T1 + ((x – x1) / (x2 – x1)).T2 (4.3)

This may be descriebed as T = N1. T1 + N2. T2, where N1 and N2 are the shape functions for the line element.

N1 = (x2 – x) / (x2 – x1)

N2 = (x – x1) / (x2 – x1)

In matrix form, the eqution may be descriebed as

T = [N1 N2] {T1}

{T2} (4.4)

The shape function of a node represents the influence exerted by the node in determining the field variable within the element. The combined influence of the nodes in an element, which is the sum of all the shape functions, is always equal to unity at any point within the element. The shape function for a node decreases from a value of unity at the node location to a value of zero in the other node locations.

4.3.1.2. Shape Function For A Four Noded Quadrilateral Element

In the case of a four noded quadrilateral element with four nodes as shown in the figure, the field variable can be expressed as;

$$T = a0 + a1.x + 02.y + a3.x.y \quad (4.5)$$

The above polynomial function contains linear terms and one higher order term. The four unknown constants a0, a1, a2 and a3 in the equation can be determined from the four nodal temperatures and the nodal coordinates. In order to simplify the analysis, the origin of the coordinate system is assumed to be located at node 1. The element has a length equal to L and width equal to W. The coordinates of the four nodes are shown in Figure 4.16. Substituting the four values of x and y, we get four equations, and by solving the equations, the values a0, a1, a2 and a3 can be obtained.

$a0 = T1$

$a1 = (T2 – T1) / L$

$a2 = (T4 – T1) / W$

$a3 = (T1 – T2 + T3 – T4)/L.W$

So the interpolation function for temperature at any point x and y can be written as

$T = T1 + (T2 - T1) / (x/L) + (T4 - T1) / (y/W) + (T1 – T2 + T3 – T4).(x/L).(y/W)$

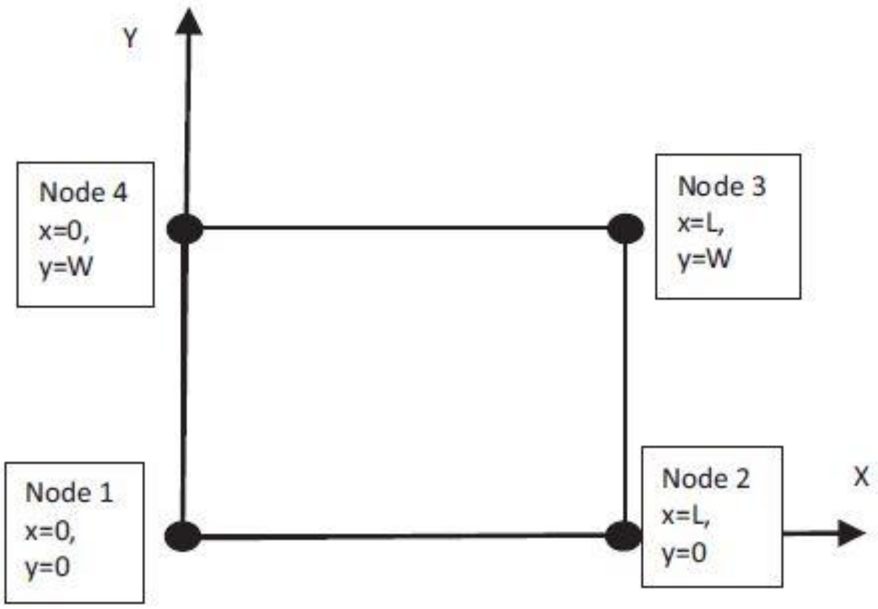

Figure 4.8. Four-noded quadrilateral element (Ravichandran, 2021)

Simplfying the equation, one can get

$$T = T1.(1 – x/L – y/W + x/L.y/W) + T2.(x/L – x/L.y/W) + T3.(x/L.y/W) + T4.(y/W – X/L.y/W) \quad (4.6)$$

The expressin can also be written as

$$T = N1.T1 + N2.T2 + N3.T3 + N4.T4 \quad (4.7)$$

$N1 = (1 – x/L –y/W + x/L.y/W) = (1 – x/L).(1 – y/W)$

$N2 = (x/L – x/L.y/W) = x/L.(1 – y/W)$

$N3 = ((x/L.y/W)$

$N4 = (y/W – x/L.y/W) = y/W.(1 – x/L)$

Alternately, if the coordinate system is selected as shown in Figure 4.17, the shape functions are more general in this case. The origin of the coordinate system is not at node 1 in this case. The coordinates at the four nodes are (0, W1), (L, W1), (L, W2) and (0, W2), respectively.

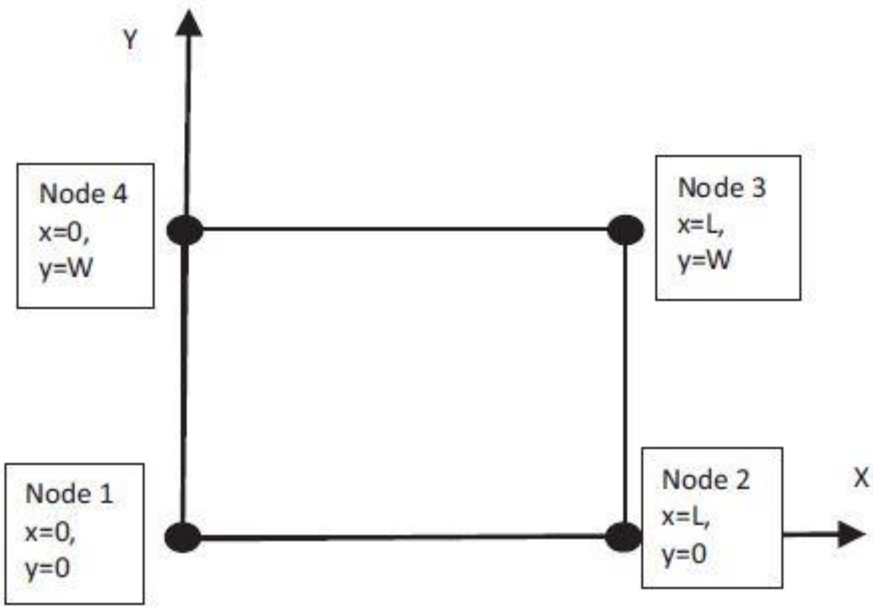

Figure 4.9. Two-dimensional rectengular element. The origin of the coordinate system does not coincide with any mode (Ravichandran, 2021)

In this case, the shape function is determined as

$N1 = (1 - x/L)(W2 - y)/(W2 - W1)$

$N2 = (x/L)(W2 - y)/(W2 - W1)$

$N3 = (x/L)(y - W1)/(W2 - W1)$

$N4 = (1 - x/L)(y - W1)/(W2 - W1)$

4.3.2. Formulation of Equation

The shape functions are a function of geometry, whereas the nodal temperatures are independent of geometry. Hence, the first derivative of the temperature with respect to x can be expressed as;

$dT/dx = [dN/dx].\{T\}$

Expressing the derivates with respect to x, y and z in matrix form.

$$\begin{Bmatrix} dT/dx \\ dT/dy \\ dT/dz \end{Bmatrix} = \begin{bmatrix} dN1/dx & dN2/dx & dN3/dx & \ldots \\ dN1/dy & dN2/dy & dN3/dy & \ldots \\ dN1/dz & dN2/dz & dN3/dz & \ldots \end{bmatrix} \times \begin{Bmatrix} T1 \\ T2 \\ T3 \\ .. \\ .. \end{Bmatrix} \quad (4.8)$$

The partial differential equations shown below serve as the governing equation for the transient thermal analysis.

$$\partial/\partial x\,(kx.\partial T/\partial x) + \partial/\partial y\,(ky.\partial T/\partial y) + \partial/\partial z\,(kz.\partial T/\partial z) = \rho c.\partial T/\partial t \quad (4.9)$$

ky, kz and kx represent the materials's thermal conductivity values in y, z and x directions, ρ is the density of the steel and c is the specific heat of the material. Within the operating domain, there are some nodes which receive the external heat flux q along a surface. Similarly, there are nodes lying at the free surface from which the heat is lost by convection. The convection heat loss is expressed as h. (T – T∞), where T∞ is the ambient temperature and h is the convection coefficient.

Incorporating the boundary conditions in the above equation, we get the equation as;

$$\partial / \partial x\,(kx.\partial T/ \partial x) + \partial / \partial y\,(ky.\partial T/ \partial y) + \partial / \partial z\,(kz.\partial T/ \partial z) + h.(T - T_{\infty}) + q = \rho c.\partial T/ \partial t \tag{4.10}$$

Using a minimization function for the functional formulation of the differential equation, the above partial differential equation is represented in matrix form as;

$$[\,c\,].\{dT/dt\} + [\,k\,]\{\,T\,\} = \{\,f\,\} \tag{4.11}$$

Where

[c] is the capacitance matrix written as $\int \rho c.\,[N]^T.[N].dV$,

[k] is the heat conductance matrix written as $\int[B]^T.[D].[B]\,dV + \int h.[N]^T.[N].dS$,

{f} is the force matrix written as $\int q.\,.[N]^T.dS + + \int h.[N]^T.T\infty.dS$, and

[B] is the matrix containing derivatives of shape functions and is written as folows.

[

[dN1/dx dN2/dx dN3/dx]

[B] = [dN1/dy dN2/dy dN3/dy]

[dN1/dz   dN2/dz   dN3/dz   ]

[D] is matrix containing thermal conductivities written as

$$[D] = \begin{bmatrix} k_x & 0 & 0 \\ 0 & k_y & 0 \\ 0 & 0 & k_z \end{bmatrix}$$

The elemental matrices [c] and [k] are assembled for all the elements and global [C] and [K] matrices are formed. The equation is then solved to get the nodal temperatures {T} for various time intervals. For solving the transient analysis, the term ∂T/∂t, T and F are written as

$\partial T/\partial t = (T2 – T1) / \Delta t$

T = (T2 + T1) / 2

F = (F2 + F1) / 2

F1 and F2 are the thermal loads corresponding to the previous time step and the current time step, respectively, and t is the time increment. T1 and T2 stand for the temperature of the previous step and the current time step, respectively. Thus the matrix form of the equation is written as,

[C]. (T2 – T1) / Δt + [K].

(T2 + T1) / 2 = (F2 + F1) / 2

Simplifying,

$$[[\,C\,]\,/\,\Delta t \;+\; [\,K\,]\,/\,2]].\{T2\} \\ = \{\,(F2 \;+\; F1)/2 \;+[[\,C\,]\,/\,\Delta t - [\,K\,]\,/2.\{T1\} \tag{4.12}$$

This simplified equation can be expressed as

[A] . {T2} = {B}

Thus, knowing the values of [C], [K], {F1}, {F2} and {T1} matrices, the unknown matrix {T2} can be evaluated. Repeating the procedure, the nodal temperature values can be determined for various time steps from the start to the end. This is known as time marching scheme. Due to the temperature dependence of material parameters like thermal conductivity and specific heat, transient thermal analysis is by its very nature non-linear. The equation then reads,

$$[\,C\,(T)\,]\,\{dT/dt\} \;+\; [\,K\,(T)\,]\,\{T\} \;=\; \{F\} \tag{4.13}$$

Where the matrices [C] and [K] are both temperature dependent. The equations cannot be solved in a single step, but an iterative technique is needed to get the temperature results. Newton Raphson's meth is usually adopted technique for such nonlinear problems. In this technique, the matrices are iteratively evaluated using the previous set of temperature results, and the error in accounting the force terms is determined. The procedure is repeated until the error due to unaccounted force is a small fraction of the initial force (Ravichandran, 2021).

4.4. Using ANSYS for Finite Element Analysis

The transient thermal analysis of welding issues may be effectively performed using ANSYS, a general-purpose finite element programme. The software consists of three modules such as preprocessor, solution, and post-processor. In the preprocessor module, the element type and the material properties are selected and the meshing of the domain of interest is carried out. In the solution module, the time interval for transient analysis, the convection heat loss and arc heat input are entered and the problem is solved for a given time step. If the analysis is of transient type, then the analysis is repeated for different time steps. In the post-processor module, the temperature results for various sets can be viewed. In addition, the animation feature enables one to visually picturize the flow of heat in the domain of interest.

The selection of element type is an important step, and the researcher has to decide whether the analysis is two-dimensional or three-dimensional in nature. ANSYS has a big library of elements, and either a lower order element or a higher order element can be selected. In some problems, multiple types of elements may be selected in the same problem. Thermal conductivity, specific heat, and density are the material characteristics that are important for the transient thermal analysis. You can enter these characteristics as a function of temperature.

Once an element type is selected and the material properties are entered, then the meshing of the domain of interest is performed. In ANSYS, the meshing of the region of interest can be done in two ways such as by direct generation of nodes and elements or by solid modelling with automatic mesh generation within the domain. The direct generation is a simpler method, and in this method, the nodes and their coordinates are defined first. Using the “ngen” command, multiple sets of nodes may be generated from a master set. The elements are defined subsequently from the nodes. Smaller element size is selected for regions close to the weld where steep temperature gradients are expected and larger element size is selected for far off points. Multiple elements may be generated from a master set using the “egen” command. This procedure is easy to apply, but the disadvantage of this procedure is that there will be elements with unfavourable shapes.

In the alternate method, which is called solid modelling, the meshing is performed by dividing the domain into various volumes or areas. The user has to generate the desired areas or volumes using keypoints and lines. Then the size of the desired mesh near each keypoint is entered using the “kesize” command. The software automatically generates the nodes and elements which satisfy the user’s requirement of mesh spacing near each keypoint. The disadvantage with this procedure is that the node numbers which are generated are not uniform. This becomes a problem when the in-plane analysis has to be performed using APDL.

The meshing of the domain is an important step, and the user may have to repeat it several times until satisfactory results are obtained. In the mesh generation through areas and volumes, the division of the domain into different areas and volumes must be attempted to get the required results.

There is no hard and fast rule in deciding whether a given mesh is satisfactory or not, but the following set of rules must be borne in mind.

The elements should not be distorted too much from the ideal shape. For example, if a triangle is selected as the element type, then an ideal shape of the triangle is an equilateral one with the corner angles of 60°. But getting such a mesh is not always possible, and it may be okay if any of the corner angle goes up to 90°. But if an element has a corner angle more than 90°, then the shape is not acceptable.

The mesh size should increase gradually along any line. If the increase of mesh size is abrupt along any line, then it is not considered to be a good meshing.

The shape factor of the element is important. The best shape for a four-noded quadrilateral element will be a square with length and breadth equal. A selection of rectangle with length being 2–3 times the width is okay, but if the length is several times compared to the width, then such a shape is not okay.

When the meshing is done, ANSYS gives out warnings if the procedure has resulted in the generation of elements with any of the above violations. However, if the researcher chooses to ignore the warnings, then the analysis will be performed anyway. It is left to the researcher to estimate the inaccuracy of such a case.

In the solution module, the researcher has to define the heat losses from the surface nodes. Likewise, the nodes which receive the arc heat at any time interval and the exact values of the heat input must be entered.

The transient analysis has to be performed for several time steps. Instead of manually executing the commands, which is prone for errors, the analysis may be performed using a program which is written in APDL language. The APDL enables a user to perform multiple analyses using a do command.

The results of the analysis can be viewed in a general post-processor or time-based post-processor. In a general post-processor, the temperature distribution corresponding to a chosen set is viewed, and in the time-based post-processor, the thermal cycle can be viewed for a selected point. In addition, the post-processor has an option to view the animated results. The progressive heat flow in the plate can be viewed to obtain an overall idea of heat transfer in the component. There is also a provision to view the temperature results along a chosen path such as longitudinal direction or any transverse direction (Ravichandran, 2021).

4.5. Heat Source Model

4.5.1. Rosenthal's Analytical Model

Simulating heating and welding has been a focus of research for many years. Rosenthal (1941) was one of the first researchers to develop an analytical solution of heat flow during welding based on conduction heat transfer using the heat conduction Fourier partial differential equation (PDE) in order to predict the geometry of the weld pool for two- and three-dimensional welds. Rosenthal developed the moving coordinate system to find remedies for the point and line heat sources. He then successfully used this to a variety of welding issues. His analytic solutions of the heat flow made it possible to investigate the process for the first time taking into account the welding parameters, particularly the current, voltage, welding speed, and weld form. Heat source for welding was grouped into three types: point type by Rosenthal, line type and area type depending on the thickness, shape and dimensions of the weldment and the pattern of heat transfer during welding process. In the case of surfacing bead welding in thick weldment, where the heat transfers in all three directions, The source of the heat might be regarded as a point source. The temperature field of this instantaneous concentrated point source can be obtained from the following formula.

$$T = \frac{2Q}{c\rho(4\pi\alpha t)^{3/2}} \exp\left(-\frac{D^2}{4\alpha t}\right) \tag{4.14}$$

Where a is the thermal diffusivity, Q represents the instantaneous heat energy provided by the welding heat source, Q = ηIU, η is the heat source's efficiency, U is the welding voltage, I is the welding current.

$Q = (x^2 + y^2 + z^2)^{1/2}$

In the case of welding in infinite and thin plate, the temperature deviation in the direction along the plate thickness can be ignored, so the heat propagates to two directions. The heat source can be regarded as a line along the plate thickness. The temperature field in this case can be calculated from the following equation.

$$T = \frac{Q}{4\pi\lambda ht} \exp\left(-\frac{d^2}{4\alpha t}\right) \quad (4.15)$$

In this equations d denotes the distance away from the line source, d = $(x^2 + y^2)^{½}$

Tthe temperature distributes uniformly in the section of the bar which is equivalent to heat propagation of a small area with constant temperature. The heat source can be defined as area source, and its temperatures field can be expressed as follows.

$$T = \frac{Q}{c\rho A(4\pi\alpha t)^{1/2}} \exp\left(-\frac{d^2}{4\alpha t}\right) \quad (4.16)$$

Where x is the separation from the area source and A is the section's area.

Mathematical approach of Rosenthal (1946) a focused heat source serves as its foundation, but it ignored latent heat, phase shifts, and changes in material characteristics with temperature. As a result, the result deviation in the heat influence section is rather large. Nevertheless, it has been frequently employed in engineering applications due to its acceptable accuracy in the low temperature zone and its simplicity (Chen 2011).

4.5.2. Gaussian Distributed Model

Following Rosenthal's landmark work, Friedman (1975) advocated utilising the Gaussian Distributed heat source to approximately characterise the heat flow in the heating region, as shown in Figure 4.10.

The expression for the heat flow q(r), at a distance r from the heat source center, is:

$$q(r) = q_{max}\left(-\frac{3r^2}{R^2}\right) = \frac{3Q}{\pi R^2} \exp\left(-\frac{3r^2}{R^2}\right) \quad (4.17)$$

where q_{max} is the highest heat flux at the heat source's center, Q is the arc's heat input energy, and R is the heating spot's radius. It has been demonstrated that the Gaussian distributed heat source modal may produce results that are accurate enough for the common welding processes, such as SMAW and GTAW (Chen 2011).

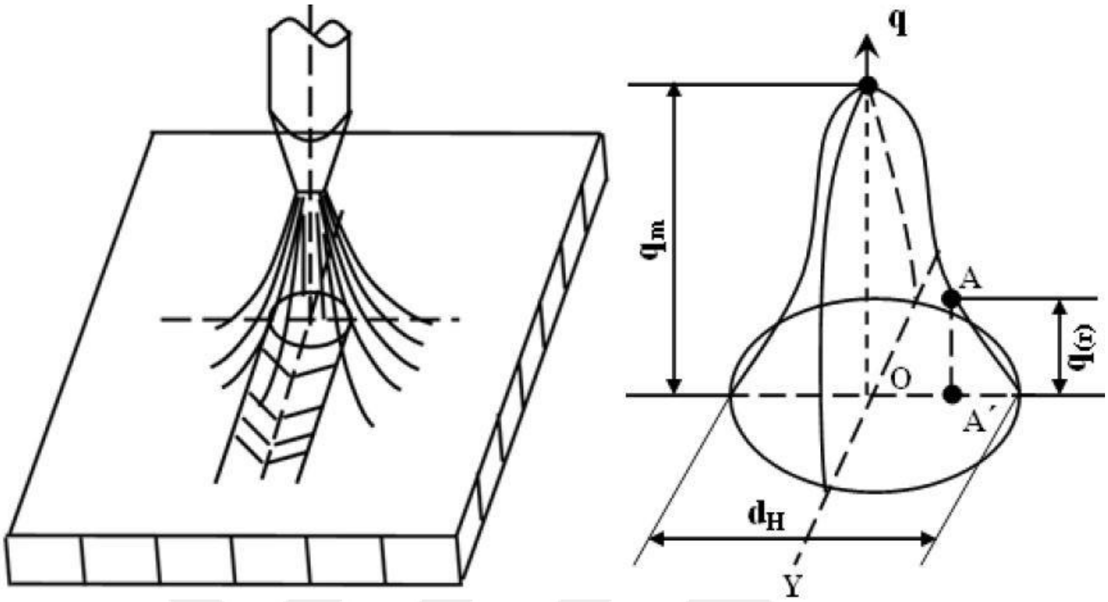

Figure 4.10. Gaussian distributed heat source (Chen, 2011).

4.5.3. Goldak’s Distributed Model

4.5.3.1. Semi-Ellipsoidal Model

The precision that results from the Gaussian distribution model has a drawback, too. Due to the arc stiffness's lack of consideration in welding processes where the arc's momentum impact is a significant factor. To solve this issue, Goldak et al. (1985) first created a semi-ellipsoidal heat source in which heat flow is distributed uniformly across volume of heat source.

The ellipsoid's semi-axes are shown in Figure 4.11 as bh, ah, and ch. The center of the heat source provided by the equation 4.18, is where heat flow reaches its highest value.

$$q(x, y, z) = q_{max}(-Ax^2 - By^2 - Cz^2) \tag{4.18}$$

where heat flow distribution coefficient are A,B,C.

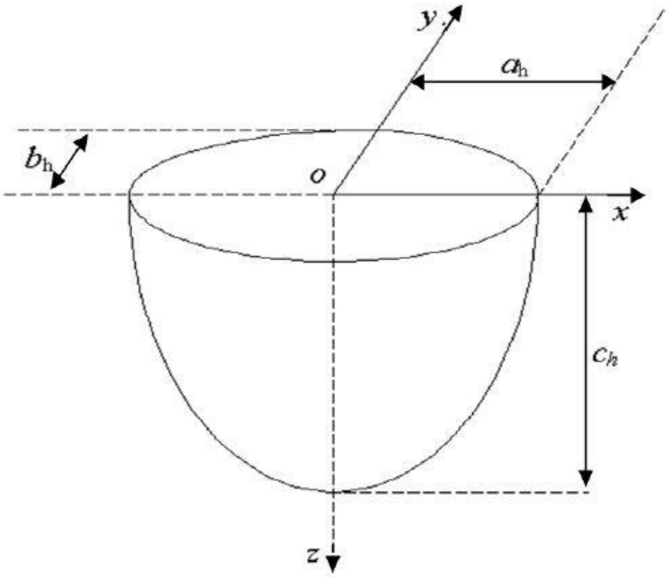

Figure 4.11. Semi-ellipsoidal distributed heat source (Chen, 2011).

Because heat is diffusing inside the semi-ellipsoid at the weldment surface, the heat flux may be defined as follows:

$$Q = \eta IU = 4\int_0^\infty\int_0^\infty\int_0^\infty q(x,y,z,)dxdydz$$

$$= 4q_{max}\int_0^\infty \exp\,(-Ax^{2)}dx\int_0^\infty \exp\,(-Byx^{2)}dy\int_0^\infty \exp\,(-Czx^{2)}dz$$

$$= 4q_{max}(\frac{1}{\sqrt{A}}\frac{\sqrt{\pi}}{2})(\frac{1}{\sqrt{B}}\frac{\sqrt{\pi}}{2})(\frac{1}{\sqrt{C}}\frac{\sqrt{\pi}}{2}) \qquad (4.19)$$

$$\frac{q_m\pi\sqrt{\pi}}{2\sqrt{ABC}}$$

Where

$$q_m = \frac{2Q\sqrt{ABC}}{\pi\sqrt{\pi}} \qquad (4.20)$$

Considering that 95% of the heat energy produces inside the semi-ellipsoid, as

$$q(a_h,0,0) = \; q_m\exp(-Aa_h^2) = 0{,}05q_m \qquad (4.21)$$

Thus

$$A = \frac{3}{a_h^2} \qquad (4.22)$$

Also

$$B = \frac{3}{b_h^2} \qquad C = \frac{3}{c_h^2} \tag{4.23}$$

Substitute Eq. 4.22 and Eq.4.23 into Eq.4.21, the heat flux Q(x, y, z) at a point (x, y, z) within the semi-ellipsoid is given by the following equation: (Chen 2011).

$$q(x,y,z) = \frac{6\sqrt{3}Q}{a_h b_h c_h \pi\sqrt{\pi}} \exp\left(-\frac{3x^2}{a_h^2} - \frac{3y^2}{b_h^2} - \frac{3z^2}{c_h^2}\right) \tag{4.24}$$

4.5.3.2. Double-Ellipsoidal Heat Source Model

Gradients behind the arc were found to be steeper than measured, while gradients in front of the arc were found to be less steep than experimentally observed ones, according to experience with this heat source. They developed a novel heat source termed heat source which becomes double ellipsoidal, as illustrated in Figure 4.12, to get around this problem by combining two semi-ellipsoids.

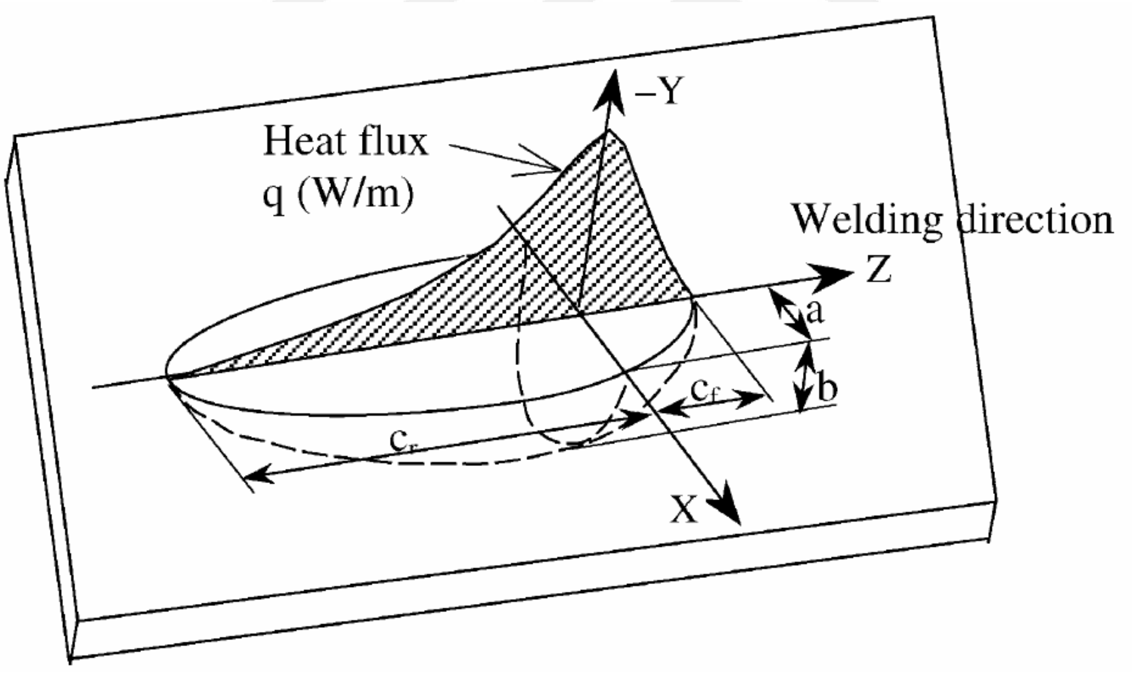

Figure 4.12. Heat source with Double-ellipsoidal (Chen, 2011).

Because the new heat source is produced by joining two separate semi-ellipsoids, the heat flow within each one is described by a different equation.

For a location inside the first semi-ellipsoid in front of the welding arc, the heat flow equation is as follows:

$$q(x,y,z) = \frac{6\sqrt{3}(f_f Q)}{abc_f\pi\sqrt{\pi}} \exp\,(-\frac{3x^2}{a^2} - \frac{3y^2}{b^2} - \frac{3z^2}{c^2}) \tag{4.25}$$

Where ff is the front portion's heat input fraction. The amount of heat input equals:

$$2\int_0^\infty\int_0^\infty\int_0^\infty q(x,y,z,)dxdydz$$

$$= \frac{6\sqrt{3}(f_f Q)}{abc_f\pi\sqrt{\pi}} \int_0^\infty \exp\left(-\frac{3x^2}{a^2}\right)dx \int_0^\infty \exp\left(-\frac{3y^2}{ab^2}\right)dy \int_0^\infty \exp\left(-\frac{3c^2}{c_f^2}\right)dx \tag{4.26}$$

$$= 2\frac{6\sqrt{3}(f_f Q)}{abc_f\pi\sqrt{\pi}} \frac{a}{\sqrt{3}} \frac{\sqrt{\pi}}{2} \frac{b}{\sqrt{3}} \frac{\sqrt{\pi}}{2} \frac{c_f}{\sqrt{3}} \frac{\sqrt{\pi}}{2} = \frac{1}{2}(f_f Q)$$

The heat flux equation is defined as follows for locations (x, y, and z) inside the second semi-ellipsoid, which covers the real section of the arc:

$$q_r(x,y,z) = \frac{6\sqrt{3}(f_r Q)}{abc_r\pi\sqrt{\pi}} \exp\left(-\frac{3x^2}{a^2} - \frac{3y^2}{b^2} - \frac{3z^2}{c_r^2}\right), x < 0 \tag{4.27}$$

where fr is the fraction of heat input in the back.

So,

$$2\int_0^\infty\int_0^\infty\int_0^\infty q_r(x,y,z,)dxdydz = \frac{1}{2}(f_f Q) \tag{4.28}$$

Since

$$\eta IU = Q = \frac{1}{2}(f_f Q) + \frac{1}{2}(f_r Q) = \frac{1}{2}Q(f_f + f_r) \tag{4.29}$$

It is obviously that

$$f_f + f_r = 2 \tag{4.30}$$

4.6. Temperature Distribution Field

4.6.1. Theory of Heat Transfer

The mechanical characteristics of the material change with temperature, melting, phase transitions, and latent heat are all present throughout the process of welding, which involves sharply localized heating to high temperatures and fast cooling thereafter. In conclusion, the investigation of the temperature field caused by welding is a well-known nonlinear transient heat transfer problem.

The temperatures of different weldment components vary significantly because of local heating that occurs during the welding process. As a result, heat is transferred both within the weldment and to its surroundings.

Three major categories may be used to classify heat transmission methods:

4.6.1.1. Conduction

Through direct molecular collisions, conduction is the process by which regions with greater molecular kinetic energy transmit their thermal energy to those with lower molecular kinetic energy. Conduction-band electrons in metals also transfer a substantial percentage of the thermal energy.

In general, the Fourier equation gives the rate of heat transfer by conduction.

$$q'' = -k\Delta T \tag{4.31}$$

Where the heat flow is q", the material's thermal conductivity is k, and the temperature is T and $\Delta = (\frac{\partial}{\partial x}, \frac{\partial}{\partial y}, \frac{\partial}{\partial z})$

It is possible to express energy conservation in a differential form as;

$$c\rho \frac{\Delta T}{\Delta t} = \frac{\partial}{\partial x}\left(k_x \frac{\partial T}{\partial x}\right) + \frac{\partial}{\partial y}\left(k_y \frac{\partial T}{\partial y}\right) + \frac{\partial}{\partial z}\left(k_z \frac{\partial T}{\partial z}\right) + \dot{Q} \tag{4.32}$$

Where is the material's density, c is its specific heat, Q is the heat produced inside the element, and t is the passage of time.

Eq. 4.35 becomes; if the thermal conductivity of the material, k, is taken to be constant.

$$\frac{\Delta T}{\Delta t} = \alpha\left(\frac{\partial^2 T}{\partial x^2} + \frac{\partial^2 T}{\partial y^2} + \frac{\partial^2 T}{\partial z^2}\right) + \dot{Q} \tag{4.33}$$

Where α is thermal diffusivity ($\alpha = \frac{k}{c\rho}$)

For an isotropic, stationary material with constant thermal conductivity, k, the differential equation for heat conduction is given by Eq. 4.36. The boundary conditions and initial circumstances have a significant impact on the solution of this equation.

4.6.1.2. Convection

A static fluid experiences a local volumetric expansion as heat transmits into it. Gravity-induced pressure gradients cause the expanded fluid parcel to swell and move about, which allows heat to be transferred both by conduction and fluid motion (convection). Free convection is the term used to describe such heat-induced fluid mobility in initially static fluids.

The two different boundary conditions for the heat transfer coefficient are radiation and convection. With regard to the latter,

$$q''_{max} = h_f \,.(T - T_\infty) \tag{4.34}$$

Where T_∞ is ambient temperature, T is body temperature, and h_f is the convection heat transfer coefficient.

4.6.1.3. Radiation

Depending on their temperature, all materials emit thermal energy, which is transported by photons of light in the infrared and visible ranges of the electromagnetic spectrum. When temperatures are constant, there is no net thermal energy exchange because the radioactive flow between objects is in equilibrium. When temperatures are not constant and thermal energy is transferred from hotter to colder surfaces, the equilibrium is disrupted.

The equation for radiation heat transfer is;

$$q''_{rad} = \sigma\varepsilon(T^4 - T_\infty^4) \tag{4.35}$$

Where ε is the emissivity, T_∞ is surrounding temperature., T is body temperature σ is Stefan-Boltmann constant,

For analytical, numerical, or experimental studies of the welding process, knowledge of heat flow theory is a prerequisite (Chen 2011).

4.7. Welding Deformation

The area closest to the welding flame experiences the greatest temperatures, therefore it grows more than areas farther away. Because the thermal expansion in this location is limited by surrounding metal with a higher yield stress and lower temperature, the stresses in the vicinity of the weld are compressive plastically during heating. The plate deforms in the opposite direction when it cools after the welding is finished. The plate would revert to its original shape with no lingering distortion if the material was entirely elastic during the whole heating and cooling cycle.

However, plastic deformations do happen to metals like steel and aluminum. The plate continues to deform after passing its original shape as a result of the compressive plastic stresses created in the areas close to the welding zone, which causes a negative final distortion when the plate cools down to its initial temperature, as shown in Figure 4.13. The thing could be so deformed that it cannot serve its original purpose or fit its intended position.

As a result, complex strains develop in the weld and its surrounding areas, creating stresses that lead to deformation of the welded component. Therefore, each welding procedure has the potential to deform the finished product in some way. Since welding-induced distortion directly affects the product quality of the connected components, distortion must be reduced in order to meet product requirements. Some possible mitigating techniques include precise weld preparation, ideal welding sequencing, pre-bending, heat sinking, thermal straightening, and thermal tensioning.

Numerical simulation of welding-induced distortion is a useful technique because it enables distortion prediction, which results in a prior description of distortion growth, and enables well-directed optimisation of welding-induced distortion evolution in practise (Chen, 2011).

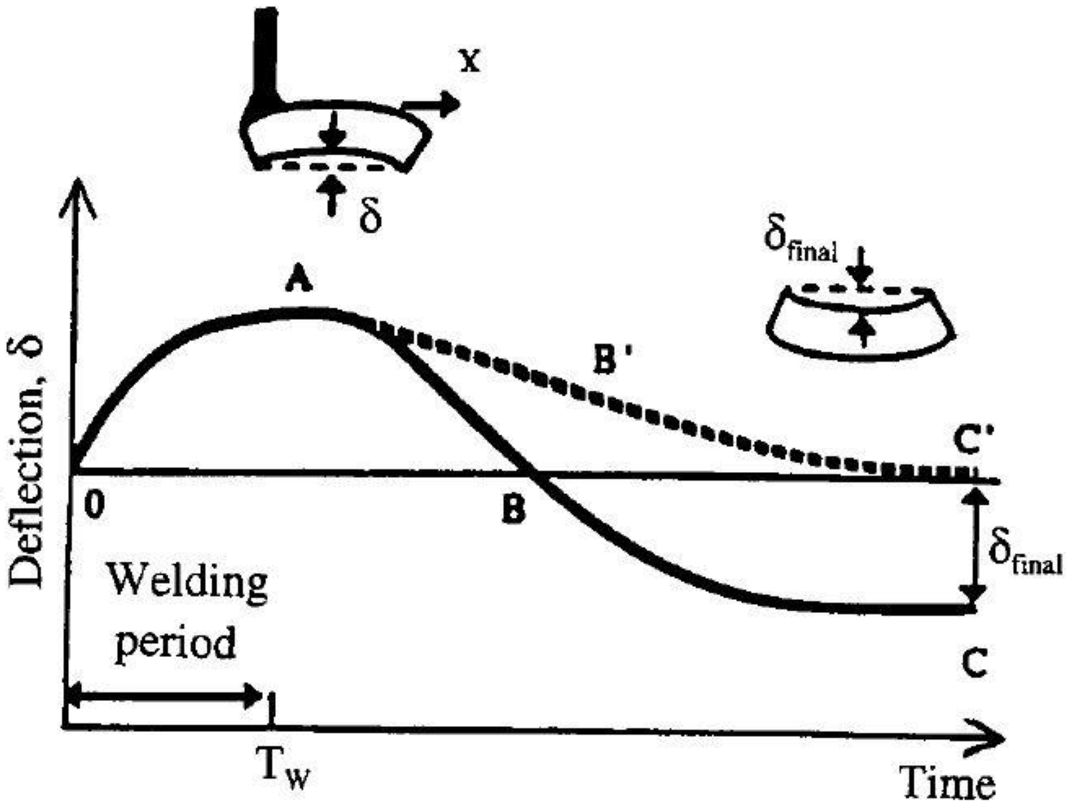

Figure 4.13. Deformation of a steel plate during and after welding (Chen, 2011)

4.7.1. Theory of Welding Deformation

The metal shrinks throughout the heating and cooling phases of the welding process due to a variety of variables. Heat alters the metal's physico-mechanical characteristics. As the temperature of the weld increases, the metal's yield strength, modulus of elasticity, and thermal conductivity all decrease while specific heat and coefficient of thermal expansion values increase.

Weisman (1976) reported on the temperature and stress variations that occur throughout the welding process. Figure 4.14 (a) depicts a bead fillet on a plate in order to graphically illustrate how residual stresses are produced during the welding process. The picture also depicts the arc, which is situated at the origin O and is travelling at a speed of v. Figure 4.14 (a) depicts the region where plastic deformation takes place during welding. It is shown by the hatching area, M-M'. The location of the metal melting is shown by the eggshaped area close to the origin O. Throughout all of the welding cycles, the metal outside of the hatching region keeps its elasticity. As illustrated in Figure 4.14 (b), numerous cross-sections are investigated to characterize the temperature variations that occur during welding. The region of A-A that is some distance in front of the welding flame has a temperature gradient that is almost zero for welding. Section B-B, where the welding arc passes, has a very substantial temperature fluctuation, and the distribution there is quite uneven. Along section C-C, some distance past the welding arc, the temperature change flattens out and becomes less sudden. Finally, at section D-D, which is far from the welding arc, the temperature differential brought on by welding has nearly completely disappeared.

The distribution of stresses x in the X-direction at cross sections A-A, B-B, C-C, and DD is depicted in Figure 4.14 (c). Shearing stresses, or τ_{xy}, exist in addition to normal y-direction stresses but are often much less than σ_x. The thermal strains brought on the welding are essentially nonexistent at section A-A. Stresses in the region below the weld pool at section B-B are also basically nonexistent since molten metal cannot maintain a load. The heat-affected zone (HAZ) experiences compressive pressures because the surrounding metal, which is at a lower temperature, prevents these areas from expanding. Given that the metal temperature at these locations is high and the material's yield strength is low, the stresses are equivalent to the material's yield strength at the corresponding temperature. The amount of compressive stress increases as the distance from the weld or temperature decreases, and eventually reaches its maximum. In places far from the weld line, tensile stresses are present to balance off compressive loads.

At section C-C, where the weld metal and heat-affected zone have cooled, there are compressive stresses at a greater distance and tensile strains in the sections near to the weld as they seek to contract. Last but not least, section D-D depicts an area that has cooled down, where the base plate is under compressive stress away from the weld and the HAZ zone is under high tensile stress (Chen, 2011).

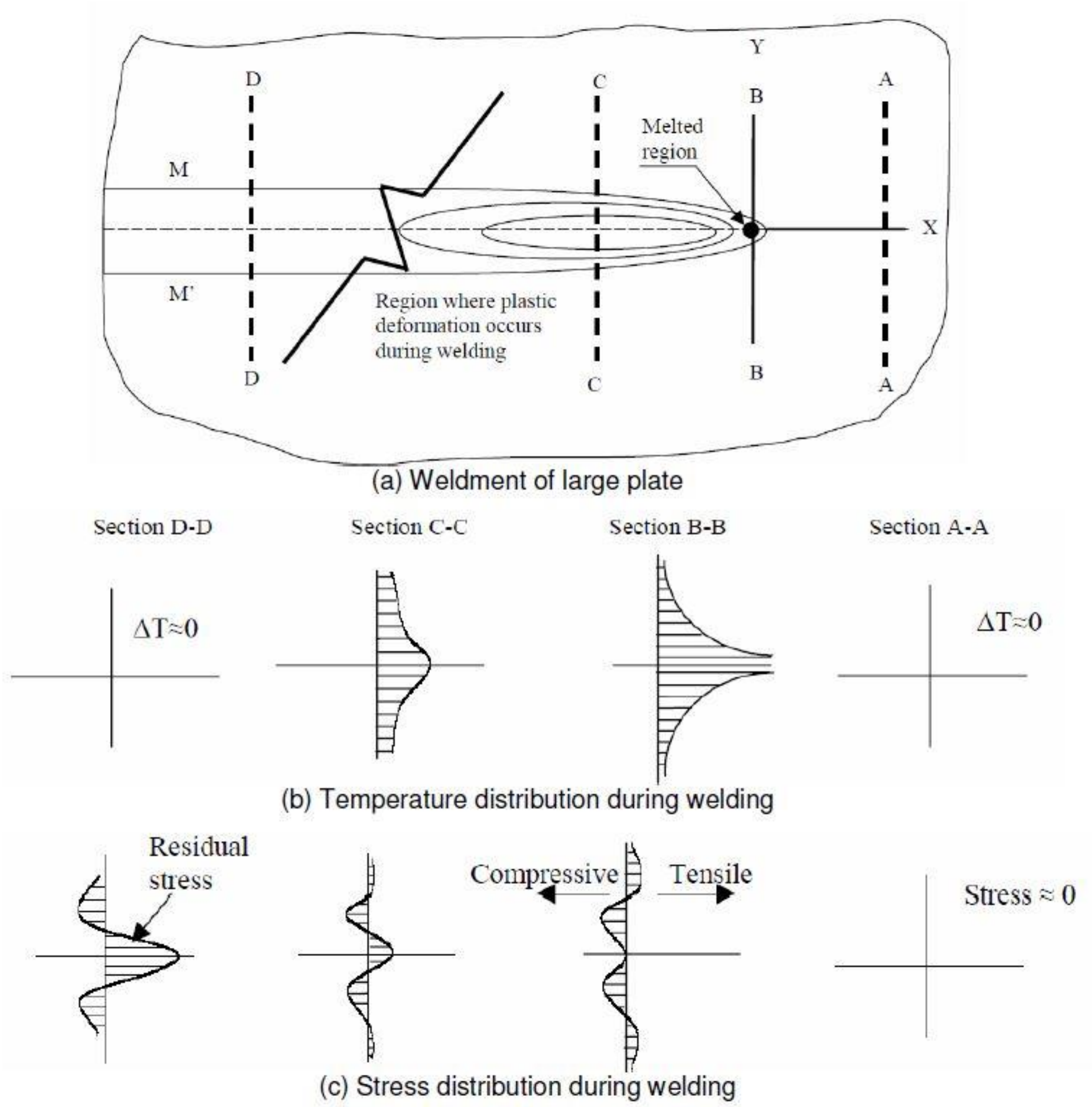

Figure 4.14. Temperature and stress changes during welding (Chen, 2011)

4.7.2. Stress Strain Relationship

The total strains increase in the elastic area may be written as

$$\{d\varepsilon\} = \{d\varepsilon\}_e + \{d\varepsilon\}_T \qquad (4.36)$$

Where $\{d\varepsilon\}_T$ is the thermal strain increment, $\{d\varepsilon\}_e$ is the elastic strains increment due to the consistency condition, The elastic matrix $[D]_e$ (related to the modulus of elasticity and Poisson's ratio) varies with temperature, then,

$$\{d\varepsilon\}_e = d[[D]_e^{-1}\{\sigma\}] = [D]_e^{-1}\{d\sigma\} + \frac{\partial [D]_e^{-1}}{\partial T}\{\sigma\}dT \tag{4.37}$$

$\{d\varepsilon\}_T$ is the differential increment of $\{\alpha_{0T})$ where α_0 is the lineer expansion coefficient of initial temperature.

$$\{d\varepsilon\}_T = \{\alpha_0 dT + T d\alpha_0\} = \{\alpha_0 + \frac{\partial \alpha_0}{\partial T}\}dT = \{\alpha\}dT \tag{4.38}$$

The linear expansion coefficient α also varies with temperature. Its effective value is,

$$\{\alpha\} = \left\{\alpha_0 + \frac{\partial \alpha_0}{\partial T} T\right\} \tag{4.39}$$

Substitute equaiton 4.40 and 4.11 into equation 4.39 then

$$\{d\sigma\} = \{[D]_e\{d\varepsilon\} - [D]_e(\{\alpha\} + \frac{\partial [D]_e^{-1}}{\partial T}\{\sigma\})dT \tag{4.40}$$

Or,

$$\{d\sigma\} = [D]_e\{d\varepsilon\} - \{C\}dT \tag{4.41}$$

Where $[D] = [D]_e$, $\{C\} = [D]_e(\{\alpha\} + \frac{\partial [D]_e^{-1}}{\partial T}\{\sigma\})$ is relevant temperature. Equation 4.43 is the stress increment-strain increment relationship in the elastic region, taking into consideration the temperature dependent material properties.

While in the plastic region, asume that the material starts to yield when the value of the yield function $f(\sigma_x, \sigma_x, \ldots)$ reaches $f_0(\sigma_y, T, K)$ which is,

$$f = f_0(\sigma_y(T), K(\varepsilon_p)) \tag{4.42}$$

Where K is the strain hardening exponen and T is the temperature

Its differential form is,

$$df = df_0 \tag{4.43}$$

The total strain increment in the plastic region may be found out by,

$$\{d\varepsilon\} = \{d\varepsilon\}_p + \{d\varepsilon\}_e + \{d\varepsilon\}_T \tag{4.44}$$

Where $\{d\varepsilon\}_p$ is the plastic strain increment.

According to the flow rule,

$$\{d\varepsilon\}_p = \xi \{\frac{\partial f}{\partial \sigma}\} \tag{4.45}$$

From the equation above, ξ can be solved as,

$$\xi = [\{\frac{\partial f}{\partial \sigma}\}^T [D]_e\{d\varepsilon\} - \{\frac{\partial f}{\partial \sigma}\}^T [D]_e(\{\alpha\} + \frac{\partial [D]_e^{-1}}{\partial T} - \frac{\partial f_0}{\partial T} dT] / s$$

$$s = \{\frac{\partial f}{\partial \sigma}\}[D]_e\{\frac{\partial f}{\partial \sigma}\} + \{\frac{\partial f_0}{\partial \sigma}\}\{\frac{\partial K}{\partial \varepsilon_p}\}^T\{\frac{\partial f}{\partial \sigma}\} \tag{4.46}$$

Then the stress-strain relationship will be,

$$\{d\sigma\} = [D]_{ep}\{d\varepsilon\}_e - ([D]_{ep}\{\alpha\} + [D]_{ep}\frac{\partial [D]_e^{-1}}{\partial T}\{\sigma\} - [D]_e\{\frac{\partial f}{\partial \sigma}\}(\frac{\partial f_0}{\partial \sigma})/S)dT \tag{4.47}$$

Where [D]ep is the elasto-plastic matrix,

$$[D]_{ep} = [D]_e - [D]_e\{\frac{\partial f}{\partial \sigma}\}\{\frac{\partial f}{\partial \sigma}\}^T [D]_e / s \tag{4.48}$$

Let [D] = [D]ep, $\{C\} = \{C\}_{ep} = ([D]_{ep}\{\alpha\} + [D]_{ep}\frac{\partial [D]_e^{-1}}{\partial T}\{\sigma\} - [D]_e\{\frac{\partial f}{\partial \sigma}\}(\frac{\partial f_0}{\partial \sigma})/S)dT$

It becomes equation 4.44.

It can be concluded that the stress – strains relationship is,

$$\{d\sigma\} = [D]\{d\varepsilon\} - \{C\}dT \tag{4.44}$$

While in the plastic region, $[D]=[D]_{ep}$, $[C]=[C]_{ep}$, in the elastic region, $[D] = [D]_e$, $[C]=[C]_e$,.

Consider one element of the entire structure. It is with temperature T nodal displacement {δ}, nodal force $\{F\}^e$, stress {σ] and strain {ε} at the time t, and with $\{F + dF\}^e$, (δ + d δ}, {ε + dε} and {σ + dσ} at time T + dt. The following formula can be obtained by appliying the virtual displacement principle.

$$d\sigma^T F + dF^e = \iint_{\Delta V} d\sigma^T [B]^T \{\sigma\} + [D]\{d\varepsilon\} - \{C) dT) dV$$
$$= d\sigma^T \iint_{\Delta V} [B]^T (\sigma + [D] d\varepsilon - CdT) dV \tag{4.49}$$

Where is relevant to the geometry of the element and [B] is geometric matrix.

At time t, the structure is in an equilibrium state.

$$\{dF\}^e = \iint_{\Delta V} [B]^T \{\sigma\} dT \tag{4.50}$$

Consider the stress-strain relationship,

$$\{dF\}^e = \iint_{\Delta V} [B]^T ([D]\{d\varepsilon\} - \{C\} dT) dV \tag{4.51}$$

Or,

$$\{dF\}^e + \{dR\}^e = [K]^e \{d\delta\} \tag{4.52}$$

Where the equivalent nodal force of the initial strain is $\{dR\}^e = \iint_{\Delta V} [B]^T \{C\} dT dV,$ the element stifness matrix is $[K]^e = \iint_{\Delta V} [B]^T [D][B] dV.$

Substitute {C} and [D] from equation 4.44 into equation 4.55, the equivalent nodal load ans stiffnes matrix of the element can be ontained and be used in the global stiffness matric and load column vector, to produce the following system of algebraic equations on order to solve the nodal displacement.

$$[K]\{d\delta\} = \{dF\} \tag{4.53}$$

Where $[K]=\Sigma[K]^e$, $\{dF\}=\Sigma(\{dF\}^e + \{dR\}^e)$, normally $\Sigma\{dF)^e$ is close to zero in the welding-related issue.

4.7.3. Thermo-elasto-plastic FEM in Welding

The nonlinear stress-strain relationship must be progressively transformed into the liner one throughout the loading process in order to resolve the thermo-elasto-plastic problems. The load is really brought on by the temperature difference because there is no outside force acting on the weld during the welding process. The solution can be obtained by dividing the temperature variation calculated from the thermal analysis into several load increments to apply to the structure gradually. In general, there are three methods to solve the elasto-plastic issues, which are tangent stiffness matrix increment method, initial strain increment method and initial stress increment method. However, in the last two of these methods, a linear system of equations with the same stiffness matrix is required, which can not be guaranteed in each step of thermo-elasto-plastic solution owing to the mechanical properties of the material may be altered with the change of the temperature. These two methods often result in non-convergence, so they are not adopted in the thermo-elasto-plastic solutions. In the tangent stiffness matrix increment method, the stiffness matrix is corrected in each loading step according to the stress state of the element. When the element yields, the stiffness matrix [K] in Eq 4.54 is relevant to the coinstantaneous stress level. So the equation is nonlinear. In order to linearize it, the load is gradually increased in a certain stress and strain level. If the load value is small enough, Eq. 4.54 can be approximately expressed as,

$$[K]\{\Delta\delta\}_i = \{\Delta F\}_i \qquad (4.54)$$

Where $\{\Delta\delta\}_i$ Dd is the displacement increment in the i th load step, $\{\Delta F\}_i$ is the applied load the the i th load step, $\{\Delta F\} = \{F\}/ n$, n is a positive integer.

In this method, The stiffness matrix [K] solely relates to the stress level prior to loading since the differentials of stress and strain are replaced by their increments. As a result, there is a linear connection between the load and the displacement increment. As a result, it is simple to obtain the increments of displacement, stress, and strain. These increments plus the outcome after the (i-1) load step can be used to determine the total displacement, strain, and stress after the load step. Nevertheless, the error if the pure increment is inevitable and it can be accumulated more and more until the result becomes equilibrium nonconvergent. To solve it, the Newton-Raphson iteration method can be used. Out-of-balance load vector, or the difference between the restoring forces (the loads corresponding to the element stresses) and the applied loads, is evaluated by the Newton-Raphson technique prior to each solution. The convergence of the linear solution will next be tested using the out-of-balance loads. A new solution is discovered once the stiffness matrix is modified, and the out-of-balance load vector is reassessed if convergence requirements are not met. Until the issue converges, this iterative process continues. (Chen, 2011). Figure 4.15 shows Newton-Raphson iterative solution methods by graphically.

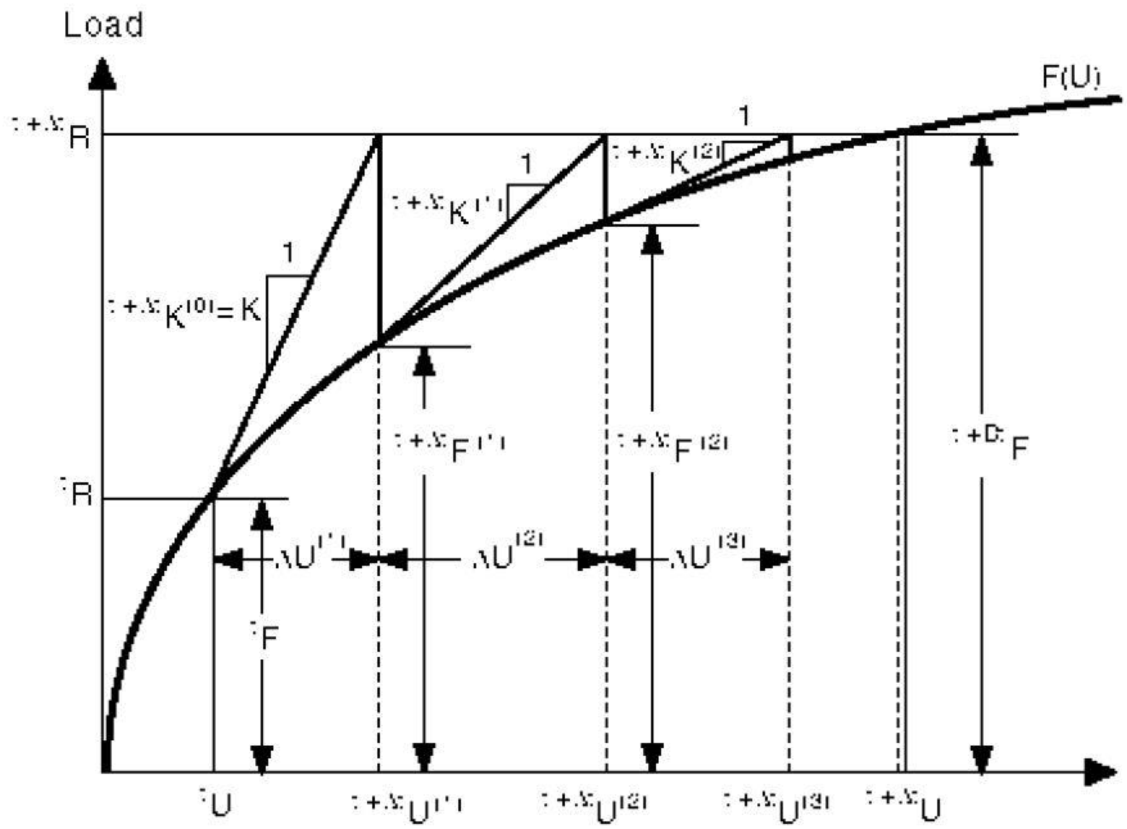

Figure 4.15. Newton-Raphson iterative solution (Chen, 2011).

4.8. Residual Stress Determination X-Ray Diffraction

By observing the angular shift of a specific Bragg reflection as a function of sample tilt (Ψ), stress may be calculated. The sample's strain is really measured by this, and the stress may subsequently be determined by graphing the variation in d-spacing versus $\sin^2\Psi$. In Figure 4.16 schematic view of determining residual stress by X-Ray Diffraction method can be seen. Figure 4.17 and 4.18 show Intensitg graph and spacing graph and Figure 4.19 shows schematic view of X-Ray Diffraction method application.

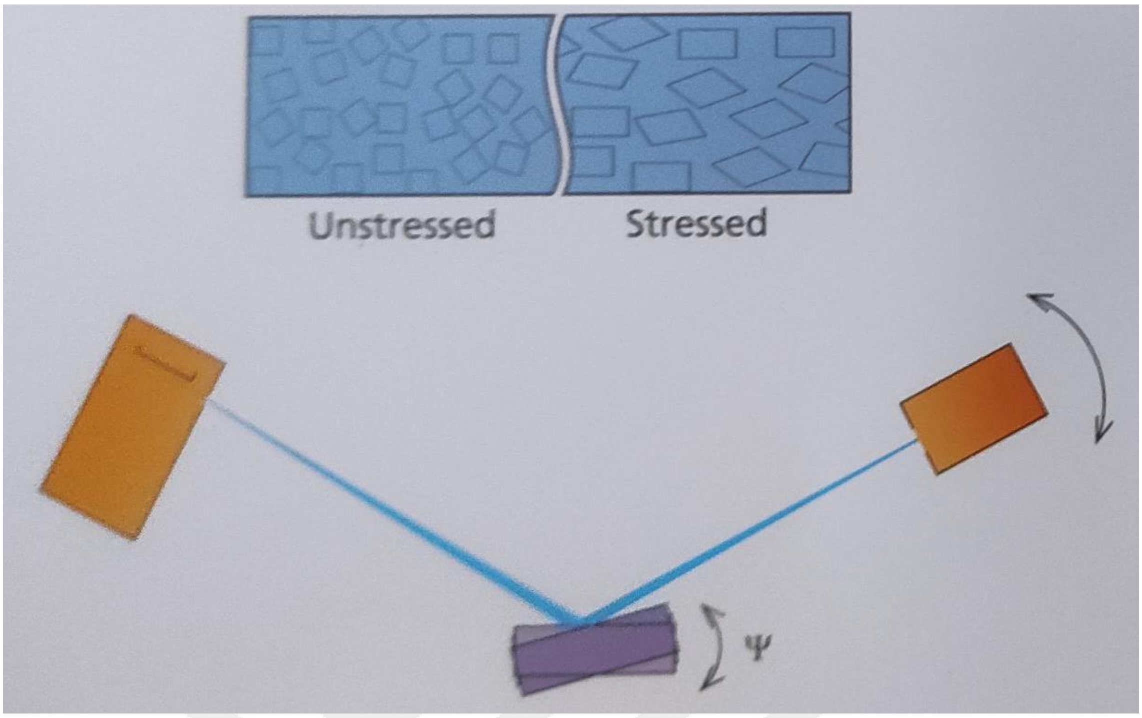

Figure 4.16. Schematic view of determining residual stress

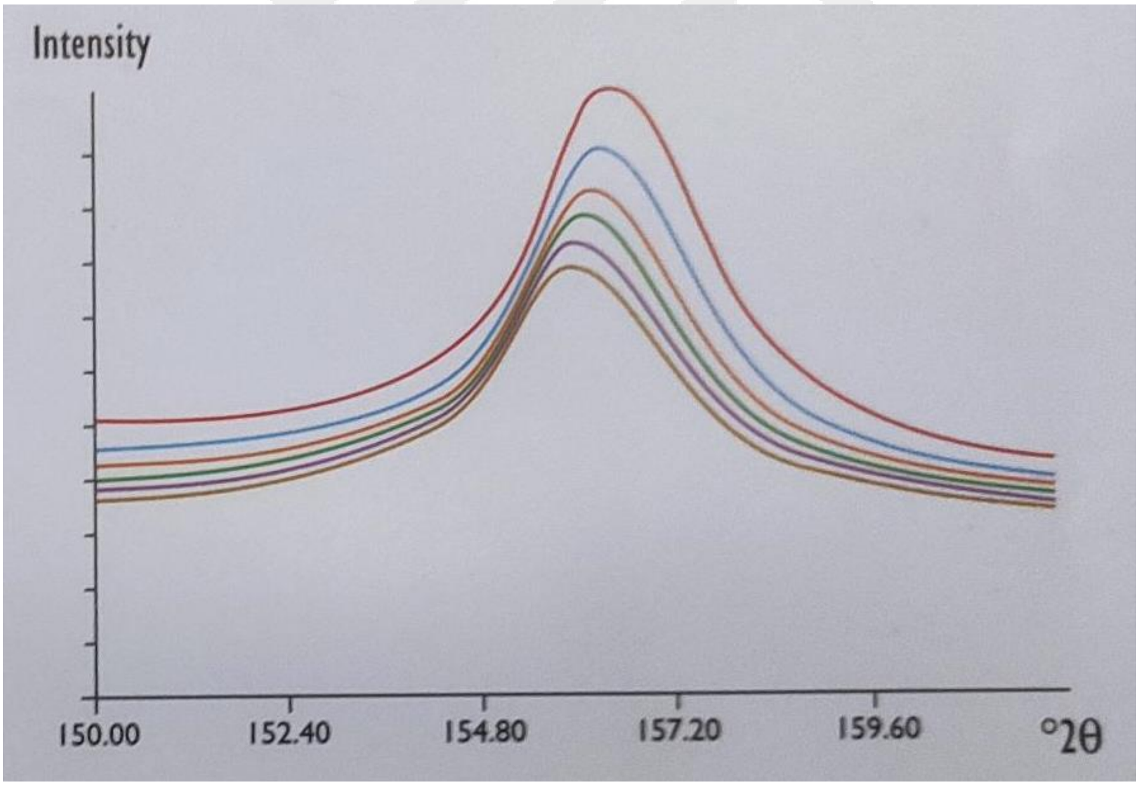

Figure 4.17. Intensity graph

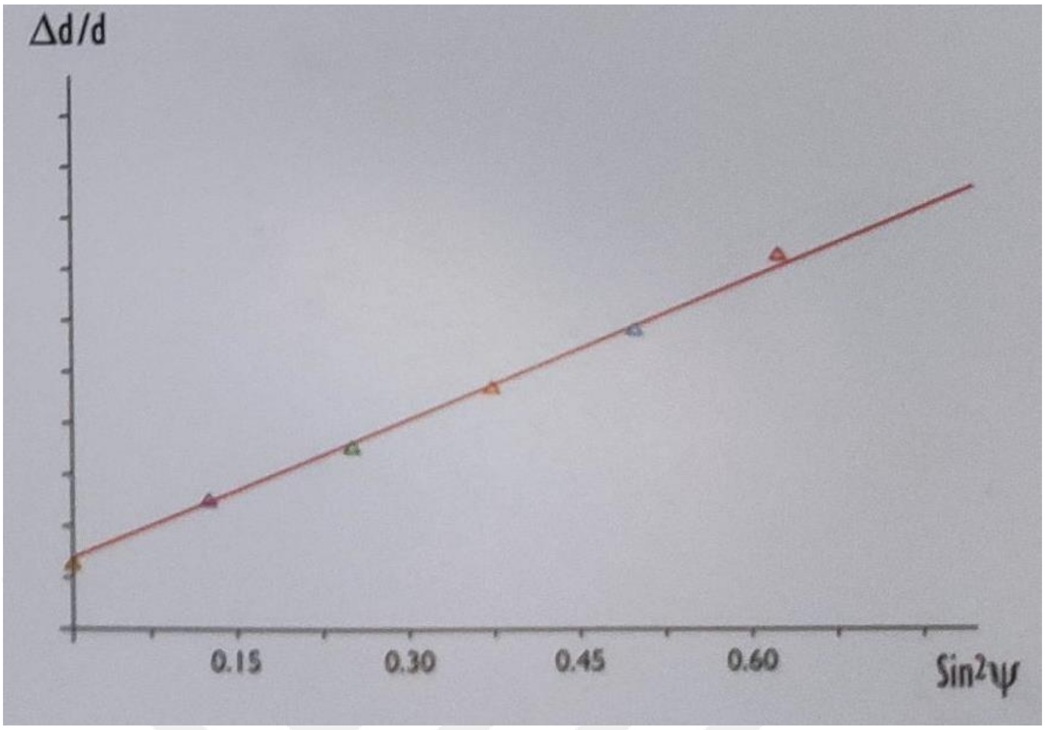

Figure 4.18. Spacing graph

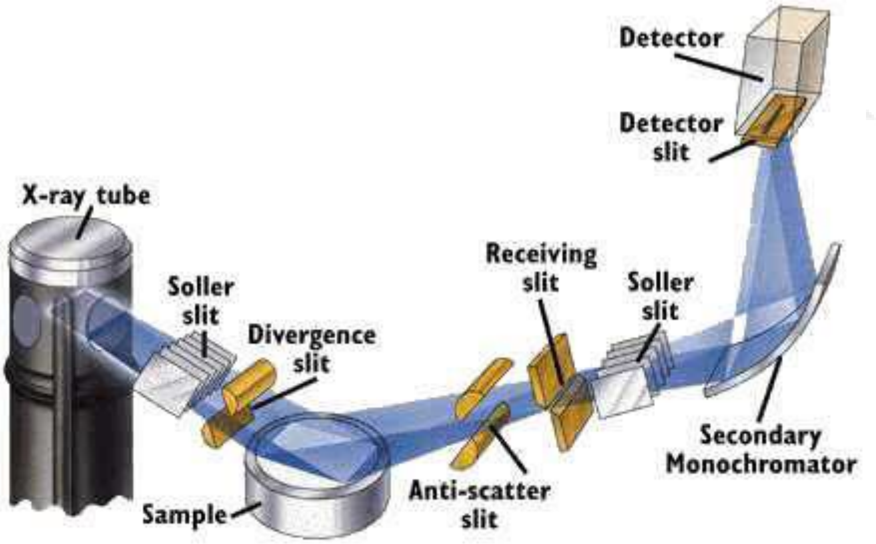

Figure 4.19. Schematic view of diffraction system

4.8.1. Principles of X-Ray Diffraction Residual Stress Measurement

When a collimated X-ray beam of wavelength (λ) is focused onto a specimen, the number of X-rays diffracted (diffracted intensity) is measured when the angle between the X-ray tube and X-ray detector (θ) changes. This makes it possible to trace diffracted intensity against 2(θ) (seen in Figure 4.20). The lattice spacing which varies between strained and non-stressed materials may be determined using the Bragg equation from these peaks.

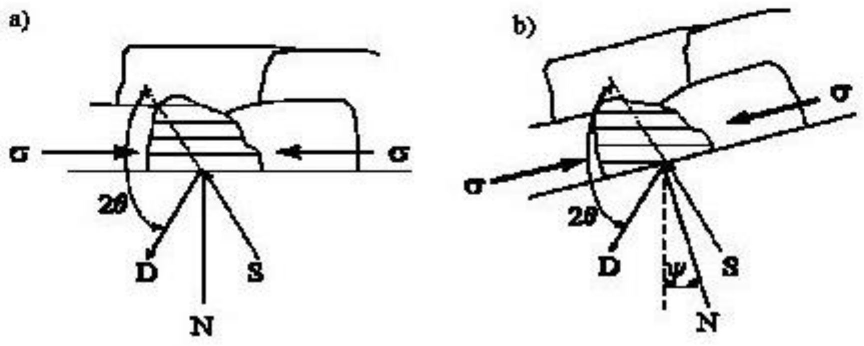

Figure 4.20. X-ray Diffraction's principle

a) Ψ = 0, b) Ψ = Ψ_i (sample is rotated by a predetermined angle, Ψ_i)

S: X-ray source, D: X ray detector, N: Surface Normal

$$n\lambda = 2dsin\theta \tag{4.55}$$

Where,

n: constant, λ: wavelength (m), d: Interplanar spacing between crystallaographic planes (m).θ: diffraction angle (º).

$$\frac{d_{\theta\Psi} - d_0}{d_0} = \frac{1 + \upsilon}{E}\,\sigma_\theta . sin^2\Psi \tag{4.56}$$

Where,

d_o : interplanar spacing for unstressed material (m), υ, $d_{\theta\Psi}$: intyerplanar spacing in the direction defined by θ and Ψ (m), E : Poisson's ratio and Elastisite modulus (Pa) respectively, σ_θ : surface stress descriebed by the angle θ (Pa).

$$\mathrm{m} = \frac{1 + \upsilon}{E}\,\sigma_\theta . d_0 \tag{4.57}$$

Where,

m: slope.

Note that the parameters υ/E and (1+υ) /E are generally as S_1 and ½ S_2 respectively, and The X-ray elastic constants are the name given to them (URL-4).

5. EXPERIMENTATION

5.1. Welding Application

5.1.1. Material Selection, Welding and Preheating

As the basic material for our experimental work, ASME SA 387 Grade 11 Class 2 type material, with dimensions of 103 mm length, 102 mm breadth, and 8 mm thickness as indicated in Figure 5.2, was selected as a pressure vessel grade steel for use in extreme temperatures service. This kind of steel is widely used and very effective, especially in the oil, gas, and petrochemical sectors where gases and liquids are frequently held at higher temperatures. Only one pass on a completely automated submerged arc welding equipment, single-sided submerged arc welding was performed. Table 5.5 contains the experiment's set of process parameters. In order to model this process using FE, the same parameters were used.

Sample parts were cut on the plasma cutting machine and then cleaned by being grounded.

To investigate the temperature history and weld-induced residual deformation, many sets of tests were conducted. Three welding parameters were used as variables: current, voltage, and welding speed, with a constant value of 2.5 mm for the length of the stick out. In order to identify the range of the welding parameters, various trial-and-error experiments were first carried out by changing only one parameter while holding the others constant. The parameters values used for the welding in the trial and error experiments can be seen in Table 5.1 and optimized welding parameters used in numerical analysis can be seen in Table 5.5.

Table 5.1. Welding parameters used in the trial and error experiments

Current (amp)	Voltage (v)	Welding speed (m/s)
430	31	0,01
530	31	0,01
560	31	0,01
600	31	0,01

Before welding, the area outside the weld zone was preheated to a desired temperature range, commonly known as the preheating temperature. Preheat temperature varies depending on a variety of elements including base metal chemical composition, heat delivered, hydrogen diffusion, and base plate thickness. For SA387 GR 11 Class 2 steels, the preheating temperature range typically ranges between 150 and 200 ºC. Pre-heat was performed using local heat treatment unit and electrical resistances.

The parent metal is fixed with clamps in order to avoid the disturbances in the movement of metals during welding application as shown in Figure 5.7.

Prior to SAW, the test plate pair was fixed wit GTAW from the upper and lower sections to prevent the samples from slipping during welding. In order tack weld weld-backing-plate, GTAW process was carreid out using Esab Origo Tig 3001i TIG welding machine which has 300 A power source. For GTAW process a filler metal ER80S-B2 which has a 2.4 mm diameter is used. Gas composition and flow rate is 99,997 Argon and 11-16 L/min respectively. The welding backing plates were welded to beginning and end of the piece shown in Figure 5.1. A weld joint's backing is the material positioned at the weld joint's base to support the molten weld metal. Its purpose is to make full joint penetration easier. In order to avoid damaging the bottom surface of the piece a ceramic protector was used by sticking it to the bottom of the part as shown Figure 5.1.

Submerged arc welding was carried out using a 1250-A constant potential power source, Miller Subarc DC 1250 (as shown in Figure 5.8). The setup of the experiments is shown Figure 5.6, 5.7. AWS A5.23: F8P2-EB2-B2 which has 3,2 mm diameter was used as filler metal and Esab Flux 10.62 agglomerated fluoride-basic flux is used.

The welding specimens were prepared with square butt joint and 1 mm gap as shown schematic in Figure 5.5.

Table 5.2. Chemical Composition of AWS A5.23 F8P2-EB2-B2

C	Mn	Si	P	S	Cr	Mo	Cu
0,09	0,80	0,25	0,013	0,008	1,10	0,45	0,03

Table 5.3. Chemical Composition of SA 387 Gr 11 Cl 2

	Carbon	Manganese	Phosphorus	Sulphur	Silicon	Chromium	Molybdenum
Heat analysis	0,05-0,17	0,40-0,65	0,035	0,035	0,50-0,80	1.00-1,50	0,45-0,65
Product Analysis	0,04-0,17	0,35-0,73	0,035	0,035	0,44-0,86	0,94-1,56	0,45-0,70

Table 5.4. Tensile Requirements for ASME SA 87 Grase 11 Alloy Steel Plates Class 2 Plates

Tensile Strength,	Yield Strength	Elongation	Elongation	Reduction of area
Ksi (MPa)	Min, ksi (MPa)/(0.2% offset)	In 8 in. (200mm), min%	İn 2 in. (50mm), min%	Min %
75 to 100 (515 to 690)	43 (310)	18	22	---

Figure 5.1. The photo of test plate prepared for welding

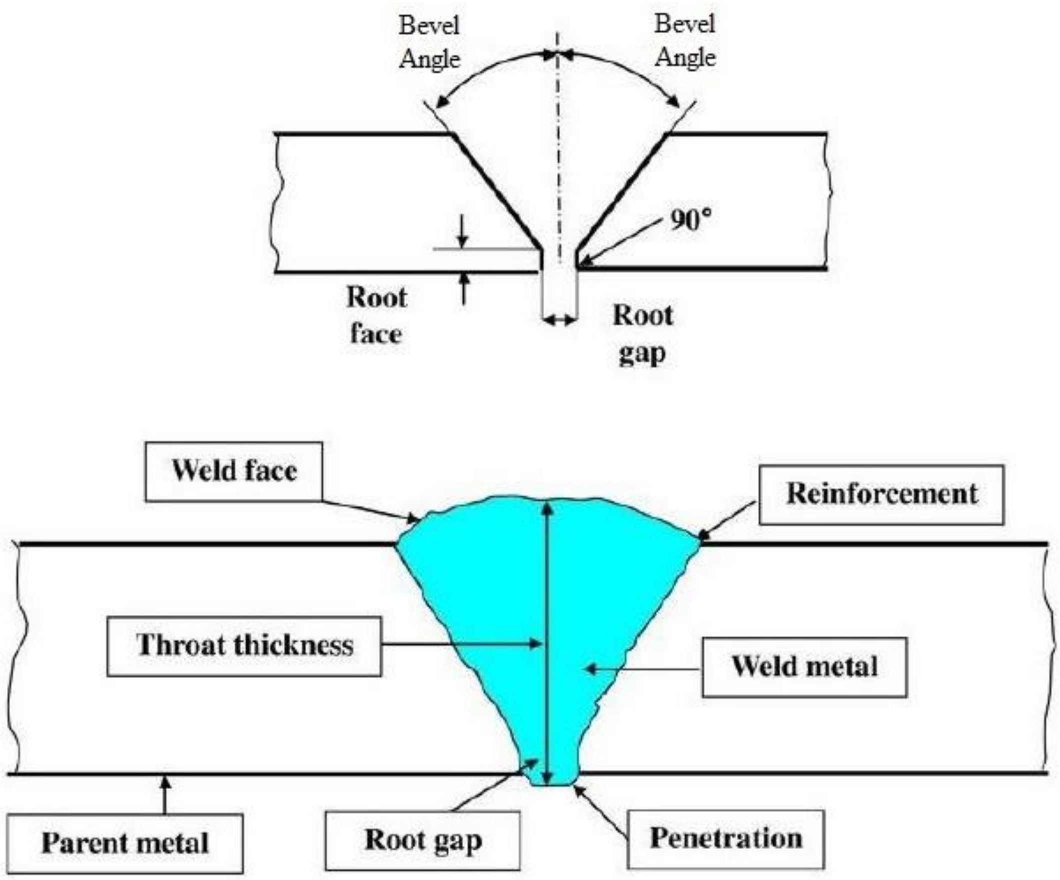

Figure 5.2. Welding Terms

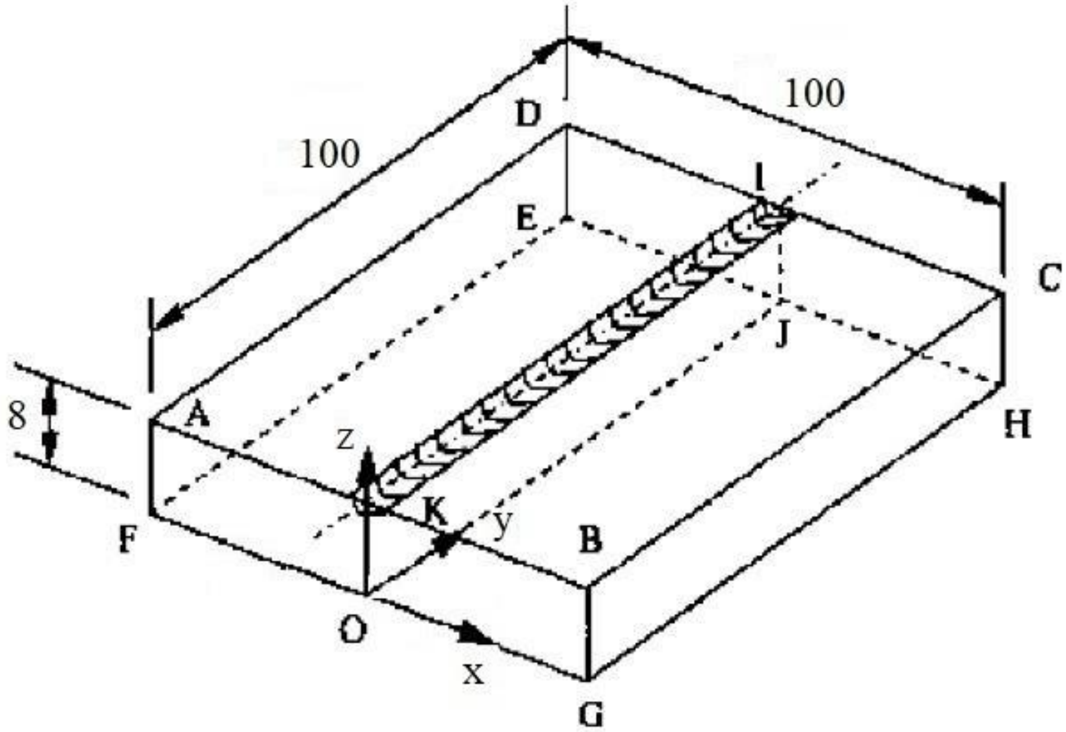

Figure 5.3. Dimensions of workpiece

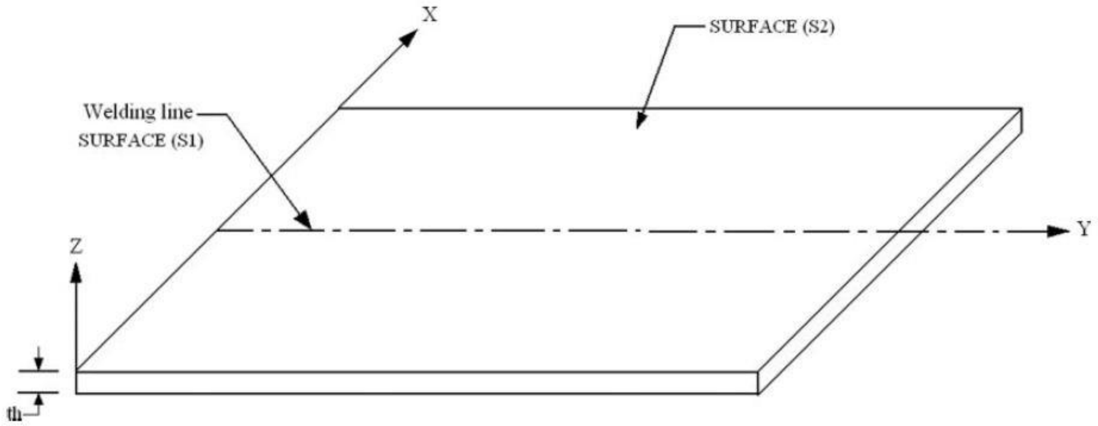

Figure 5.4. Axis system

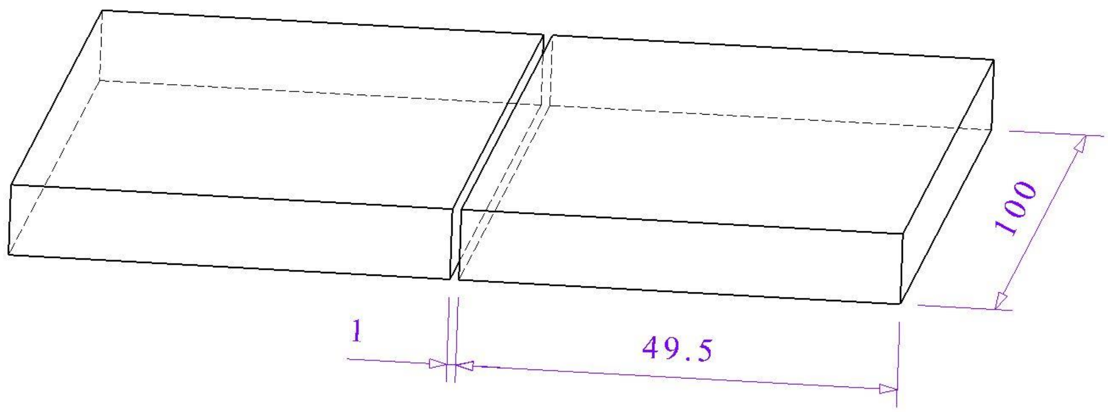

Figure 5.5. Schematic diagram of square butt joint

Heat input and welding speed are calculated as;

$$Q = \eta * VI \quad (5.1)$$

$$welding\ speed = \frac{welding\ length}{Welding\ time} \quad (5.2)$$

$$efficiency\ of\ heat\ source\ (\eta) = \frac{energy\ transfered\ to\ the\ workpiece}{energy\ generated\ by\ the\ heat\ source} \quad (5.3)$$

Table 5.5. Parameters used in SAW

Current (A)	Voltage (V)	Root gap (mm)	Welding Time (s)	Welding Speed (mm/s)
600	31	1	10	10

Figures 5.6, 5.7, 5.8, 5.9, 5.10, 5.11, 5.12, 5.13 below show the pictures of work before, during and after welding.

Figure 5.6. Setup of test plate for SAW

Figure 5.7. The view of ceramic protector after welding process

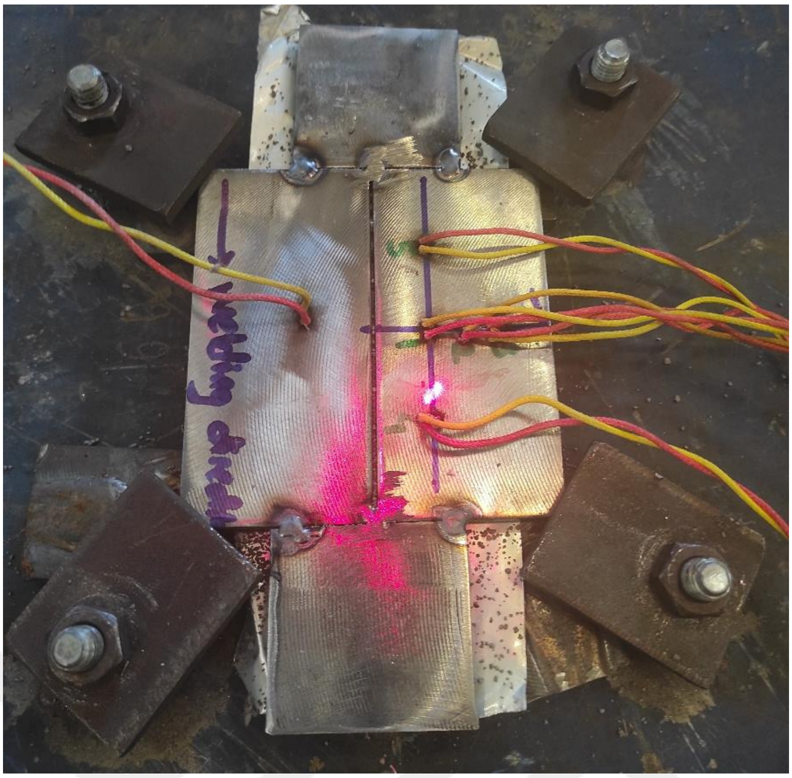

Figure 5.8. Fixing of test plate.

Figure 5.9. SAW welding machine

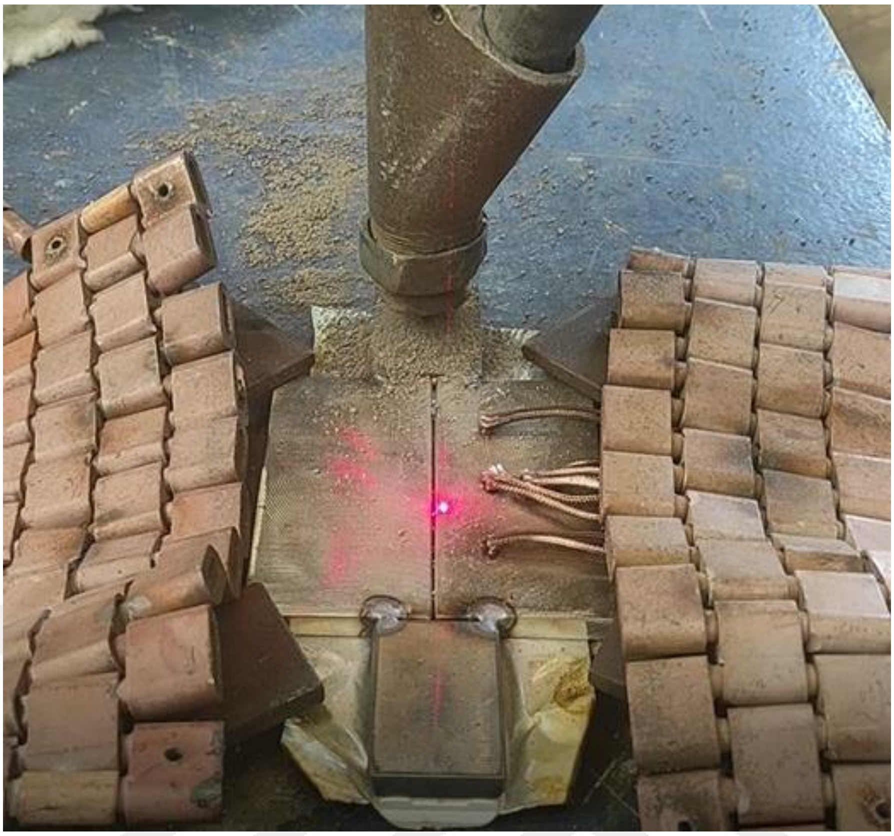

Figure 5.10. Submerged arc welding beginning of process

Figure 5.11. Welded sample

Figure 5.12. The weld bead surface

Figure 5.13. Bottom surface of welded part

5.1.2. Temperature Measurement During Welding Process

Temperature history was recorded using K type thermocouple wires which is chrome/nickel aliminum termocouple wire, insulated with high temperature glass braid and Honeywell eZtrend paperless recoder with 6 directly connected analog inputs as shown Figure 5.14. Thermocouple wires were attached directly to the workpiece using “Termocouple Atttachment Unit”. 5 thermocouples were used in the temperature collection process and Figure 5.15 and 5.16 show their locations. TC1, TC4 and TC5 were placed 15 mm away from weld centre line of weld joint. TC2 and TC3 were positioned 10 mm in x direction away from TC1. The positions of thermocouples are tabulated in Table 5.6.

The data recorded inside to Digital Honeywell Recorder was taken with Pro version of TrendViewer which is own application of Honeywell in MS Excel format.

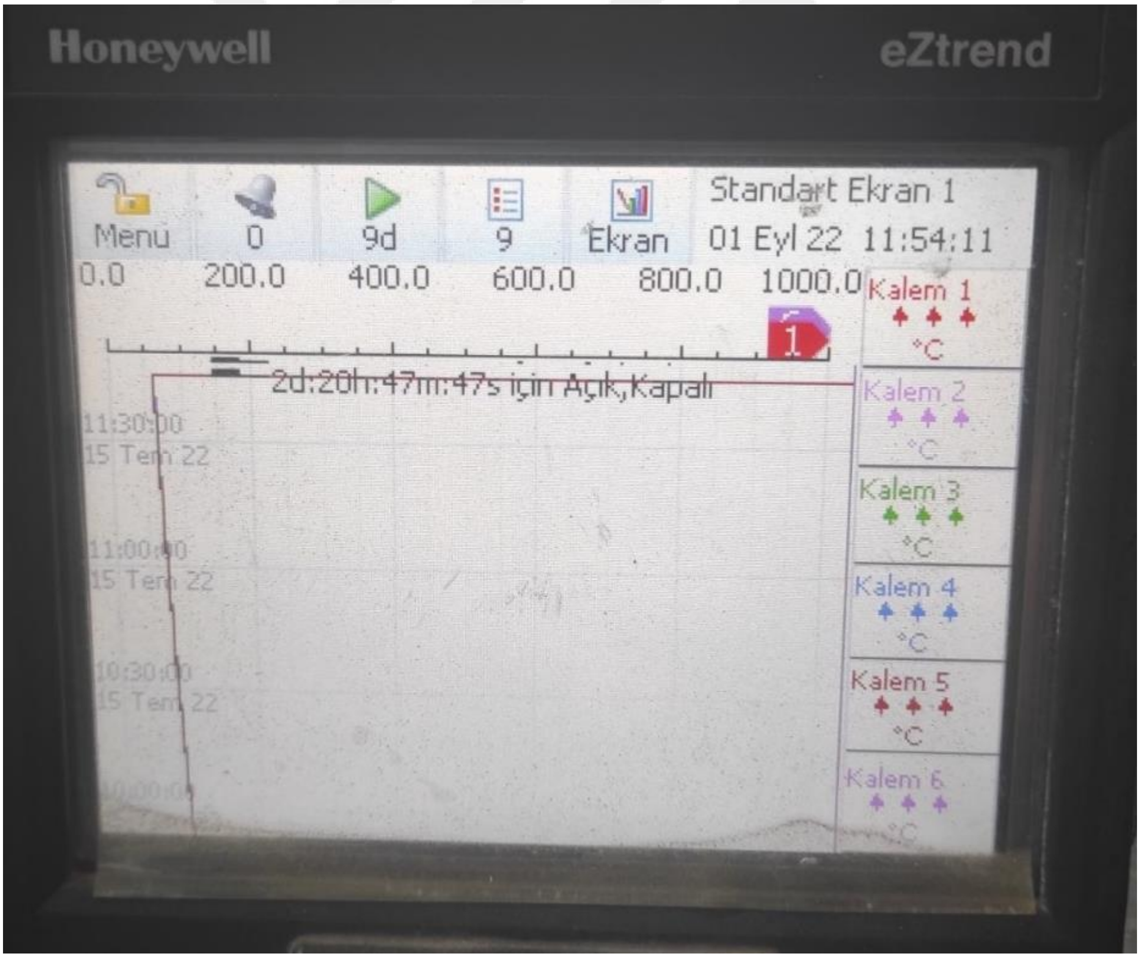

Figure 5.14. Temperature recorder device

Table 5.6. Thermocouple mean position

TC number	X	Y	Z
T-1	15	0	0
T-2	25	0	0
T-3	35	0	0
T-4	15	-26	0
T-5	15	26	0

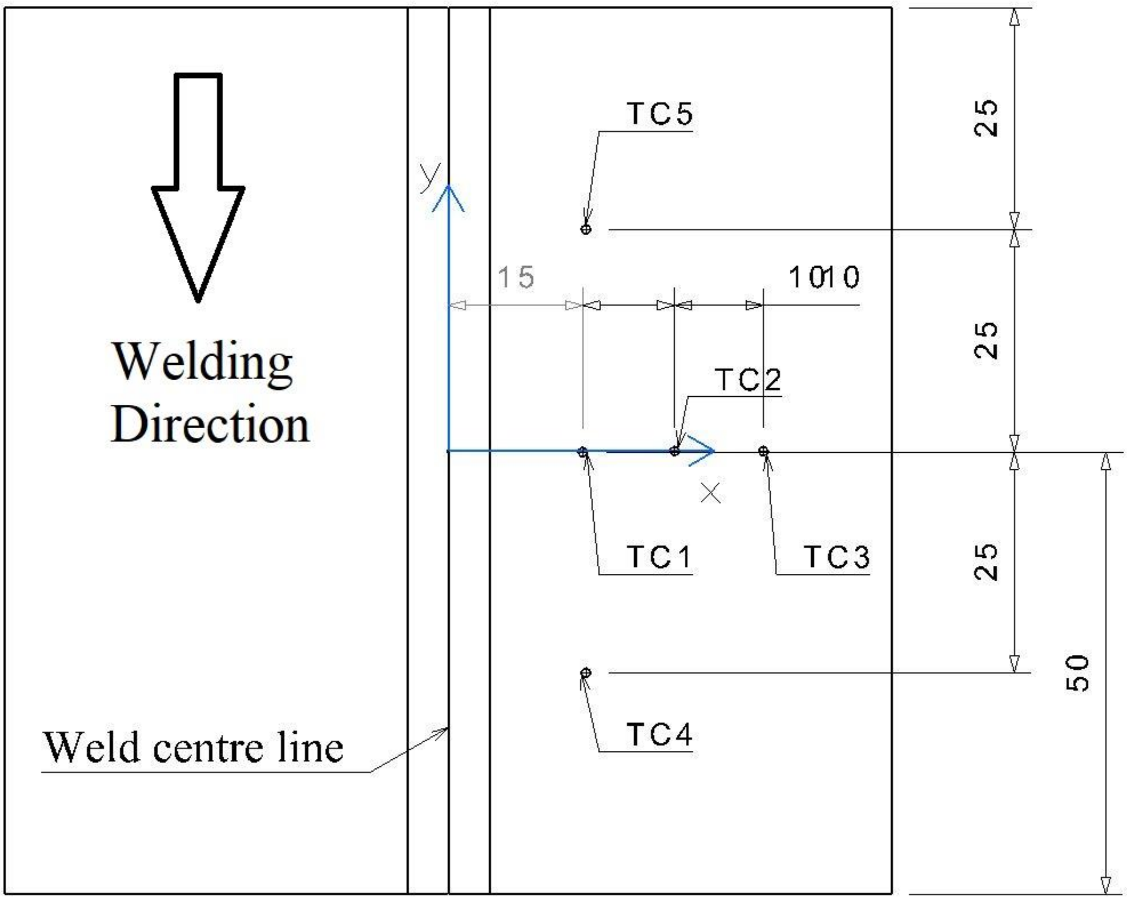

Figure 5.15. Distribution of measurement points

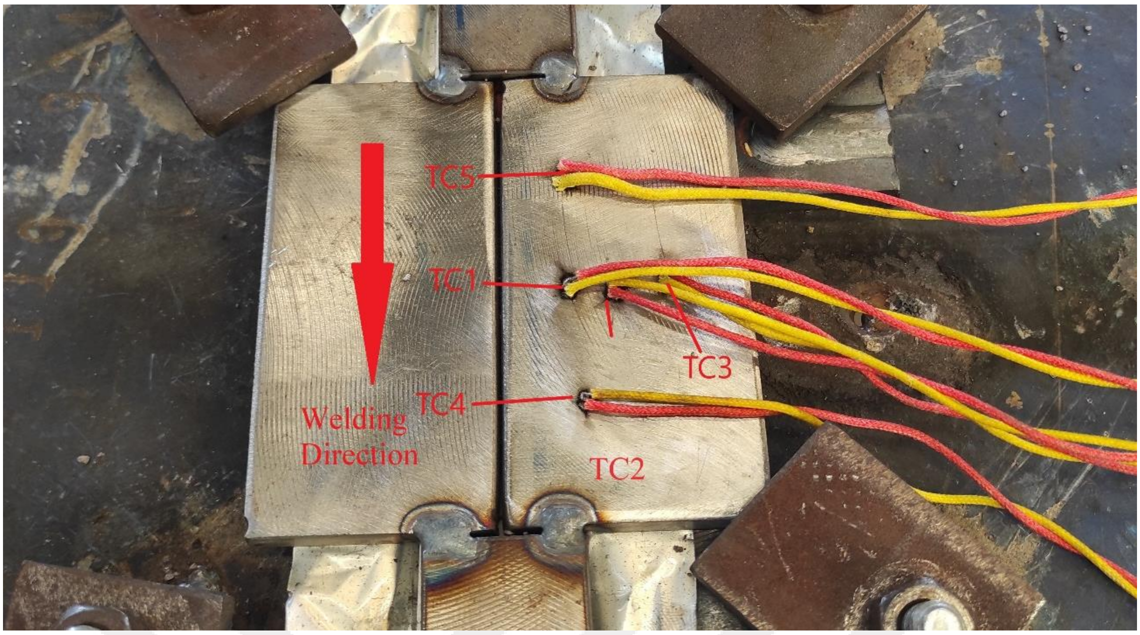

Figure 5.16. Photo of TC locations on work piece

5.1.3. Measurement of Residual Stress of Welded Part

Residual stresses of welded parts was measured at Marmara Research Center Tubitak by Panalytical X’Pert Pro MPD (shown in Figure 5.17 amd 5.18). Figure 5.19 and 5.20 show the points at which the residual stress was determined.

Figure 5.17. Panalytical X’Pert Pro MPD

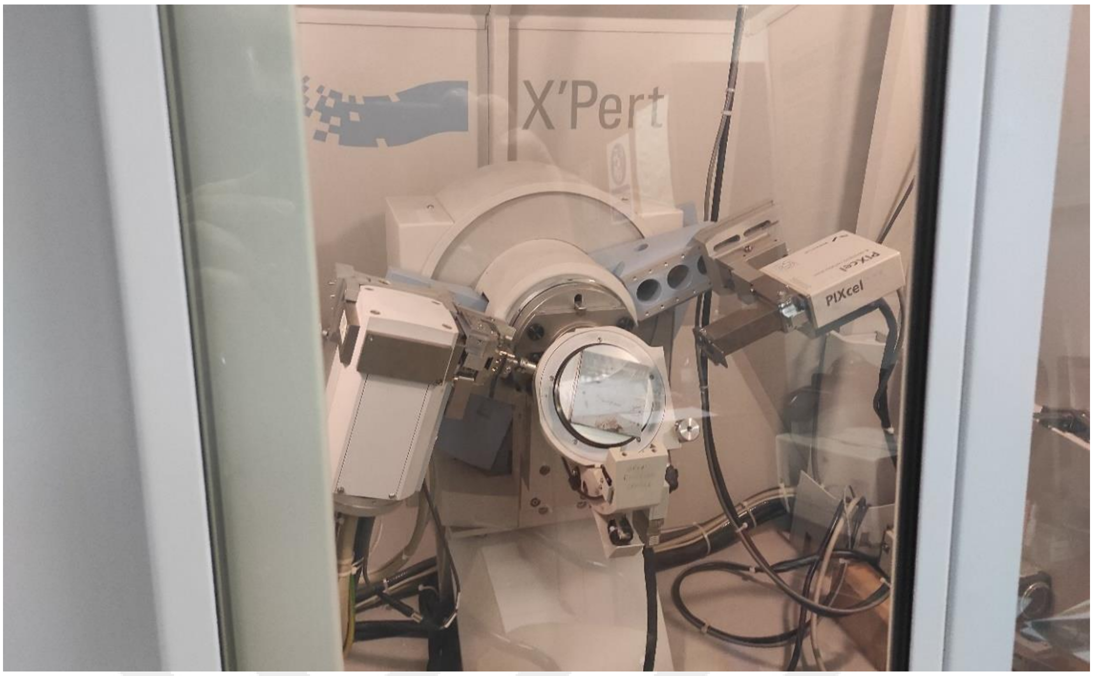

Figure 5.18. Meausring of residual stress on welded part

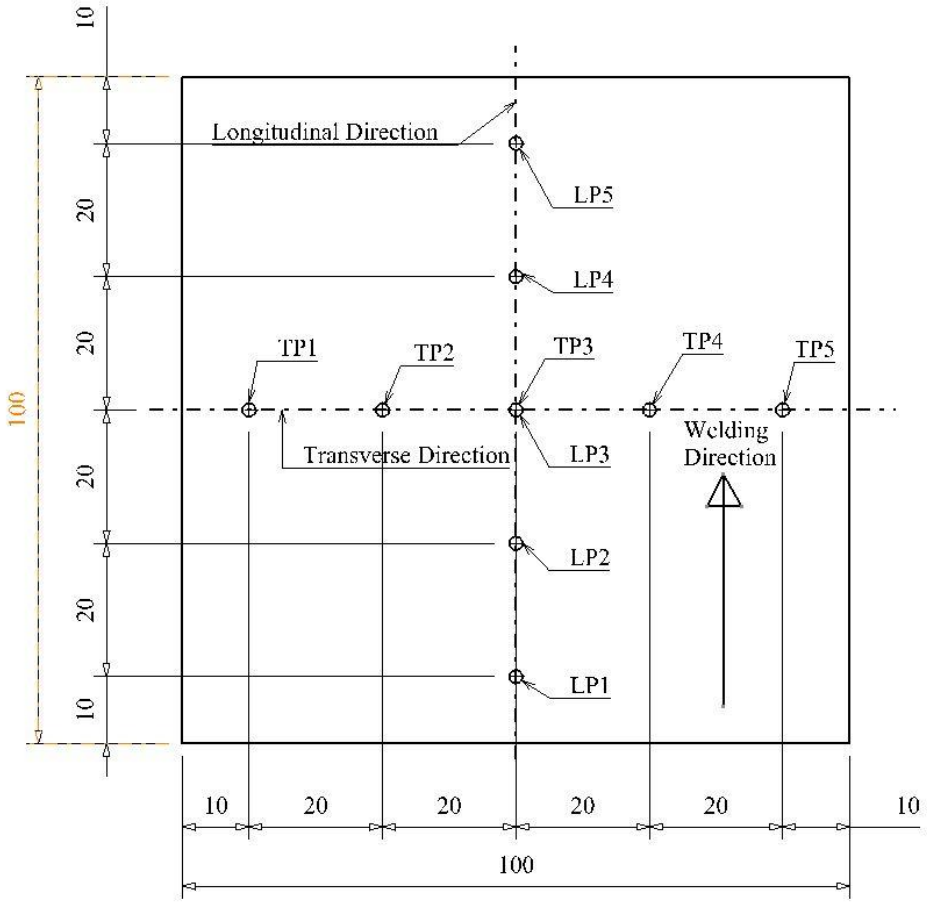

Figure 5.19. The location of points at which residual stress was determined

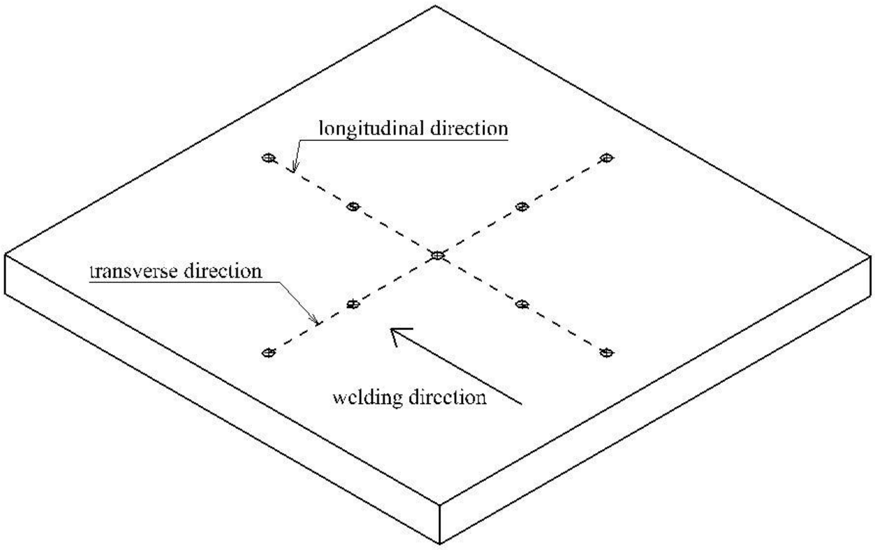

Figure 5.20. The layout of points at which residual stress was determined

5.2. Welding Simulation by FEM

The major goal of creating a FEA model is to be able to accurately anticipate the SAW thermal cycle and residual stress compared to experiment data. The numerical simulation of the welding process was performed in ANSYS 2020 R2 Workbench by dividing into two steps to get results, thermo-mechanical analysis (Transient thermal and Transient Structural analysis). Although temperature calculations are done in thermal analysis, calculating thermal strains requires a structural analysis. Thermal analysis and structural analysis are two steps sequentially followed in the solving process. A three-dimensional coupled thermo-mechanical analysis may be used to define the finite element analysis of the welding process. Pre-processing, solution, and post-processing make up the finite element analysis process in general. A 3D FE model of the welding is used, followed by a transient thermomechanical analysis, to forecast the residual stress. To determine the nodal transient temperatures, a first thermal analysis was conducted with the assumption that the heat source was of the Gaussian distributed kind. The flow diagram for the transient thermo-mechanical analysis model is shown in Figure 5.21. Using the findings from the transient heat transfer study, a nonlinear elasto-plastic analysis was conducted in the second section.

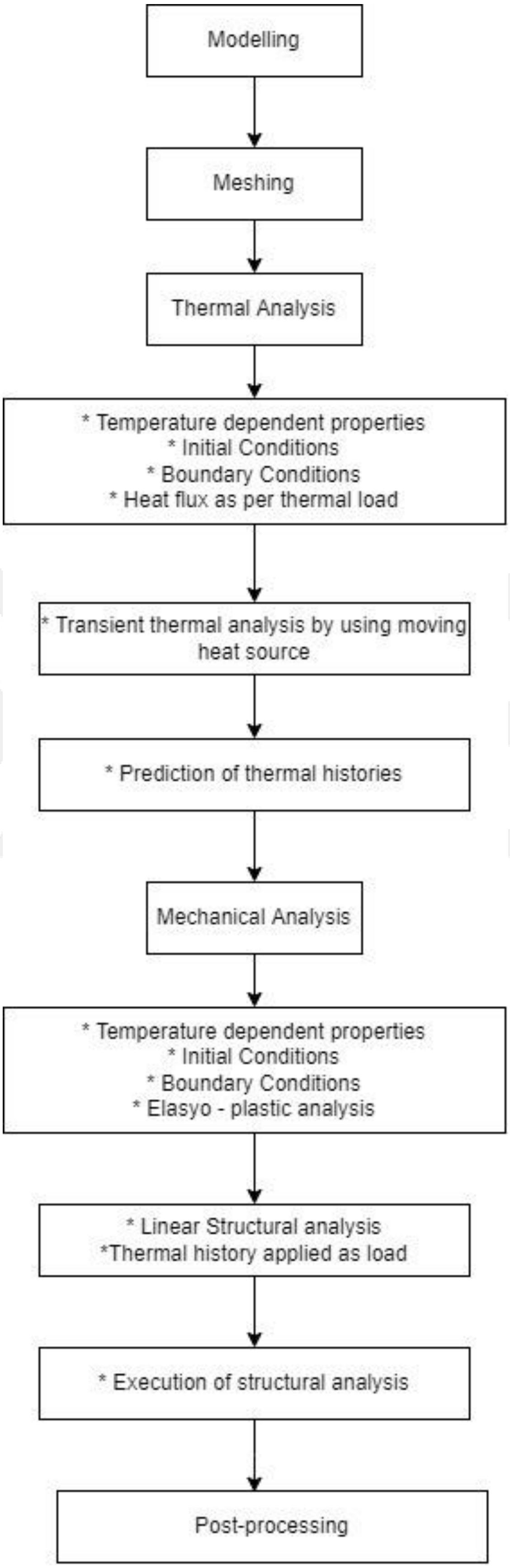

Figure 5.21. Flow diagram of transient thermo-mechanical analysis model

5.2.1. Material Properties

The material properties can be classified in two groups, thermal properties and physical properties of SA 387 GR 11 Class 2 steel. Thermal properties shown in Table 5.7 are thermal conductivity (W /m ºC), specific heat (J kg ºC) and physical properties shown Table in 5.8 are density ($kg/m^{3)}$, Elastisite modulus (GPa) and thermal expansion (W/m ºC). The material's characteristics were presumptively affected by temperature through cycles of heating and cooling. Accurate information on temperature-dependent material characteristics could not be found in the literature.

Table 5.7. Thermal properites of SA 387 Gr 11 Cl.2 (ASME BPVC.II.D.M-2021, 2021)

Temperature	Density	Thermal Conductivity	Specific heat
(ºC)	(kg/m^3)	(W/m-ºC)	(J/kg-ºC)
20	7750	41	470
100	7750	40,6	487
200	7750	40,1	529
300	7750	38,7	564
400	7750	36,8	605
500	7750	34,8	666
600	7750	32,8	760
700	7750	29,1	1008
800	7750	27,5	803
900	7750	24	650
1000	7750	20,1	650
1100	7750	15,8	650
1200	7750	11,1	650
1300	7750	6	650

Table 5.8. Physical properties of SA 387 Gr 11 Cl.2 (ASME BPVC.II.D.M-2021, 2021)

Temperature	Thermal Expansion	Young's modulus	Poisson ratio
(ºC)	(W/m-ºC)	(Pa)	-
20	$11,5x10^{-6}$	204	0,3
100	$12,1x10^{-6}$	200	0,31
200	$12,7x10^{-6}$	193	0,32
300	$13,3x10^{-6}$	186	0,33
400	$13,8x10^{-6}$	179	0,34
500	$14,4x10^{-6}$	169	0,35
600	$14,8x10^{-6}$	157	0,36
700	$15,1x10^{-6}$	142	0,37
800	$15,4x10^{-6}$	125	0,38
900	$15,9x10^{-6}$	108	0,39
1000	$16,1x10^{-6}$	90	0,40
1100	$16,3x10^{-6}$	69	0,41
1200	$16,4x10^{-6}$	48	0,42
1300	$16,4x10^{-6}$	24	0,43

The material properties of SA 387 were used as given by ASME Boiler and Pressure Vessel Code ASME BPVC.II.D.M-2021. The SA 387 GR 11 Class 2 material was considered 1 ¼ Cr – ½ Mo carbon – moly steels. Temperature dependent enthalpy is shown in Table 5.9 and temperature dependent yield strentgh and tangential modules is shown in Table 5.10.

Table 5.9. Temperature dependent enthalpy for steel

Temperature (ºC)	0	100	200	300	400	500	600	700	800	900	1000	>2500
Enthalpy (MJ/m³)	0	360	720	1100	1500	1980	2500	3000	3700	4500	5000	9000

Table 5.10. Temperature-dependent yield stress and Tangential modulus

Temperature	ºC	40	100	300	525	720	800
Yield Stress	MPa	310	290	256	201	10	10
Tangential Modulus	MPa	9,45	9	6,9	1,85	0,9	0,4

Unit system used in APDL commands and Workbench unit system should be the same. Otherwise APDL commands will not work. In this study Metric system was selected, kg., m., sn., ºC, V., A., and the parameters was written in these units in APDL Commands.

```
MKS UNITS SPECIFIED FOR INTERNAL
 LENGTH        (l)  = METER (M)
 MASS          (M)  = KILOGRAM (KG)
 TIME          (t)  = SECOND (SEC)
 TEMPERATURE   (T)  = CELSIUS (C)
 TOFFSET            = 273.0
 CHARGE        (Q)  = COULOMB
 FORCE         (f)  = NEWTON (N) (KG-M/SEC2)
 HEAT               = JOULE (N-M)

 PRESSURE           = PASCAL (NEWTON/M**2)
 ENERGY        (W)  = JOULE (N-M)
 POWER         (P)  = WATT (N-M/SEC)
 CURRENT       (i)  = AMPERE (COULOMBS/SEC)
 CAPACITANCE   (C)  = FARAD
 INDUCTANCE    (L)  = HENRY
 MAGNETIC FLUX      = WEBER
 RESISTANCE    (R)  = OHM
 ELECTRIC POTENTIAL = VOLT
```

Figure 5.22. Unit Sytem to be used in analysis

5.2.2. Modelling and Meshing

The engineering issue was resolved using a three-dimensional finite element model. Using SpaceClaim 2020 R2 and Ansys Mechanical Workbench, single-sided single-pass butt joints were developed and simulated using submerged arc welding. A model's accuracy is influenced by its element size, node count, and time step size. Not only does the number of nodes enhance the model's precision, but it also lengthens the model's computation time. Figure 5.25 and 5.27 show the model of test plate.

The element type in thermal analysis is SOLID90 and in structural analysis is SOLID186. The finite element model consists of 358743 nodes and 80800 elements with 0,001 m element size. More elements give more accurate results but significantly increase the computational time. Mesh model was shown in Figure 5.26 and 5.28.

The 3-D eight node thermal element (SOLID70) has a higher order variant called SOLID90 shown in Figure 5.23. The element has 20 nodes, each of which has just one degree of freedom—temperature. The 20-node elements are ideally suited to modeling curved boundaries since they have comparable temperature forms. The 20-node thermal element can be used in a 3-D, steady-state, or transient thermal investigation. The corresponding structural element, such as SOLID186, should be used in lieu of this element if the model containing it is also going to be subjected to structural analysis.

SOLID186 shown in Figure 5.24, a 20-node higher order 3-D solid element, exhibits quadratic displacement behaviour. The element is defined by twenty nodes, each having three degrees of freedom for translations in the nodal x, y, and z directions. The element supports capabilities for plasticity, hyperelasticity, creep, stress stiffening, large deflection, and huge strain. Additionally, it offers the capacity to use mixed formulations to simulate the deformation of completely incompressible hyperelastic materials as well as virtually incompressible elastoplastic materials.

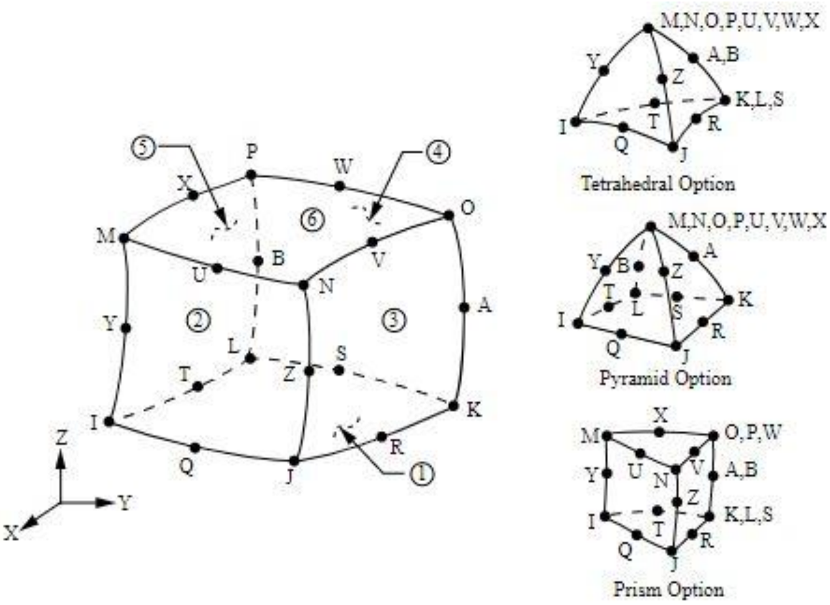

Figure 5.23. Geometry of SOLID90 Element

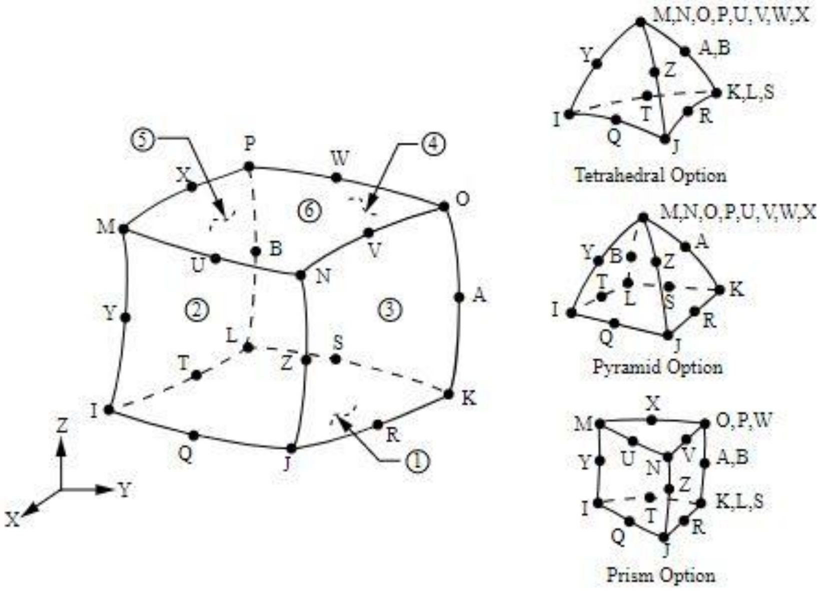

Figure 5.24. Geometry of SOLID186 Element

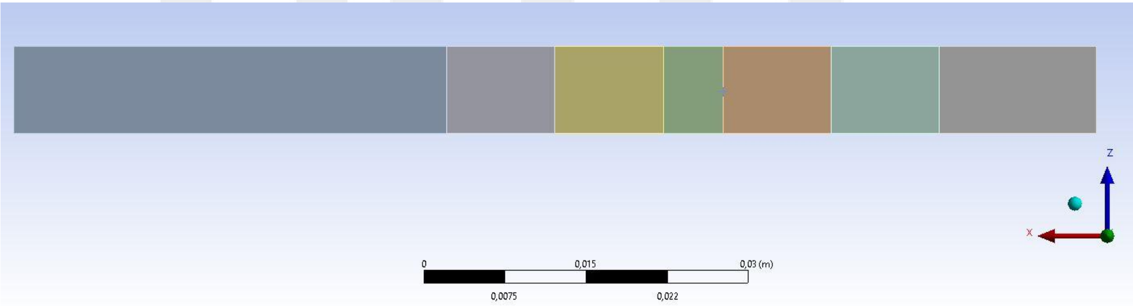

Figure 5.25. Finite Element Model Front view

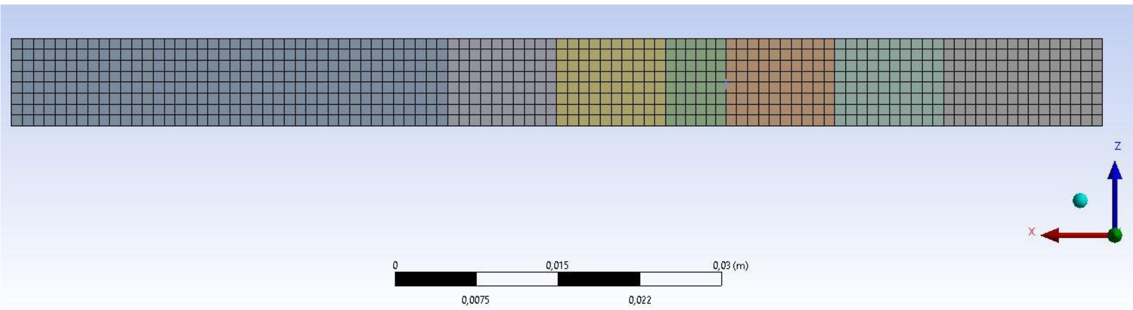

Figure 5.26. Mesh model front view

Mesh density (shown in Figure 5.26) is a crucial parameter for accuracy management. Accuracy is also impacted by element type and form. A high-density mess will provide findings with great precision, if there aren't any singularities. However, if a mesh is excessively thick, it will use a lot of memory and take a long time to execute, especially for multiple-iteration runs, which are characteristic in nonlinear and transient analysis.

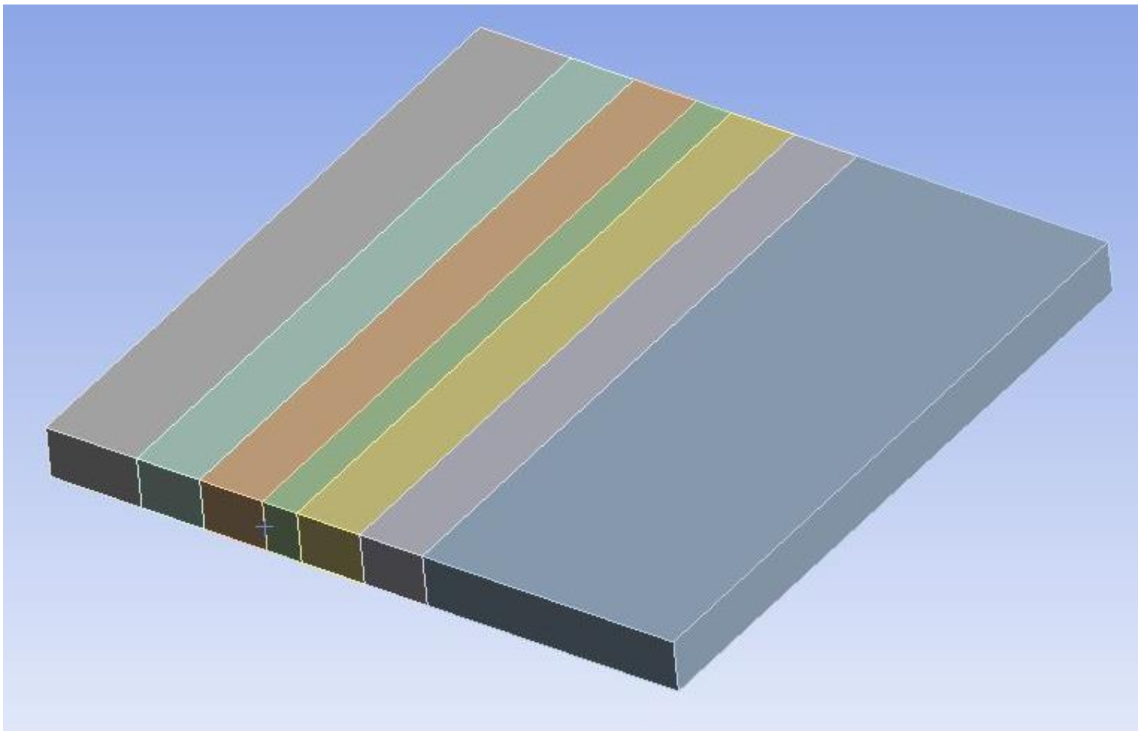

Figure 5.27. FE model isometric view

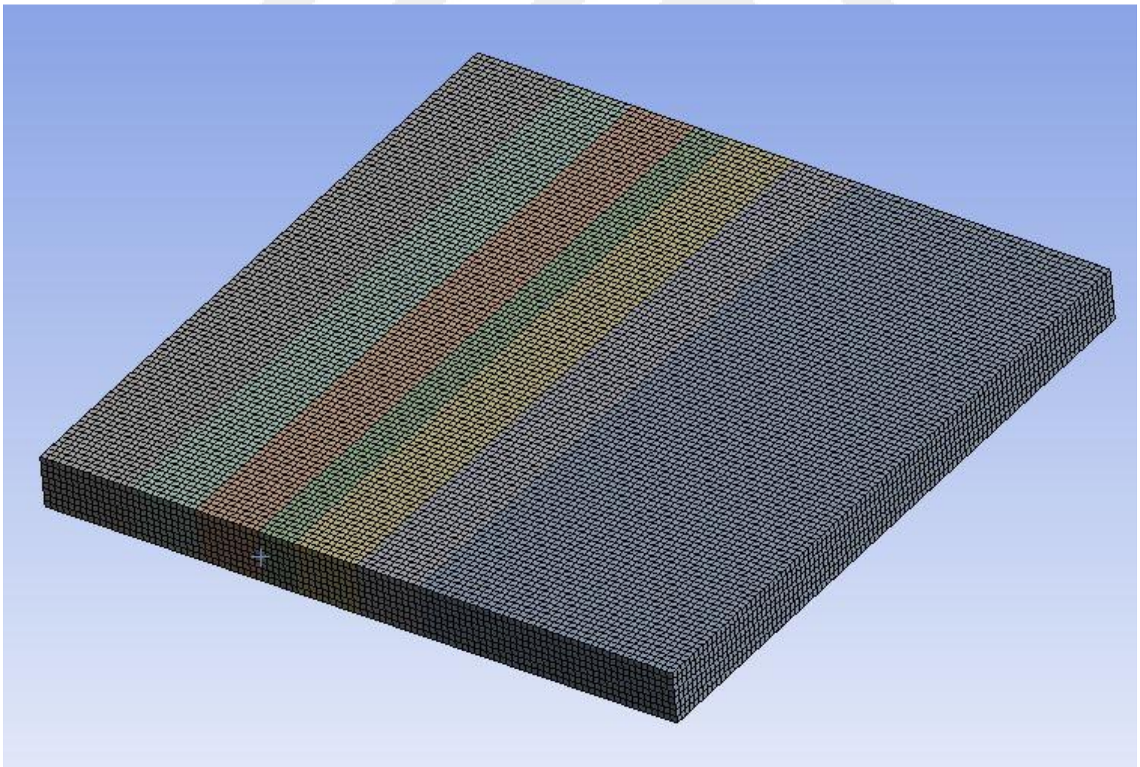

Figure 5.28. Mesh model isometric view

5.2.3. Thermal Model

The simulation's status in one potential design configuration is defined by boundary conditions, which are a collection of loads, limitations, and contact conditions. Before beginning to transient thermal and static structural analysis the set of boundary conditions should be applied on to the model with a sequence of experimental procedures. The set of loading and few constraints are in the form of mathematical expressions. For thermal analysis, the boundary conditions involves the convection and specific heat flux. For static structural analysis, it involves forces, moments and displacements (Kumar, 2020).

The heat flow at the weld is essential for melting. At the source, heat is emitted in significant amounts through radiation from the melt pool's surface and the high temperature area's surface. The material receives a significant amount of the heat needed for melting simultaneously through conduction and convection (Taskaya and et al., 2019).

Conduction, convection, and radiation (descriebed in Figure 5.29) are the three basic categories into which heat transmission techniques may typically be divided.

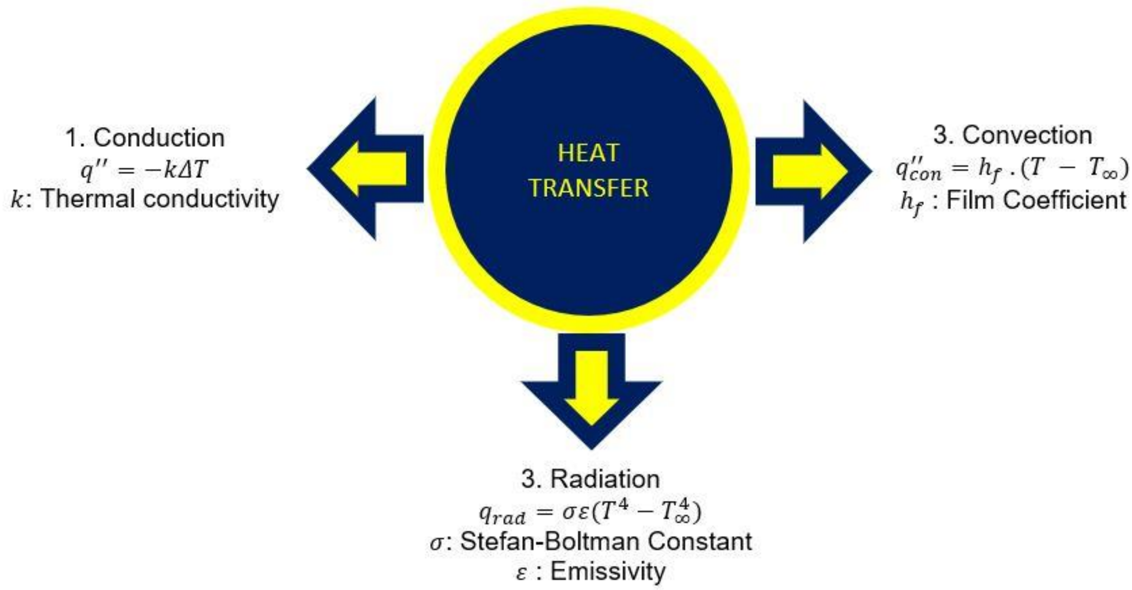

Figure 5.29. Basis of heat transfer during welding process

The thermal analysis's non-linear heat transfer equation establishes the welded portion's transient temperature field T as a function of time and the spatial coordinates (x, y);

$$\frac{\partial}{\partial x}\left(k_x \frac{\partial T}{\partial x}\right) + \frac{\partial}{\partial y}\left(k_y \frac{\partial T}{\partial y}\right) + q_{in} + q_{lat} = \rho c \frac{\partial T}{\partial t} \tag{5.4}$$

The rate of internal heat production is denoted by q_{in} the rate of latent heat generation is denoted by q_{lat}, the coefficients of thermal conduction in the x and y directions are denoted by k_x and k_y, respectively, the specific heat is denoted by c, and the density of the plate material is denoted by ρ. The model accounts for the latent heat produced during the phase shift. As a result, the enthalpy formulation is utilized since, aside from density and thermal conductivity, it contains all the additional information needed to compute the latent heat release (Nart et al., 2013).

The heat source is applied to the welded component to begin the heat transfer process between the welded part and its surroundings during welding, and as a result, both convection and radiation cooling occur. During the analysis, forced convection is not taken into account. Equations are provided below that show the heat flow caused by convection and radiation on the surfaces of the welded plate.

$$q_{con} = h\,(T - T_\infty) \tag{5.5}$$

$$q_{rad} = \varepsilon\sigma\,(T^4 - T_\infty^4) \tag{5.6}$$

Where (5,67 x 10-8 W/(m^2 ºC^{-4}) is the Stefan-Boltzmann constant, T_∞ is the ambient temperature, T is the boundary temperature exposed to the environment, ε is the emissivity. All of the plate's surfaces, save the top surface, have a convection coefficient of h = 100 W/ m^2. When the torch is directly on the surface, it is believed that the top surface immediately beneath the welding arc is insulated (Nart et al., 2013). The base metal's temperature-dependent thermal characteristics are taken into account in every analysis. The model is developed under the following presumptions as shown in Figure 5.30:

1. The test plate’s beginning temperature is 150 ºC and the weldments’ ambient temperature is 25 ºC.
2. The material’s thermal characteristics are temperature-dependent (like specific heat and conductivity)

3. Material's physical characteristics, such as Elastisite Moduli abd thermal expansion are temperature-dependent.
4. Density is constant 7750 kg/m3 and Poisson ratio is 0,3.
5. Considered the convection heat transfer coefficient is as 5 W/m^{2}°C.
6. The emissivity of radiation is assumed as 0,90.
7. It was thought that the welded part's top face was properly insulated.

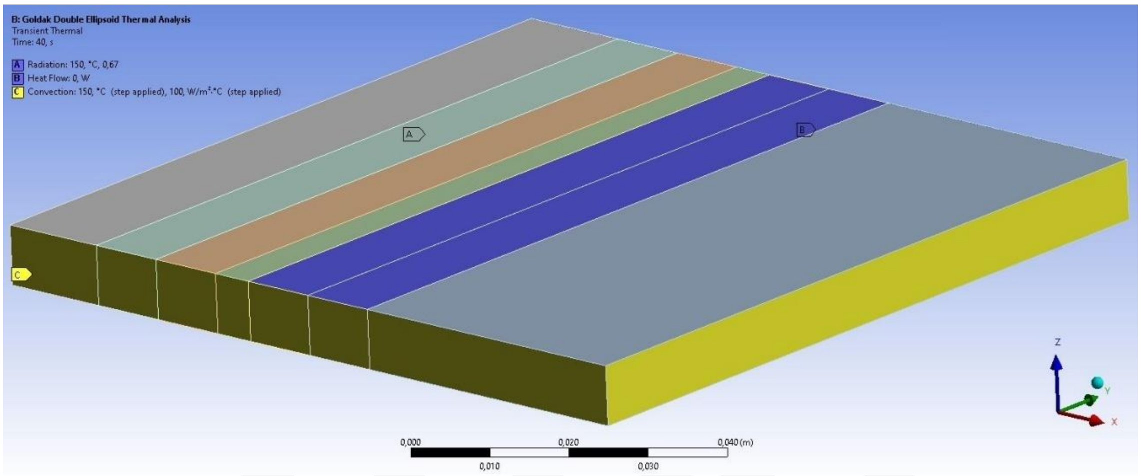

Figure 5.30. Boundary conditions for transient thermal analysis

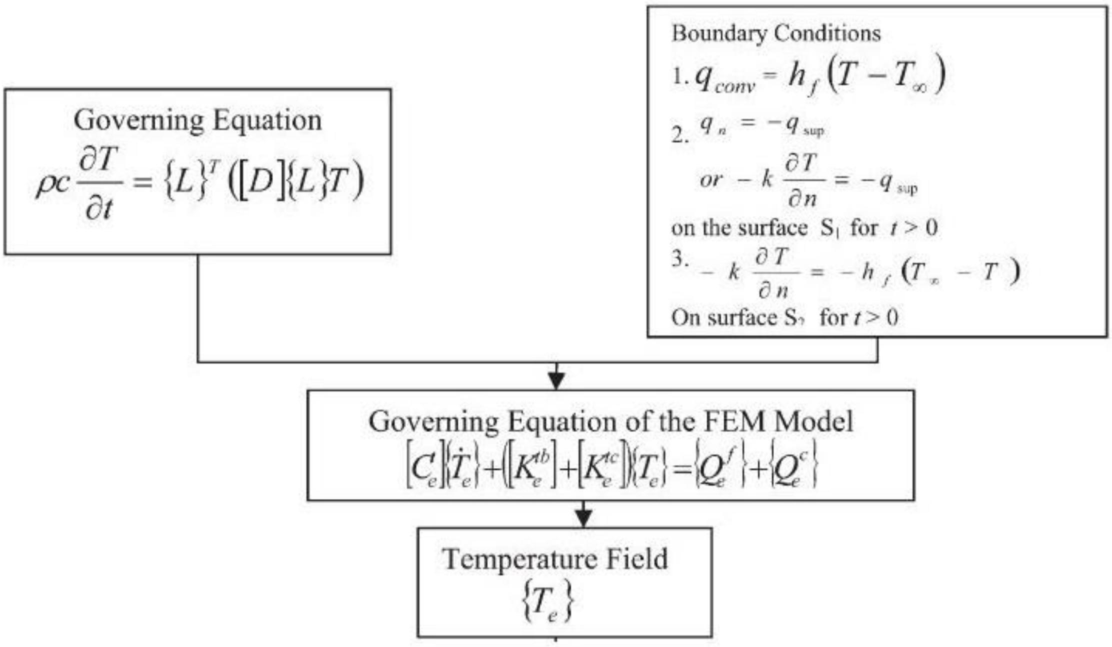

Figure 5.31. Flow diagram for thermal analysis (Biswas et.al., 2009)

5.2.4. Structural Model

To examine the precise residual stress and strain distributions around the weld bead as well as the transverse distortion of the welded component, the structural analysis should employ the same mesh as was used in the thermal analysis. The results of the transient heat transfer study were used in the second portion of the nonlinear elasto-plastic analysis. Figure 5.32 depicts the flow diagram of the FE mechanical analysis model for forecasting residual stresses.

Von-Mises yield criteria and related flow rules were utilised in this investigation. The models depicted in Figures 5.36 and 5.37 took rigid body boundary conditions into account. The uniform meshing was considered throughout the whole piece. The minimum element was used as 1 x 1 x 1 mm^3.

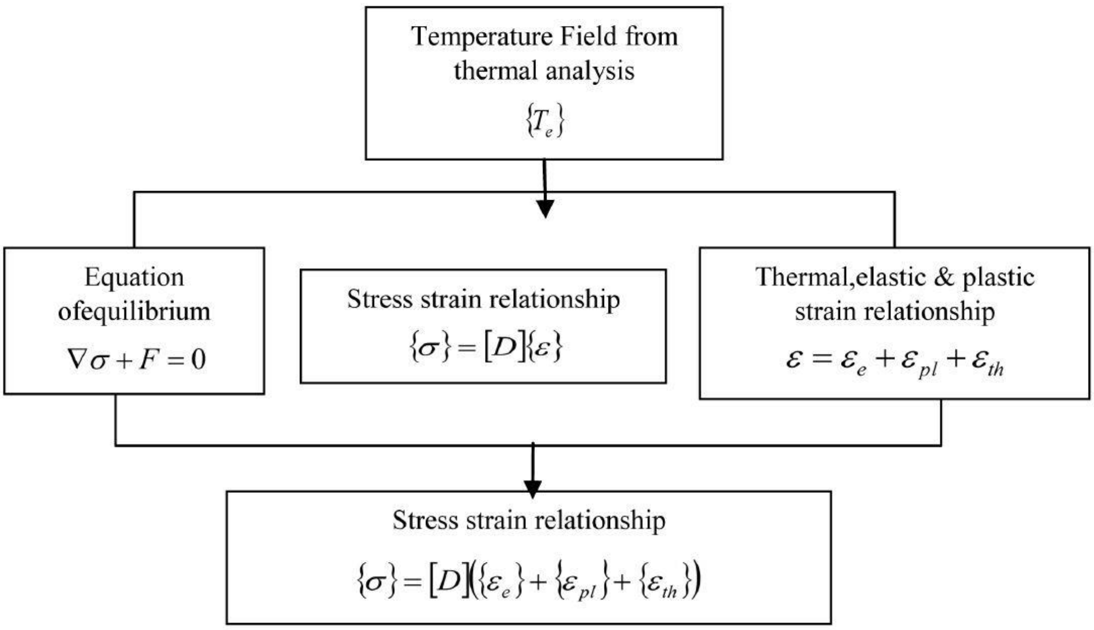

Figure 5.32. Flow chart for predicting of residual stresses (Mondal at al., 2017)

The main causes of stress distortions in welds are thermally induced expansion and contraction as well as phase transformation-driven volume change. The residual stresses are estimated using the temperature distribution identified by thermal analysis as input data. Examples of material properties include Young's modulus, yield strength, Poisson's ratio, and thermal expansion coefficient. Equation 5.7 illustrates how utilising the properties of the elastic-plastic material, the total strain in the SAW weld can be divided into three components.

$$\varepsilon = \varepsilon^{e} + \varepsilon^{p} + \varepsilon^{t} \tag{5.7}$$

Where the letters ε^e, ε^p, ε^t stand for elastic, plastic, and thermal strains, respectively. The isotropic Hooke's law, along with a temperature-dependent Young's modulus and Poison's ratio, is used to simulate elastic strain. The thermal strain is calculated using the temperature-dependent coefficient of thermal expansion. The plastic strain is accounted for using a plastic model with the von Mises yield requirements, temperature-dependent mechanical properties, and a bilinear isotropic hardening model. The bilinear isotropic hardening model attributes the tangent modulus, yield stress, and linear area to the post-yielding plastic part of the curve.

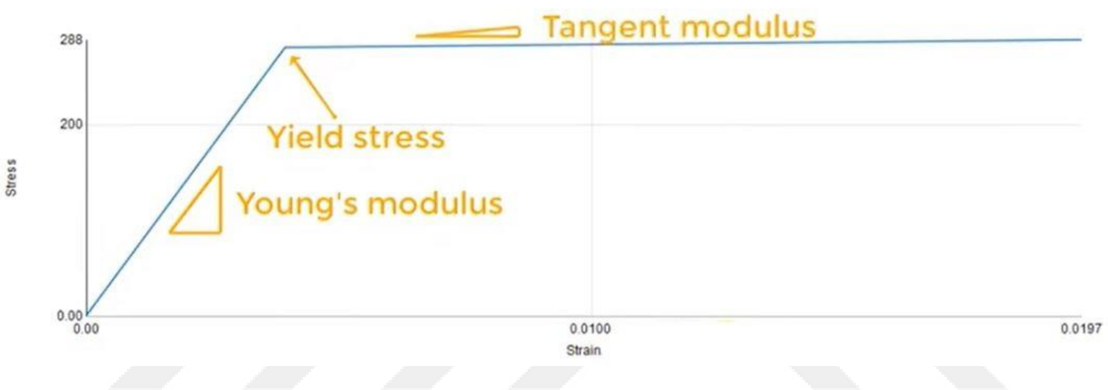

Figure 5.33. Bilinear isotropic model

As shown in Figure 5.36 comprasion support boundary condition is applied to the surface to where the fixture is contacted and for the bottom surface of the test place u_x, u_y and u_z displacement are applied as 0 mm as shown in Figure 5.34, also this surface was assumend as no any movement through x-y and z directions.

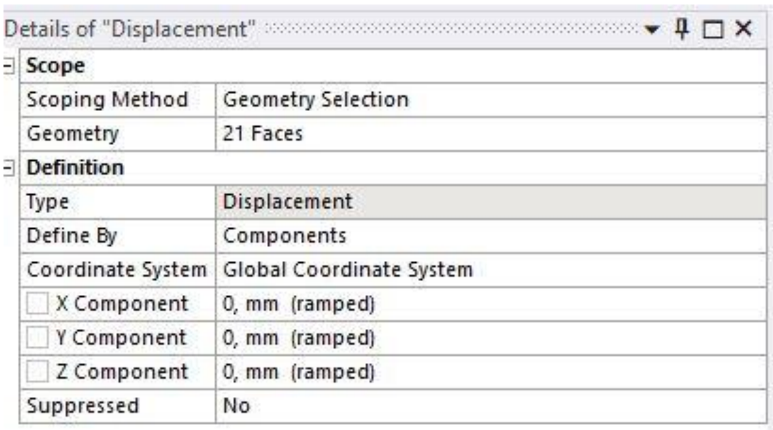

Details of "Displacement"

Scope	
Scoping Method	Geometry Selection
Geometry	21 Faces
Definition	
Type	Displacement
Define By	Components
Coordinate System	Global Coordinate System
X Component	0, mm (ramped)
Y Component	0, mm (ramped)
Z Component	0, mm (ramped)
Suppressed	No

Figure 5.34 Details of displacement boundary condition

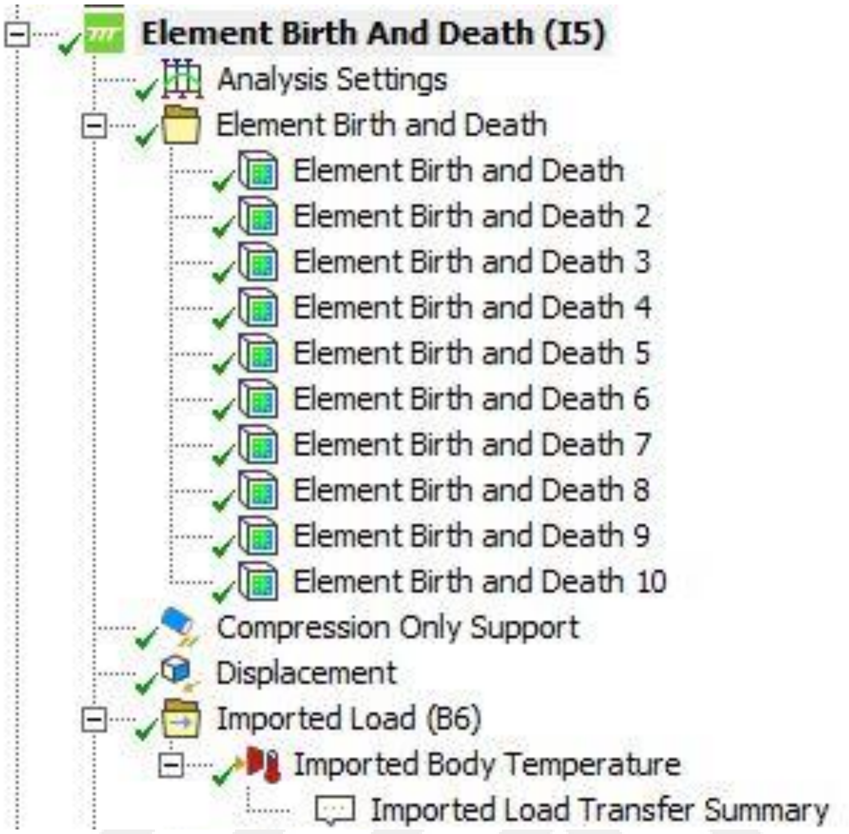

Figure 5.35. Boundary Conditions.

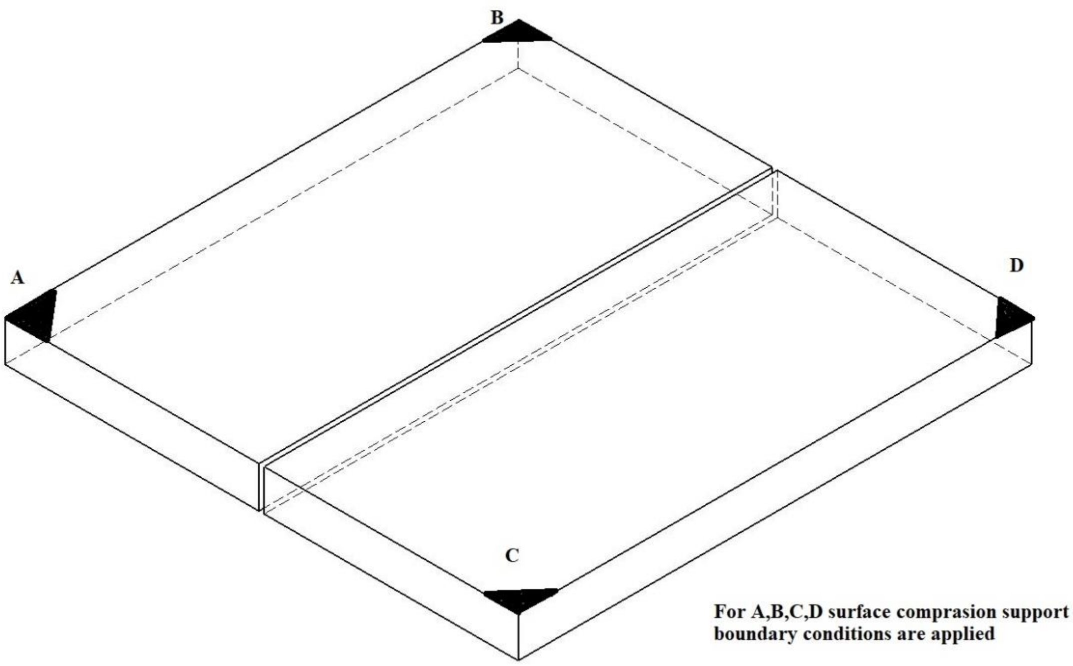

Figure 5.36. Rigid body boundary conditions

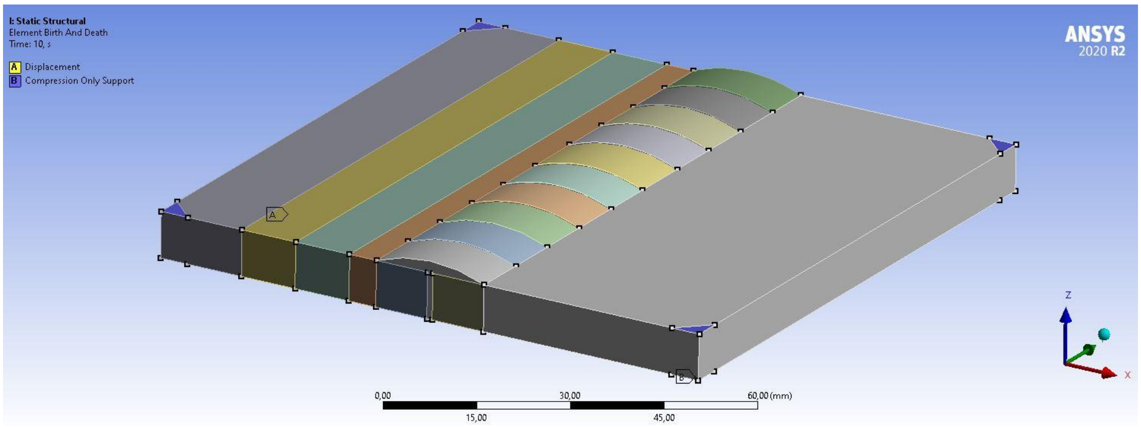

Figure 5.37. Boundary conditions for transient structural analysis

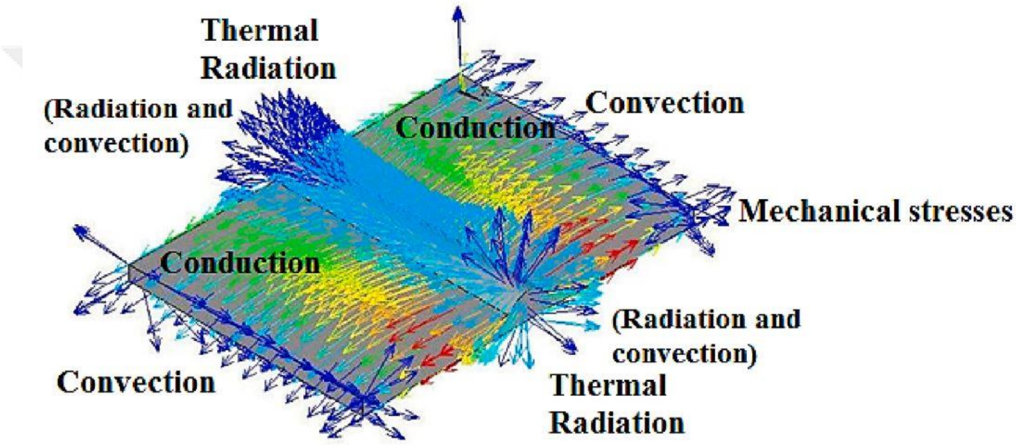

Figure 5.38. Thermo-mechanical transfer mechanism of welding (Taskata and et al., 2019)

Details of "Analysis Settings"

Step Controls	
Number Of Steps	12,
Current Step Number	10,
Step End Time	10, s
Auto Time Stepping	On
Define By	Substeps
Carry Over Time Step	Off
Initial Substeps	250,
Minimum Substeps	50,
Maximum Substeps	10000
Solver Controls	
Solver Type	Iterative
Weak Springs	On
Spring Stiffness	Program Controlled
Solver Pivot Checking	Program Controlled
Large Deflection	On

Figure 5.39. Details of Analysis Settings.

It is specified 250 initial subsequents 50 for the minimum and 10.000 for the maximum as shown Figure 5.39.

5.2.5. Heat Source Model

A unique transient thermal process involves simulating a moving heat source. Using Parametric Design Language (APDL) codes, ANSYS 2020 R2 simulates the moving heat source. The general-purpose finite element solver known as Ansys Mechanical APDL is used to run a variety of simulations, including stress analysis, spectrum analysis, vibro-acoustics, and even heat transfer analysis. It is intended to move continuously at each brief interval. The heat energy remains constant while the heat source is in motion, although the centre of the source occasionally shifts. The idea is to gradually alter the parameters of the function that models the locations of the heat source.

The Goldak's Double Ellipsoidal Heat Source Model describes the production of the heat flux/torch in the Submerged Arc Welding (SAW) in order to construct the temperature distribution in the analysis.

A created model's power density is dispersed throughout a volume and across the front and back quadrants of the heat source.

$$q\ (x, y, z) = \frac{6 * (\sqrt{3}) * f * \eta * Q}{a * b * c * \pi * \sqrt{\pi}} \exp\left(-\frac{3x^2}{a^2} - \frac{3y^2}{b^2} - \frac{3z^2}{c^2}\right) \tag{5.8}$$

The heat flux equation for the welding arc in the front quadrant of the heat source model is given as follows:

$$q\ (x, y, z) = \frac{6 * (\sqrt{3}) * f_f * \eta * Q}{a * b * c * \pi * \sqrt{\pi}} \exp\left(-\frac{3x^2}{a^2} - \frac{3y^2}{b^2} - \frac{3z^2}{c_f^2}\right) \tag{5.9}$$

The following is a description of the heat flux equation for the heat source model/welding arc in the back quadrant:

$$q\ (x, y, z) = \frac{6 * (\sqrt{3}) * f_r * \eta * Q}{a * b * c * \pi * \sqrt{\pi}} \exp\left(-\frac{3x^2}{a^2} - \frac{3y^2}{b^2} - \frac{3z^2}{c_r^2}\right) \tag{5.10}$$

a, b,c_f and c_r are the geometric parameters, c_r and cf are rear and front semi ellipsoidal heat source dimensions, f_r and f_f are fraction of heat deposited represent the rear and front quadrants heat apportionments of the heat flux, f_f + f_r=2. Q is the heat input. x, y, z are the coordinates of the heat flux. ɳ is the efficiency of the welding process (Goldak et al., 1984).

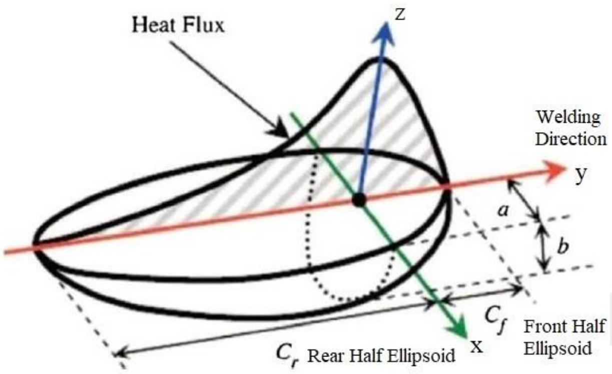

Figure 5.40. Double-ellipsoidal distributed heat source (Goldak et al, 1984)

The Goldak's double-ellipsoidal is used to define volumetric heat flux in the Arc welding process. It is the most famous and widely used model fır simulating the arc welding process. To define Goldak's double ellipsoid model in Ansys APDL commands should be used.

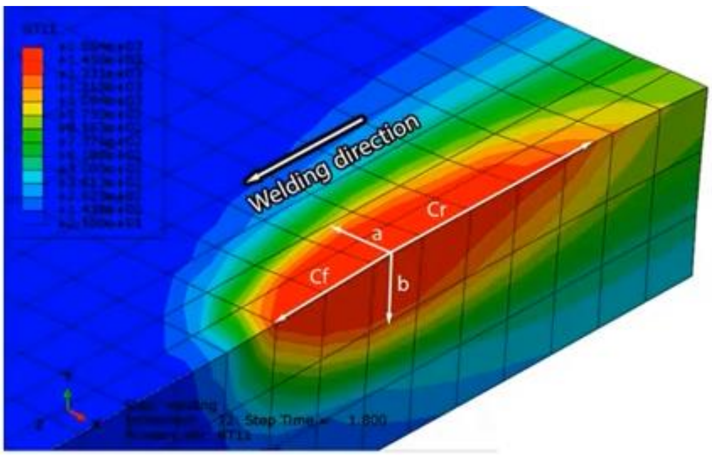

Figure 5.41. Goldak's double ellipsoidal parameters

f_f and f_r parameters are calculated using these formulas;

$$f_f = \frac{2 * c_f}{c_f + c_r} \tag{5.11}$$

$$f_r = \frac{2 * c_r}{c_f + c_r} \quad (5.12)$$

$$f_f + f_r = 2 \quad (5.13)$$

The energy input rate Q (I = 600 A, V = 31, ɳ= 0.95) and welding speed (Q = 0.01 m/s) in the experiment employed in this investigation.

Heat source parameters were determined by looking at the weld portion and the cross-section in Figure 5.42, 5.43, 5.44, and they were determined to be a = 10, b = 8, cr = 10, cf = 3 x cr = 30, ff = 0, and fr = 1.5.

Table 5.11. Goldak model parameters used in FE Analysis (mm.)

Goldak Parameters	a	b	c_f	c_r	f_f	f_r	q
Weld reinforcement	10	8	10	30	0.5	1.5	0.35VI
Fusion Zone	10	2	10	30	0.5	1.5	0.35VI

Table 5.12. Welding Parameters used in SAW

Power A	Voltage V	Heat Input Q=I*V*ɳ W	Progression Speed mm/sec
600	31	17670	10

Table 5.13. The efficiency of welding processes

Welding Process	GTAW Ar, Steel	GTAW He, Al	GTAW Ar, Al	SMAW Stell	GMAW Ar, Steel	SAW Steel
ɳ	25-75 %	55-80 %	22-46 %	66-85 %	66-70 %	91-99 %

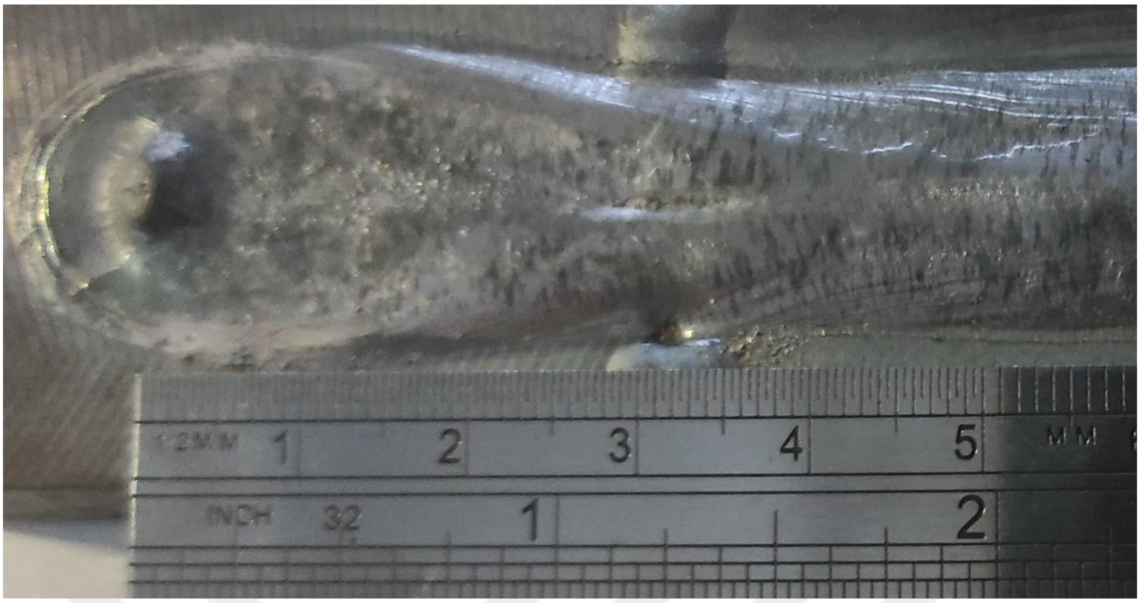

Figure 5.42. Goldak’s double elipsoidal parameters view on test plate

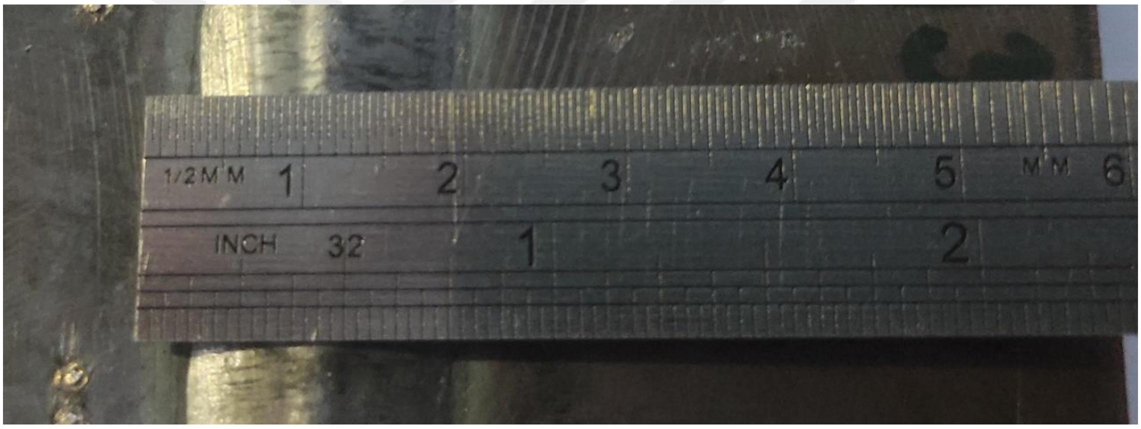

Figure 5.43. Goldak’s double elipsoidal parameters view on test plate

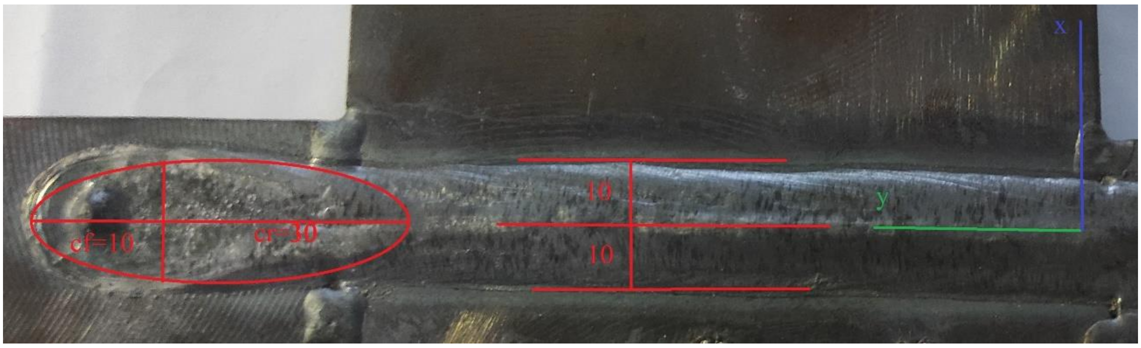

Figure 5.44. Goldak’s double elipsoidal parameters view on test plate

5.2.6. Element of Birth and Death Technique

Elements of birth and death have been used in this study to approximate the injection of filler metal during the welding process. This approach multiplies the stiffness by a very tiny amount in the order of 10-6 rather than killing or deleting the element. The components along the weld centerline are first killed or deactivated during the simulation of the structural model. Depending on the movement of the source, they are either triggered or born later at the chosen moment.

Test plate was 100 mm long and the welding speed was 10 mm/sec. So in the Ansys Mechanical the test plate was divided into 10 pieces which is 10 mm long as shown in Figure 5.45. This pieces with 10 mm long was activated at 1 second intervals.

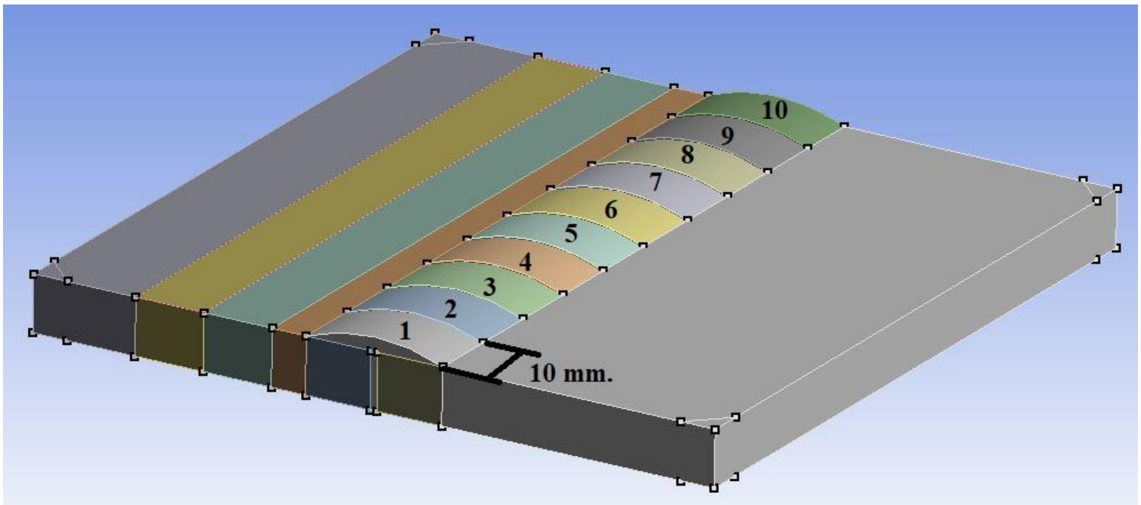

Figure 5.45. Pieces divided 10 mm long.

6. RESULTS AND DISCUSSION

The main aim of this study is to develop a 3D-FEA model which can predict the SAW thermal cycle, residual stresses and distortion with higher accuracy compare to the experimental work. The transient thermal and structural analysis were performed by using ANSYS 2020 R2 Software. The 3D FE model was carried out using Intel(R) Core (TM) i7-10750H CPU @ 2.60GHz with 16 GB ram. The CPU time needed for thermal analysis is about 20 hours and for structural analysis is about 2,5 hours.

The predicted temperatures, residual stresses and distortion were compared with temperatures residual stresses and distortions obtained from experiments.

(a) (b)

Figure 6.1. (a) The top view (b) the bottom view of specimens welded with 430 A, 530 A and 560 A respectively

Firstly, it was aimed to determine the most suitable Amper value in order to weld SA 387 GR 11 Cl 2 material with 8 mm thickness and some tests were carried out by changing the amperage value while keeping the voltage and welding speed values constant. At the values 430, 530 and 560 the penetration of the welding flux to underside of the part was low as seen Figure 6.1.

At 600 amper welding flux was provided as seen Figure 6.3. In some experiments, there were cases where complete penetration could not be achieved due to flux entering root gap as shown in Figure 6.2.

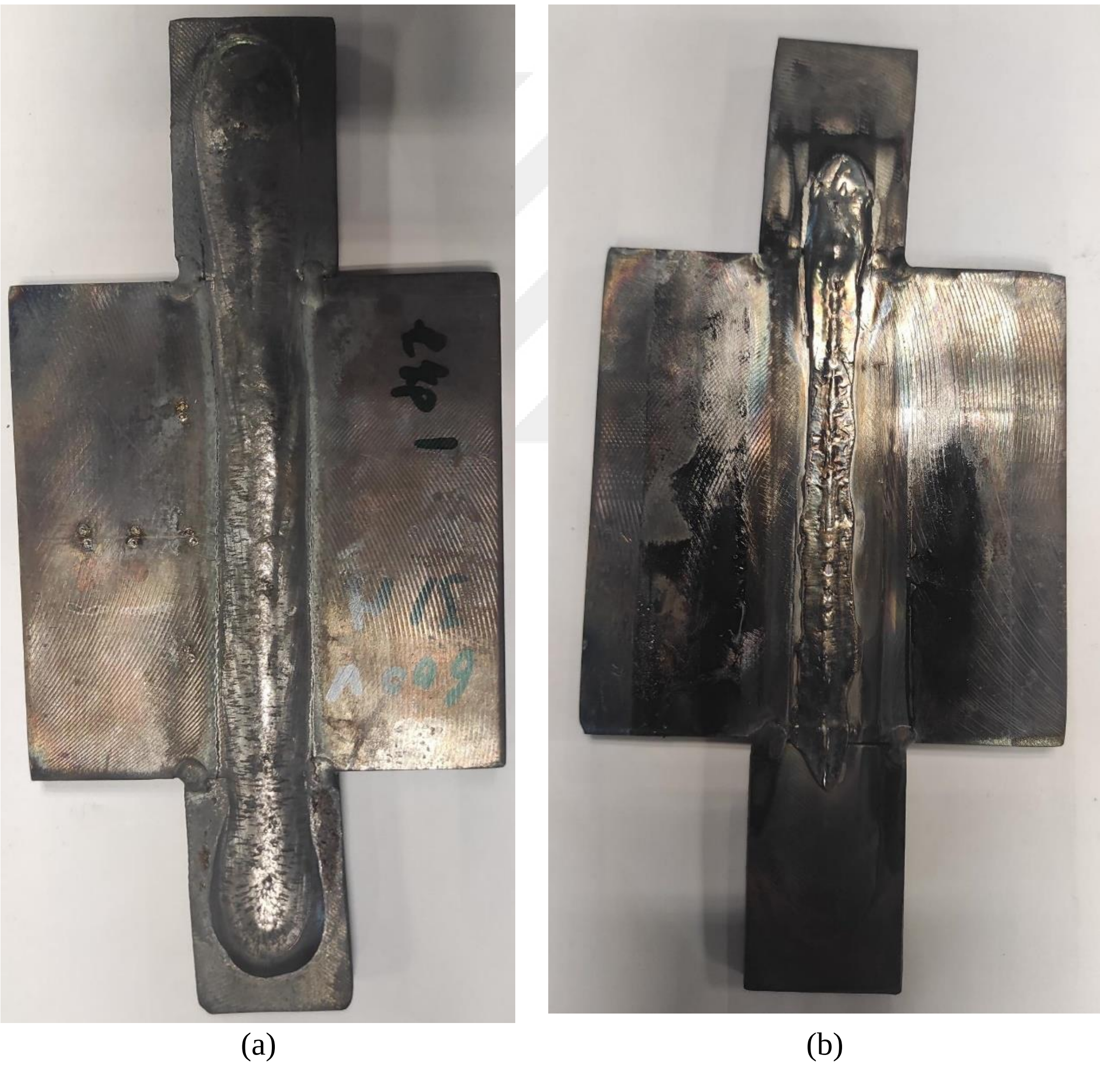

(a) (b)

Figure 6.2. (a) Top face of the welded part (b) bottom face of the welded part

(a) (b)

Figure 6.3. (a) the top face of welded part (b) the bottom face of welded part

6.1. Thermal Analysis

Thermal cycles were obtained at certain measuring places on the surface of the welded sheets based on an experimental test that was conducted. The acquired findings were contrasted with those from FEM modelling on a shared graph.

The heat source fitting process used a bead-on-plate weld with the same heat input characteristics as the plate for the butt joint weld. The butt joint plate was subjected to a transient thermal analysis employing a heat source fitting as an input. Figures 5.15 and 5.16 illustrate the temperature distribution along the weld line at the top of the weld joint for various locations. Temperatures measured by TC were recorded by Honeywell eztrend digital redorder and these temperature values can be monitored by Trendviewer application. In experiments, for measuring temperature distribution chrome/nickel aliminum termocouples with 0,71 mm diameter were used tom record the temperature history durimg welding process by using Honeywell eztrend temperature recorder and the temperature data recorded by Honeywell recorders was exported to Excel.

Figure 6.2, 6.3, 6.4, 6.5, 6.6, 6.7, 6.8, 6.9, 6.10, 6.11, 6.12, 6.13 show thermal field at different times during FE analysis and Figure 6.14 and 6.15 show the temperature values obtained from experiment and temperature values obtained from FE Analysis. Each TC value obtained from experiment was compared with the temperature value which is at the corresponding node in FEA in separate graphs Figure 6.16, 6.17, 6.17, 6.19, 6.20. The sample part was welded at approximately 150 ºC preheat temperature. At the beginning of welding the temperature of TC's (TC1, TC2, TC3, TC4, TC5) were 129.4, 158.7, 157.2, 139, 153.1ºC respectively. Prior the welding the heating elemets were taken from the part. For that reason a drop in temperature occured on the part.

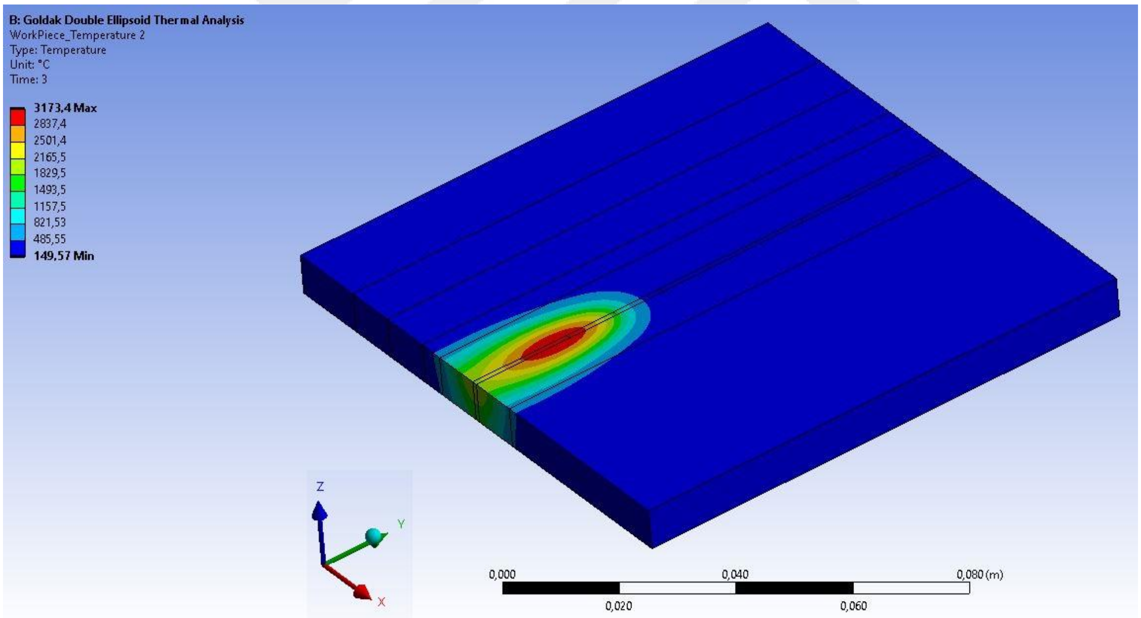

Figure 6.4. Isometric view of moving heat source after 3 seconds

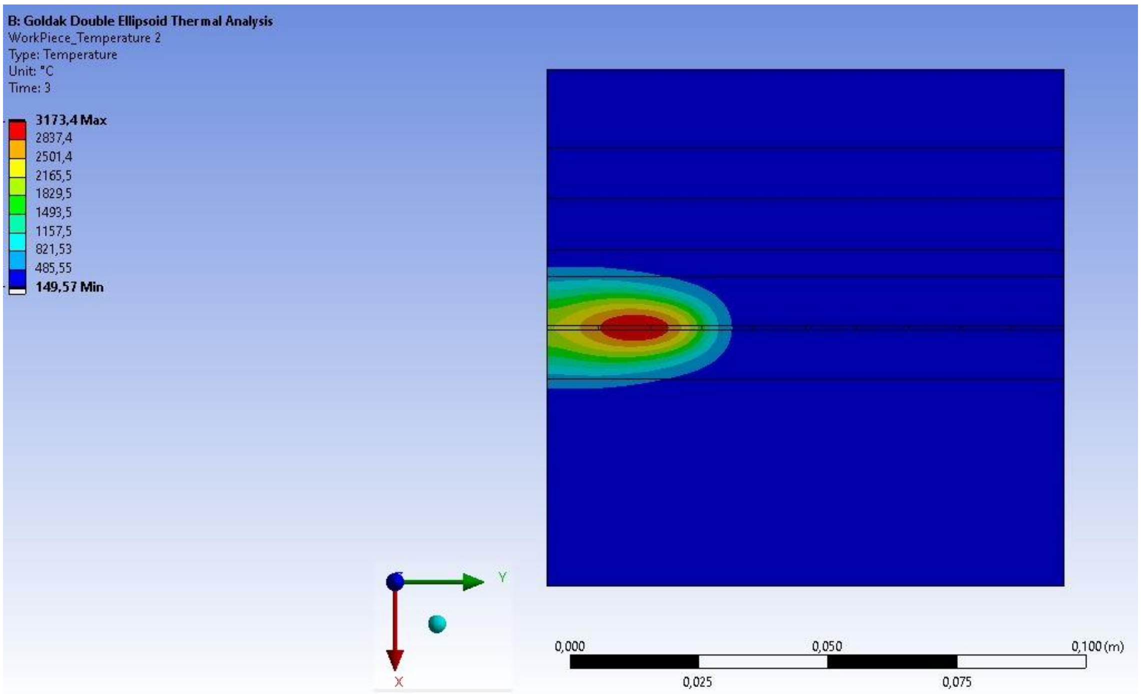

Figure 6.5. Top view of temperature distribution after 3 seconds

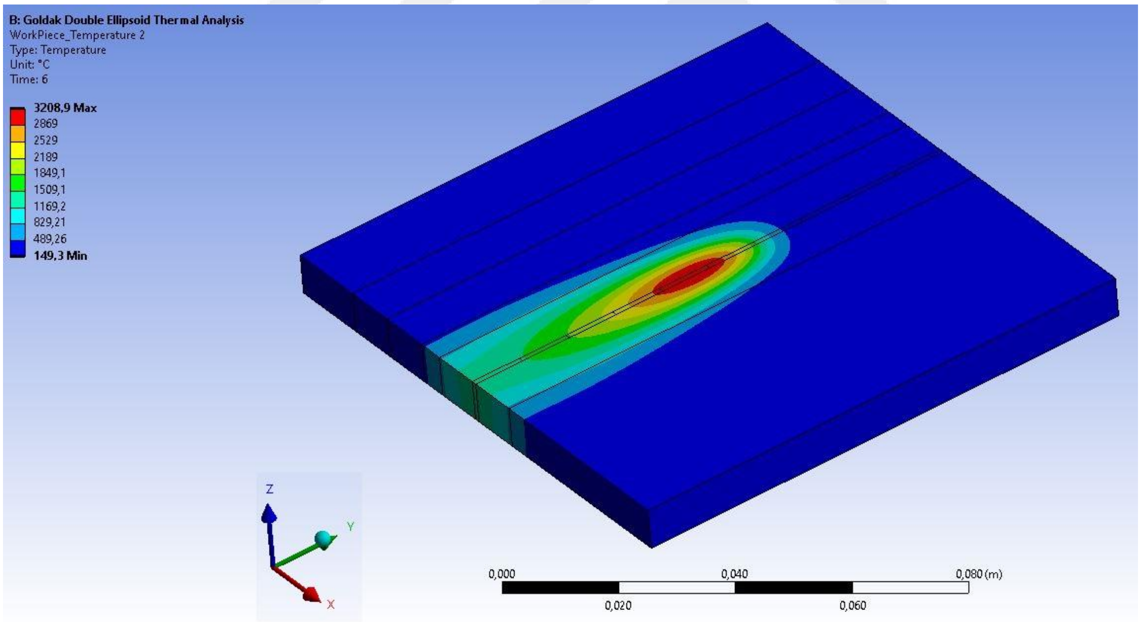

Figure 6.6. Isometric view of temperature distribution after 6 seconds

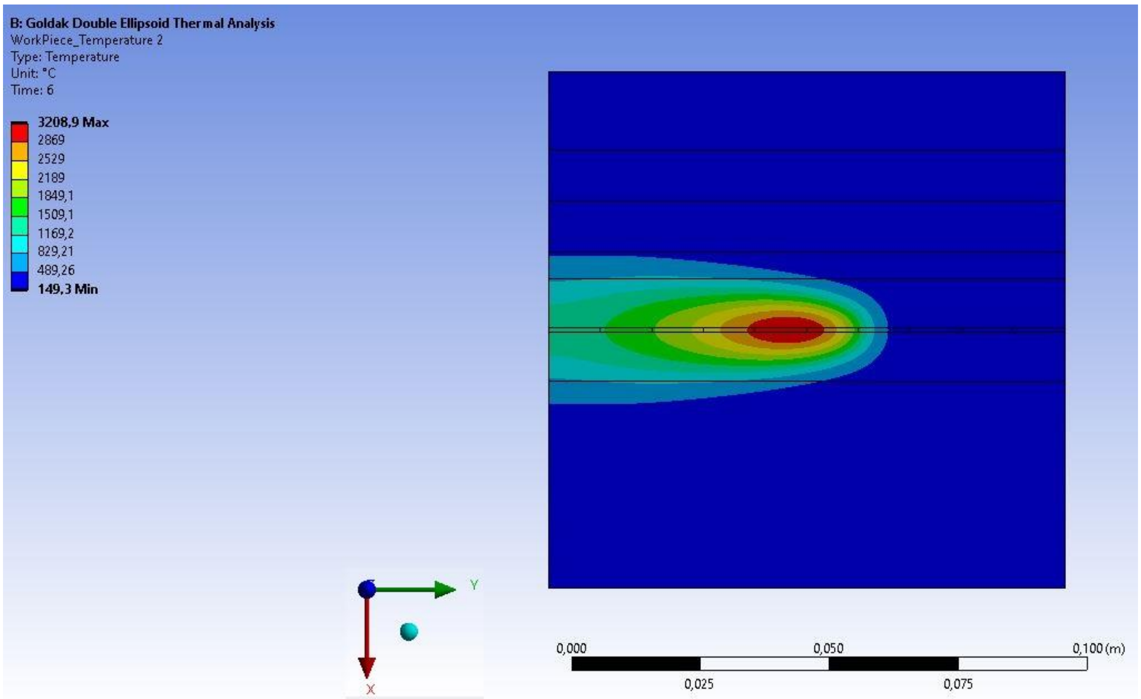

Figure 6.7. Top view of temperature distribution after 6 seconds

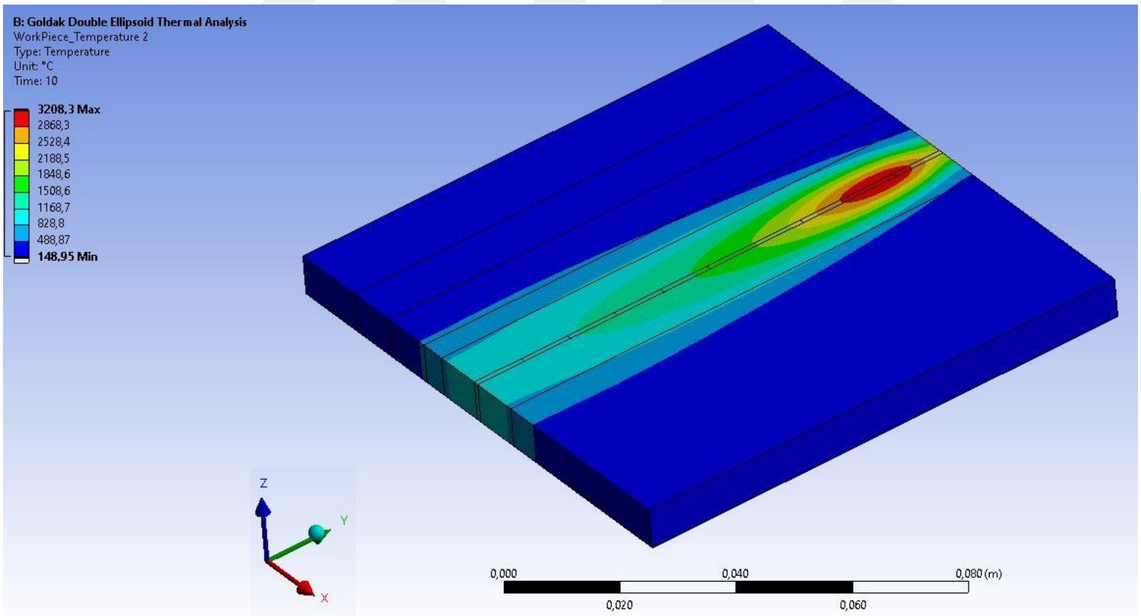

Figure 6.8. Isometric view of moving heat source after 10 seconds

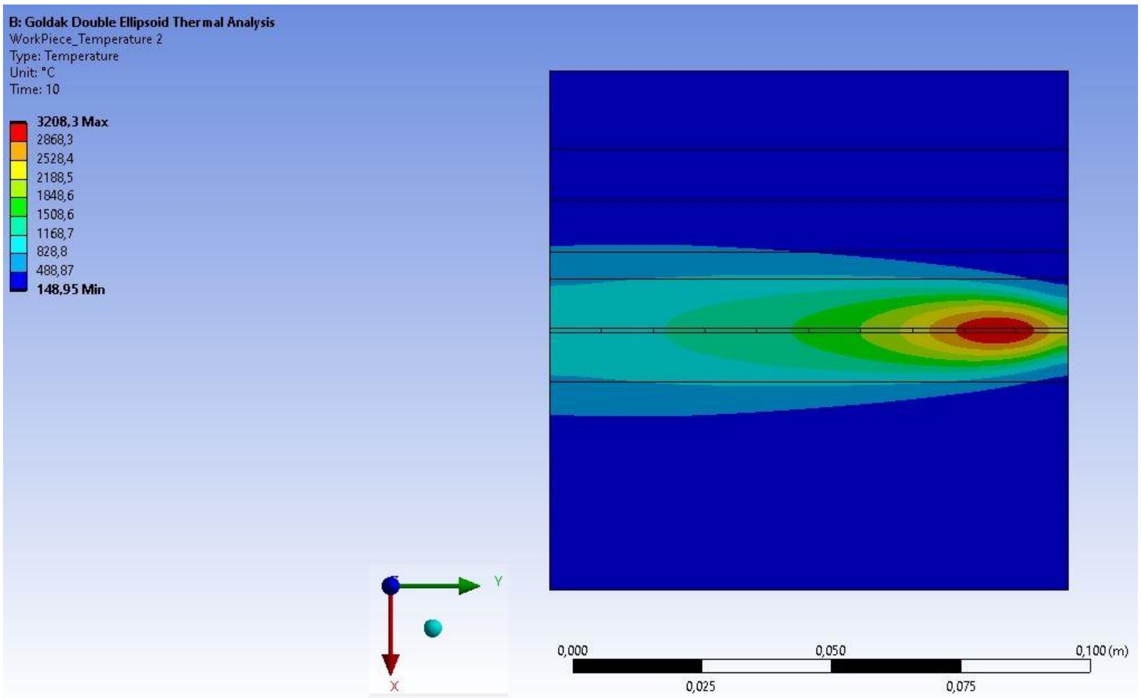

Figure 6.9. Top view of temperature distribution after 10 seconds

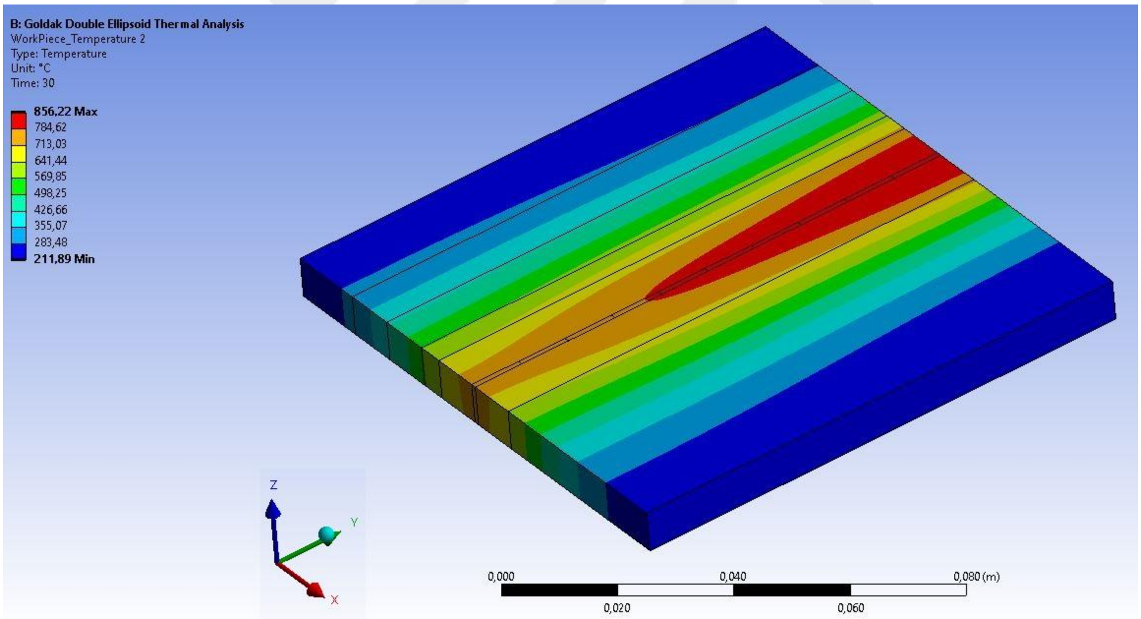

Figure 6.10. Isometric view of moving heat source after 30 seconds

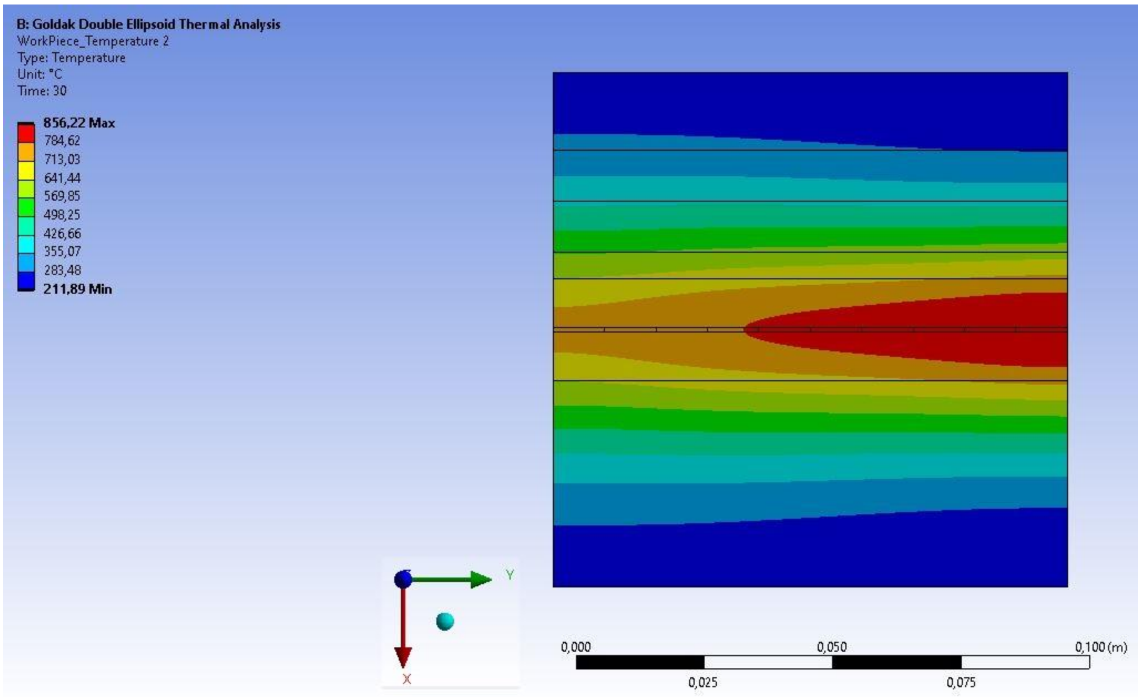

Figure 6.11. Top view of temperature distribution after 30 seconds

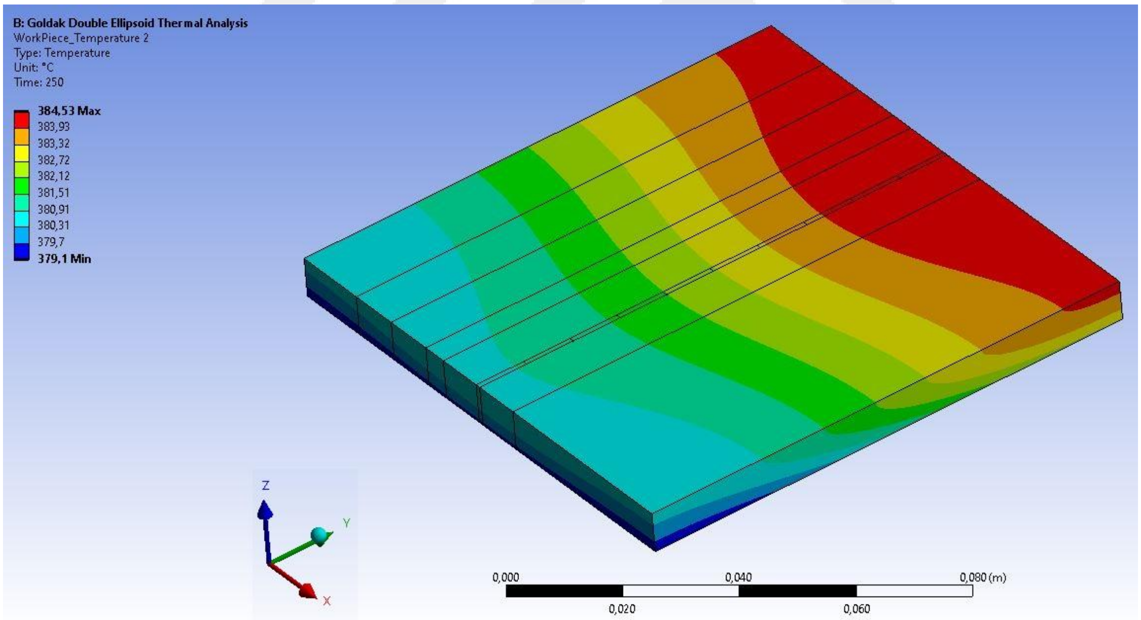

Figure 6.12. Isometric view of temperature distribution after 250 seconds

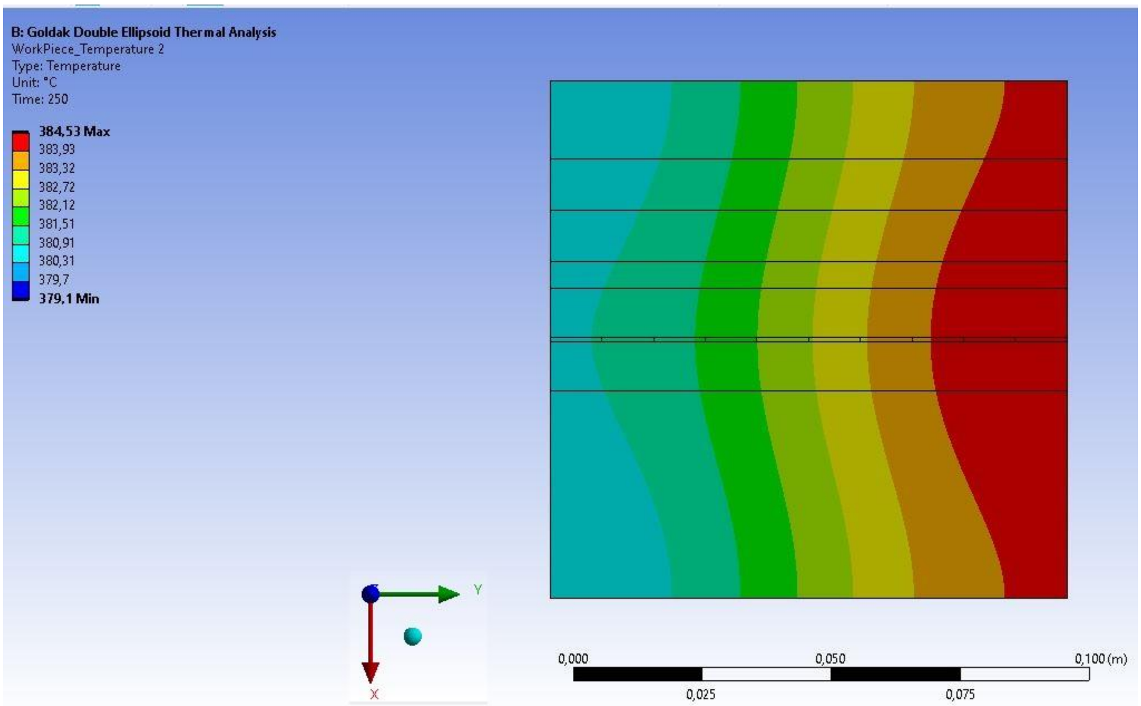

Figure 6.13. Top view of temperature distribution after 250 seconds

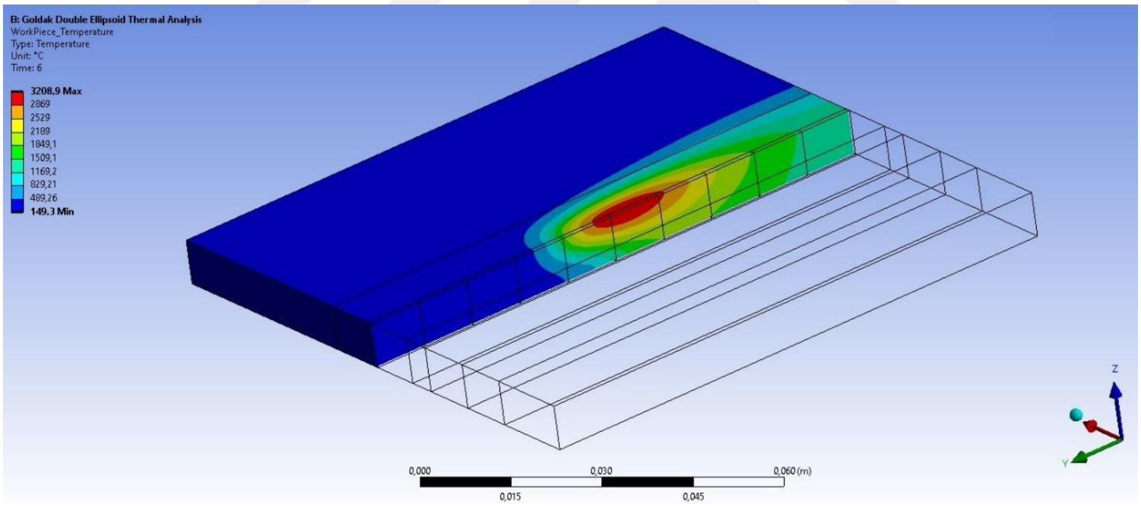

Figure 6.14. Temperature distribution at weld line after 6 seconds

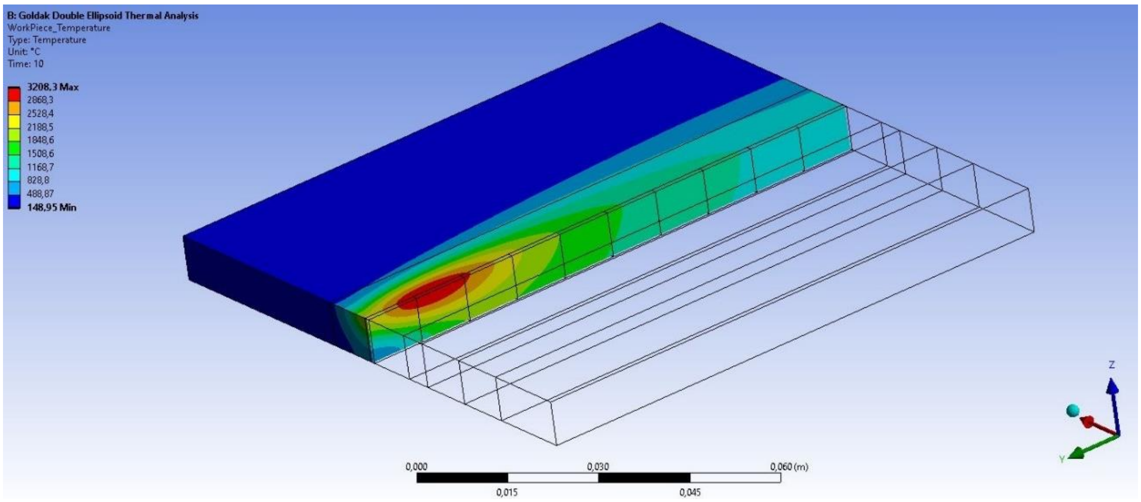

Figure 6.15 Temperature distribution at weld line after 10 seconds

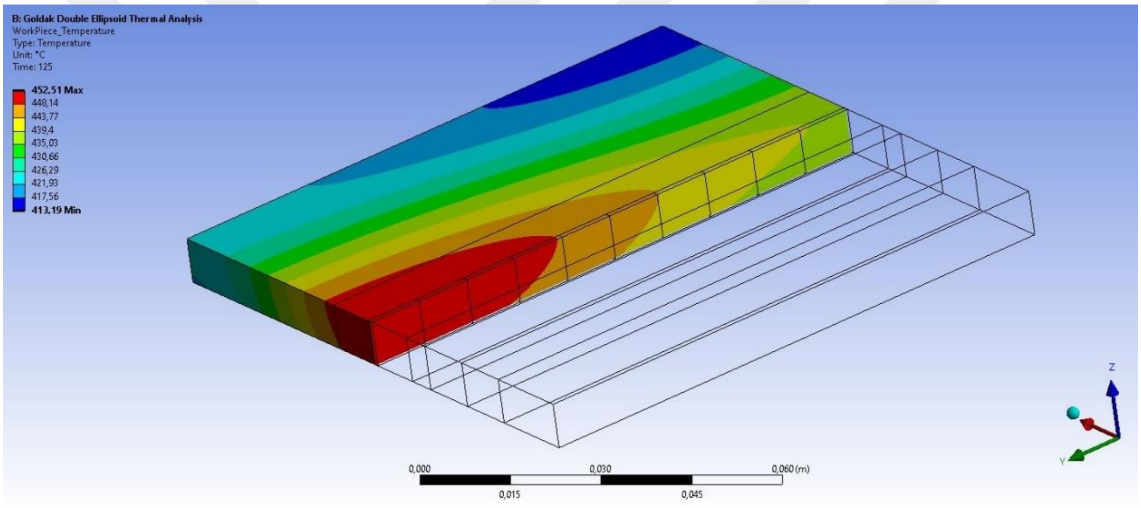

Figure 6.16. Temperature distribution at 125 sec.

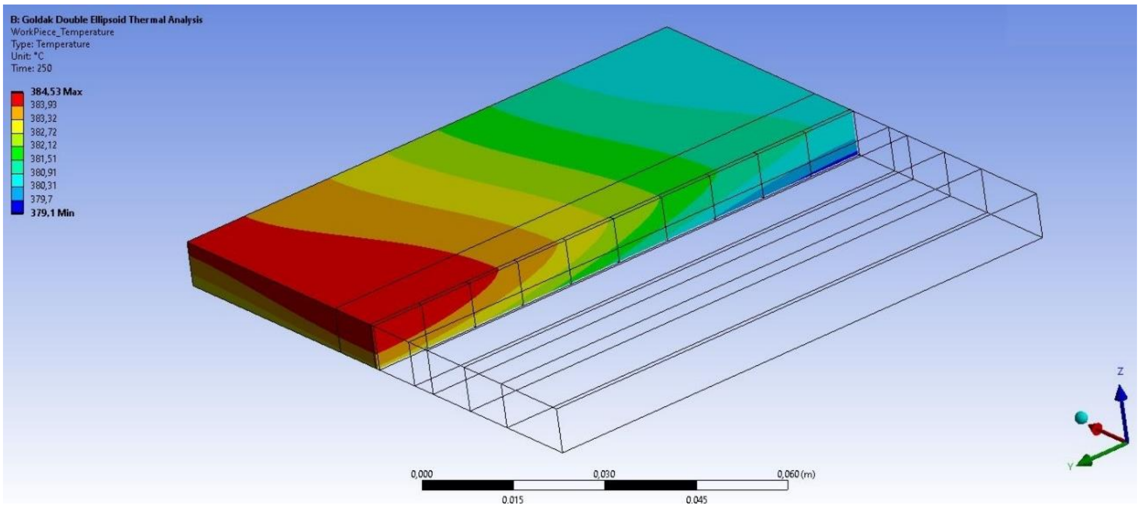

Figure 6.17. Temperature distribution at 250 sec.

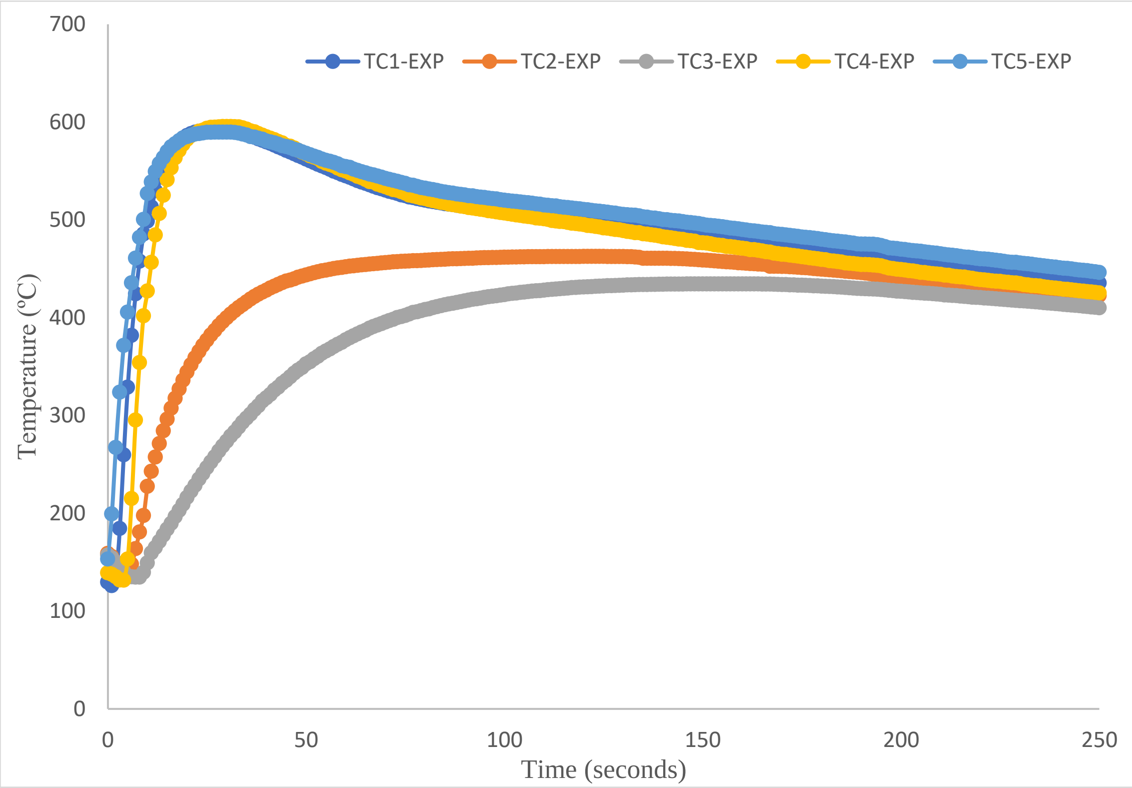

Figure 6.18. Temperature distribution obtained during experiment

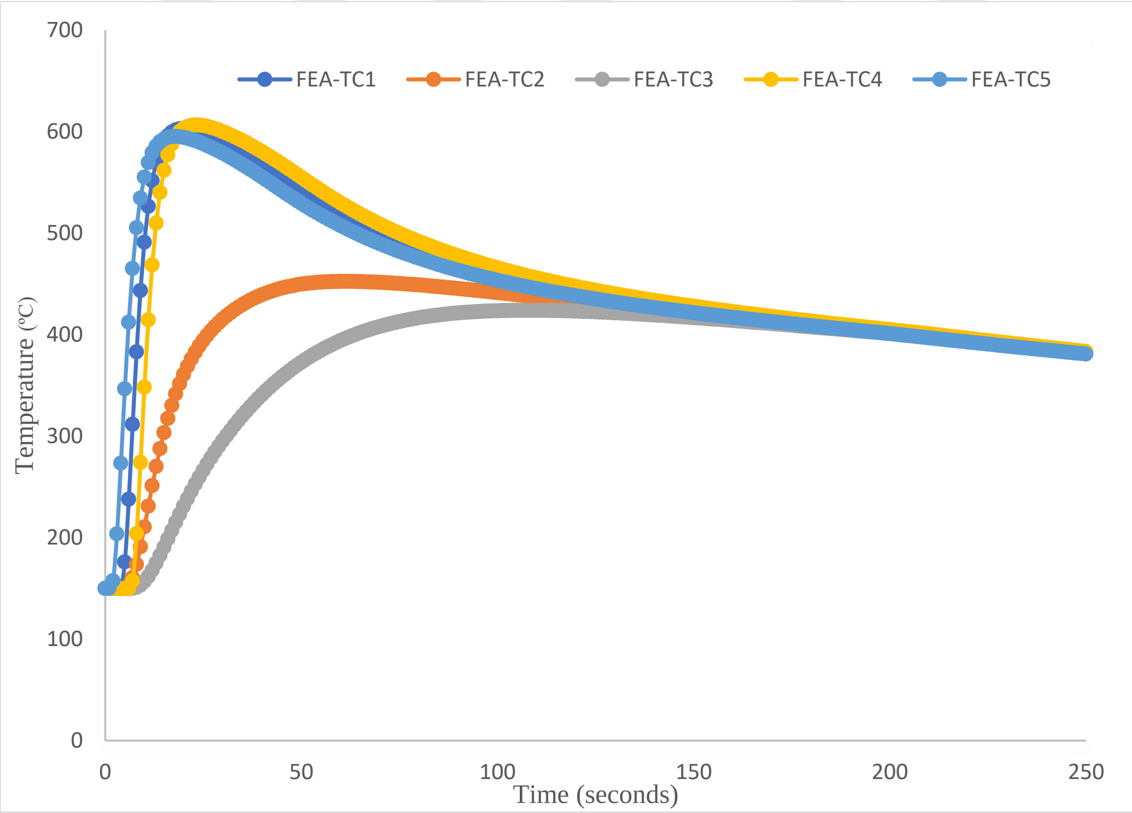

Figure 6.19. Temperature distribution obtained from FEA

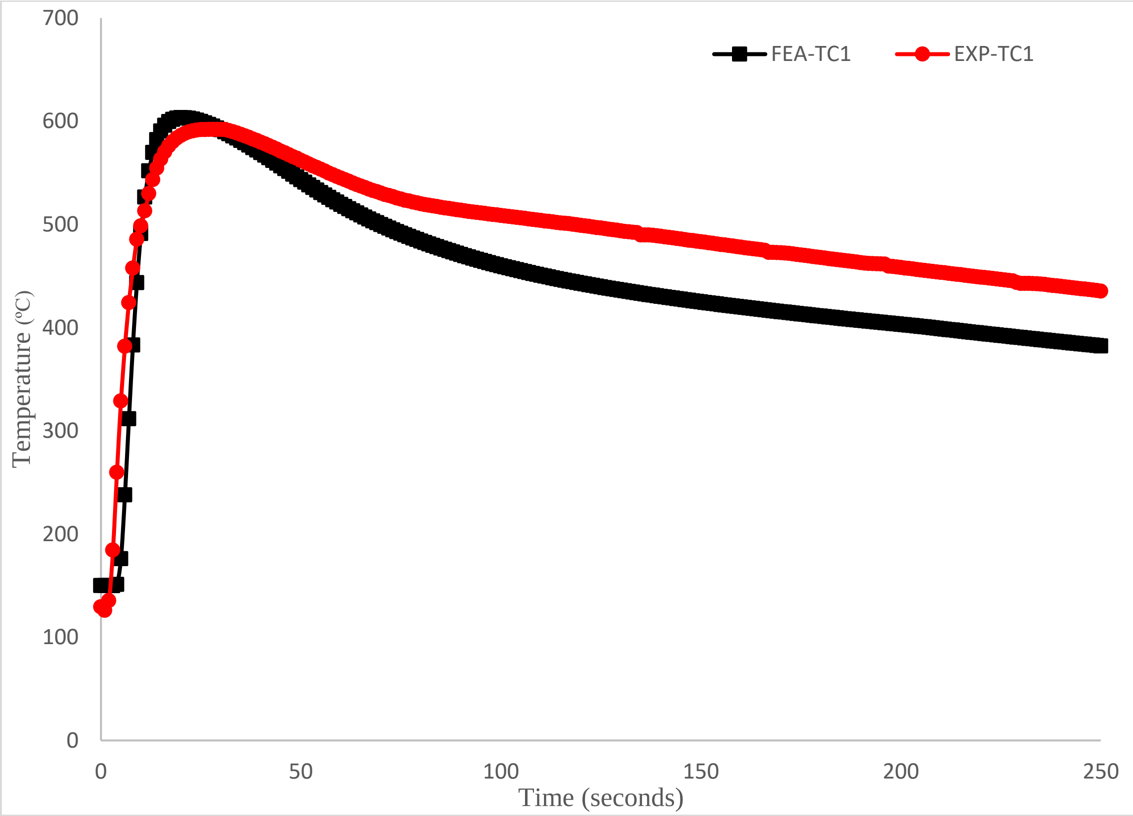

Figure 6.20. Comparison of the predicted temperature with experimental data at temperature measuring point 1

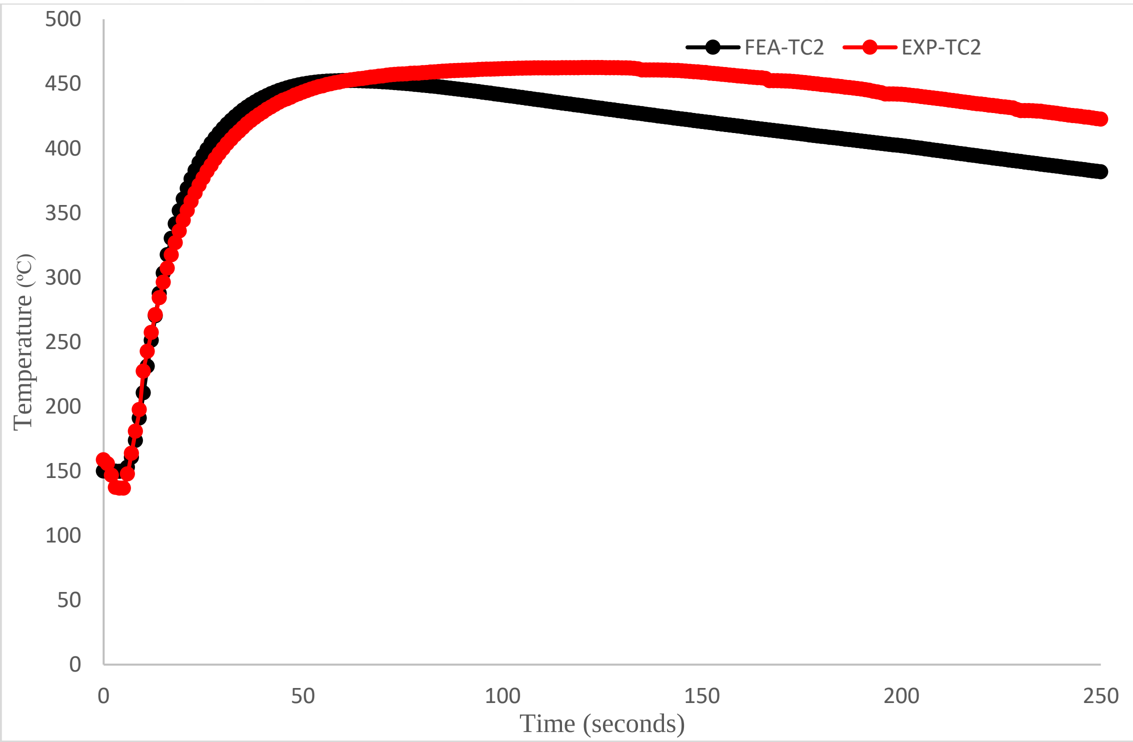

Figure 6.21. Comparison of the predict temperature with experimental data at temperature measuring point 2

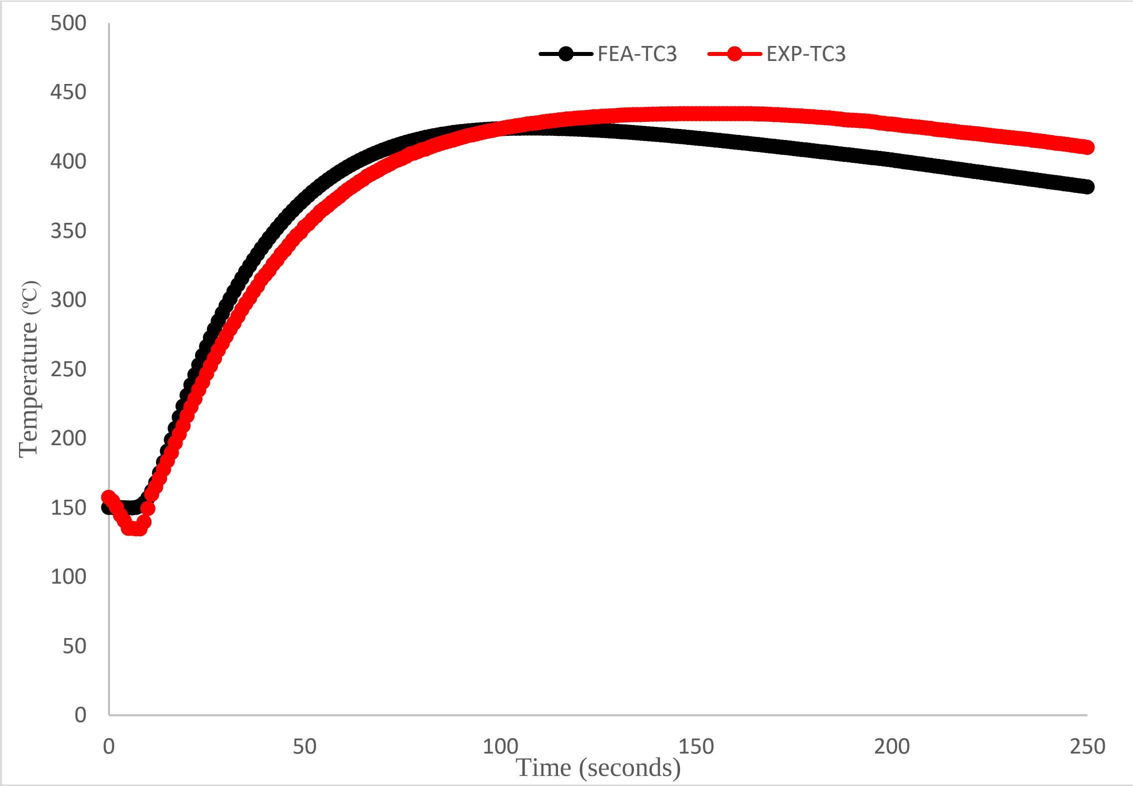

Figure 6.22. Comparison of the predict temperature with experimental data at temperature measuring point 3

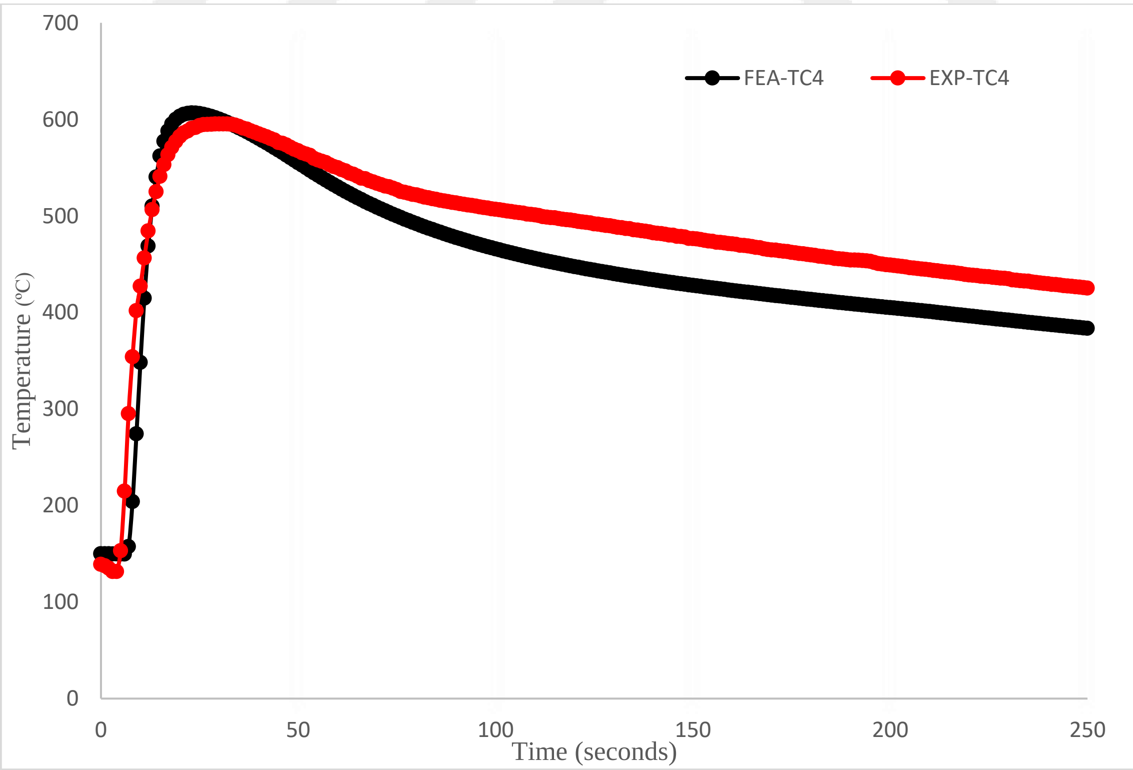

Figure 6.23. Comparison of the predict temperature with experimental data at temperature measuring point 4

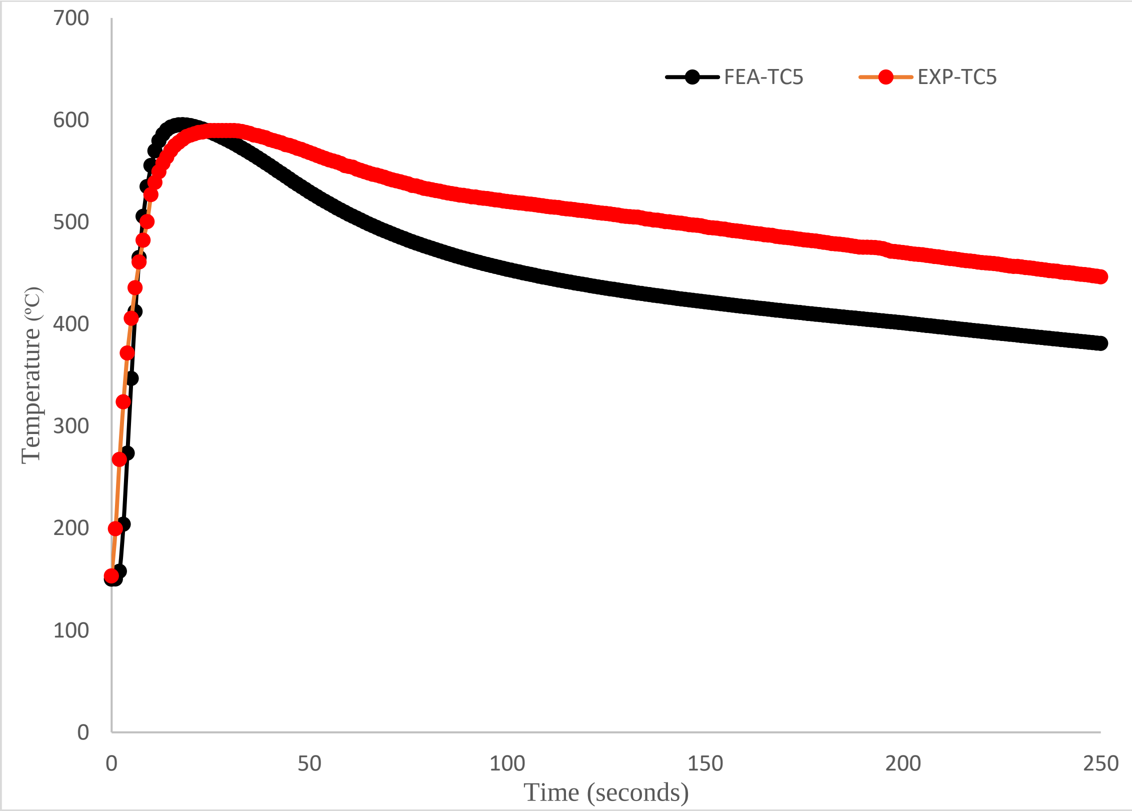

Figure 6.24. Comparison of the predict temperature with experimental data at temperature measuring point 5

Figures 6.10 and 6.11 show that as a heat source gets closer to a point, the temperature of the point gradually rises, and when it goes further away, the temperature of the point gradually drops. The temperature at point 1, 4 and 5 near the heat source is greater than the temperatures at point 2 and 3 and the temperature at point 2 is greater than the temperature at point 3. On the whole, a good agrement was found between the predicted and experimental temperatures.

At point 1 when welding began the temperature measured by TC1 was 129,4 ºC in the experiment work. The maximum temperature was reached to 591,9 ºC at 27 seconds and thermocople measured maximum temperature value for the next 4 seconds. According to predicted temperature value obtained from FEA on the node corresponding TC1 the maximum temperature was 603,34 ºC at 20 sec. This time difference is due to the response time of the recorder. Recorder meauseres the temperatures momentarily 4 or 5 seconds late. At 250 sec the temperature on the specimen was 435,3ºC and predicted temperature by FEA was 382,17 ºC. So for point 1 at the maximum temperature it is observed about % 2 and for the temperature at 250 sec it is observed about % 13.

At point 2 when welding began the temperature measured by TC2 was 158,7 ºC in the experiment work. The maximum temperature was reached to 462,5 ºC at 120 seconds and thermocople measured maximum temperature value for the next 6 seconds. According to predicted temperature value obtained from FEA on the node corresponding TC2 the maximum temperature was 452,43 ºC at 60 sec. At 250 sec the temperature on the specimen was 422,6 ºC and predicted temperature by FEA was 381,8 ºC. So for point 2 at the maximum temperature it is observed about %2 and for the temperature at 250 sec it is observed about %10.

At point 3 when welding began the temperature measured by TC3 was 157,2 ºC in the experiment work. The maximum temperature was reached to 434,4 ºC at 149 seconds and thermocople measured maximum temperature value for the next 14 seconds. According to predicted temperature value obtained from FEA on the node corresponding TC2 the maximum temperature was 423,94 ºC at 108 sec. At 250 sec the temperature on the specimen was 410,0 ºC and predicted temperature by FEA was 381,49 ºC. So for point 3 at the maximum temperature it is observed about %2,4 and for the temperature at 250 sec it is observed about %7.

At point 4 when welding began the temperature measured by TC4 was 139,0 ºC in the experiment work. The maximum temperature was reached to 595,2 ºC at 29 seconds and thermocople measured maximum temperature value for the next 3 seconds. According to predicted temperature value obtained from FEA on the node corresponding TC4 the maximum temperature was 606,58 ºC at 23 seconds. At 250 sec the temperature on the specimen was 425,1 ºC and predicted temperature by FEA was 400,09 ºC. So for point 4 at the maximum temperature it is observed about %2 and for the temperature at 250 sec it is observed about %10.

At point 5 when welding began the temperature measured by TC5 was 153,1 ºC in the experiment work. The maximum temperature was reached to 589,5 ºC at 27 seconds and thermocople measured maximum temperature value for the next 5 seconds. According to predicted temperature value obtained from FEA on the node corresponding TC5 the maximum temperature was 599,25 ºC at 18 seconds. At 250 sec the temperature on the specimen was 446,2 ºC and predicted temperature by FEA was 380,89 ºC. So for point

4 at the maximum temperature it is observed about %1 and for the temperature at 250 sec it is observed about %15.

Table 6.1. Comparison of Experimental and Predicted temperatures

Points	FEA Model			Experiment			Deviation	Deviation
	Peak Temp.(ºC)	Time (sec.)	Temp. At 250 sec.	Peak Temp.(ºC)	Time (sec.)	Temp. At 250 sec.	At Peak Temp.	At 250 sec Temp.
TC1	603,34	20	382,17	591,9	27	435,3	%2	%13
TC2	452,43	60	381,8	462,5	108	422,6	%2	%10
TC3	423,94	108	381,49	434,4	149	410,0	%2,4	%7
TC4	606,58	23	400,9	595,2	29	425,1	%2	%10
TC5	599,25	18	380,89	589,5	27	446,2	%1	%16

It is found a good analogy between the measured and predicted temperatures.

6.2. Structural Analysis

Engineering's field of stress analysis is based on solid mechanics. Stress analysis is a key technique used by engineers to determine the stress and strain of a design or structure. A mathematical model is created by an engineer from a real-world engineering challenge.

A mechanical assembly may experience large temperature variations in many engineering applications. Such temperature variations cause thermal strains, which in some cases can also result in stresses. The thermal-stress analysis is required to determine how much warpage is brought on by thermal strains and to prevent failure due to excessive thermal stresses. We may first need to conduct a thermal study to gather data on the temperature distribution over the mechanical assembly in order to estimate thermal strains and stresses.

Remaining tension was created in the weldment as a result of the uneven cooling and contraction of the weld material. Residual stress may have contributed to the failure of several welds. The mobility of the heat flux creates residual stresses, which lead to uneven expansion and contraction of the weld material. Fixtures are used to clamp the workpiece at each of its corners The distribution of residual stress in the weldment is significantly influenced by the clamping of the workpiece. The thermal model is solved to calculate and depict residual stresses. The mechanical model receives the thermal profile data as input. To get rid of non-linearities, the mechanical model is solved using the Newton-Raphson technique.

Table 6.2. Residual Stress values along the longitudinal direction of welding

Measurement Point	Result (MPa)	Standart Deviation	X coordinates	Y coordinates
LP1	255,4	±141,8	0	10
LP2	206,9	±76,1	0	30
LP3	235,8	±111,9	0	50
LP4	236,1	±141,3	0	70
LP5	204,4	±83,5	0	90

Table 6.3. Residual Stress values along the transferse direction of welding

Measurement Point	Result (MPa)	Standard Deviation	X coordinates	Y coordinates
TP1	217,0	±86,9	-30	50
TP2	192,4	±69,9	-20	50
TP3	235,8	±111,9	0	50
TP4	213,9	±70,5	20	50
TP5	210,0	±73,8	30	50

On the graphs three geometrical shapes appear, these are rectangular, triangle and cross. Rectangular and tirangle means measurements at points corresponding to 180 degrees. The Table to where the test part was located is moving with an incline of approximately 5 degrees and in every movement it is measuring at that point and the corresponding 180 degree point. Cross shapes on the graphs means the point which is not taken into account also it is the ignored measuring points. The roughness of the surface affects the accuracy of measurement.

Table 6.4. The number of points to be ignored along longitudinal direction

Measuring Point	LP1	LP2	LP3	LP4	LP5
Number of points ignored	0	0	2	1	5

Table 6.5. The number of points to be ignored along longitudinal direction

Measuring Point	TP1	TP2	TP3	TP4	TP5
Number of points ignored	0	4	2	5	8

Figure 6.25, 6.26, 6.27, 6.28 and 6.29 show spacing graph to determine the residual stresses at longitudinal direction at point LP1, LP2, LP3, LP4 and LP5 which is given in Tab.

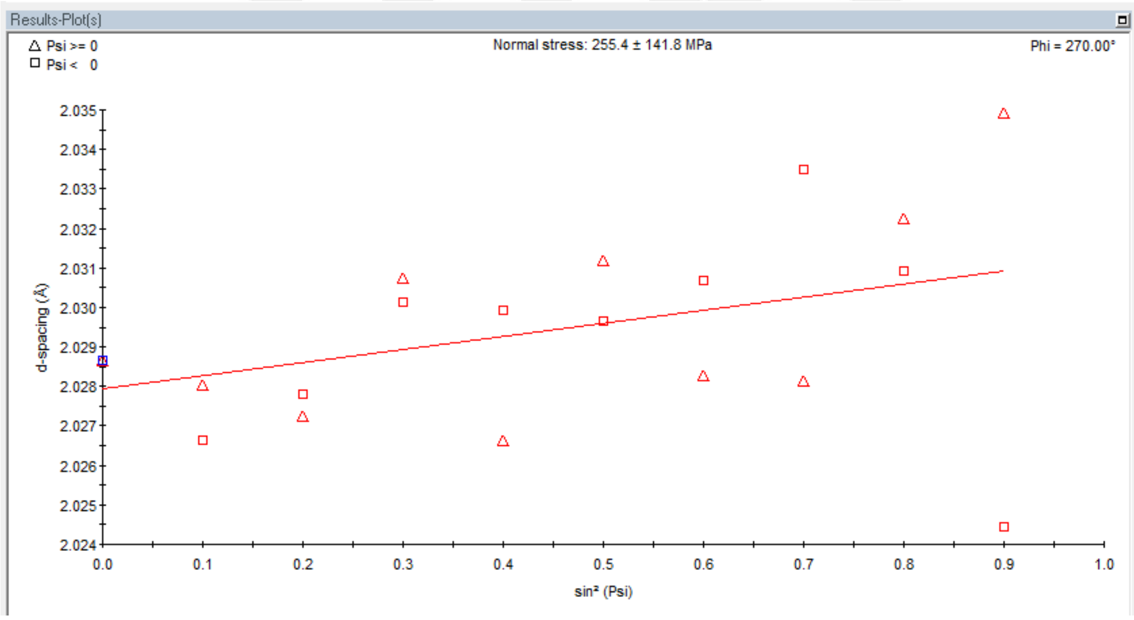

Figure 6.25. Residual stress at measuring point LP1

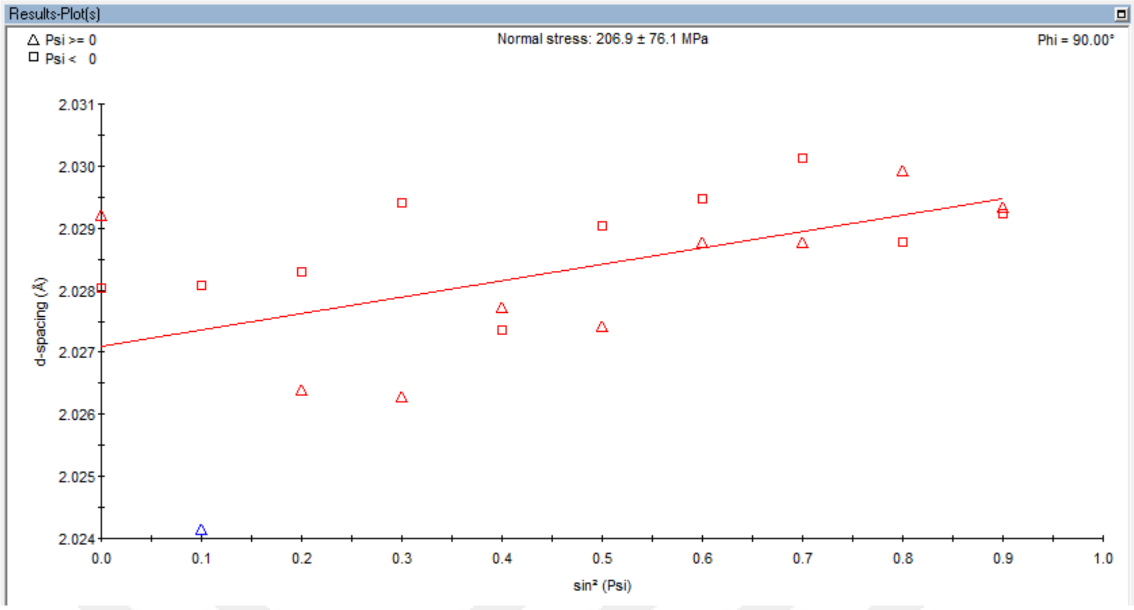

Figure 6.26. Residual stress at measuring point LP2

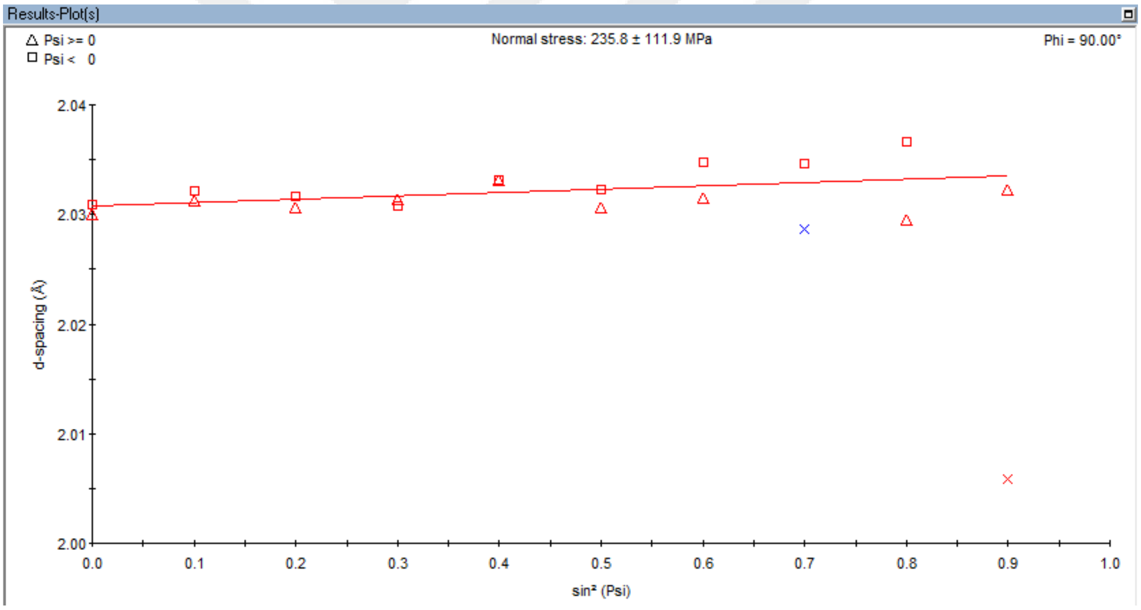

Figure 6.27. Residual stress at measuring point LP3

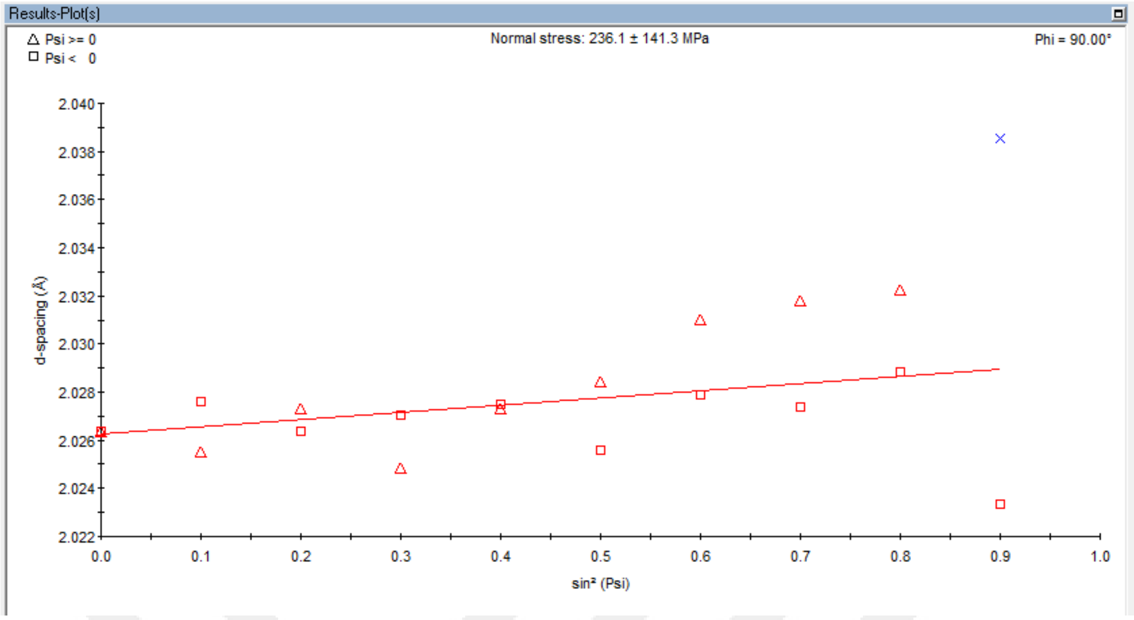

Figure 6.28. Residual stress at measuring point LP4

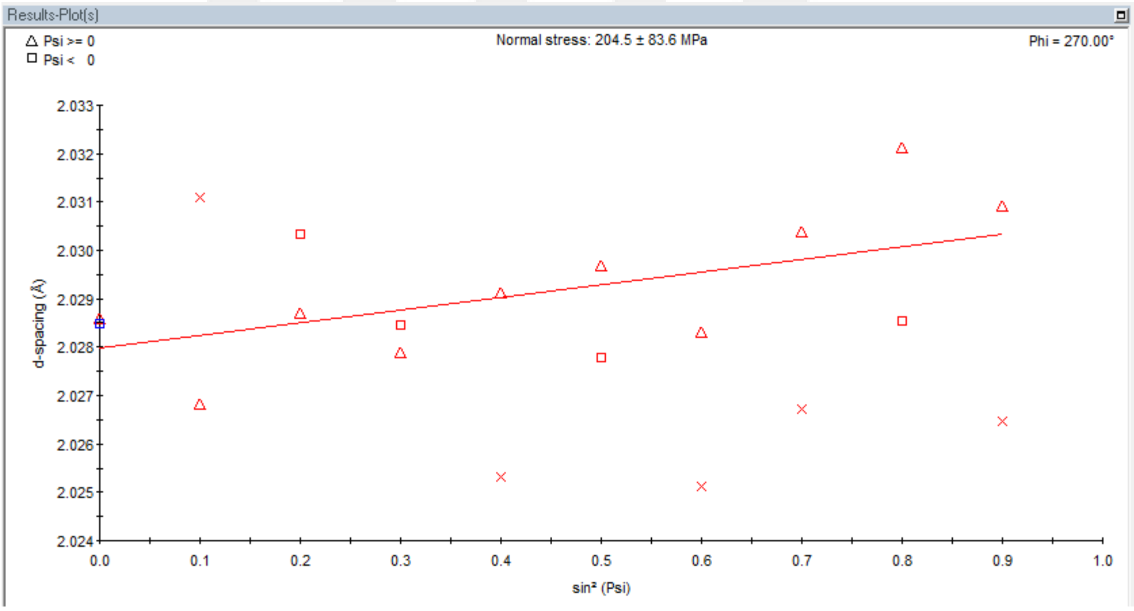

Figure 6.29. Residual stress at measuring point LP5

Figure 6.30, 6.31, 6.32, 6.33 and 6.34 show spacing graph to determine the residual stresses at transverse direction at point TP1, TP2, TP3, TP4 and TP5 which is given in Table 6.3. LP3 and TP3 is the same point it is the common intersection point in the longitdunal and transverse direction.

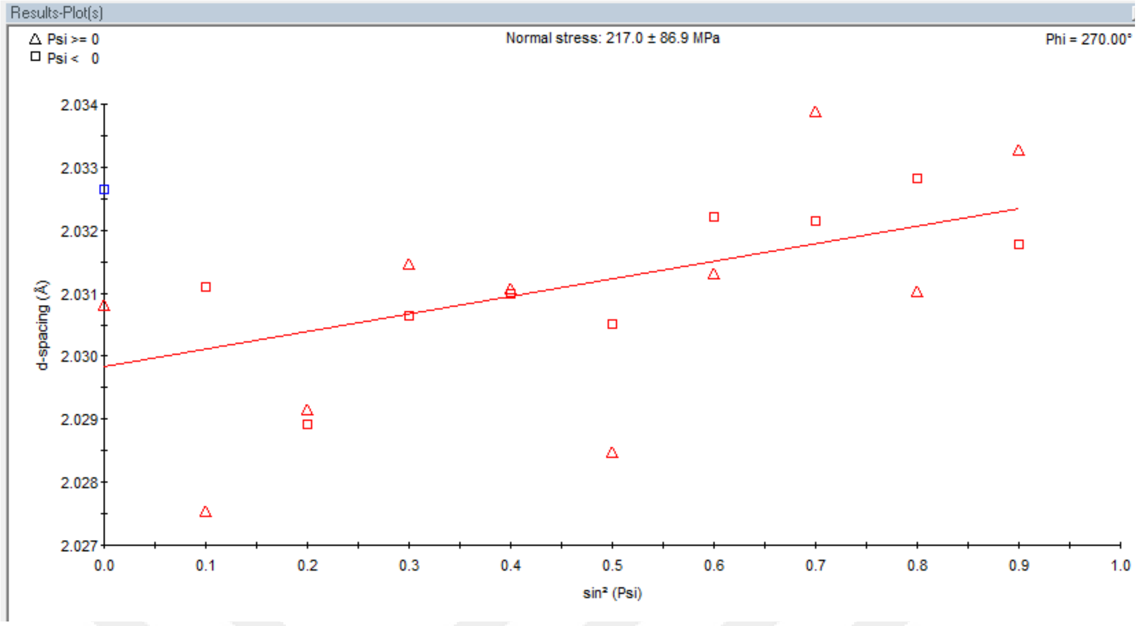

Figure 6.30. Residual stress at measuring point TP1

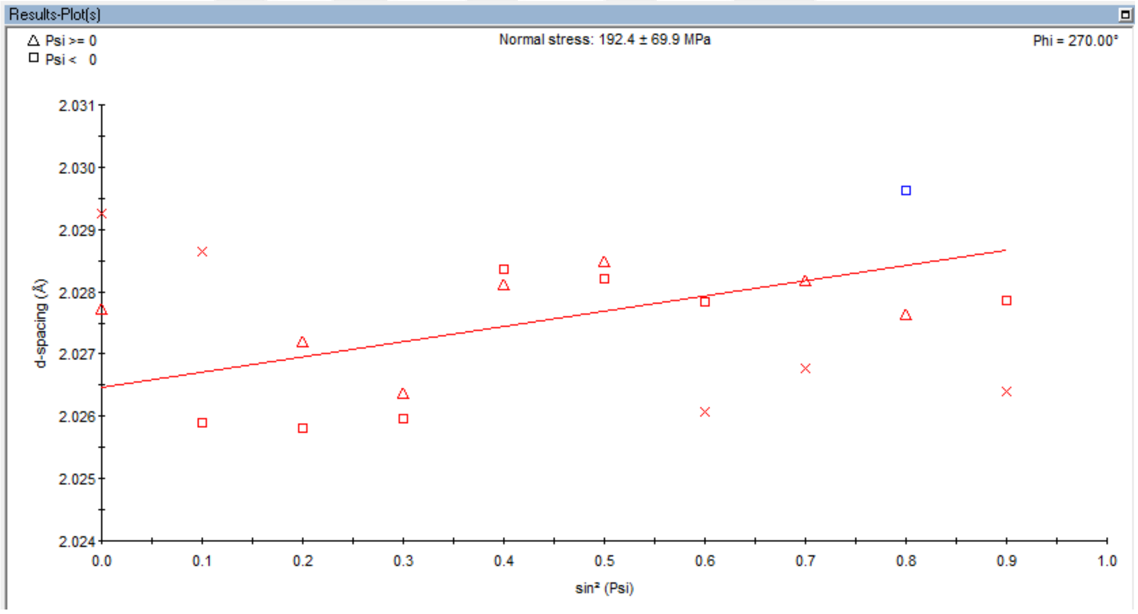

Figure 6.31. Residual stress at measuring point TP2

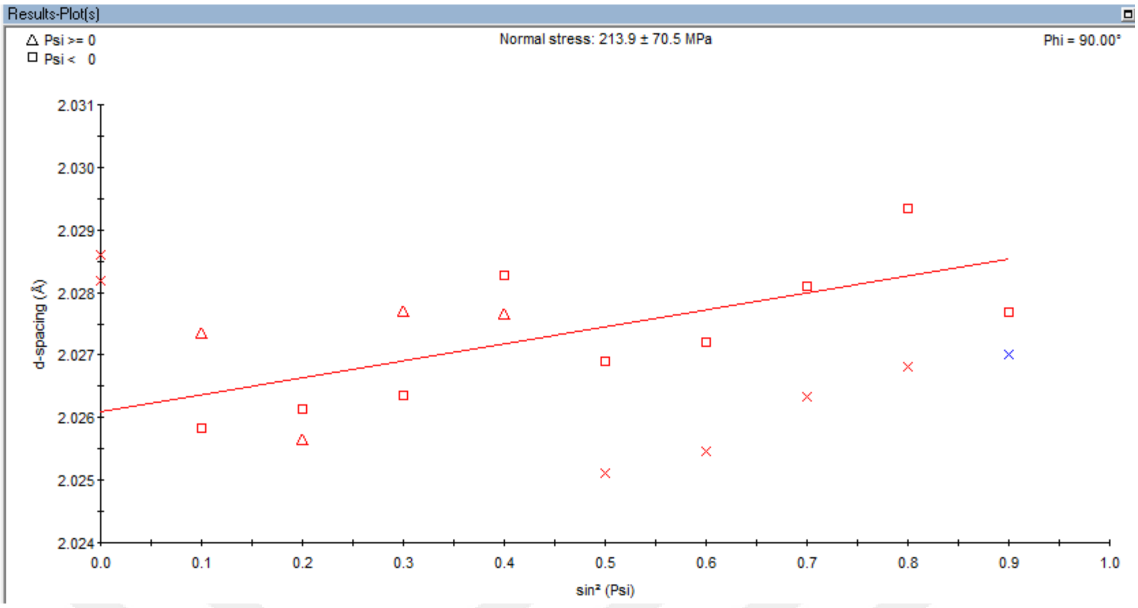

Figure 6.32. Residual stress at measuring point TP4

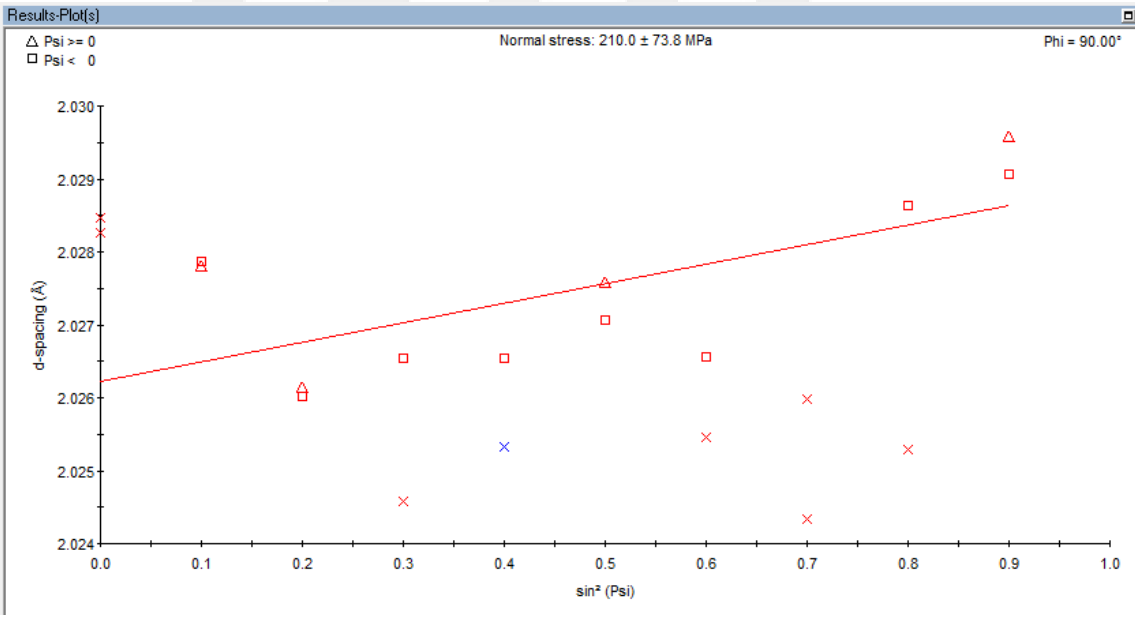

Figure 6.33. Residual stress at measuring point TP5

Panalytical X'Pert Pro MPD measures residual stress with X-ray diffraction method. X-ray diffraction is the only method to determine macro and micro residual stresses non-destructively. As known with $\sin^2$psi(Ψ) method, residual stress is calculated with changes of distance between the planes in the crystal lattice. Also, focally stress ans stress types of the material in the desired direction is calculated individually.

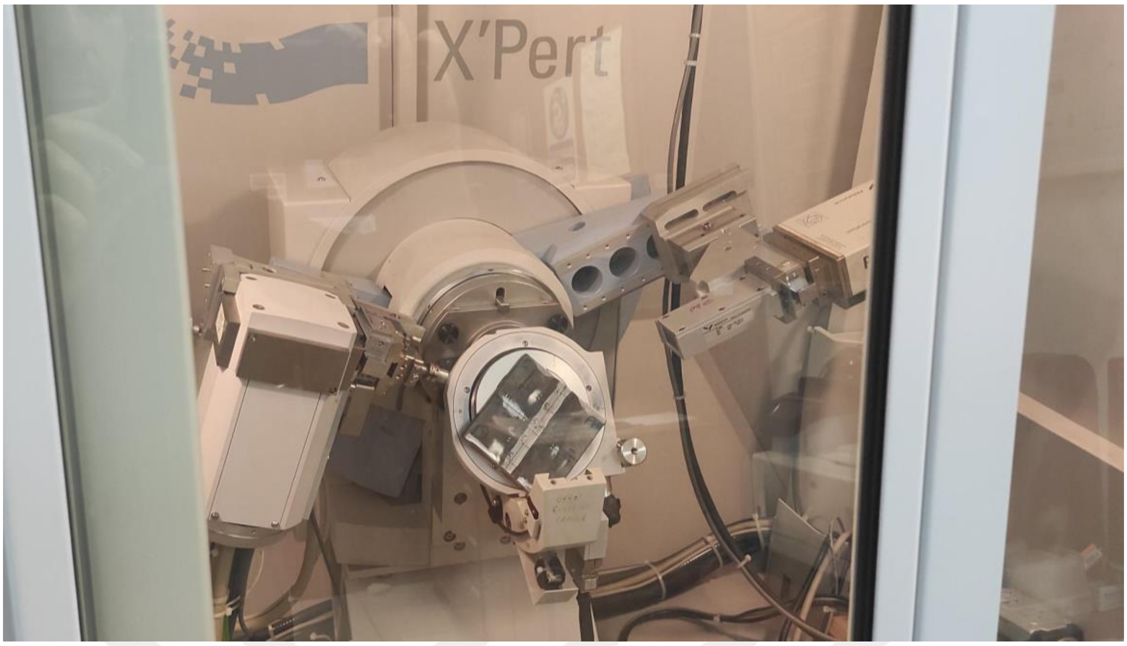

Figure 6.34. The part located to X-pert Pro MPD

Figure 6.35. Residual stress measurement

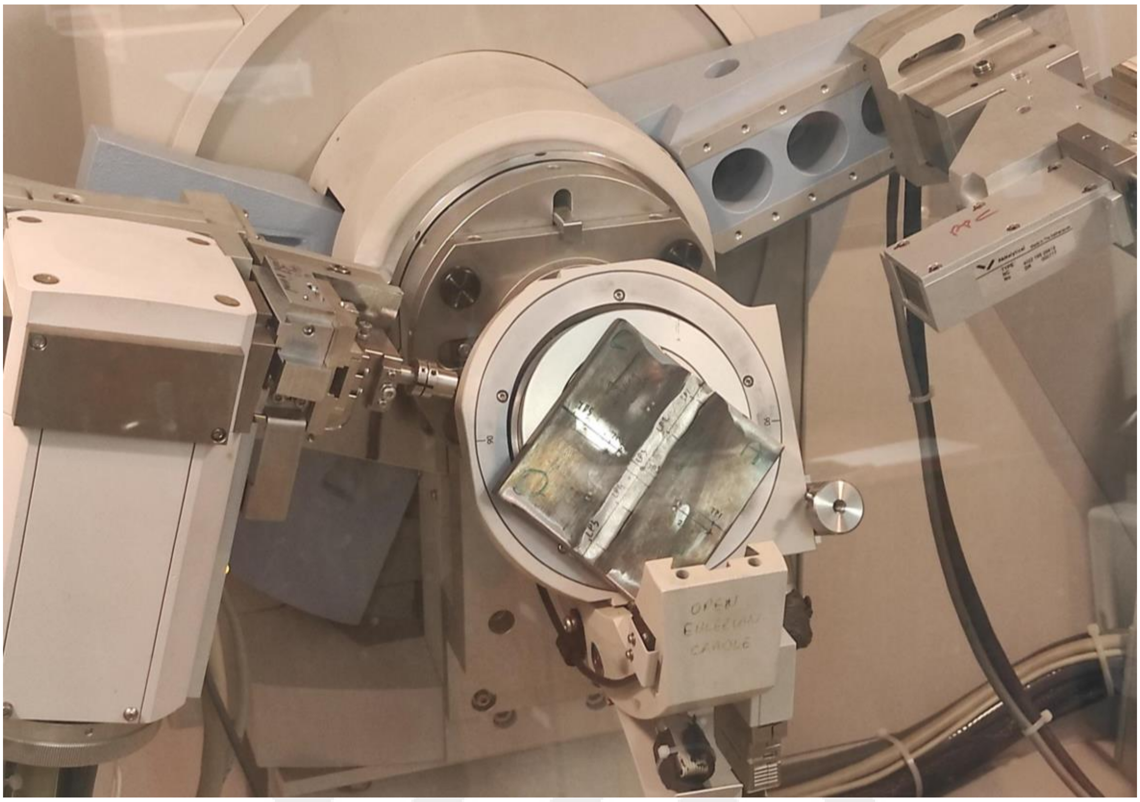

Figure 6.36. Residual stress measurement

The test part is sticked to the sample with double-sided adhesive tape. It is aimed to prevent the part to move. Sample is moving in the angular direction and at every angular position it takes values. These values can be seen as a point in software of X-Pert Pro MPD. In order to obtain an exact value software makes lineer fit regression acording to the points. Some points can be neglicable. In order for the result to be correct, the number of canceled points should not be too much. The deviation is increased with the values of points canceled. Using double sided tape we were unable to prevent the sample piece to move. When sample moves upward direction the piece slowly moved down direction. That means the angle measured by X-Pert Pro MPD changed and some points produced inaccuratr results. When we ignore these point the deviation value increased. The residual stresses were obtained with using “Birth and Death” feature and non-using Birth and Death” feature in FEA in both transverse and longitudinal directions. Figure 6.38 and 6.39 show residual stresses along longitudinal and transverse direction obtained with Birth and Death” feature respectively. The "death element" effect is produced by ANSYS code, which does not really modify the model element. Instead, the weld components are first turned off by greatly reducing their stiffness (or conductivity, or other comparable quality). In the meanwhile, Ansys Mechanical reactivates the "death element" by letting its stiffness, mass, and other qualities return to their initial values in order to get the "birth element" effect. Relative stress analysis at 3 seconds is shown in Figure 6.34.

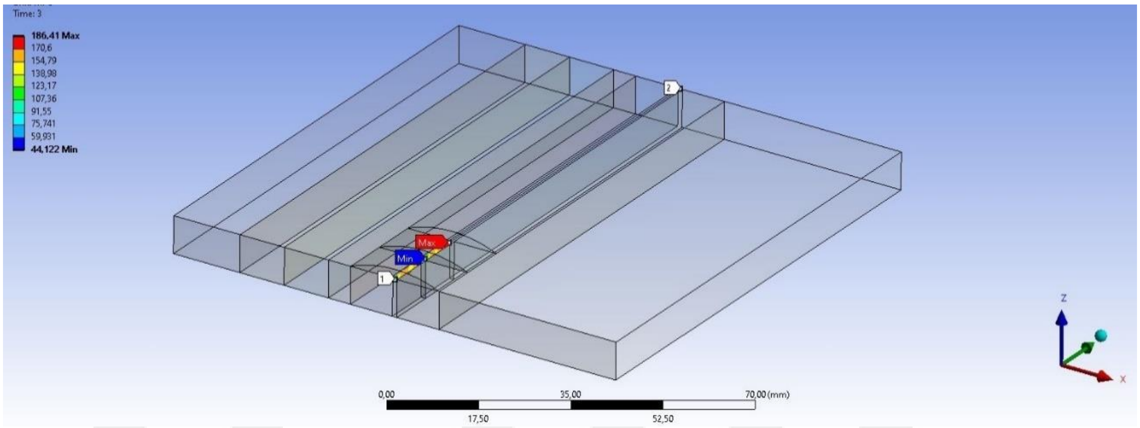

Figure 6.37. Residual Stress analysis with element Birth and Death Technique at 3 seconds

Table 6.6. Residual Stress values on measurement points both longitudinal and transverse directions in FEA and Test results

		FEA RESULTS with element Birth and Death			TEST RESULTS	
	Measurement Point	Maximum (MPa)	Minimum (MPa)	Average (MPa)	Results	Standart Deviation
Longitudinal Direction	LP1	277,73	247,04	262,39	255,4	±141,8
	LP2	275,5	245,72	260,61	206,9	±76,1
	LP3	275,95	246,11	261,02	235,8	±111,9
	LP4	281,29	246,77	264,03	236,1	±141,3
	LP5	277,95	248,83	263,39	204,4	±83,5
Transverse Direction	TP1	265,46	265,46	265,46	217,0	±86,9
	TP2	277,09	277,09	277,09	192,4	±69,9
	TP3	275,92	246,11	261,02	235,8	±111,9
	TP4	271,1	271,1	271,1	213,9	±70,5
	TP5	265,46	265,46	265,46	210,0	±73,8

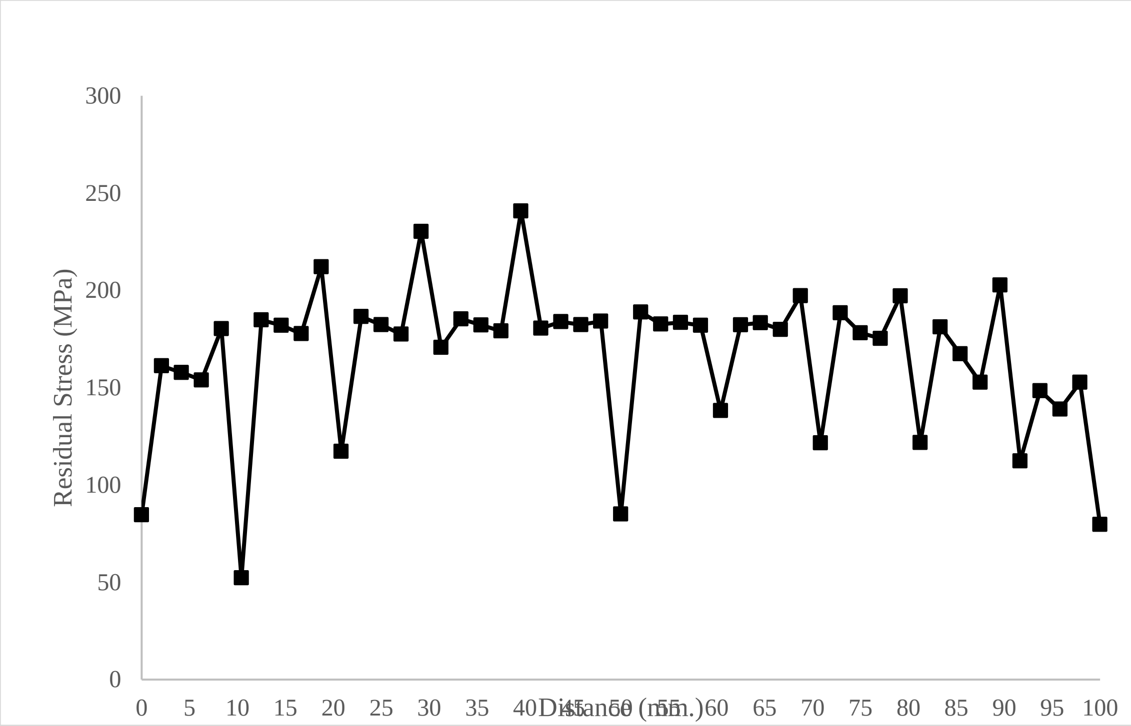

Figure 6.38. Residual stresses along the longitudinal direction obtained with Element Birth and Death Technique

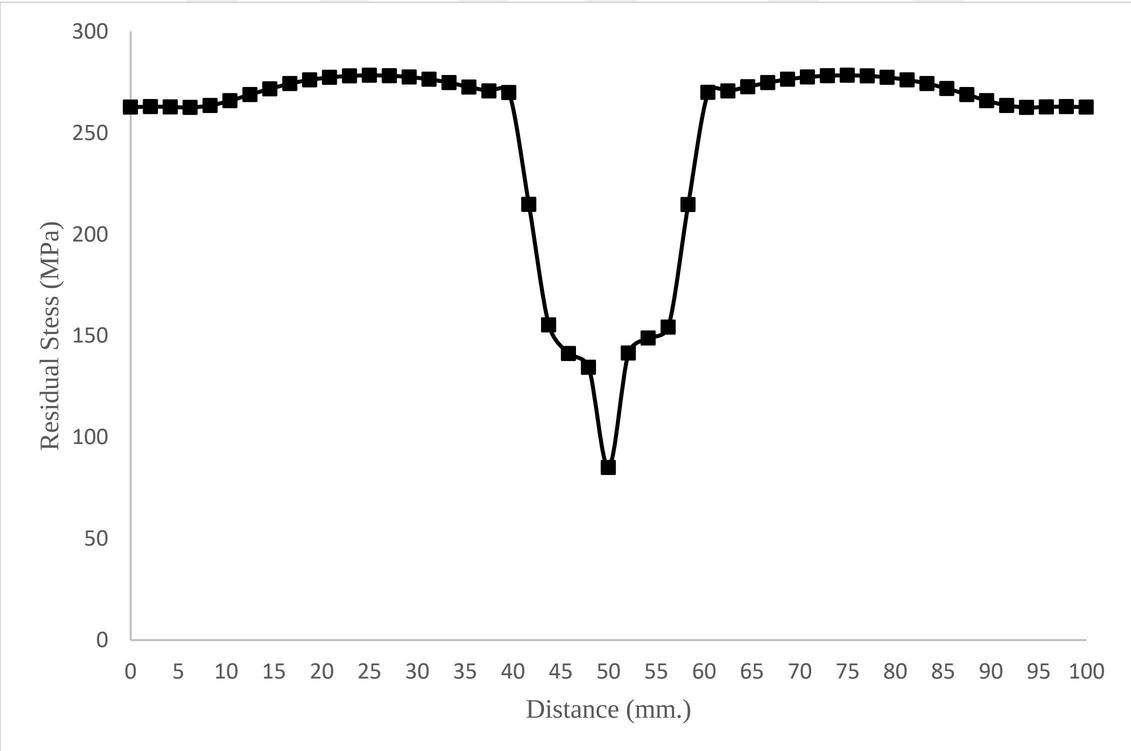

Figure 6.39. Residual stresses along the transverse direction obtained with Element Birth and Death Technique

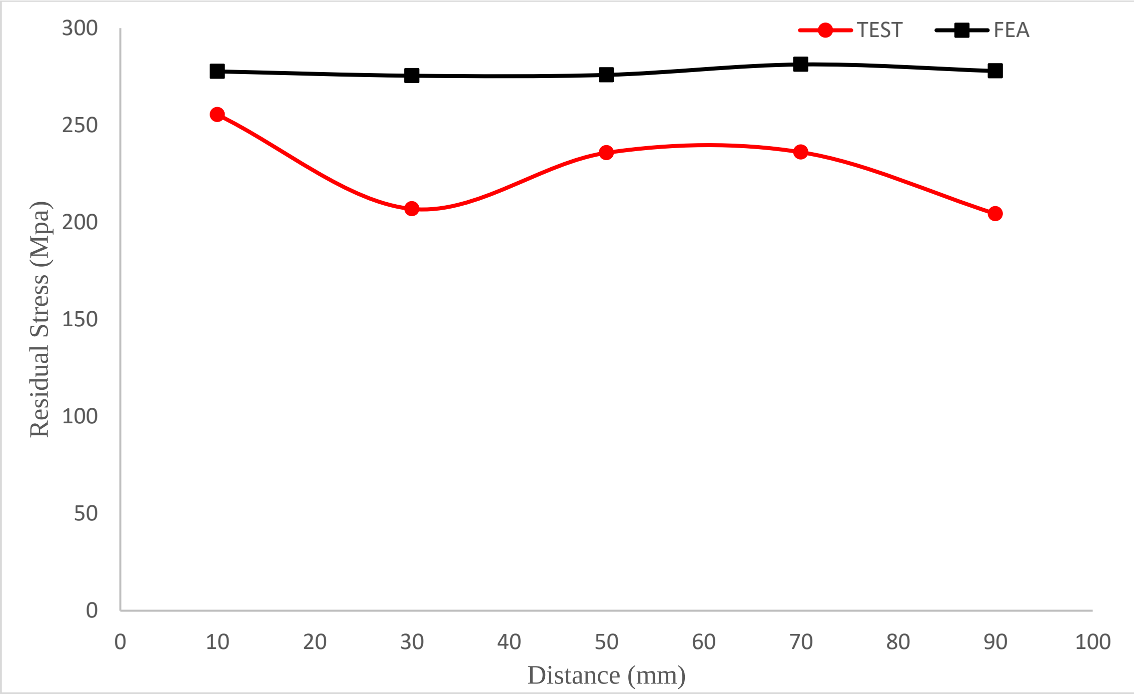

Figure 6.40. Comparison of residual stress along longitudinal direction on measurement points FEA with EBD technique

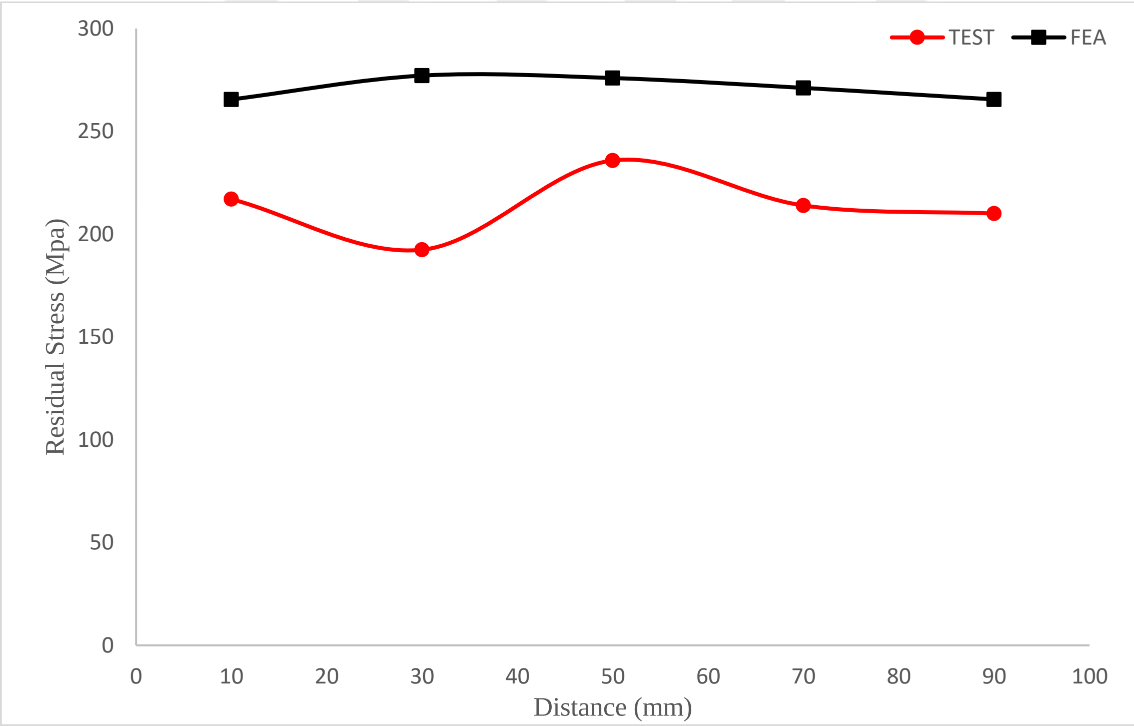

Figure 6.41. Comparison of residual stress along transverse direction on measurement points FEA with EBD technique

Table 6.7. Residual Stress values on measurement points both longitudinal and transverse directions in FEA and Test results (non using Element Birth and Death Technique)

		FEA RESULTS not using element Birth and Death			TEST RESULTS	
	Measurement Point	Maximum (MPa)	Minimum (MPa)	Average (MPa)	Results	Standart Deviation
Longitudinal Direction	LP1	241,58	241,4	241,49	255,4	±141,8
	LP2	265,32	265,08	265,2	206,9	±76,1
	LP3	270,02	270	270,01	235,8	±111,9
	LP4	264,68	264,42	264,55	236,1	±141,3
	LP5	240,91	240,98	240,95	204,4	±83,5
Transverse Direction	TP1	265,73	265,73	265,73	217,0	±86,9
	TP2	287,79	287,79	287,79	192,4	±69,9
	TP3	270,02	270	270,01	235,8	±111,9
	TP4	287,79	287,79	287,79	213,9	±70,5
	TP5	265,73	265,73	265,73	210,0	±73,8

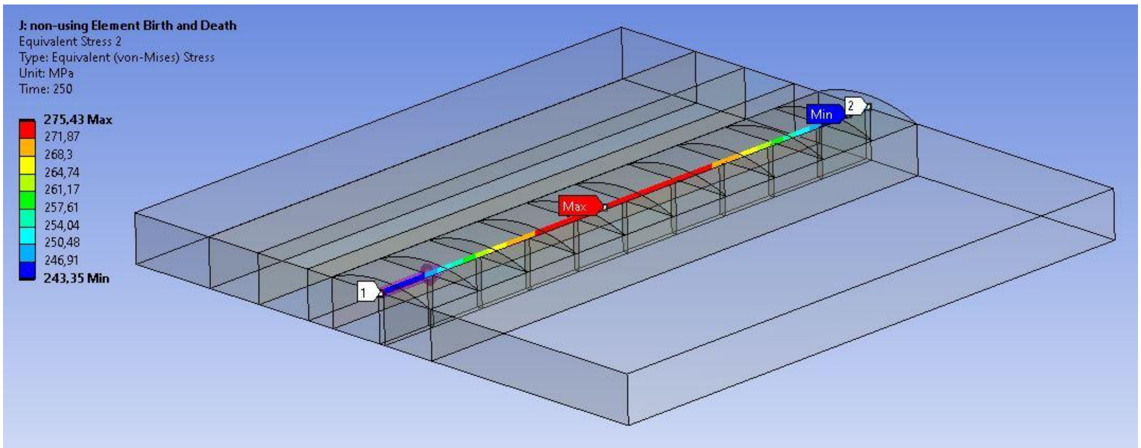

Figure 6.42. Residual Stress along longitudinal path direction

These residual stresses shown on Figure 6.43 and 6.45 obtained through path line along transverse direction. Residual stresses which is used for comparing with test results are nodal stresses which is corresponding nodal on FEA.

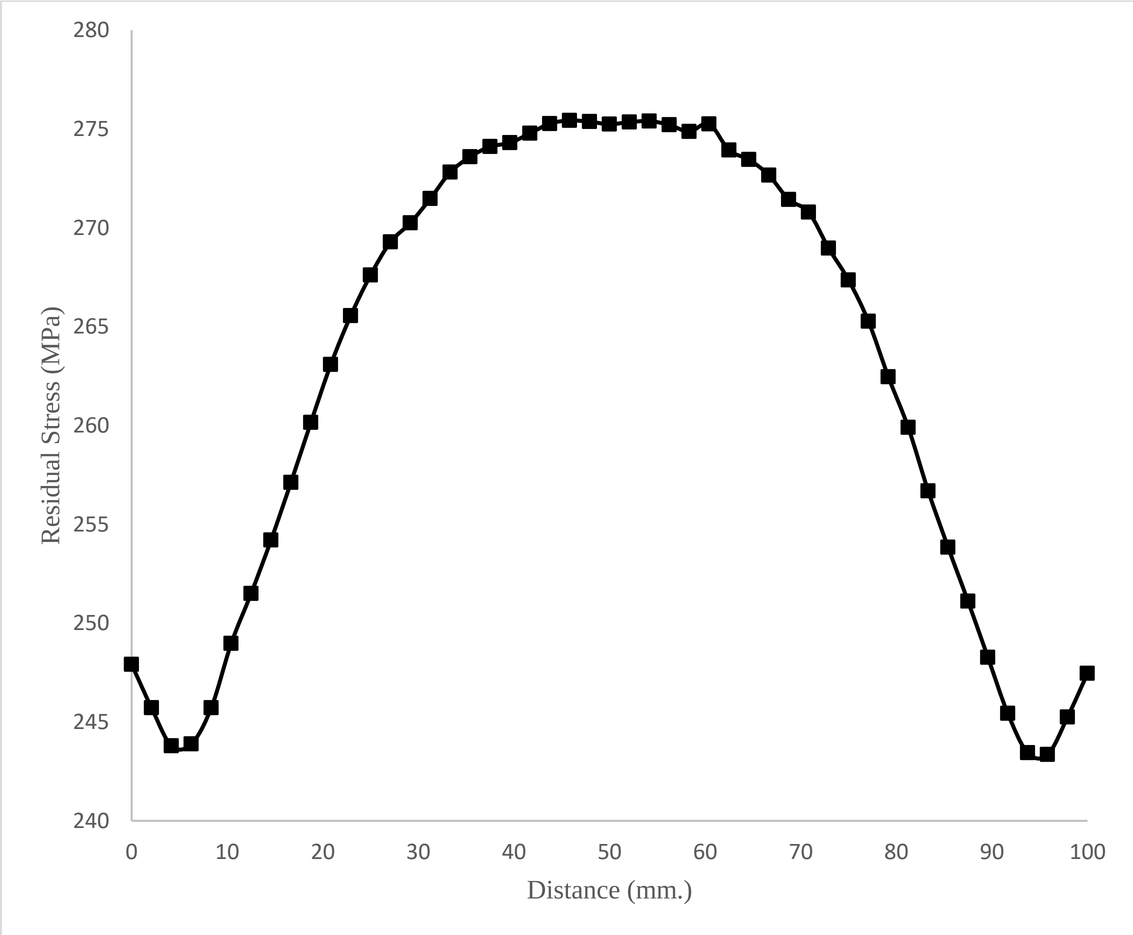

Figure 6.43. Residual stresses along the longitudinal direction obtained by without using Element Birth and Death Technique

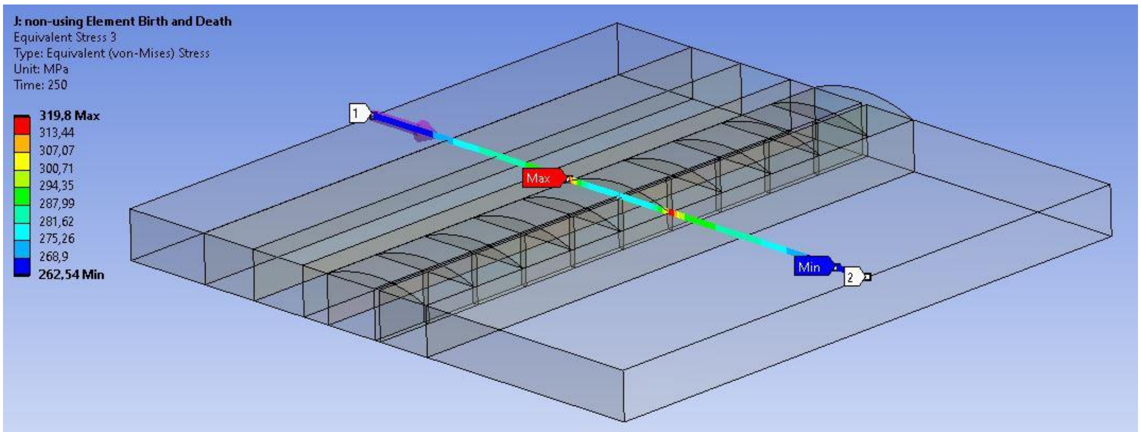

Figure 6.44. Residual Stress along transverse Path direction

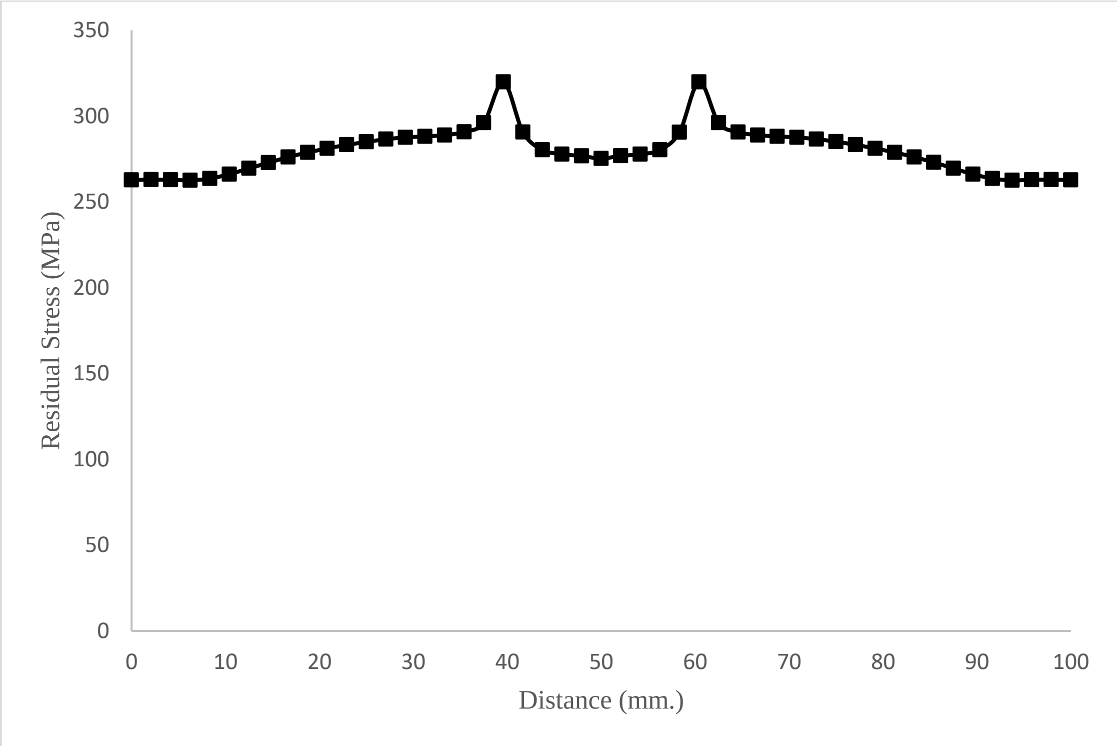

Figure 6.45 Residual stresses along the transverse direction obtained by without using Element Birth and Death Technique

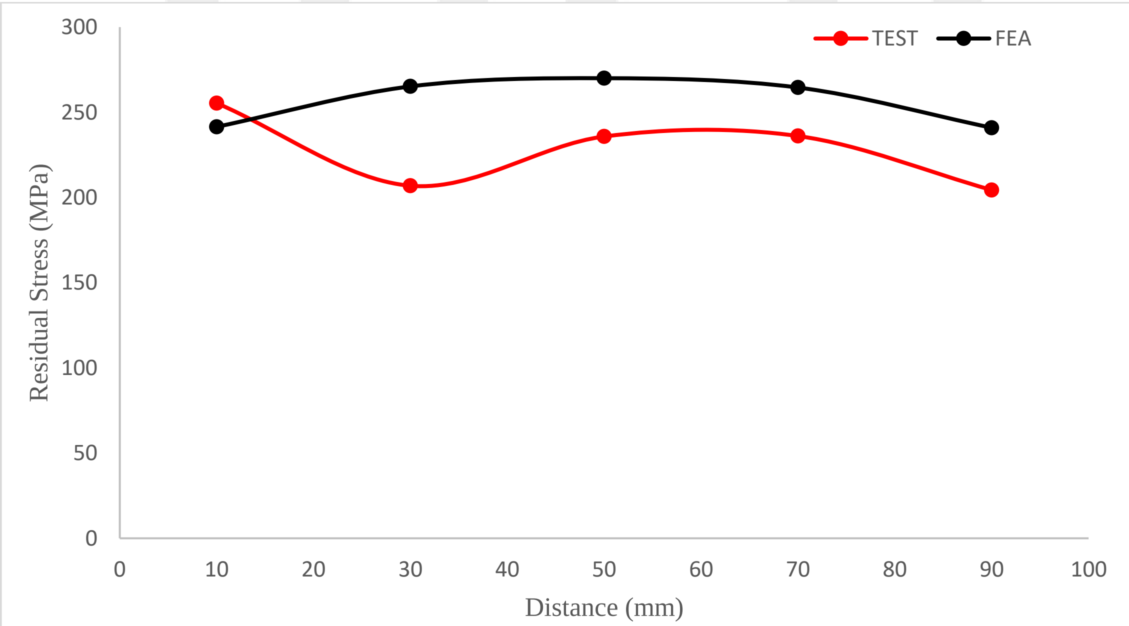

Figure 6.46. Comparison of residual stress along longitudinal direction on measurement points FEA without using EBD Technique

These residual stresses shown on Figure 6.46 and 6.47 are nodal stresses obtained corresponding nodes to the residual stress measurement points.

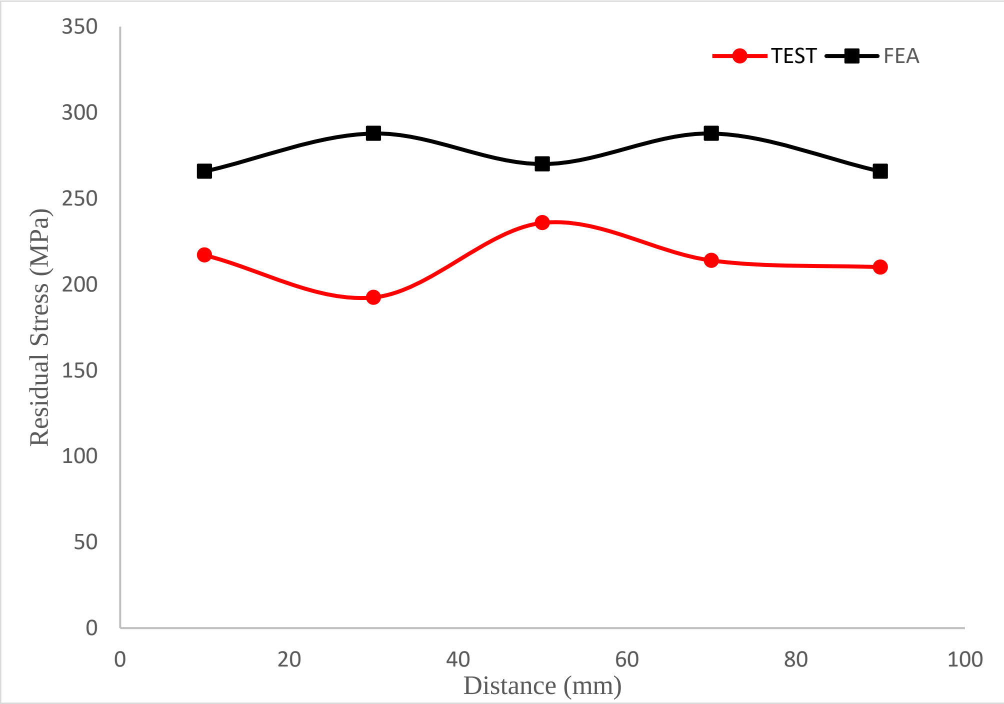

Figure 6.47. Comparison of residual stress along transverse direction on measurement points FEA without using EBD Technique

Table 6.8. Comprasion of result on measurement nodal obtained with using Element Birth/Death technique and non using Element Birth/Death Technique along longitudinal direction

		FEA RESULTS with element Birth and Death			FEA RESULTS with non using element Birth and Death		
	Measurement Point	Maximum (MPa)	Minimum (MPa)	Average (MPa)	Maximum (MPa)	Minimum (MPa)	Average (MPa)
Longitudinal Direction	LP1	277,73	247,04	262,39	241,58	241,4	241,49
	LP2	275,5	245,72	260,61	265,32	265,08	265,2
	LP3	275,95	246,11	261,02	270,02	270	270,01
	LP4	281,29	246,77	264,03	264,68	264,42	264,55
	LP5	277,95	248,83	263,39	240,91	240,98	240,95
Transverse Direction	TP1	265,46	265,46	265,46	265,73	265,73	265,73
	TP2	277,09	277,09	277,09	287,79	287,79	287,79
	TP3	275,92	246,11	261,02	270,02	270	270,01
	TP4	271,1	271,1	271,1	287,79	287,79	287,79
	TP5	265,46	265,46	265,46	265,73	265,73	265,73

The maximum and minimum residual stresses obtained by using Element Birth/Death Technique are 240,75 and 52,206 MPa along the longitudinal direction, 278,3 and 85,046 MPa along the transverse direction like shown on Figure 6.48 and 6.49.

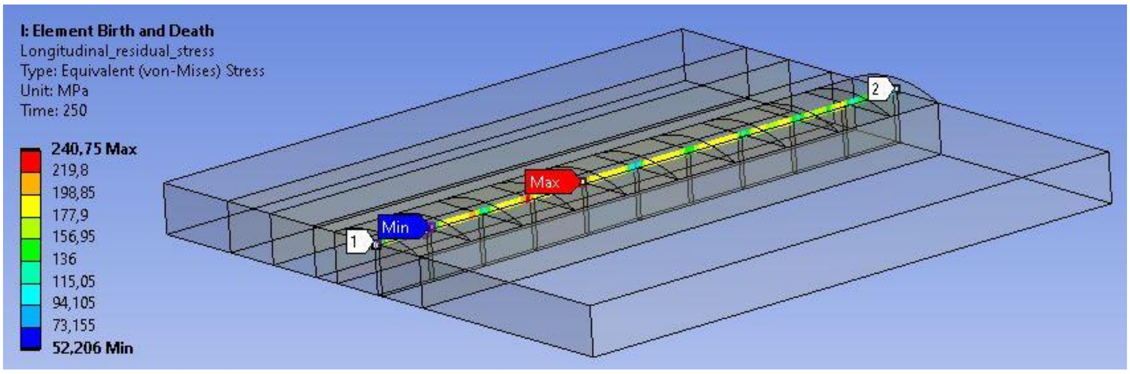

Figure 6.48. Residual stresses along longitudinal direction by using element birth-death technique

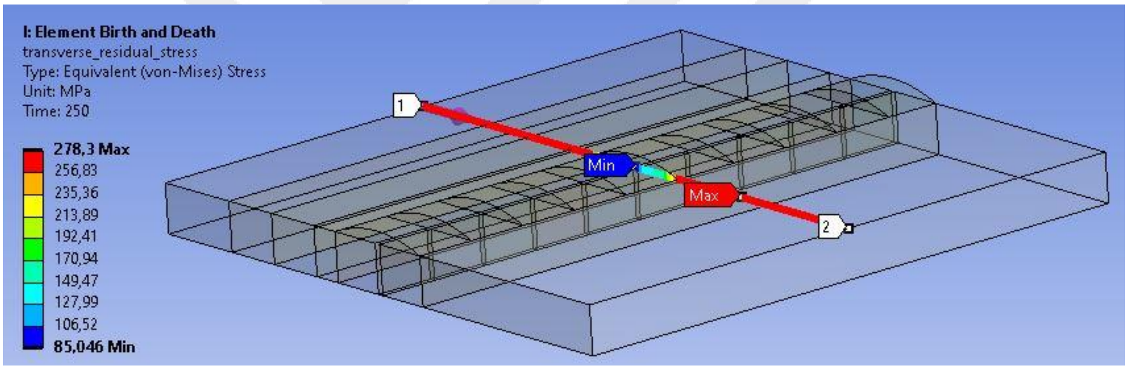

Figure 6.49. Residual stresses along longitudinal direction by using element birth/death technique

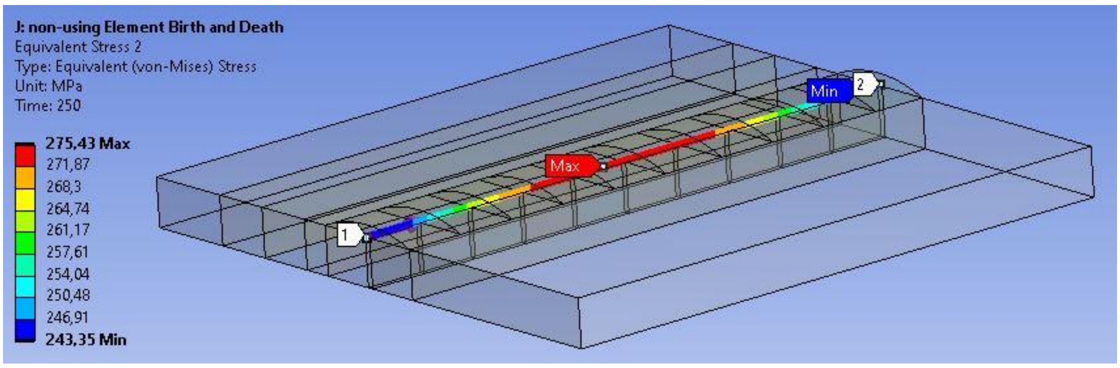

Figure 6.50 residual stresses along longitudinal direction by not using element birth/death technique

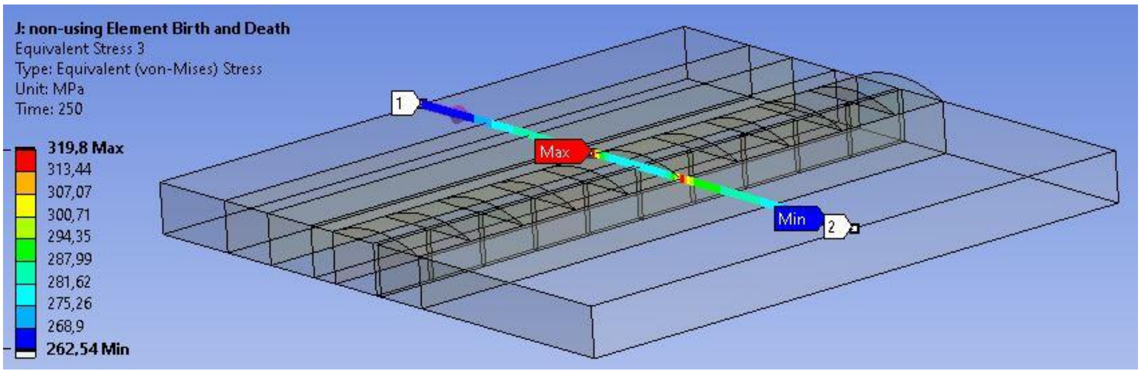

Figure 6.51. Residual stresses along transverse direction by not using element birth/death technique

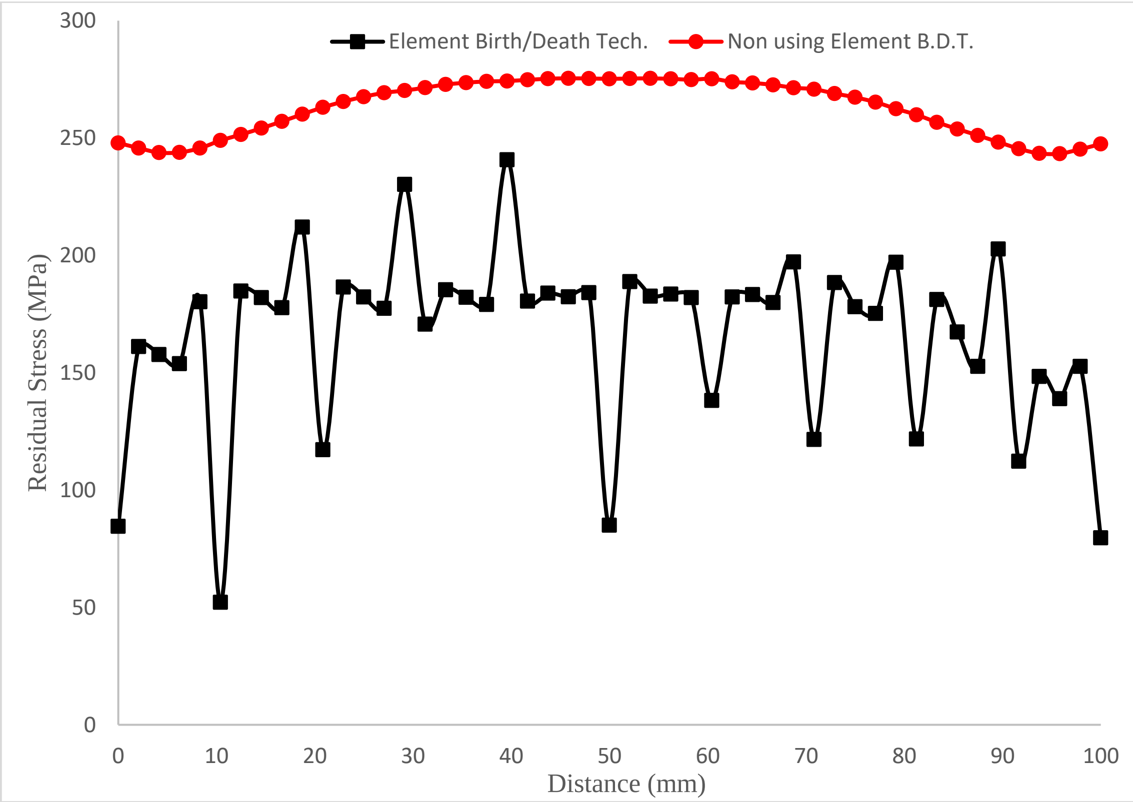

Figure 6.52. Comprasion of result obtained with using Element Birth/Death technique and non using Element Birth/Death Technique along longitudinal direction

The maximum and minimum residual stresses obtained by not using Element Birth/Death Technique are 275,43 and 243,35 MPa along the longitudinal direction, 319,8 and 262,54 MPa along the transverse direction like shown on Figure 6.50 and 6.51 .

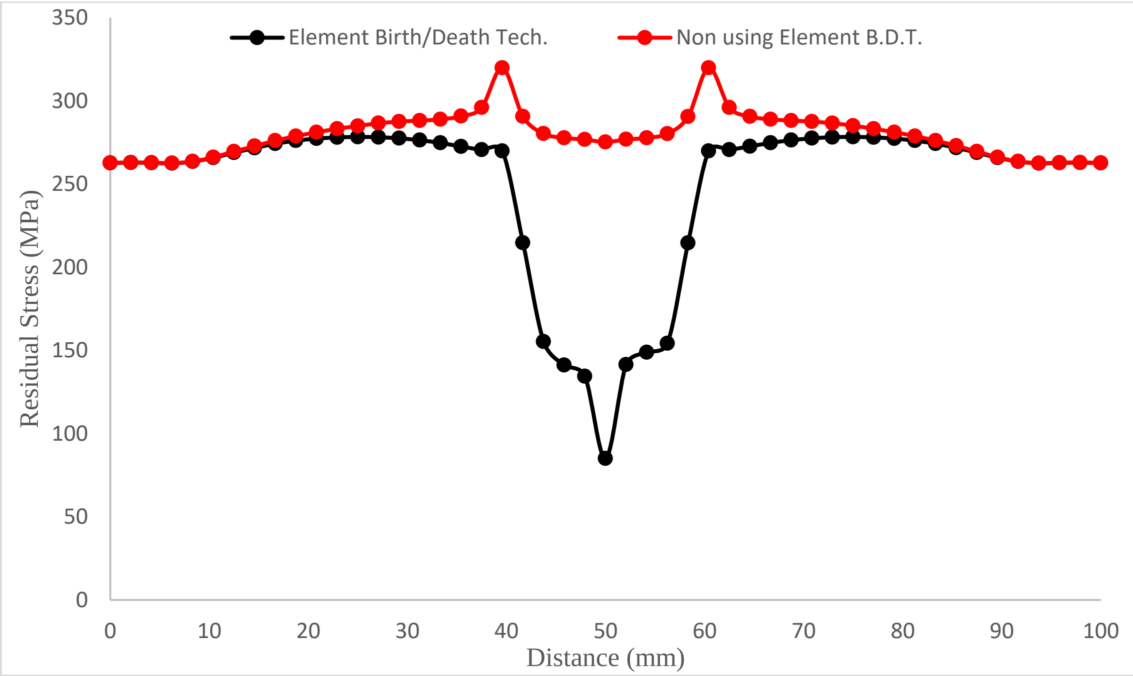

Figure 6.53. Comprasion of result obtained with using Element Birth/Death technique and non using Element Birth/Death Technique along transverse direction

We all desire accurate simulation results and generally speaking this takes two forms.

1. Numerical accuracy
2. Correct model respresentation

In numerical accuracy, we answer the question of whether the mesh is fine enough to get a mesh-dependent solution. While in correct model represantation, we focus on the question of whether the model is accurately representing our understanding of physical system.

While performing an analysis, we should always have a rough idea of the deformation or stress we expect to be generated in the system. In Ansys Mechanical, users can view the animations of deformed shapes while analyzing results. It is a very good practice to verify these animations and ensure that the structure is deforming in the manner which we expect. By verifying the deformation results, we can also identify whether or not our applied loads and supports are correct, especially to identify common problems like over sontraining the model (Url 5).

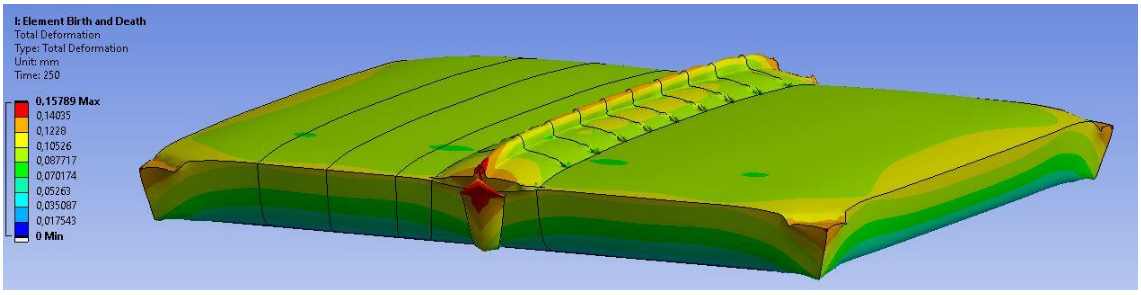

Figure 6.54. Total deformation obtained by using EBD Technique

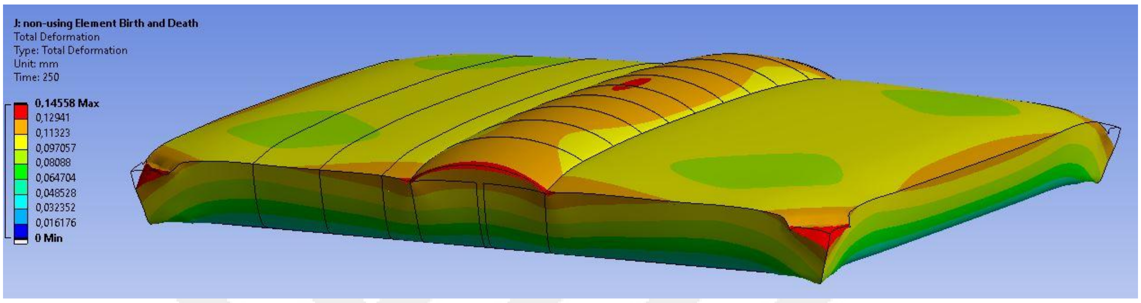

Figure 6.55. Total deformation obtained by using without element Birth/Death Technique

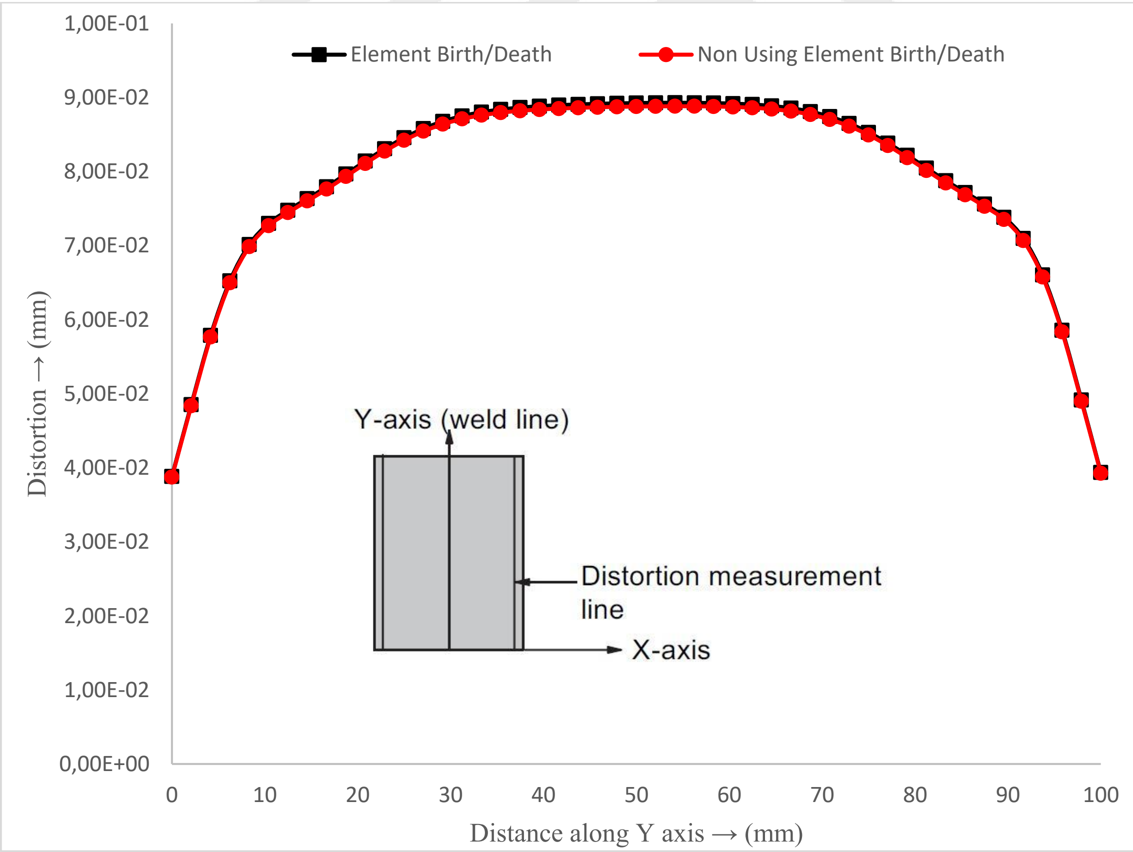

Figure 6.56. Comparing of distortion results on FEA

In order to prevent test piece to move freely test piece was clamped with its all corners like shown Figure 6.57. so the bottom surface of test place was fixed to surface that means there was no movement in any direction x,y and z. Thermal strains lead to stress when the structure is prevented from freely expanding or contracting.

For example there is a bar with a uniform cross section and no constraint applied and let the reference temperature for the bar of material be 20 ºC. If the bar is heated to a uniform of 30 ºC we can see that the bar can expand freely due to lack of any constraints. İn this case we see non-zero thermal strains. But since there are no constraints to prevent free expansion of the bar the stress produced are zero. Now let's fix the two ends of the bar and heat it again to a uniform temperature of 30 ºC. Since the bar is no longer allowed to expand freely non-zero stresses are produced in the bar.

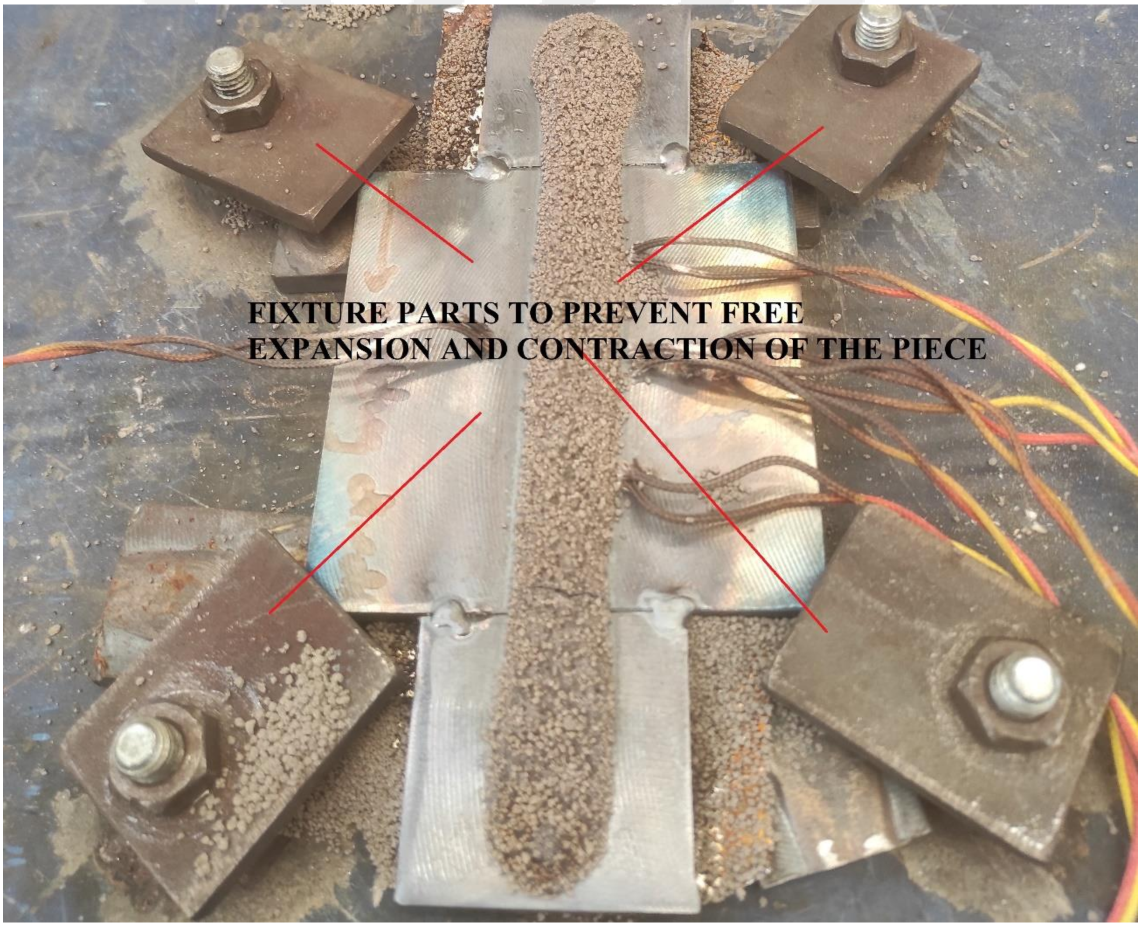

Figure 6.57. Clamping of the piece with fixtures

7. CONCLUSION

For any stress stress analysis, the engineers will have to specify appropriate boundary conditions to get the expected results. The structure should be constrained with appropriate supports and excitations are provided via loads. Changes in temperature produce thermal strains and thermal strains can cause mechanical stresses. In this study, residual stress and temperature distribution were compared using both experimental and finite element methods.

A submerged arc single pass double sided welded square butt joint of SA 387 GR 11 Class 2 pressure vessel steel was prepared to estimate both temperature distribution and residual stress distribution across the weld in both longitudinal and transverse directions. A test plate with 100 mm long, 100 mm width and 8 mm thick was used. Firstly Welding speed and voltage were kept constant and tested at different amperage values to determine suitable amperage value. At 430, 530 and 560 amperage values it was observed that lack of penetraiton has been occured. At 600 an appropriate welding penetration achieved. And all the test were performed with 600 A, 31 voltage and 10 mm/sec welding speed.

A finite element thermo-mechanical elastic-plastic analysis was carried out to predict residual stresses and temperature distribution using ANSYS 2020. Double-ellipsoidal distributed heat source model was used for moving heat source model. All the temperature dependent properties of SA 387 GR 11 Class 2 Steel was taken from Asme Boiler And Pressure Vessel Code Section II, Materials.

Based on the results presented in this study the following observations and conclusions can be made:

For thermal results it was observed;

1. Experimental findings were used to validate the model, and they showed a satisfactory level of agreement with the numerical model.
2. 15% is discovered to be the highest possible percentage of inaccuracy between experimental and numerical data.

3. As mesh size has been made finer, the findings of finite elements have grown closer to those of experimental measurements. Dimensions of the mesh were determined to be 1x1x1 mm.

4. The penetration and bead width increase in supply current, according to experimental data.

For residual stress analysis it was observed;

1. For the first time FEA has been applied for determination of residual stress in weldment of pressure vessel steel.
2. Time and cost saving can be available due to calculated residual stress levels. No matter what is the stress level, the industry always applies stress relieving process by heat treatment. The result of this type analysis can give a idea about whether stress relieving process should be applied necessary or not for design engineers.
3. Finite Element results are dependent on the mesh size specified. Mesh size affects the accuracy of the finite element results. Coarse meshes may give inaccurate results if the stress gradients are too large for the elements to capture properly. Seeing high gradients through the element of dericed quantities suc as stress or strain, is a good first indication that the element size may be too large.
4. Too small of an element size will unnecessarily increase the computation costs and solution times.
5. While we may not know the mesh size required to give accurate results before solving, using the results one can check and add mesh sizing as necessary.
6. Residual stresses obtained along the trasnverse and longitudinal direction on FEA analysis were the results through the path line along transverse and longitudinal direction.
7. Residual stresses which is used for comparing with test results are nodal stresses which is corresponding nodal on FEA.
8. Due to the boundary conditions our piece is symmetric so we are expecting the residual stress along the transverse direction to be the same symmetrically. The part had been clamped from its all corners with the same condition. Both FEA results by using EBD technique and by not-using EBD technique are symmetric as we are expecting.
9. The surface roughness and flatness of the sample piece in which residual stress is measured is very important to get accurate results. Surface roughness affects the results

meausered by XRD method and the surface should be flat. For that reason the reinforcement was removed by grinding.

10. On the first studies the deviation values on test result were too much. The reason why deviation values were too much was the roughness of the surface. In order to get acceptable results some points should be ignored. According to the curve the stress values are obtained.

11. The test piece was sticked to sample by using double-sided tape. But although we used double side tape we could not prevent the part to move down direction while sample was moving up direction.

12. The FE modelling of SA 387 Gr 11 Class 2 steel weld has not taken into account the solid-state phase transformation effect.

Further work, it is recommended :

1. While measuring residual stress with XRD method, in order to fix the work piece, different method can be used.
2. For determining residual stress different methods like deep hole drilling or ultrasonic technique can be used.
3. It should be considered the surface roughness should be very high to get more accurate results by using XRD method.
4. Microstructure and mechanical properties of the welded part can be analysed. Especially By applying tensile and charpy tests the mechanical properties of the welded part can be determined and the results of welding process can be observed.
5. The solid-state phase transformation effect can be considered in FE modelling of SA 387 GR 11 Class 2 steel weld.

REFERENCES

Biswas, P., Mandal, N.R. (2009). A Comparative Study of Three Different Approaches of FE Analysis For Prediction of Welding Distortion of Orthogonally Stiffened Plate Panels. *Journal of Ship Production and Design, vol 25*(No 4), 1-7. DOI: 10.5957/jsp.2009.25.4.191

Biswas, P., Mandal, A.K. (2009). Thermomechanical Finite Element Analysis and Experimental Investigation of Single-Pass Single Sided Submerged Arc Welding of C-Mn Stell Plates. *Proceedings of the Institution of Mechanical Engineers, Part B: Journal of Engineering Manufacture, 2010*(224), 627-639. DOI: 10.1243/09544054JEM1624

Biswas, P., Mahapatra, M.M., Mandal, N.R. (2010). Numerical and Experimental Study on Prediction of Thermal History and Residual Deformation of Double-Sided Fillet Welding. *Proceedings of the Institution of Mechanical Engineers, Part B: Journal of Engineering Manufacture, 2010*(224), 125-134. DOI: 10.1243/09544054JEM1666

British Standart. (1987). *Specification for Class I Arc Welding of Ferritic Steel Pipework for Carrying Fluids* (BS 2633: 1987). England

Chen, B.Q. (2011). Prediction of Heating Induced Temperature Fields and Distortions in Steel Plates. MSc Thesis, Universidade Tecnica de Lisboa, Instituto Sperior Tecnico, Lisbon

Croft, D.N. (1996). *Heat Treatment of welded structures* (First published). Cambridge England: Abington Publishing, Woodhead Publishing Ltd in association with The Welding Institute.

Çelik, B. (2009). Thermally Induced Distortion and Residual Stresses in Welded Joints. Master Thesis, Çukurova University, Institute of Natural and Applied Science, Adana, 284120

Ghosh, A., Barman, N., Chattopadhay, H. Bag, S. (2013). Modelling of Heat Transfer in Submerged Arc Welding. *Proceedings of the Institution of Mechanical Engineers, 227*(10), 1467–1473. DOI: 10.1177/0954405413489291

Goldak, J., Chakravarti, A., Bibby, M., (1984). A New Finite Model for Welding Heat Sources, *Metallurgical Transactions B, Volume 15B*, 299-305.

Ueda, Y., Murakawa, H., Ma, N. (2012). *Welding Deformation and Residual Stress Prevention* (1rd ed.). United States of America: Butterworth-Heinemann

Kumar, S.K. (2020). Thermal Field and Residual Stress Analyses of GTAW Dissimilar Weldments Between AA 5052 and AA 7075 By Numerical Simulation and Experimentation. Master Thesis, CMR Institute of Technology, Department of Mechanical Engineering, India

Mondal, A.K., Biswas, P., Bag, S. (2017). Experimenatal and FE Analysis of Submerged Arc Weld Induced Residual Stress and Angular Deformation of Single and Double Sided Fillet Welded Joint. *International Journal of Steel Structures, 17*(1), 9-18. DOI: 10.1007/s13296-016-0093-9

Nart, E., Celik, Y. (2013). A Practical Approach for Simulating Submerged Arc Welding Process Using FE Method. *Journal of Construcional Steel Research, 84,* 62-71. DOI: 10.1016/j.jcsr.2013.02.005

Nezamdost, M.R., Esfahani, M.R.N., Hashemi, S.H., Mirbozorgi, A.S. (2016). Investigation of Temperature and Residual Stresses Field of Submerged Arc Welding by Finite Element Method and Experiments. *Int J Adv Manuf Technol, 87,* 615-624. DOI 10.1007/s00170-016-8509-4

Radaj, D. (1992). *Heat Effects of Welding, Temperature Fields, Residual Stress, Distortion.* (First Published). Berlin: Springer-Verlag.

Ravichandran, G. (2021). *Finite Element Analysis of Weld Thermal Cycles Using ANSYS.* (First Published). USA Florida: CRC Press

Suman, S., Biswas, P. (2020). Comparative Study on SAW Welding Induced Distortion and Residual Stresses of CSEF Steel Considering Solid State Phase Transformation and Preheating. *Journal of Manufacturing Processes, 51,* 19-30 *https://doi.org/10.1016/j.jmapro.2020.01.012*

Suman, S., Biswas, P. (2022). Microstructural Strength and Residual Stress Studies on Single and Double-Side Single-Pass Submerged Arc Welding of 9Cr-1Mo-V Steel Plate. *Journal of The Institution of Engineers (India), Series C.,* 1177–1191 https://doi.org/10.1007/s40032-022-00870-4

Suman, S., Biswas, P., Patel, S.,K., Singh, V.,P., Kumar, A., Kuriachen, B. (2019). Measurement of Residual Stresses in Submerged Arc Welded P91 Steel Using Surface Deformation. *Materials Today Proceedings, 2019,* 1707-1712. DOI: https://doi.org/10.1016/j.matpr.2019.12.049

Sarkar, S.S., Das, A., Paul, S., Mali, K., Hosh, A., Sarkar, R., Kumar, A. (2020). Machine Learning Method to Predict and Analyse Transient Temperature in Submerged Arc Welding. *Measurement, Volume 170(*108713), DOI:https://doi.org/10.1016/j.measurement.2020.108713.

Singh, R. (2021). *Arc Welding Processes Handbook* (First published). USA: Scrivener Publishing WILEY

Sirivella, V.B. (2014). Investigation on Temperature Distribution in SAW Weld Using 2D Mesh Model. *International Journal of Engineering Trends and Technology (IJETT), Volume 18*(Number 6), 252-255. DOI: 10.14445/22315381/IJETT-V18P252

Taskaya, S., Gur, A.K., Ozay, C. (2019). Joining of Ramor 500 Steel with SAW (Submerged Arc Welding) and its Evaluation of Thermomechanical Analysis in ANSYS Package Software. *Thermal Science and Engineering Progress, 13*(100396), DOI: 10.1017/j.step.2019.100396

The American Society of Mechanial Engineers ASME. (2016). *ASME Code for Pressure Piping, B31* (B31.3-2016). New York USA

The American Society of Mechanical Engineers ASME. (2021). *Asme Boiler And Pressure Vessel Code Section II, Materials, ASME BPVC.II.D.M.-2021*, New York USA.

URL-1: https://qaqctips.blogspot.com/2019/05/what-is-preheat-temperature-for-carbon-steel-bsen-1011-2.html, (Visit Date: 10 August 2022)

URL-2:https://www.rextonsteel.com/sa-387-gr-11-cl-2-alloy-steel-plate-supplier-stockist.html, (Visit Date: 11 August 2022)

URL-3:https://www.alloysteelplates.com/asme-sa-387-grade-11-class-2.html,(Visit Date: 11 August 2022)

URL-4:https://sites.google.com/site/temfemguy/research/residual-stress-in-aluminium-forgings/residual-stress-determination---x-ray-diffraction, (Visit Date: 15 October 2022)

URL-5:https://courses.ansys.com/index.php/courses/reviewing-results-validation-and-insight-using-ansys-mechanical/, (Visit Date: 22 December 2022)

Uzun, F. (2014). Effect of Carbon Content in Carbon steels on formation of Welding Residual Stress. Doctoral Thesis, Yeditepe University, Institute of Graduate Studies in Science and Engineering, 438687

Yildiz, A. (2011). Analysis of Welded Part by Finite Element Method. Msc Thesis, Uludağ University, Graduate School of Natural and Applied Sciences Department of Mechanical Engineering, 284799

APPENDICES

APPENDICES-A

The APDL Code for Moving Heat Source

```
!   Commands inserted into this file will be executed just prior to the ANSYS SOLVE command.

!   These commands may supersede command settings set by Workbench.

!   Active UNIT system in Workbench when this object was created:  Metric (m, kg, N, s, V, A)

!   NOTE:  Any data that requires units (such as mass) is assumed to be in the consistent solver unit system.

!                See Solving Units in the help system for more information.

!**************

! APDL COMMANDS FOR GOLDAK DOUBLE ELLIPSOID MODEL

! retrieves a value and stores it as a scalar parameter or part of an array parameter. Name of parameter = EMAX/EMIN, Entity=Element

CMSEL,ALL

*GET,EMAX,ELEM,,NUM,MAX

*GET,EMIN,ELEM,,NUM,MIN

! used constant in the equation

ALLSEL

TIME_WELD=25        ! Welding Time

DT=0.01
```

A=0.01 ! ellipsoid semi-axe 1

B=0.008 ! ellipsoid semi-axe 2

C1=0.01 ! ellipsoid semi-axe 3 front

C2=0.03 ! ellipsoid semi-axe 3 rear

TAU=0 ! Time Delay

FF=0.5 ! ff = Fraction of heat on the front part of the heat source

FR=1.5 ! fr = Fraction of heat on the rear part of the heat source

Q=12000 ! Welding Energy J/S (W) Q = (n*I*U) ; I=welding current 600 A, U=welding voltage 31, n=thermal efficiency 0.9 is selected,

VEL=1E-2 ! welding speed m/sn

NPT=TIME_WELD/DT

NROPT,FULL ! NROPT = specifies the Newton-Raphson options in a static or full transient analysis. Use full Newton-Raphson

!Defining Parametric variables

! Welding Pass

*DO,i,1,NPT,1 ! Loop for every time steps, Time increment

WTIME=(i/10)

TIME,WTIME

HCENTER=VEL*WTIME ! HEAT SOURCE CENTER : This defines the moving centre of the double ellipsoid heat soource

*DO,jj,EMIN,EMAX,1 ! SELECT THE CENTROID OF EVERY ELEMENT. Picking of element cetroids

X=CENTRX(jj) ! Centroid X-coordinate of jj-th element in global Cartesian Coordinate System.

Y=CENTRY(jj) ! Centroid Y-coordinate of jj-th element in global Cartesian Coordinate System.

Z=CENTRZ(jj) ! Centroid Z-coordinate of jj-th element in global Cartesian Coordinate System.

CSI=Y+VEL*(TAU-WTIME) ! MOVING COORDINATE (IT MOVES THROUGH Y AS TIME PASSES), Y is moving direction.

*IF,Y,GT,HCENTER,THEN ! defines whether it is the front part of the heat source or rear

! loop for heat source application

C=C1

F=FF

*ELSE

C=C2

F=FR

*ENDIF

PART1=(6*(3**0.5)*F*Q)/(A*B*C*3.14*(3.14**0.5)) ! First part of Goldak Double ellipsoid model in fixed CSYS

PART2=(EXP(-3*(X/A)**2))*(EXP(-3*(Z/B)**2))*(EXP(-3*(CSI/C)**2)) ! second part of Goldak Double ellipsoid model in fixed CSYS

QF=PART1*PART2 ! Heat source equation

BFE,jj,HGEN,,QF ! Defines an elemnt body force load BFE, ELEM, Lab, STLOC, VAL1, VAL2, VAL3, VAL4

```
*ENDDO

SOLVE

*ENDDO

CMSEL,ALL                    ! Select a subset of components and assemblies

BFEDELE,ALL,ALL              ! Deletes element body force loads. BFEDELE, ELEM,
Lab

ALLSEL
```

PERSONAL PUBLICATION AND WORKS

Şenol M.T., Makaraci, M. (2022). Estimation in Submerged Arc Welding Process Applied to A387 Chromium-Molybdenum Alloy Steel Using Goldak's Double Ellipsoidal Heat Source Model. *International Azerbaijan Academic Research Congress*, Online, 28-29 May 2022

BIOGRAPHY

Mert Turgut Şenol gratuated from Mechanical Department of Kocaeli Anatolian Technical High School in 2000 and from Mechanical Department of Kullar Vocational High School of Kocaeli University in 2002 respectively. He has earned his Bachelor of Science degree from the Mechanical Engineering Department of Çukurova University in 2007. He completed his master of science of education in Mechatronics Enginering of Kocaeli University in 2018.

He began his master of science studies at the Department of Mechanical Engineering of Kocaeli University in 2020.

He began to work as maintenance engineer in 2010 in Tekfen Manufacturing and Engineering Company and since 2013 he is continuing to work as maintenance chief engineer.